

**LABORATORY STUDIES OF EDDY STRUCTURES AND EXCHANGE  
PROCESSES THROUGH TIDAL INLETS**

A Thesis

by

FRANCISCO NICOLAU DEL ROURE

Submitted to the Office of Graduate Studies of  
Texas A&M University  
in partial fulfillment of the requirements for the degree of  
MASTER OF SCIENCE

August 2007

Major Subject: Ocean Engineering

**LABORATORY STUDIES OF EDDY STRUCTURES AND EXCHANGE  
PROCESSES THROUGH TIDAL INLETS**

A Thesis

by

FRANCISCO NICOLAU DEL ROURE

Submitted to the Office of Graduate Studies of  
Texas A&M University  
in partial fulfillment of the requirements for the degree of

MASTER OF SCIENCE

Approved by:

Co-Chairs of Committee,	Scott A. Socolofsky
	Kuang-An Chang
Committee Members,	Patrick Lynett
	Achim Stössel
Head of Department,	David Rosowsky

August 2007

Major Subject: Ocean Engineering



physical parameters such as the position on the basin of the vortex, the equivalent diameter, and the maximum vorticity among others.

The mixing number accurately predicts the behavior of the vortex for the first cycle on idealized inlets for the subsequent cycles; the structures behave differently than predicted by  $K_W$ , because the blocking effect of the vortex formed in the previous cycle. For characteristic times  $t^* = tU / W$  less than about 2, the dipole is attached to the inlet and forms rapidly. For later times, the dipole advects downstream, and slowly dissipates.

Numerical experiments are also presented. Comparing the numerical data with the laboratory data, good agreement is reached, but important limitations are identified for the grid resolution and domain size.

## ACKNOWLEDGMENTS

This research was supported by the Texas Sea Grant. The title of the principal project funded by this grant is “Laboratory Studies of Exchange Processes through Tidal Inlets on the Texas Coast”.

In addition to financial support, I deeply appreciate the invaluable motivation and guidance extended to me by my advisor Dr. Scott A. Socolofsky. I am thankful for all the time that he spent helping me with the Matlab and FORTRAN codes, and for his support in answering my questions and doubts regarding the project and fluid mechanics in general. I especially thank the Institute of Hydromechanics of the University of Karlsruhe, in Karlsruhe, Germany for lending me their facilities to simulate my experiments, especially to Wernher Brevis for his knowledge in the use of the shallow water basin and his assistance to run the experiments with Leticia Tarrab. I also appreciate the support of the Co-Chair of the committee Dr. Kuang-An Chang, the members of my research committee and Dr. Patrick Lynett for the participation in useful discussions concerning this investigation in our monthly meetings, and Dr. Achim Stössel who gave me unconditional help when I needed.

Finally, I would like to thank my parents that always believe in me, and gave me words of inspiration and support in moments that I needed the most.

## TABLE OF CONTENTS

		Page
ABSTRACT.....		iii
ACKNOWLEDGMENTS.....		v
TABLE OF CONTENTS.....		vi
LIST OF FIGURES.....		vii
LIST OF TABLES.....		xxiii
CHAPTER		
I	INTRODUCTION.....	1
	1.1 Background.....	1
	1.2 Problem Definition.....	6
	1.3 Objectives.....	9
	1.4 Outline.....	9
II	LABORATORY STUDIES OF EDDY STRUCTURES AND EXCHANGE PROCESSES THROUGH TIDAL INLETS	11
	2.1 Introduction.....	11
	2.2 Experimental Design.....	15
	2.3 Data Analysis.....	18
	2.4 Results.....	25
	2.5 Discussion.....	39
	Summary and Conclusions.....	46
III	NUMERICAL MODELING.....	48
	3.1 Model Description.....	48
	3.2 Methodology.....	48
	3.3 Results.....	49
	3.4 Application Discussion.....	52
IV	CONCLUSIONS.....	53

	Page
REFERENCES.....	56
APPENDIX A      METHODOLOGY OF THE EXPERIMENTS.....	59
APPENDIX B      DATA ANALYSIS.....	73
APPENDIX C      ELECTRONIC SUPPLEMENT.....	158
VITA.....	159

## LIST OF FIGURES

	Page
Figure 1 Chlorophyll concentration off the Queen Charlotte Islands, CANADA (Courtesy NASA SeaWiFS, 2004).....	3
Figure 2 Parameters that define a tidal vortex dipole.....	4
Figure 3 a) Laboratory where the experiments were taken. b) Dye studies visualization. c) PIV simulation.....	8
Figure 4 Layouts with different geometries: A) Idealized Inlet; B) Inlet with jetties with equal length of the width of the inlet; C) Inlet with jetties with length longer than the inlet; and D) Inlet with a thicker barrier island with length longer than the width of the inlet. ....	17
Figure 5 Example of a result for the data analysis of and image for the Life- history Type I of the idealized case: a) Velocity field; b) Vorticity field; c) Vortex formation identification.....	22
Figure 6 Dye experimental studies for the idealized inlet. a) Life-history Type I ( $K_W = 0.11$ ), the vortex dipole remains stationary in the vicinity of the mouth of the inlet. b) Life-history Type II ( $K_W = 0.26$ ), the vortex dipole gets drawn back to the estuary. c) Life-history Type III ( $K_W = 0.06$ ), the vortex dipole escapes away from the inlet to never come back.....	26
Figure 7 Example of a result for the data analysis of and image for the Life- history Type II of the idealized case: a) Velocity field; b) Vorticity field; c) Vortex formation identification.....	29
Figure 8 Example of a result for the data analysis of and image for the Life- history Type III of the idealized case: a) Velocity field; b) Vorticity field; c) Vortex formation identification.....	30



- Figure 9 Life-history Type I for Layout A: a) Cross sectional average velocity at the mouth of the inlet. b) Longitudinal position of the center of the main vortex starting from the edge of the barrier island. c) Lateral position of the center of the main vortex starting from the edge of the barrier island. d) Circulation around the main vortex. e) Maximum vorticity in the main vortex. f) Equivalent diameter of the main vortex. g) Upwelling flowing from the main vortex. ....32
- Figure 10 Life-history Type II for Layout A: a) Cross sectional average velocity at the mouth of the inlet. b) Longitudinal position of the center of the main vortex starting from the edge of the barrier island. c) Lateral position of the center of the main vortex starting from the edge of the barrier island. d) Circulation around the main vortex. e) Maximum vorticity in the main vortex. f) Equivalent diameter of the main vortex. g) Upwelling flowing from the main vortex. ....34
- Figure 11 Life-history Type I for Layout A: a) Cross sectional average velocity at the mouth of the inlet. b) Longitudinal position of the center of the main vortex starting from the edge of the barrier island. c) Lateral position of the center of the main vortex starting from the edge of the barrier island. d) Circulation around the main vortex. e) Maximum vorticity in the main vortex. f) Equivalent diameter of the main vortex. g) Upwelling flowing from the main vortex. ....36

Figure 12 1) Layout A. 2) Layout B. 3) Layout C. 4) Layout D. a) Cross sectional average velocity at the mouth of the inlet. b) Longitudinal position of the center of the main vortex starting from the edge of the barrier island. c) Lateral position of the center of the main vortex starting from the edge of the barrier island. d) Circulation around the main vortex. e) Maximum vorticity in the main vortex. f) Equivalent diameter of the main vortex. g) Upwelling flowing from the main vortex. ....	38
Figure 13 a) Circulation around the main vortex for life-history Type I, Layout A. b) Circulation around the main vortex for life-history Type II, Layout A. c) Circulation around the main vortex for life-history Type III, Layout A. d) Circulation around the main vortex for life-history Type I, Layout B. e) Circulation around the main vortex for life-history Type I, Layout C. a) Circulation around the main vortex for life-history Type I, Layout D.	41
Figure 14 Numerical simulation of Layout A. Life-history Type II ( $K_W = 0.26$ )....	50
Figure 15 Numerical simulation of Layout A. Life-history Type III ( $K_W = 0.06$ )...	51
Figure 16 Layout A: Idealized inlet.....	64
Figure 17 Layout B: Inlet with jetties with equal length than the inlet.....	64
Figure 18 Layout C: Inlet with jetties length longer than the inlet.....	65
Figure 19 Layout D: Inlet with a wider width, simulating a barrier island.....	65
Figure 20 Layout E: Inlet with obstacles in the mouth of the inlet. Case A .....	66
Figure 21 Layout F: Inlet with obstacles in the mouth of the inlet. Case B.....	66
Figure 22 Layout G: Inlet with obstacles in the mouth of the inlet. Case C.....	67
Figure 23 Layout H: Inlet in an oblique angle .....	67
Figure 24 Layout A: Idealized inlet ( $K_W = 0.11$ ).....	74
Figure 25 Layout A: Idealized inlet ( $K_W = 0.26$ ).....	75

Figure 26 Layout B: Inlet with jetties with equal length than the inlet ( $K_W = 0.06$ ).....	76
Figure 27 Layout D: Inlet with a wider width, simulating a barrier island ( $K_W = 0.13$ ).....	77
Figure 28 Layout H: Inlet in an oblique angle: $20^\circ$ ( $K_W = 0.13$ ).....	78
Figure 29 Example of a result for the data analysis of and image for the Life- history Type I of the idealized case: a) Velocity field; b) Vorticity field; c) Vortex formation identification.....	85
Figure 30 Example of a result for the data analysis of and image for the Life- history Type II of the idealized case: a) Velocity field; b) Vorticity field; c) Vortex formation identification.....	86
Figure 31 Example of a result for the data analysis of and image for the Life- history Type III of the idealized case: a) Velocity field; b) Vorticity field; c) Vortex formation identification.....	87
Figure 32 Life-history Type I for Layout A, repetition 1: a) Average cross sectional velocity at the mouth of the inlet. b) Longitudinal position of the center of the main vortex starting from the edge of the barrier island. c) Lateral position of the center of the main vortex starting from the edge of the barrier island.....	92
Figure 33 Life-history Type I for Layout A, repetition 1: a) Circulation around the main vortex b) Maximum vorticity in the main vortex c) Equivalent diameter of the main vortex. d) Upwelling flowing from the main vortex.....	93

Figure 34 Life-history Type I for Layout A, repetition 2: a) Average cross sectional velocity at the mouth of the inlet. b) Longitudinal position of the center of the main vortex starting from the edge of the barrier island. c) Lateral position of the center of the main vortex starting from the edge of the barrier island.....	94
Figure 35 Life-history Type I for Layout A, repetition 2: a) Circulation around the main vortex b) Maximum vorticity in the main vortex c) Equivalent diameter of the main vortex. d) Upwelling flowing from the main vortex.....	95
Figure 36 Life-history Type II for Layout A, repetition 1: a) Average cross sectional velocity at the mouth of the inlet. b) Longitudinal position of the center of the main vortex starting from the edge of the barrier island. c) Lateral position of the center of the main vortex starting from the edge of the barrier island.....	96
Figure 37 Life-history Type II for Layout A, repetition 1: a) Circulation around the main vortex b) Maximum vorticity in the main vortex c) Equivalent diameter of the main vortex. d) Upwelling flowing from the main vortex.....	97
Figure 38 Life-history Type II for Layout A, repetition 2: a) Average cross sectional velocity at the mouth of the inlet. b) Longitudinal position of the center of the main vortex starting from the edge of the barrier island. c) Lateral position of the center of the main vortex starting from the edge of the barrier island.....	98

Figure 39 Life-history Type II for Layout A, repetition 2: a) Circulation around the main vortex b) Maximum vorticity in the main vortex c) Equivalent diameter of the main vortex. d) Upwelling flowing from the main vortex.....	99
Figure 40 Life-history Type III for Layout A, repetition 1: a) Average cross sectional velocity at the mouth of the inlet. b) Longitudinal position of the center of the main vortex starting from the edge of the barrier island. c) Lateral position of the center of the main vortex starting from the edge of the barrier island.....	100
Figure 41 Life-history Type III for Layout A, repetition 1: a) Circulation around the main vortex b) Maximum vorticity in the main vortex c) Equivalent diameter of the main vortex. d) Upwelling flowing from the main vortex.....	101
Figure 42 Life-history Type III for Layout A, repetition 2: a) Average cross sectional velocity at the mouth of the inlet. b) Longitudinal position of the center of the main vortex starting from the edge of the barrier island. c) Lateral position of the center of the main vortex starting from the edge of the barrier island.....	102
Figure 43 Life-history Type III for Layout A, repetition 2: a) Circulation around the main vortex b) Maximum vorticity in the main vortex c) Equivalent diameter of the main vortex. d) Upwelling flowing from the main vortex.....	103
Figure 44 Life-history Type I for Layout B, repetition 1: a) Average cross sectional velocity at the mouth of the inlet. b) Longitudinal position of the center of the main vortex starting from the edge of the barrier island. c) Lateral position of the center of the main vortex starting from the edge of the barrier island.....	104

Figure 45 Life-history Type I for Layout B, repetition 1: a) Circulation around the main vortex b) Maximum vorticity in the main vortex c) Equivalent diameter of the main vortex. d) Upwelling flowing from the main vortex.....	105
Figure 46 Life-history Type I for Layout B, repetition 2: a) Average cross sectional velocity at the mouth of the inlet. b) Longitudinal position of the center of the main vortex starting from the edge of the barrier island. c) Lateral position of the center of the main vortex starting from the edge of the barrier island.....	106
Figure 47 Life-history Type I for Layout B, repetition 2: a) Circulation around the main vortex b) Maximum vorticity in the main vortex c) Equivalent diameter of the main vortex. d) Upwelling flowing from the main vortex.....	107
Figure 48 Life-history Type II for Layout B, repetition 1: a) Average cross sectional velocity at the mouth of the inlet. b) Longitudinal position of the center of the main vortex starting from the edge of the barrier island. c) Lateral position of the center of the main vortex starting from the edge of the barrier island.....	108
Figure 49 Life-history Type II for Layout B, repetition 1: a) Circulation around the main vortex b) Maximum vorticity in the main vortex c) Equivalent diameter of the main vortex. d) Upwelling flowing from the main vortex.....	109
Figure 50 Life-history Type II for Layout B, repetition 2: a) Average cross sectional velocity at the mouth of the inlet. b) Longitudinal position of the center of the main vortex starting from the edge of the barrier island. c) Lateral position of the center of the main vortex starting from the edge of the barrier island.....	110

Figure 51 Life-history Type II for Layout B, repetition 2: a) Circulation around the main vortex b) Maximum vorticity in the main vortex c) Equivalent diameter of the main vortex. d) Upwelling flowing from the main vortex.....	111
Figure 52 Life-history Type III for Layout B, repetition 1: a) Average cross sectional velocity at the mouth of the inlet. b) Longitudinal position of the center of the main vortex starting from the edge of the barrier island. c) Lateral position of the center of the main vortex starting from the edge of the barrier island.....	112
Figure 53 Life-history Type III for Layout B, repetition 1: a) Circulation around the main vortex b) Maximum vorticity in the main vortex c) Equivalent diameter of the main vortex. d) Upwelling flowing from the main vortex.....	113
Figure 54 Life-history Type III for Layout B, repetition 2: a) Average cross sectional velocity at the mouth of the inlet. b) Longitudinal position of the center of the main vortex starting from the edge of the barrier island. c) Lateral position of the center of the main vortex starting from the edge of the barrier island.....	114
Figure 55 Life-history Type III for Layout B, repetition 2: a) Circulation around the main vortex b) Maximum vorticity in the main vortex c) Equivalent diameter of the main vortex. d) Upwelling flowing from the main vortex.....	115
Figure 56 Life-history Type I for Layout C, repetition 1: a) Average cross sectional velocity at the mouth of the inlet. b) Longitudinal position of the center of the main vortex starting from the edge of the barrier island. c) Lateral position of the center of the main vortex starting from the edge of the barrier island.....	116

Figure 57 Life-history Type I for Layout C, repetition 1: a) Circulation around the main vortex b) Maximum vorticity in the main vortex c) Equivalent diameter of the main vortex. d) Upwelling flowing from the main vortex.....	117
Figure 58 Life-history Type I for Layout C, repetition 2: a) Average cross sectional velocity at the mouth of the inlet. b) Longitudinal position of the center of the main vortex starting from the edge of the barrier island. c) Lateral position of the center of the main vortex starting from the edge of the barrier island.....	118
Figure 59 Life-history Type I for Layout C, repetition 2: a) Circulation around the main vortex b) Maximum vorticity in the main vortex c) Equivalent diameter of the main vortex. d) Upwelling flowing from the main vortex.....	119
Figure 60 Life-history Type II for Layout C, repetition 1: a) Average cross sectional velocity at the mouth of the inlet. b) Longitudinal position of the center of the main vortex starting from the edge of the barrier island. c) Lateral position of the center of the main vortex starting from the edge of the barrier island.....	120
Figure 61 Life-history Type II for Layout C, repetition 1: a) Circulation around the main vortex b) Maximum vorticity in the main vortex c) Equivalent diameter of the main vortex. d) Upwelling flowing from the main vortex.....	121
Figure 62 Life-history Type III for Layout C, repetition 1: a) Average cross sectional velocity at the mouth of the inlet. b) Longitudinal position of the center of the main vortex starting from the edge of the barrier island. c) Lateral position of the center of the main vortex starting from the edge of the barrier island.....	122



Figure 63 Life-history Type III for Layout C, repetition 1: a) Circulation around the main vortex b) Maximum vorticity in the main vortex c) Equivalent diameter of the main vortex. d) Upwelling flowing from the main vortex.....	123
Figure 64 Life-history Type III for Layout C, repetition 2: a) Average cross sectional velocity at the mouth of the inlet. b) Longitudinal position of the center of the main vortex starting from the edge of the barrier island. c) Lateral position of the center of the main vortex starting from the edge of the barrier island.....	124
Figure 65 Life-history Type III for Layout C, repetition 2: a) Circulation around the main vortex b) Maximum vorticity in the main vortex c) Equivalent diameter of the main vortex. d) Upwelling flowing from the main vortex.....	125
Figure 66 Life-history Type I for Layout D, repetition 1: a) Average cross sectional velocity at the mouth of the inlet. b) Longitudinal position of the center of the main vortex starting from the edge of the barrier island. c) Lateral position of the center of the main vortex starting from the edge of the barrier island.....	126
Figure 67 Life-history Type I for Layout D, repetition 1: a) Circulation around the main vortex b) Maximum vorticity in the main vortex c) Equivalent diameter of the main vortex. d) Upwelling flowing from the main vortex.....	127
Figure 68 Life-history Type I for Layout D, repetition 2: a) Average cross sectional velocity at the mouth of the inlet. b) Longitudinal position of the center of the main vortex starting from the edge of the barrier island. c) Lateral position of the center of the main vortex starting from the edge of the barrier island.....	128

Figure 69 Life-history Type I for Layout D, repetition 2: a) Circulation around the main vortex b) Maximum vorticity in the main vortex c) Equivalent diameter of the main vortex. d) Upwelling flowing from the main vortex.....	129
Figure 70 Life-history Type II for Layout D, repetition 1: a) Average cross sectional velocity at the mouth of the inlet. b) Longitudinal position of the center of the main vortex starting from the edge of the barrier island. c) Lateral position of the center of the main vortex starting from the edge of the barrier island.....	130
Figure 71 Life-history Type II for Layout D, repetition 1: a) Circulation around the main vortex b) Maximum vorticity in the main vortex c) Equivalent diameter of the main vortex. d) Upwelling flowing from the main vortex.....	131
Figure 72 Life-history Type II for Layout D, repetition 2: a) Average cross sectional velocity at the mouth of the inlet. b) Longitudinal position of the center of the main vortex starting from the edge of the barrier island. c) Lateral position of the center of the main vortex starting from the edge of the barrier island.....	132
Figure 73 Life-history Type II for Layout D, repetition 2: a) Circulation around the main vortex b) Maximum vorticity in the main vortex c) Equivalent diameter of the main vortex. d) Upwelling flowing from the main vortex.....	133
Figure 74 Life-history Type III for Layout D, repetition 1: a) Average cross sectional velocity at the mouth of the inlet. b) Longitudinal position of the center of the main vortex starting from the edge of the barrier island. c) Lateral position of the center of the main vortex starting from the edge of the barrier island.....	134

Figure 75 Life-history Type III for Layout D, repetition 1: a) Circulation around the main vortex b) Maximum vorticity in the main vortex c) Equivalent diameter of the main vortex. d) Upwelling flowing from the main vortex.....	135
Figure 76 Life-history Type III for Layout D, repetition 2: a) Average cross sectional velocity at the mouth of the inlet. b) Longitudinal position of the center of the main vortex starting from the edge of the barrier island. c) Lateral position of the center of the main vortex starting from the edge of the barrier island.....	136
Figure 77 Life-history Type III for Layout D, repetition 2: a) Circulation around the main vortex b) Maximum vorticity in the main vortex c) Equivalent diameter of the main vortex. d) Upwelling flowing from the main vortex.....	137
Figure 78 Life-history Type I for Layout E, repetition 1: a) Average cross sectional velocity at the mouth of the inlet. b) Longitudinal position of the center of the main vortex starting from the edge of the barrier island. c) Lateral position of the center of the main vortex starting from the edge of the barrier island.....	138
Figure 79 Life-history Type I for Layout E, repetition 1: a) Circulation around the main vortex b) Maximum vorticity in the main vortex c) Equivalent diameter of the main vortex. d) Upwelling flowing from the main vortex.....	139
Figure 80 Life-history Type I for Layout E, repetition 2: a) Average cross sectional velocity at the mouth of the inlet. b) Longitudinal position of the center of the main vortex starting from the edge of the barrier island. c) Lateral position of the center of the main vortex starting from the edge of the barrier island.....	140

Figure 81 Life-history Type I for Layout E, repetition 2: a) Circulation around the main vortex b) Maximum vorticity in the main vortex c) Equivalent diameter of the main vortex. d) Upwelling flowing from the main vortex.....	141
Figure 82 Life-history Type I for Layout F, repetition 1: a) Average cross sectional velocity at the mouth of the inlet. b) Longitudinal position of the center of the main vortex starting from the edge of the barrier island. c) Lateral position of the center of the main vortex starting from the edge of the barrier island.....	142
Figure 83 Life-history Type I for Layout F, repetition 1: a) Circulation around the main vortex b) Maximum vorticity in the main vortex c) Equivalent diameter of the main vortex. d) Upwelling flowing from the main vortex.....	143
Figure 84 Life-history Type I for Layout F, repetition 2: a) Average cross sectional velocity at the mouth of the inlet. b) Longitudinal position of the center of the main vortex starting from the edge of the barrier island. c) Lateral position of the center of the main vortex starting from the edge of the barrier island.....	144
Figure 85 Life-history Type I for Layout F, repetition 2: a) Circulation around the main vortex b) Maximum vorticity in the main vortex c) Equivalent diameter of the main vortex. d) Upwelling flowing from the main vortex.....	145
Figure 86 Life-history Type I for Layout G, repetition 1: a) Average cross sectional velocity at the mouth of the inlet. b) Longitudinal position of the center of the main vortex starting from the edge of the barrier island. c) Lateral position of the center of the main vortex starting from the edge of the barrier island.....	146

Figure 87 Life-history Type I for Layout G, repetition 1: a) Circulation around the main vortex b) Maximum vorticity in the main vortex c) Equivalent diameter of the main vortex. d) Upwelling flowing from the main vortex.....	147
Figure 88 Life-history Type I for Layout G, repetition 2: a) Average cross sectional velocity at the mouth of the inlet. b) Longitudinal position of the center of the main vortex starting from the edge of the barrier island. c) Lateral position of the center of the main vortex starting from the edge of the barrier island.....	148
Figure 89 Life-history Type I for Layout G, repetition 2: a) Circulation around the main vortex b) Maximum vorticity in the main vortex c) Equivalent diameter of the main vortex. d) Upwelling flowing from the main vortex.....	149
Figure 90 Life-history Type I for Layout H, 10 Degrees: a) Average cross sectional velocity at the mouth of the inlet. b) Longitudinal position of the center of the main vortex starting from the edge of the barrier island. c) Lateral position of the center of the main vortex starting from the edge of the barrier island.....	150
Figure 91 Life-history Type I for Layout H, 10 Degrees: a) Circulation around the main vortex b) Maximum vorticity in the main vortex c) Equivalent diameter of the main vortex. d) Upwelling flowing from the main vortex.....	151
Figure 92 Life-history Type I for Layout H, 20 Degrees: a) Average cross sectional velocity at the mouth of the inlet. b) Longitudinal position of the center of the main vortex starting from the edge of the barrier island. c) Lateral position of the center of the main vortex starting from the edge of the barrier island.....	152

Figure 93 Life-history Type I for Layout H, 20 Degrees: a) Circulation around the main vortex b) Maximum vorticity in the main vortex c) Equivalent diameter of the main vortex. d) Upwelling flowing from the main vortex..... 153

## LIST OF TABLES

	Page
Table 1 Summary of vortex life-history types described by Kashiwai (1984).....	5
Table 2 Typical ranges of $K_W$ for inlets on the Texas coast.....	6
Table 3 Summary of vortex life-history types of vortex described by Kashiwai (1984) and Wells (2003).....	14
Table 4 Flow parameters used in the different types of life-history.....	18
Table 5 Nominal and real values of $K_W$ , and maximum mean cross sectional velocity over a tidal cycle obtain from the PIV data.....	24
Table 6 Non-dimensional factors used for the calculation of the physical parameters of the vortex evolution.....	24
Table 7 Slopes of the fitted curves for the growth and decay of the circulation of the main vortex for the first cycle,with an associated error of $\pm 0.020$ .....	42
Table 8 Frequency of the formation of the secondary vortices in the peak of the first and second tidal cycles, with an associated error of $\pm 0.1$ [Hz]..	44
Table 9 Strouhal Number of the secondary vortices present in the first and second cycles of the tidal flow, with an associated error of $\pm 0.1$ [Hz]....	44
Table 10 Geometric parameters and the characteristic of the flow for different life-history types of vortex dipole formation.....	49
Table 11 Summary of the researchers done by Kashiwai (1984) and Van Heijst (2003) of the interpretation of the mixing number.....	62
Table 12 Geometric parameters used in the different layouts.....	69
Table 13 Flow parameters used in the different type of the life-history.....	69
Table 14 Nominal and real values of the mixing number $K_W$ , and maximum cross sectional average velocity over a tidal cycle for the first and the following cycles of each experiments.....	89

Table 15 Non-dimensional factors used for the calculation of the physical parameters of the vortex evolution.....	90
Table 16 Slopes of the fitted curves for the growth and decay of the circulation Of the main vortex for the first cycle, with an associated error of $\pm 0.020$ .....	155
Table 17 Frequency of the formation of the secondary vortices in the peak of the first and second tidal cycle, with an associated error of $\pm 0.1$ [Hz].....	157
Table 18 Strouhal Number of the secondary vortices present in the first and second cycles of the tidal flow, with an associated error of $\pm 0.1$ .....	157



## CHAPTER I

### INTRODUCTION

#### 1.1 Background

Mixing through tidal inlets is affected mainly by exchange processes due to currents driven by tides. The transport of constituents along the coastal waters has an effect on the environment by carrying mass and momentum in and out from estuaries and bays to the open coast. Understanding these processes is critical, because in the Gulf of Mexico, estuarine niches provide significant habitat for more than 98% of the commercial fisheries catch (Brown et al. 2000). Among the important processes influencing fisheries recruitment are transport of nutrients, sediments, pollutants, temperature, salinity, fish larvae, and many other important parameters that comes from rivers and the exchange of flows driven by tidal currents from the estuaries to the open coast, or vice versa, through tidal inlets. Transport in coastal waters is driven mostly by advection, and also dominated by the presence of two-dimensional coherent vortical structures (Socolofsky and Jirka 2004). These 2DCS are much broader than the water depth and the flows where these structures are formed are considered to be shallow, like most of the fluids in nature. Velocity shear, which drives the generation of 2DCS, is set up in the environment by riverine inflow, flow around islands, tidal wetlands, bridge piers, jetties, breakwaters, among other factors (Socolofsky 2006). Unfortunately, the formation of 2DCS is not predicted accurately by typical numerical models, such as the U.S Army Corps of Engineers depth-average model ADCIRC, and their effects on mixing cannot be extracted from existing correlations to the mean flow field or turbulence statistics. Furthermore, there is little known about the transport of mass by these

structures or the effect of a randomized field of such coherent structures on the transport of mass and momentum (Rummel et al. 2005).

This thesis is part of a broader project funded by the Texas Sea Grant, which is an environmental stewardship in charge of economic development and responsible use of the USA's coastal, ocean and Great Lakes resources. The title of this principal project is "Laboratory Studies of Exchange Processes through Tidal Inlets on the Texas Coast".

Figure 1 shows an example of transport by 2DCS in a coastal environment. The light regions in the figure are areas of high chlorophyll concentration, resulting from phytoplankton blooms. The boxed region shows the chlorophyll concentration contained in a dipole vortex formed by the transport of mass and momentum generated by a tidal jet in the inlet. Observing this figures is clear that to predict mixing and transport of nutrients in this region and to understand the phytoplankton dynamics would require an accurate prediction of the 2DCS dominating the advection in this coastal zone. In this case, the colors are representing phytoplankton, but it could be any other passive tracer such as nutrients or fish larvae.

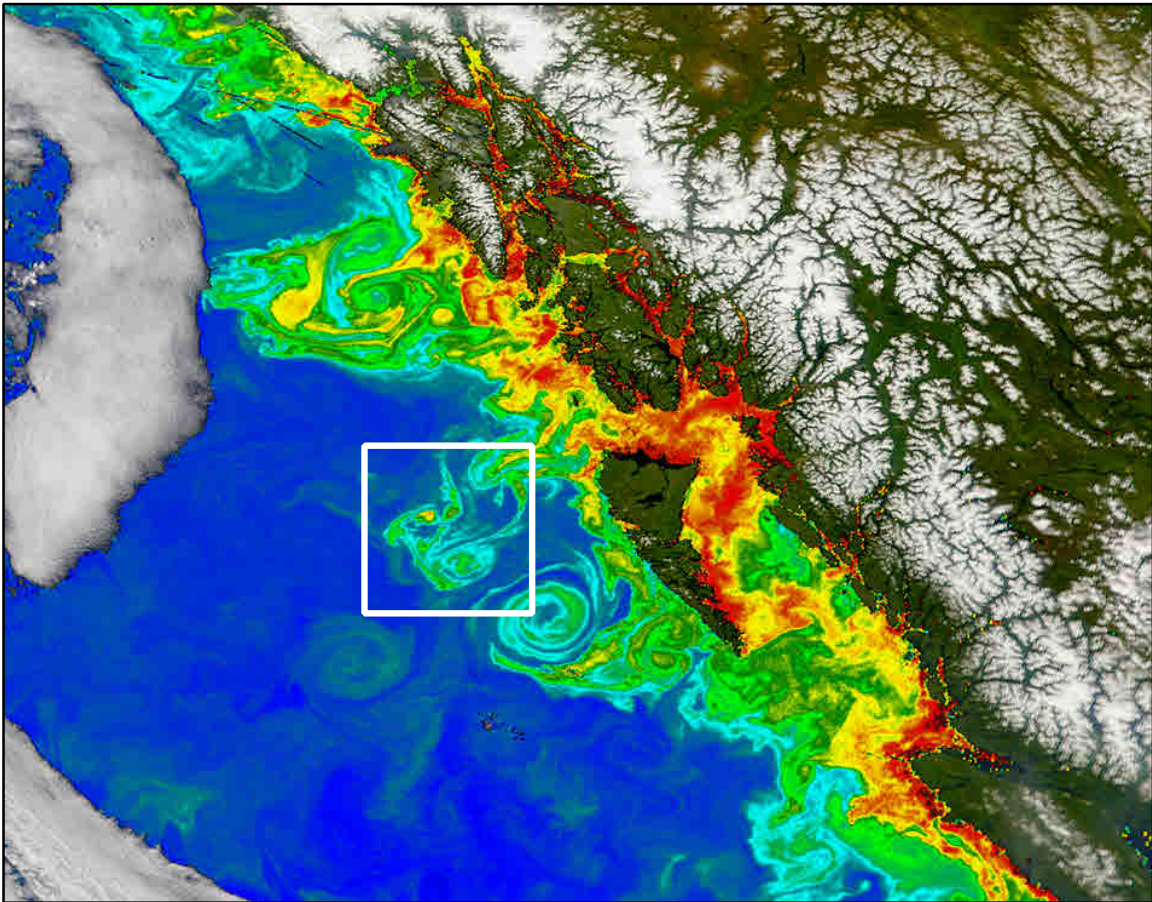


Figure 1 Chlorophyll concentration off the Queen Charlotte Islands, CANADA  
(Courtesy NASA SeaWiFS, 2004)

The dipole vortex appears in nature when a continuous or impulsive force is applied locally to some volume of fluid (Afanasyev 2006). In the case of a tidal inlet, the 2DCS is formed as a result of flow separation at the abrupt widening of a channel entrance followed by rolling up of the discontinuity surface around its free end (Afanasyev 2006). The parameters that define how these vortex dipoles behave are numerous, but there are specific factors that are more important than the others, and in the specific case of a tidal inlet vortex these parameters are: the width of the inlet  $W$ , the tidal period of the inlet  $T$ , and the maximum cross sectional mean velocity in the middle of the inlet over a tidal cycle  $U_{MAX}$

(Figure 2), assuming that the depth  $h$  of the inlet and the region where the vortex dipoles are forming is shallow. Depending on the combination of these 3 parameters ( $W$ ,  $T$ ,  $U_{MAX}$ ), Kashiwai (1984) identified 3 life-history cases for this tidal vortex:

- Type I: The tidal vortex flows out to the open coast and there amalgamates with successive vortex cores into a core of tidal residual circulation.
- Type II: The tidal vortex core flows out to the open coast not very far from the entrance of the channel (inlet) on the ebb, but returns back into the bay (estuary) on the subsequent flood.
- Type III: The tidal vortex core flows out to the open sea and never comes back.

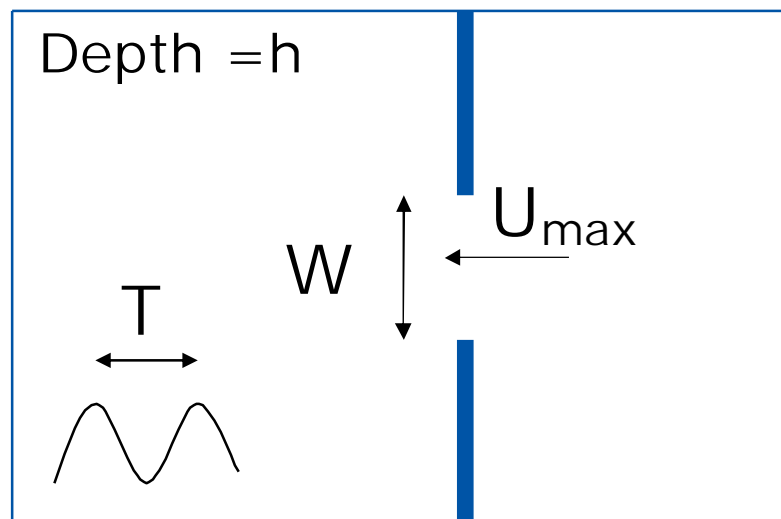


Figure 2 Parameters that define a tidal vortex dipole

In 1984, Kashiwai also identified in his studies conducted at the laboratory scale, that the 3 types of propagation of the tidal dipoles were defined by the dimensionless ratio  $W / U_{MAX}T$ . If this ratio was bigger or less than a critical value, the 2DCS would be Type II or III. If it was similar to that critical value, the dipole would have a life-history Type I.

Using a sinusoidal wave to simulate the tidal regime and perform the laboratory experiments, the critical value was found to be 0.13 (Wells and van Heijst 2003). This signifies that if the non-dimensional parameter  $W / U_{MAX}T$ , which is referred to as  $K_W$ , is less than 0.13 the vortex dipole will escape from the inlet, and if  $K_W$  is larger 0.13 the structure will get drawn back into the estuary. Although the critical value was set to be  $K_W \approx 0.13$ , there is a transition stage between the Type II and Type III life-history, therefore the dimensionless parameter has a critical value between  $K_W = 0.085$  and  $0.182$  (Kashiwai 1984). Table 1 presents a summary of the cases that were found in the experiments conducted by Kashiwai (1984) and Wells (2003). Also, in Table 1, the mixing efficiency is presented as a new category.

Table 1 Summary of vortex life-history types described by Kashiwai (1984)

$K_W$	LIFE-HISTORY TYPE	CASE	MIXING
$\approx 0.13$	Type I	Stationary	Intermediate
$\gg 0.13$	Type II	Entrain	Poor
$\ll 0.13$	Type III	Escape	Efficient

It is possible that all of these types of life history cases appear in nature. In the case of the Texas coast also happens the same. In the Table 2 we can observe that for different times of the year in the Texas coast are appearing the 3 kinds of mixing.

Table 2 Typical ranges of  $K_W$  for inlets on the Texas coast

<b>INLET</b>	<b>W</b>	<b>U<sub>MAX</sub></b>	<b>T</b>	<b>K<sub>w</sub></b>
	[m]	[m/s]	[hrs]	[]
<b>Packary Channel</b>	100	0.5 to 1.0	12.42	0.02 to 0.01
<b>Galveston Ship Channel</b>	3900	0.5 to 2.0	12.42	0.18 to 0.05
<b>Aransas Path</b>	1100	0.5 to 2.0	12.42	0.06 to 0.02

## 1.2 Problem Definition

In the past years, researchers have investigated the phenomenon of mixing through tidal inlets with a variety of different perspectives, focusing on different topics of this particular flow. However, all of the past work converges to the same point, which is to try to understand the behavioral character of the formation of the 2DCS, and the mechanisms that are behind it.

In the present investigation, laboratory experiments were done with different configuration of inlets, to study the geometric effects on tidal vortex; in some cases, the simulations were executed with 3 or 5 tidal cycles. The experimental

model was set up with different values of the mixing number  $K_W$ , in a range that goes from the entrain case to the case that the 2DCS escapes away from the inlet to the open coast, analyzing as well a  $K_W$  near the critical value of 0.13.

The experiments were conducted at the Institute of Hydromechanics of the University of Karlsruhe, in Karlsruhe, Germany, during the summer of 2006. The laboratory has a shallow water basin of 13 meters by 5.5 meters, with the capability to force flow in two directions along the longest side (Figure 3 a)). The tidal forcing in this case is simulated with a sinusoidal tidal current.

Simulations with colored dye were performed to visualize how the tidal vortex behaves with the different set up configurations (Figure 3 b)). Particle Image Velocimetry (PIV) experiments were carried out to develop movies of the velocity and vorticity field (Figure 3 c)). A qualitative analysis was performed to analyze the dye and PIV movies, and a quantitative study was done to calculate the circulation around the vortex to estimate the vortex evolution, using the PIV data.

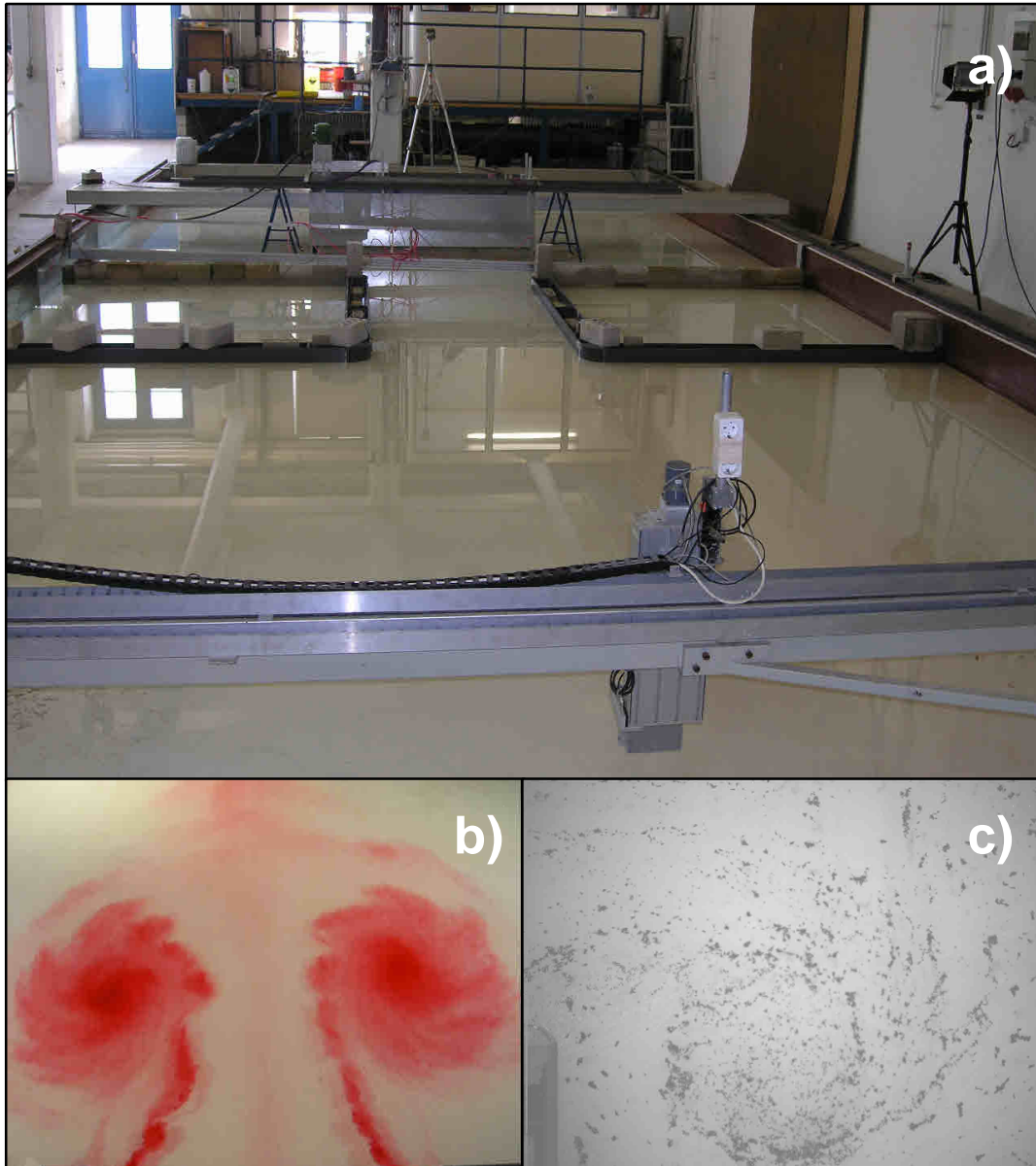


Figure 3 a) Laboratory where the experiments were taken. b) Dye studies visualization. c) PIV simulation.

Figure 3 provides the following: a) Peripheral view of the laboratory where the experiments were developed; b) Formation of the 2DCS on an idealized inlet by means of the visualization (dye) studies; c) Image of the seeding particles used for the PIV technique, where the core of an eddy can be observed.



### 1.3 Objectives

The main goal of the Sea Grant Project: “Laboratory Studies of Exchange Processes through Tidal Inlets on the Texas Coast” is to identify and understand the mechanism in tidal inlet flows responsible for the generation of the 2DCS and to incorporate their dynamics into two-dimensional coastal numerical models, such as ADCIRC.

The objectives of this Thesis, which will help to accomplish the general goal of the Sea Grant Project, are the following:

- Model typical flows through tidal inlets in the laboratory and measure their mixing and transport properties using advanced experimental techniques.
- Visualize the formation of large-scale eddies in laboratory tidal inlets using colored dye.
- Measure velocity fields by using the PIV surface method in laboratory tidal inlets.
- Analyze the PIV by means of calculating the velocity and vorticity field, identifying the coherent structures, and measuring the vortex evolution.
- Compare limited experimental results with numerical data (ADCIRC), to give suggestions and interpretation for modeling.

### 1.4 Outline

The thesis is divided into four Chapters and three Appendixes. Chapter I describes the background and purpose of the thesis, by doing a brief literature review and stating the problem that will be analyzed. In Chapter II, a Journal Article is presented that will be submitted to the *Journal of Geophysical Research* in the near future, presenting laboratory experiments of mixing processes on tidal inlets, velocity and vorticity fields from a PIV analysis,

evolution plots of the vortex strength, and a discussion of the topic. Chapter III contains a brief explanation of the numerical modeling done, and some applications to take into account when shallow water flows are modeled. Chapter IV encloses the conclusions of the research and a summary of the remaining issues for further research. The appendixes provide a complete description of the methodology used for the experimental and analytical processes, movies of the dye studies, and the simulations of the velocity and vorticity fields, which are contained in the Texas A&M University Library.

## CHAPTER II

### LABORATORY STUDIES OF EDDY STRUCTURES AND EXCHANGE PROCESSES THROUGH TIDAL INLETS

#### 2.1 Introduction

Transport in coastal waters is driven mostly by advection, and also dominated by the presence of two-dimensional coherent vortical structures (dipole vortex) (Socolofsky and Jirka 2004). The flows where these structures are formed are considered to be shallow, like most of the fluids in nature. In these kinds of flows the cross sectional extent of the flow is bigger than the flow depth (Jirka 2001). In shallow flows, the eddies are vulnerable to stretching, and this leads to the growth of the eddy by means of transport of turbulent kinetic energy (Negretti et al. 2005). Another characteristic of shallow flows is that they are intrinsically unstable to lateral viscosity shear, which results in the formation of a two-dimensional coherent structure (Socolofsky and Von Carner 2003; Socolofsky and Adams 2005).

The dipole vortex appears in nature when a continuous or impulsive force is applied locally to some volume of fluid (Afanasyev 2006). The velocity shear stress generated by this force is what drives the generation of the dipole vortex. In the case of tidal inlet flows or a flow past a sharp headland, the generated separation leads to the formation of eddies (Hench et al 2002; Wells and Van Heijst 2003). In the case of a tidal jet passing through an inlet, the relevant parameters that define how the tidal vortex dipole will behave are the width of the inlet  $W$ , the tidal period in the geographic zone where the inlet is located  $T$ , and the maximum cross sectional mean velocity at the mouth of the inlet over a tidal cycle  $U_{MAX}$ . The condition of shallowness of the flow  $h \ll W$  must be added to the mentioned parameters.

A universal definition of vortex has not been accepted yet, but it can be described as a tube shaped structure with persistent and coherent rotation along the axis of its center of mass, and is formed due to the velocity shear stress (Zhou et al. 1999). The formation and asymmetric nature of the tidal vortex are due to topographic effects, and the Coriolis force has no influence on the behavior of them (Brown et al. 2000; Hensch and Luettich 2003). Furthermore, the inclusion of the Coriolis Effect has a dynamical role in the interaction of the topography with the flow when the characteristic velocity scale of the tidal flow is sufficiently small (Davies et al. 1995). This is given when the Ekman number  $Ek$ , and the Rossby number  $Ro$  are both significantly less than one (Davies et al. 1990; Davies et al. 1995).

$$Ek = \frac{\nu}{2L^2\Omega \sin \varphi} \quad (1)$$

$$Ro = \frac{U}{2L\Omega \sin \varphi} \quad (2)$$

Where  $\nu$  is the viscosity of the fluid,  $L$  and  $U$  are respectively, characteristic length and velocity scales of the phenomenon,  $\Omega$  is the angular velocity of the rotation of the earth, and  $\varphi$  is the latitude. In the particular case of tidal jets the Coriolis Effect is not relevant on the behavior along the lifetime of a tidal vortex.

In the laboratory experiments conducted by Kashiwai (1984), he identified three types of propagation of the tidal vortex jets that were defined by the non-dimensional parameter  $W/U_{MAX}T$ . Depending on the value of the given parameter compared with a critical value, the tidal vortex would have a life-history Type I, II or III (Kashiwai 1984; Kashiwai 1985; Kashiwai 1985). Type I) the tidal vortex flows out to the open coast and there merges with successive vortexes cores into a core of tidal residual circulation, Type II) the tidal vortex

flows out to the open coast not very far from the mouth of the inlet on the ebb, and then returns back into the estuary on the following flood tide, and Type III) the tidal vortex flows out to the open sea to escape away from the inlet and never come back (Kashiwai 1984).

Using a sinusoidal wave to simulate a tidal regime and perform laboratory studies, Wells and Van Heijst (2003) establish that the critical value for the non-dimensional parameter  $K_w = W / U_{MAX} T$  is 0.13. This means that if  $K_w \ll 0.13$  (Type III), the vortex dipole will escape away from the inlet, and if  $K_w \gg 0.13$  (Type II), the structures will get drawn back into the estuary. Although the critical value was set to be  $K_w \approx 0.13$ , there is a transition stage between the Type II and III life-history of the vortex. Then the critical value range from  $K_w = 0.085$  to 0.182. Table 3 presents a summary of the experiments conducted by Kashiwai (1984) and Wells (2003). Also in the Table 3 the mixing efficiency is presented as another way of classification for the regime of the tidal vortex dipoles.

Table 3 Summary of vortex life-history types of vortex described by Kashiwai (1984) and Wells (2003).

<b><math>K_w</math></b>	<b>LIFE-HISTORY TYPE</b>	<b>CASE</b>	<b>MIXING</b>
$\approx 0.13$	Type I	Stationary	Intermediate
$\gg 0.13$	Type II	Entrain	Poor
$\ll 0.13$	Type III	Escape	Efficient

Over the past years, researchers have worked to understand the eddy structures using the dual plane Particle Image Velocimetry (PIV) technique (Lin et al. 2003; Shinneeb et al. 2004; Feng et al. 2005; Ganapathisubramani et al. 2005; Ganapathisubramani et al. 2006). Because of these previous studies the PIV method in two-dimensional plane is well known for the analysis of dipole vortex using tracer floating plastic particles to obtain the surface water velocity, which is an indicative of the depth average velocity in shallow water flows.

The PIV method is based on the position of the tracer particles contained in the images to determine the velocity of the flow. Subdividing the image into interrogation areas, a vector is found for each of these sub areas using cross-correlation techniques (Shinneeb et al. 2004). The PIV method is subject to errors that occur from the resolution of the images, the density of the seeding, large velocity gradients, or poor image quality, among others (Foucaut and Stanislas 2002). Then, is necessary to apply post processing techniques to find and fix these errors. Most of them can be easily found.

In the present research the PIV method was applied to investigate the flow field and vorticity field of the formation and life-history of the tidal vortex. The PIV data provide detailed time-evolution information of the tidal vortex that was formed in the experiments, so a quantitative analysis was developed. Also, animations were created with the PIV data. Using the animations and performing experiments with color dye tracers, a qualitative visualization study was carried out.

## 2.2 Experimental Design

The experiments were conducted in the laboratory of the Institute of Hydromechanics of the University of Karlsruhe, in Karlsruhe, Germany. The laboratory has a shallow water basin with dimensions of 13 x 5.5 meters, with the capability to force flow in two directions along the longest side. A sinusoidal tidal current forcing was imputed to simulate a flow going back and forth through an inlet.

A proper scaling analysis was developed to take the formation of the dipole vortex from the actual field scale to the laboratory scale, matching the behavior of both flows with physical relations. There are 4 main parameters that define the formation of the vortices at the mouth of an inlet: a) Tidal period  $T$ ; b) Width of the inlet  $W$ ; c) Depth of the flow  $h$ ; and d) Maximum cross sectional mean velocity over one tidal cycle at the mouth of the inlet  $U_{MAX}$ . Using the mentioned parameters, three dimensionless relations were used to match the nature flow with flow on the inlet, Geometric relation (3), Froude number (4), and Mixing number (5).

$$\frac{W}{h} \geq 10 \quad (3)$$

$$Fr = \frac{U_{MAX}}{\sqrt{gh}} \quad (4)$$

$$K_w = \frac{W}{U_{MAX} T} \quad (5)$$

Four different types of layouts were set up for the simulations: A) Idealized Inlet; B) Inlet with jetties with equal length of the width of the inlet; C) Inlet with jetties with length longer than the inlet; and D) Inlet with a thicker barrier island with length longer than the width of the inlet. In Figure 4 are shown the layouts of the simulations.



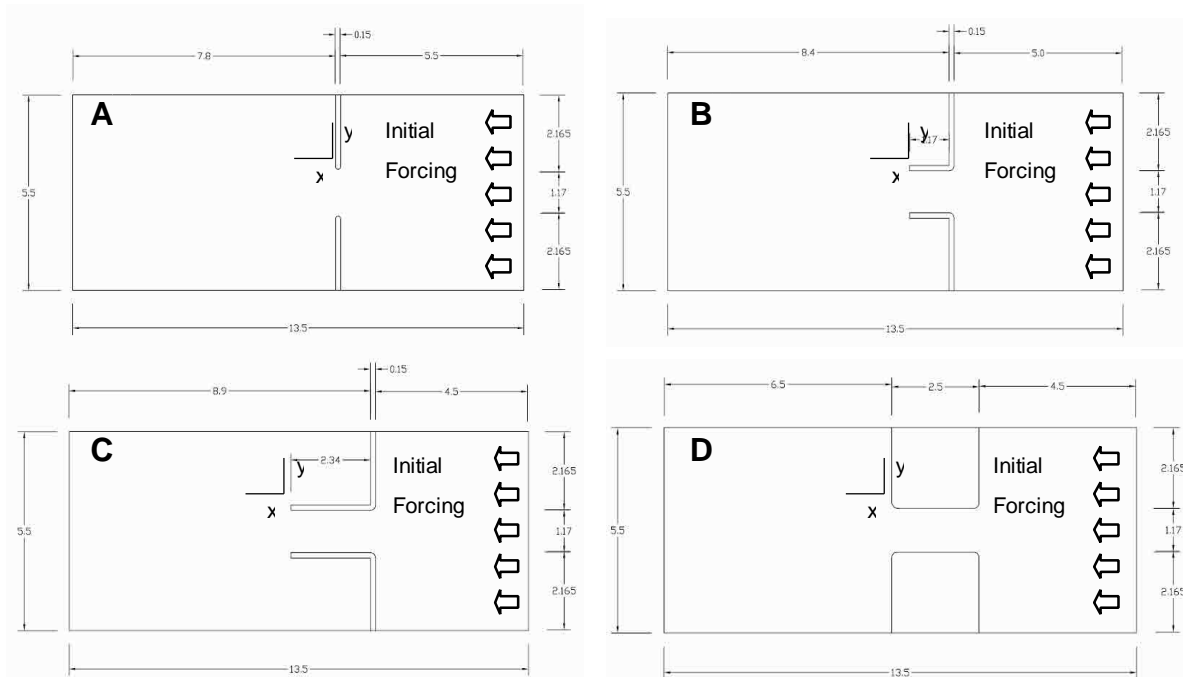


Figure 4 Layouts with different geometries: A) Idealized Inlet; B) Inlet with jetties with equal length of the width of the inlet; C) Inlet with jetties with length longer than the inlet; and D) Inlet with a thicker barrier island with length longer than the width of the inlet.

For Layout A three types of flows were developed, reproducing the Stationary Case ( $K_W \approx 0.13$ ), Entrain Case ( $K_W \gg 0.13$ ), and the Case that the structure Escape ( $K_W \ll 0.13$ ), with 4 tidal cycles each. The characteristics of the regimes were selected and calculated in order to achieve the restrictions that the physical relations needed to meet, and also taking in account the limitations of the shallow water basin. For layouts B through D only the stationary case was reproduced, with 1 tidal cycle. The flows simulated a sinusoidal tide. This sinusoidal tide was forced with a current, not with a head. This was possible because the shallow water basin had the capability to reverse the flow by operating 4 valves in order to overturn the direction of the flow. In the Table 4 the characteristics of the imputed flows are shown.

Table 4 Flow parameters used in the different types of life-history

LIFE-HISTORY TYPE	WIDTH	DEPTH	PERIOD	FLOW	VELOCITY	FROUDE
	W	H	T	$Q_{MAX}$	$U_{MAX}$	$F_r$
	[m]	[m]	[s]	[l/s]	[m/s]	[]
Type I	1.17	0.1	55	23	0.20	0.20
Type II	1.17	0.1	37	14	0.12	0.12
Type III	1.17	0.1	100	23	0.20	0.20

After reviewing the movies from the dye visualizations, two cameras were mounted in a crane 3 meters above of the inlet mouth in the shallow water basin, in a position to maximize the vortex time in focus. Each camera has a resolution of 1024x768 pixels. Using the PIV technique the cameras took 10 images per second of the surface of the velocity flow that was seeded with floating particles. It was assumed that the surface of the water was representative of the depth average flow velocity since the flow was shallow. The whole basin domain was seeded with the floating particles, and a seeding dispensator was positioned in the “estuary” side of the basin that was continuously spreading more particles once the tide started.

### 2.3 Data Analysis

The PIV system measure the fluid velocity of the surface water seeded with particles, by taking two digital images in quick succession. Then, the MPIV toolbox written in Matlab developed by Mori and Chang (2003), was applied to analyze the images taken in the shallow water basin, using the minimum quadratic difference method (MQD), with a process windows size of 32x32 pixels, and a overlap of 50%. To analyze the obtained sets of data a complete

Matlab code was developed to calculate the velocity field for the two cameras, the vorticity field, and to identify the region where the vortex were forming. The two cameras joined together have a resolution of 1884x768 pixels. Then, using the velocity field data, physical parameters of the vortexes were calculated along the time series of each experiment, to understand the vortex evolution.

Two main processes were applied to the velocity field data, filtering and interpolation. It was necessary to filter the data to remove the vectors that did not represent accurately the velocity field in the region that they were characterizing (Foucaut and Stanislas 2002). The removal of this noise was completed using the median filter in several sub-regions. The threshold to eliminate these bad neighboring vectors was 0.8. The velocity field data obtained after removing the bad vectors had missing information in some regions of the images. For good visualization and further limitations in the calculation, the data was interpolated using the Kriging method by applying a modified version of the DACE Kriging toolbox (Lophaven et al. 2002). This means that the Kriging interpolation was not applied to the whole domain of the velocity field all at once, it was divided into sub-windows. Each image was initially divided into 20 windows in the current direction, and 10 windows in the wall normal direction, if the method did not found more than 3 vectors to interpolate any sub-window the program automatically drop the resolution until it was able to perform the interpolation. There was a 50% of overlap between sub-windows. Using this methodology the data turn out to be smoother than the whole region interpolated straight away.

The vorticity field was obtained by calculating the circulation (6) at each data point of the velocity field, using for this the 8 surrounding vectors of a specific location. It was necessary to calculate the velocity gradients using the least

squared method (7) for every data point of the velocity field. The vorticity of a specific data point is given by Equation (8).

$$\Gamma = \int_A \omega dA \quad (6)$$

$$\left( \frac{df}{dx} \right)_i \approx \frac{2f_{i+2} + f_{i+1} - f_{i-1} - 2f_{i-2}}{10\Delta x} \quad (7)$$

$$\omega = \frac{\Gamma}{A} \quad (8)$$

Where  $\omega$  is the vorticity of a specific data point;  $\Gamma$  is the circulation; and  $A$  is the area in which the circulation is calculated.

To identify the vortex formation in the different experiments, the method proposed by Adrian and Christiansen (2000) that uses an equivalent 2-dimensional velocity gradient tensor (9) computed in the plane where the PIV data was acquired.

$$D^{2-D} = \begin{pmatrix} \frac{du}{dx} & \frac{du}{dy} \\ \frac{dv}{dx} & \frac{dv}{dy} \end{pmatrix} \quad (9)$$

Where  $(x,y)$  and  $(u,v)$  the direction and velocities stream-wise and normal to the direction of the initial flow. The matrix  $D^{2-D}$  will have two real eigenvalues  $\lambda_r$ , or a pair of complex conjugate eigenvalues  $\lambda_{ci}$ . If the matrix has two real eigenvalues the region is dominated by strain, and if it has a pair of complex conjugate eigenvalues, the region is dominated by vorticity. Taking the positive value of the complex values,  $\lambda_{ci} > 0$ , and plotting the iso-regions of these values, the location where the vortices are forming can be identified.

Figure 5 shows an example of the results of the data analysis. Figure 5 a) shows the velocity field. A strong tidal ebb current flowing from the inlet and the formation of a coherent structure can be appreciated. Figure 5 b) shows the vorticity field. A high vorticity area can be observed in the same area where the vortex was forming in a). Figure 5 c) shows the vortex formation identification. Besides the main vortex, three other smaller structures can be identified. These structures are secondary vortices formed due to the separation of the flow in the edge of the inlet. These structures cause a high vorticity region where they are formed, but they cannot be identified in the velocity field data.

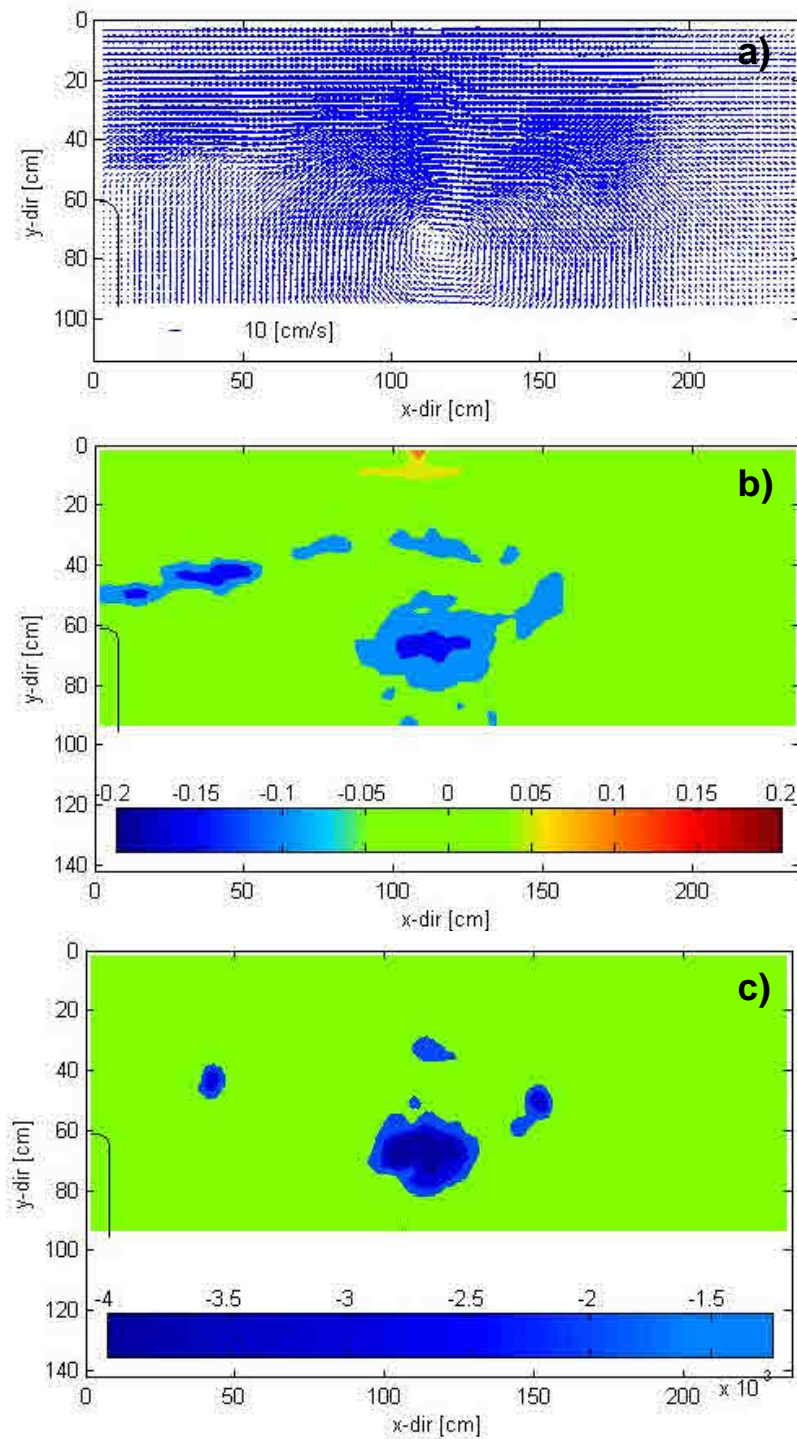


Figure 5 Example of a result for the data analysis of and image for the Life-history Type I of the idealized case: a) Velocity field; b) Vorticity field; c) Vortex formation identification.

To understand the behavior of the vortex evolution of each experiment, physical parameters were computed along the time series of the simulations. The calculated parameters were: a) mean cross sectional velocity at the mouth of the inlet,  $u$ ; b) longitudinal position of the center of the main vortex,  $X$ ; c) lateral position of the center of the main vortex,  $Y$ ; d) circulation around the main vortex,  $\Gamma$ ; e) maximum vorticity inside the main vortex,  $\omega_{MAX}$ ; f) equivalent diameter of the main vortex,  $D$ ; and g) total upwelling generated by the main vortex  $Q_{up}$ . The parameters  $X$ ,  $Y$ ,  $D$ , and  $\omega_{MAX}$  were used previously by Davies (1995)

The original (nominal) values of the mixing number  $K_W$ , were calculated using the maximum mean cross sectional velocity  $U_{MAX}$ , obtained from the formula (10).

$$Q = \frac{U_{MAX}}{A} \quad (10)$$

Where  $Q$  is the flow from the pump, and  $A$  is the cross sectional area filled with water in the inlet. For more accurate vortex evolution and physical parameters calculations the real value of  $K_W$  in each cycle and layout were calculated using the analyzed PIV data. The results are shown in the Table 5.

The  $K_W$  values were equal to the nominal value in the first cycle of the Layout A, and slightly different for the rest of the layouts. In the following cycles of the idealize inlet simulation, the values of  $K_W$  are similar to the nominal value, but the life-history Type II case the difference is significant. The Mixing number may be different in the following cycles because the mass of water has a momentum in the moment of inputting the next cycle.

Table 5 Nominal and real values of  $K_w$ , and maximum mean cross sectional velocity over a tidal cycle obtain from the PIV data.

LAYOUT	LIFE-HISTORY TYPE	MAXIMUM VELOCITY		K <sub>w</sub> NOMINAL VALUE	K <sub>w</sub> REAL VALUE	
		1 <sup>st</sup> Cycle	Following Cycles		1 <sup>st</sup> Cycle	Following Cycles
		[m/s]	[m/s]	[]	[]	[]
A	I	0.19	0.22	<b>0.11</b>	0.11	0.10
A	II	0.19	0.18	<b>0.06</b>	0.06	0.06
A	III	0.11	0.16	<b>0.26</b>	0.29	0.19
B	I	0.18	-	<b>0.11</b>	0.12	-
C	I	0.16	-	<b>0.11</b>	0.13	-
D	I	0.20	-	<b>0.11</b>	0.11	-

Using the real values of the mixing number and the maximum average velocity, the physical parameters were non-dimensionalized. The parameters are shown in the Table 6.

Table 6 Non-dimensional factors used for the calculation of the physical parameters of the vortex evolution

PHYSICAL PARAMETER	NON-DIMENSIONAL PARAMETER
$u$	$u^* = u / U$
$X$	$X^* = X / UT$
$Y$	$Y^* = Y / UT$
$\Gamma$	$\Gamma^* = \Gamma / UW$
$\omega_{MAX}$	$\omega_{MAX}^* = \omega_{MAX} W / U$
$D$	$D^* = D / UT$
$Q_{up}$	$Q_{up}^* = Q_{up} / (UWh / \pi)$



Where  $T$  is the tidal period of the cycle,  $W$  is the width of the inlet,  $h$  is the depth of the shallow water basin, and  $U$  is the maximum average velocity of the tidal cycle in the mouth of the inlet. The value of  $U$  varies depending on which cycle the calculation is made. As the physical parameters were calculated in time series evolution, it was necessary to non-dimensionalize the time scale too.

$$t^* = tU / W \quad (11)$$

In this case the value of  $U$  was taken as the average of the maximum average velocities of the tidal cycles in each experiment.

## 2.4 Results

In order to simulate different cases of the formation of tidal vortex, three experiments with an idealized tidal inlet (Layout A) were developed. Main control parameters as the maximum mean cross sectional velocity over a tidal cycle  $U_{MAX}$ , the tidal period  $T$ , and the width of the inlet  $W$ , were varied to obtain different Mixing number  $K_W$ , and consequently three kinds of vortex formation and evolution. These three kinds of vortex formation can be observed in Figure 6. The sample images were taken when the tidal current was flowing back to the estuary (flood stage), at the same non-dimensional tidal period time  $T = 0.6T^*$ .

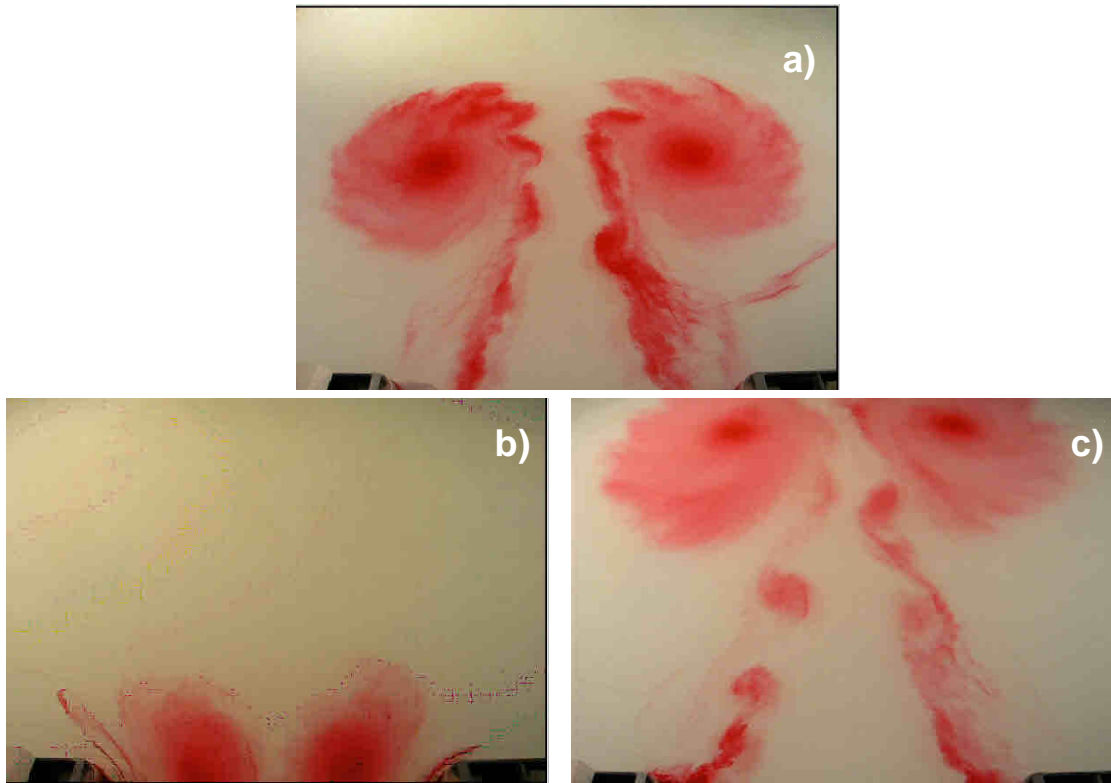


Figure 6 Dye experimental studies for the idealized inlet. a) Life-history Type I ( $K_W = 0.11$ ), the vortex dipole remains stationary in the vicinity of the mouth of the inlet. b) Life-history Type II ( $K_W = 0.26$ ), the vortex dipole gets drawn back to the estuary. c) Life-history Type III ( $K_W = 0.06$ ), the vortex dipole escapes away from the inlet to never come back.

We can observe in the Figure 6 that the vortex dipole behaves different in each three cases: a) the vortex remains stationary near the inlet as flood tide is going back towards the inlet; b) the vortex dipole gets drawn back to the estuary side of the inlet in the flood tide; c) the vortex dipole escapes away from the inlet to never come back.

The information of Figures 5, 7 and 8 were taken at the same time in the tidal cycle,  $T = 0.35T^*$ . Observing the three figures, it is clear that the vortex is forming in different spots. In the life-history Type I case, the main vortex is forming in the middle of the field of view of the cameras, in the Type II at the mouth of the inlet, and in the Type III far away from the inlet. The formation of the secondary vortices only appears in the life-history case I and III.

Figure 5 show the result for the data analysis of the Layout A for the life-history Type I ( $K_W = 0.11$ ). The velocity field, vorticity field, and the identification of the vortical structure are shown in the figure. This data corresponds to the images taken at  $t^* = 3.1$ , that matches the time of the tidal period  $T = 0.35T^*$ . The tidal period of this case is  $T = 55$  seconds. Observing the velocity field data the presence of a vortex can be clearly identify in the vicinity of the inlet. Also, at the mouth of the inlet, a strong inflow current is going towards the “open coast”, generated by the ebb tide. In c) the method proposed by Adrian and Christiansen (2000) identifies precisely where the main vortex is forming, matching what is observed in the velocity field data. Also, the method identifies three secondary vortices that appear due to the separation of the flow at the edge of the inlet. The vorticity field shows the locations where the main vortex and the secondary vortex are positioned. In addition, strong vorticity appear at the mouth of the inlet, generated by the effect of the shear stress of the velocity gradients as the flow is increasing in intensity towards the center of the inlet.

Figure 7 show the result for the data analysis of the Layout A for the life-history Type II ( $K_W = 0.26$ ). The velocity field, vorticity field, and the identification of the vortical structure are shown in the figure. This data corresponds to the images taken at  $t^* = 1.8$ , that matches the time of the tidal period  $T = 0.35T^*$ . The tidal period of this case is  $T = 37$  seconds. Observing the velocity field data, the presence of a vortex can be clearly identified almost at the mouth of the inlet.

The current generated by the ebb tide is not as strong as the current of the life-history Type I. In c) the method proposed by Adrian and Christiansen (2000) identifies precisely where the main vortex is forming. A strong consistency of the three images can be observed, since the vorticity field, the vortex identification, and the vertical structure in the velocity field data correlates precisely in the same spot at the mouth of the inlet.

Figure 8 show the result for the data analysis of the Layout A for the life-history Type III ( $K_W = 0.06$ ). The velocity field, vorticity field, and the identification of the vortical structure are shown in the figure. This data corresponds to the images taken at  $t^* = 5.7$ , that matches the time of the tidal period  $T = 0.35T^*$ . The tidal period of this case is  $T = 100$  seconds. Observing the velocity field data the presence of a vortex can be clearly identify far away from the inlet in the edge of the field of view of the cameras (right side). The jet generated by the inflow current going towards the “open coast” is larger in this case. In c) the method proposed by Adrian and Christiansen (2000) identifies precisely where the main vortex is forming, matching what is observed in the velocity field data. Also, the method identifies the secondary vortices that appear due to the separation of the flow at the edge of the inlet. The vorticity field shows the locations where the main vortex and the secondary vortex are positioned.

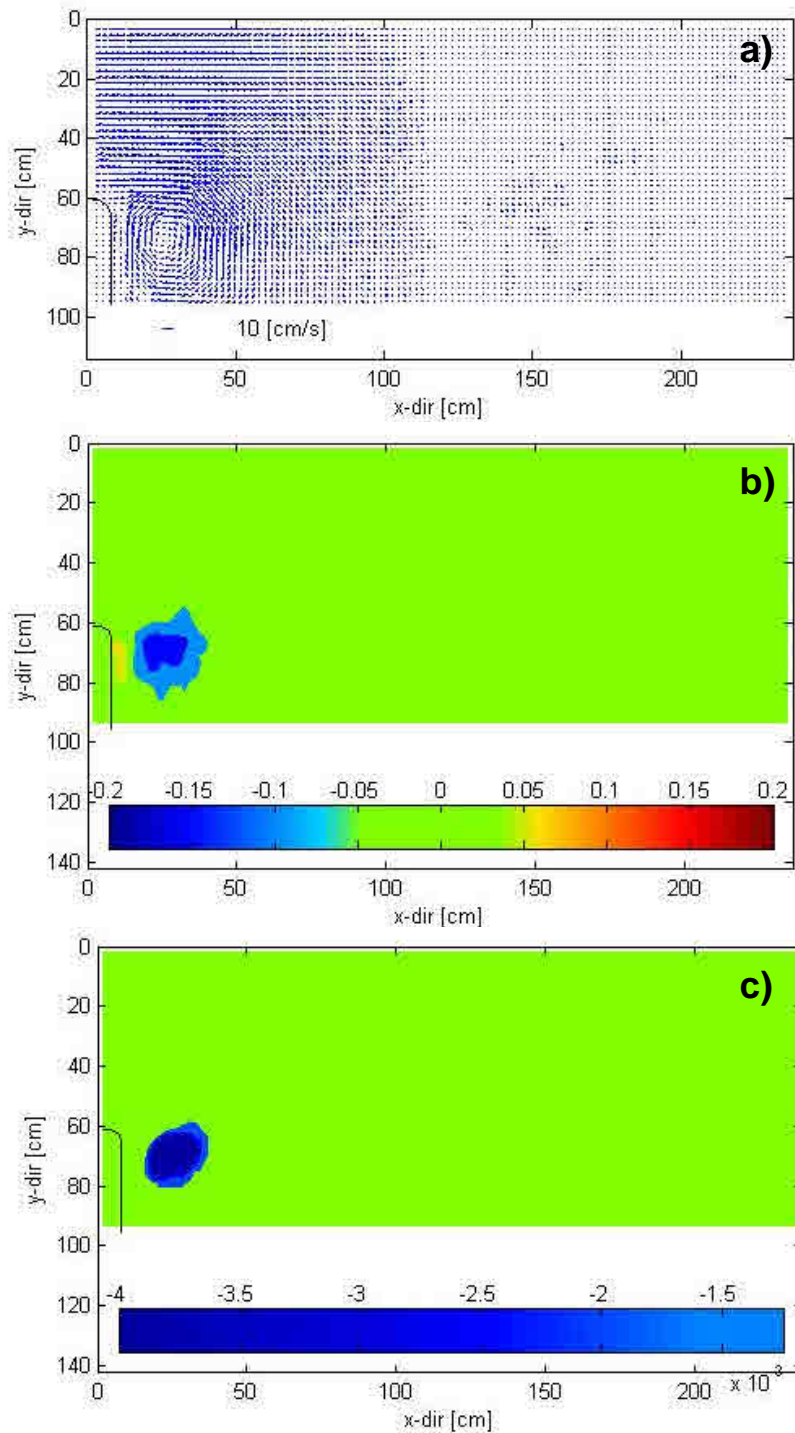


Figure 7 Example of a result for the data analysis of and image for the Life-history Type II of the idealized case: a) Velocity field; b) Vorticity field; c) Vortex formation identification.

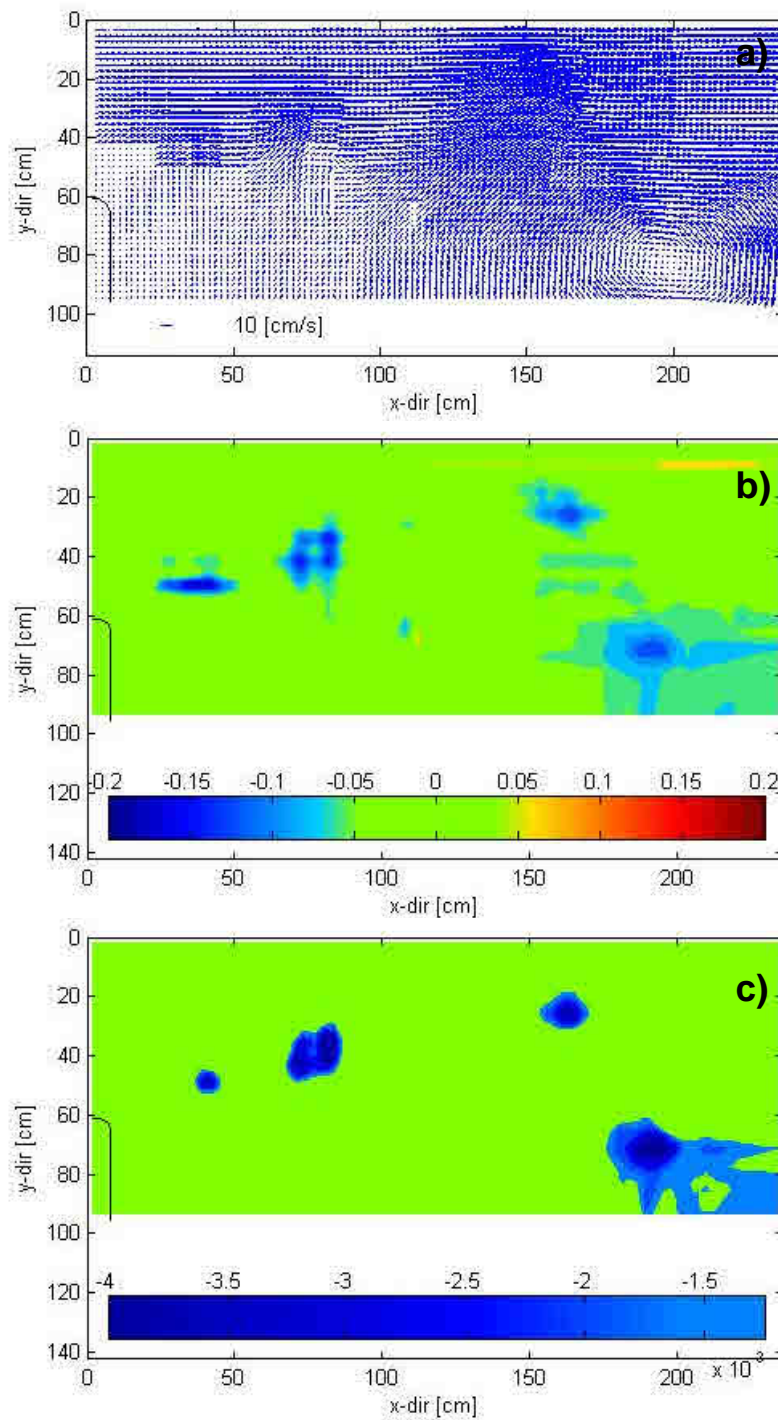


Figure 8 Example of a result for the data analysis of and image for the Life-history Type III of the idealized case: a) Velocity field; b) Vorticity field; c) Vortex formation identification.

Figure 9 shows the result of the vortex evolution analysis for the life-history Type I of the idealize inlet. The parameters were calculated only for the vortex formed by the ebb tide. All the physical parameters described previously are shown. The cross sectional average velocity  $U^*$ , is not symmetric over the tidal cycles, and is not symmetric either on the ebb and flood tides. It reaches a maximum value of 1.0 and a minimum of -0.6. The center of the main vortex flows away from the inlet. Towards the end of each cycle, the slope of the curve tends to go horizontal. The maximum value that gets to is 0.24 in the first cycle, and 0.20 in the following cycles. In the  $Y^*$  axis, the vortex flows to the right hand side of the inlet (in the direction of the ebb of the tide) in the first cycle, and then returns to the initial position. This repeats for the second cycle, but in the third and fourth cycles the center of the main vortex never flows to the right side of the inlet and never reaches back the original starting  $Y^*$  value. In the first cycle the circulation  $\Gamma^*$  increases to a maximum (-0.55) and then gradually decreases until it reaches a point that decreases faster and goes to zero. All the tidal cycles behave similarly for the circulation around the main vortex. For all cycles the maximum vorticity  $\omega_{MAX}^*$  rapidly reaches a maximum value and then decreases for a short period to later standstill at  $-4 \times 10^{-4}$ . The equivalent diameter of the main vortex the first cycle increases to reach 0.025 and then remains stationary at 0.02. In the stationary stage a sinusoidal behavior can be detected, as well in the following cycles

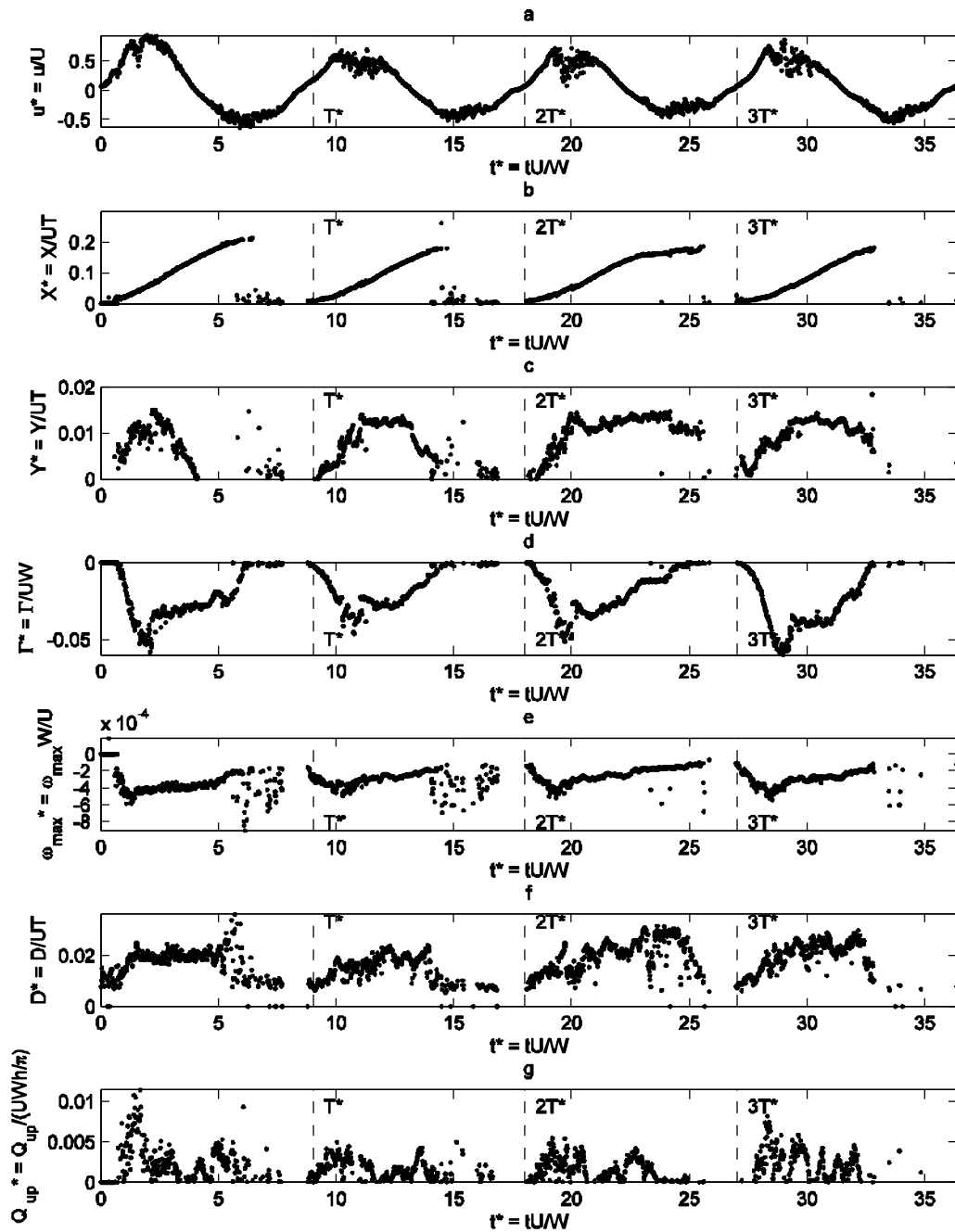


Figure 9 Life-history Type I for Layout A: a) Cross sectional average velocity at the mouth of the inlet. b) Longitudinal position of the center of the main vortex starting from the edge of the barrier island. c) Lateral position of the center of the main vortex starting from the edge of the barrier island. d) Circulation around the main vortex. e) Maximum vorticity in the main vortex. f) Equivalent diameter of the main vortex. g) Upwelling flowing from the main vortex.



Figure 10 shows the result of the vortex evolution analysis for the life-history Type II of the idealize inlet. The parameters were calculated only for the vortex formed by the ebb tide. All the physical parameters described previously are shown. The cross sectional average velocity  $U^*$ , is not symmetric over the tidal cycles, and is not symmetric either on the ebb and flood tides. It reaches a maximum value of 0.7 and a minimum of -0.6. The center of the main vortex flows away from the inlet reaching a value of 0.1 and then get drawn back to the estuary in the first cycle. In the following cycles the vortex moves away from the inlet getting a value of 0.25 for the second and third cycle, and 0.15 for the fourth cycle. In the  $Y^*$  axis, the vortex flows to the right hand side of the inlet (in the direction of the ebb of the tide) in the first cycle, then returns and pass the initial position and goes towards the center of the basin. This repeats for the following cycles, but with the values from the boundaries smaller than the first cycle. In the first cycle the circulation  $\Gamma^*$  increases to a maximum (-0.30) and then gradually decreases until it reaches a point that decreases faster and goes to zero. All the tidal cycles behave similarly for the circulation around the main vortex, but the maximum value for the following cycles is greater (0.50). For all the tidal cycles the maximum vorticity  $\omega_{MAX}^*$  increase to a maximum of  $-8 \times 10^{-4}$  and then gradually decrease. The equivalent diameter of the main vortex remains stationary but varying between 0.02 and 0.04, for all the cycles. A sinusoidal variation can be detected.

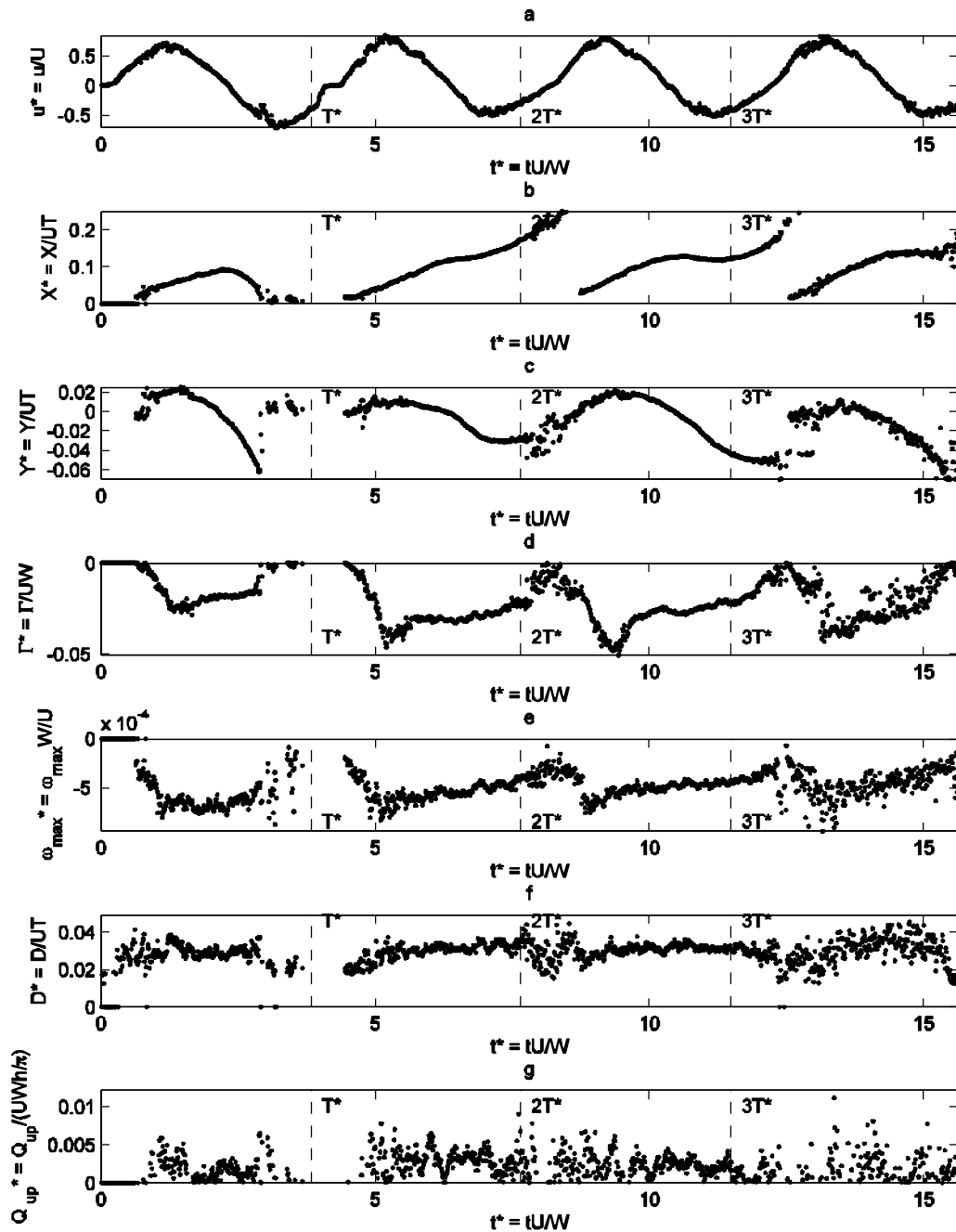


Figure 10 Life-history Type II for Layout A: a) Cross sectional average velocity at the mouth of the inlet. b) Longitudinal position of the center of the main vortex starting from the edge of the barrier island. c) Lateral position of the center of the main vortex starting from the edge of the barrier island. d) Circulation around the main vortex. e) Maximum vorticity in the main vortex. f) Equivalent diameter of the main vortex. g) Upwelling flowing from the main vortex.

Figure 11 shows the result of the vortex evolution analysis for the life-history Type III of the idealize inlet. The parameters were calculated only for the vortex formed by the ebb tide. All the physical parameters described previously are shown. The cross sectional average velocity  $U^*$ , is not symmetric over the tidal cycles, and is not symmetric either on the ebb and flood tides. It reaches a maximum value of 1.0 and a minimum of -0.6. The center of the main vortex flows away from the inlet. The maximum value is 0.13 in the first cycle, similarly in the following cycles. In the  $Y^*$  axis, the vortex flows to the right hand side of the inlet (in the direction of the ebb of the tide) in the first cycle, then returns and pass the initial position and goes towards the center of the basin. In the first cycle the circulation  $\Gamma^*$  increases to a maximum (-0.45) and then gradually decreases until it reaches a point that reduces faster and goes to zero. The same phenomenon repeats in the third tidal cycle. The circulation of the second cycle once it reaches a maximum (-0.20) remains almost stationary.

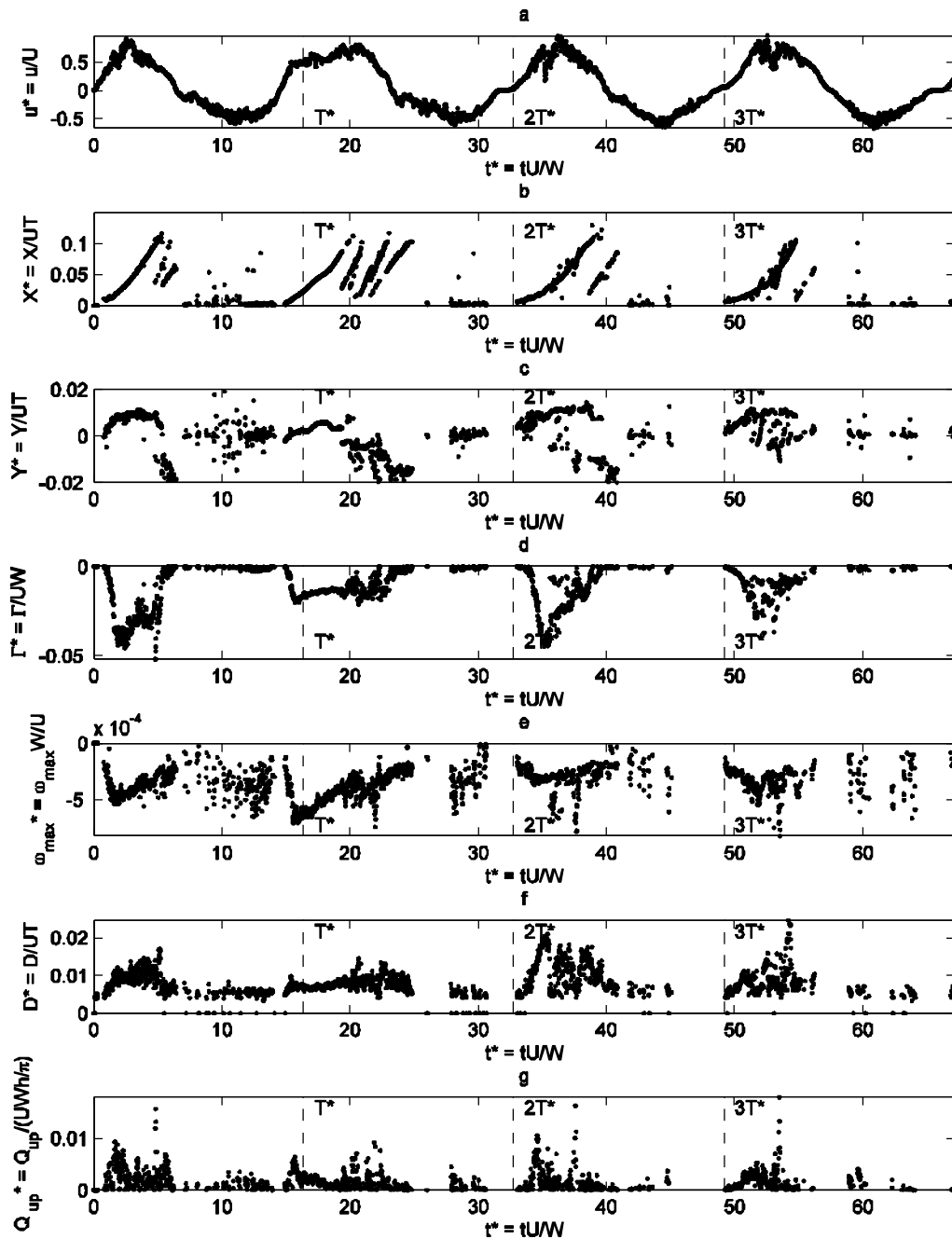


Figure 11 Life-history Type I for Layout A: a) Cross sectional average velocity at the mouth of the inlet. b) Longitudinal position of the center of the main vortex starting from the edge of the barrier island. c) Lateral position of the center of the main vortex starting from the edge of the barrier island. d) Circulation around the main vortex. e) Maximum vorticity in the main vortex. f) Equivalent diameter of the main vortex. g) Upwelling flowing from the main vortex.

Figure 12 has a comparison of the physical parameters of the first tidal cycle between the layouts A, B, C and D, that corresponds respectively to numbers 1, 2, 3 and 4 in the figure. The cross sectional average velocity  $U^*$ , has a more define sinusoidal behavior in Layout A than for the rest of the layouts. The center of the main vortex flows away from the inlet up to a value of 0.2 in the idealize case. The vortex flows away from the inlet reaching a value of 0.08 for Layout B, 0.07 for Layout C, and 0.05 for Layout D, to then travel back to the inlet about half way. In the  $Y^*$  axis, the vortex flows to the right hand side of the inlet (in the direction of the ebb of the tide) in the first cycle, then returns and pass the initial position and goes towards the center of the basin. We can observe that Layouts B, C and D have similar values among them, and larger values compared with Layout A. The circulation  $\Gamma^*$  increases to a maximum (-0.55) and then gradually decreases until it reaches a point that decreases faster and goes to zero for Layout A. For the other Layouts it behaves similarly, but with smaller maximum values: -0.20 for Layout B, -0.30 for Layout C, and -0.35 for Layout D. For all the layouts the maximum vorticity  $\omega_{MAX}^*$  increase to a maximum of and then gradually decrease with different intensities. The maximum value is:  $-8 \times 10^{-4}$  for A,  $-6 \times 10^{-4}$  for B,  $-5 \times 10^{-4}$  for C, and  $-4 \times 10^{-4}$  for D. The equivalent diameter of the main vortex increases to reach 0.025 and then remains stationary at 0.02 in Layout A. In the stationary stage a sinusoidal behavior can be detected. The rest of the layouts perform likewise Layout A, but achieving different values for the maximum and the stationary stage.

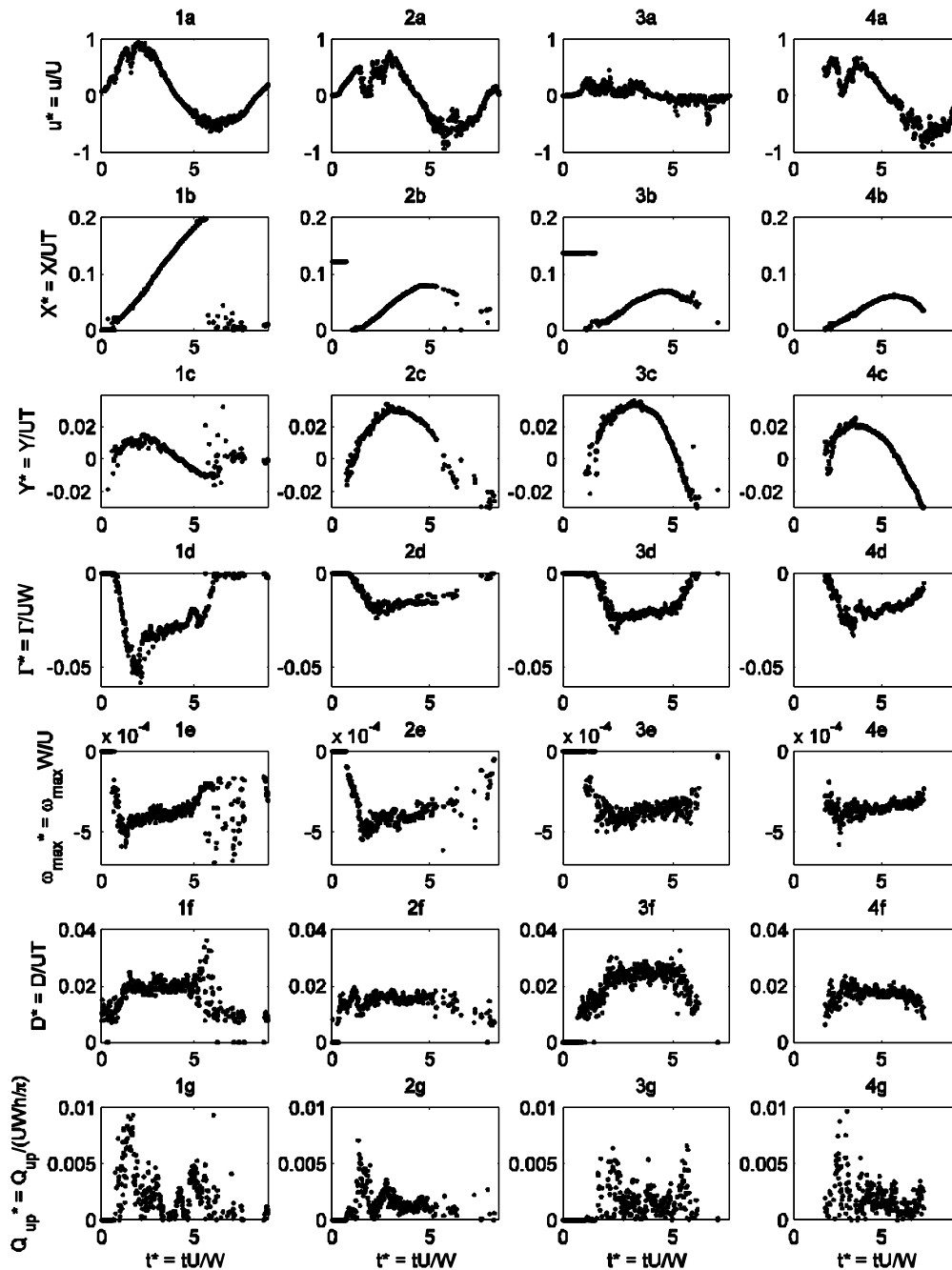


Figure 12 1) Layout A. 2) Layout B. 3) Layout C. 4) Layout D. a) Cross sectional average velocity at the mouth of the inlet. b) Longitudinal position of the center of the main vortex starting from the edge of the barrier island. c) Lateral position of the center of the main vortex starting from the edge of the barrier island. d) Circulation around the main vortex. e) Maximum vorticity in the main vortex. f) Equivalent diameter of the main vortex. g) Upwelling flowing from the main vortex.

## 2.5 Discussion

Observing the Figures 5 through 8 (PIV results and dye studies snapshots), it is clear that the Mixing number  $K_W$  predicts accurately how is going to be the behavior of the vortexes for the first cycle of idealized inlets. For the same tidal period  $T = 0.35T^*$ , the position of the vortex varies as the input Mixing number changes. For the life-history Type I, the eddy remains stationary near to the mouth of the inlet; for Type II case, the vortex stays at the mouth of the inlet, and in the flood this gets drawn back to the estuary; finally for the life-history Type III, the vortex goes away from the inlet to never come back.

This is corroborated by the information of the longitudinal position of the main vortex in Figures 9 through 11 that shows the exact phenomenon described above. For the life-history Type I, at the end of each tidal cycle the curve of the  $X^*$  position tends to go horizontal, which can be viewed that the vortex reaches a stationary position. Similarly, for life-history Type II the curve goes to a maximum and the returns to zero, which means that the structure gets drawn back to the estuary; and for the Type III case the curve just goes straight until the vortex gets out of the field of view.

For the life-history Type II, in which the structure is suppose to get drawn back the estuary, we can observe that this happens for the first cycle, but does not for the following ones. Table 5 shows that for the first cycle  $K_W = 0.29$ , and for the following ones  $K_W = 0.19$ . The value of the mixing number for the subsequent cycles is closer to the critical value  $K_W = 0.13$ , so the vortex of the following cycles does not get entrains to the estuary. For the life-history Types I and III, the values for the Mixing number shown in the Table 5, are similar for the first and following cycles. The behavior of the vortex on the second cycle is different than the conduct of the structure for the first tidal cycle. This is because, despite that the  $K_W$  values are similar, the presence of the vortex of the preceding cycle

acts as a blocking structure and affects the behavior of the new structure coming out from the mouth of the inlet.

The asymmetry on the cross sectional average velocity of the tidal cycles explains the different values for  $K_W$  in the same experiment. This asymmetry may be caused because the inlets were not in the middle of the basin. Other reason may be that in the first tidal cycle the water is standing still, and for the following cycles the mass of water has a momentum in the moment of inputting the next cycle.

Layout A behaves different than the other layouts. For the longitudinal position  $X^*$  the vortex in Layout A flows away and remain stationary at the end of the curve. In the other layouts, the vortex flows away and then goes back towards the inlet around half of the travel distance. For the lateral position  $Y^*$  in the layouts B, C and D the vortex flows towards the wall of the basin in the beginning of the cycle, and towards the middle of the basin at the end of the cycle in a more dramatic way than for the Layout A. This two phenomenon may be explained because of the stronger tidal jet generated by the channel constructed by the jetties or barrier island. When the flow is driven by the flood tide, this stronger jet drives the vortex towards the inlet in the  $X^*$  position, and towards the middle in the  $Y^*$  position.

Figure 13 shows a comparison between the circulation of the first tidal cycle of the life-history Type I, II and III, for Layout A, and life-history Type I, for Layout B, C and D. The plots have fitted curves to the growth of the value of circulation, and a curve fitted to the decay of the strength of the circulation. A third curve could be adjust at the end of the cycle, when the circulation goes down to zero, but it has no physical meaning because at that point the main vortex start leaving the image, and that is the reason why the decaying rate is faster.



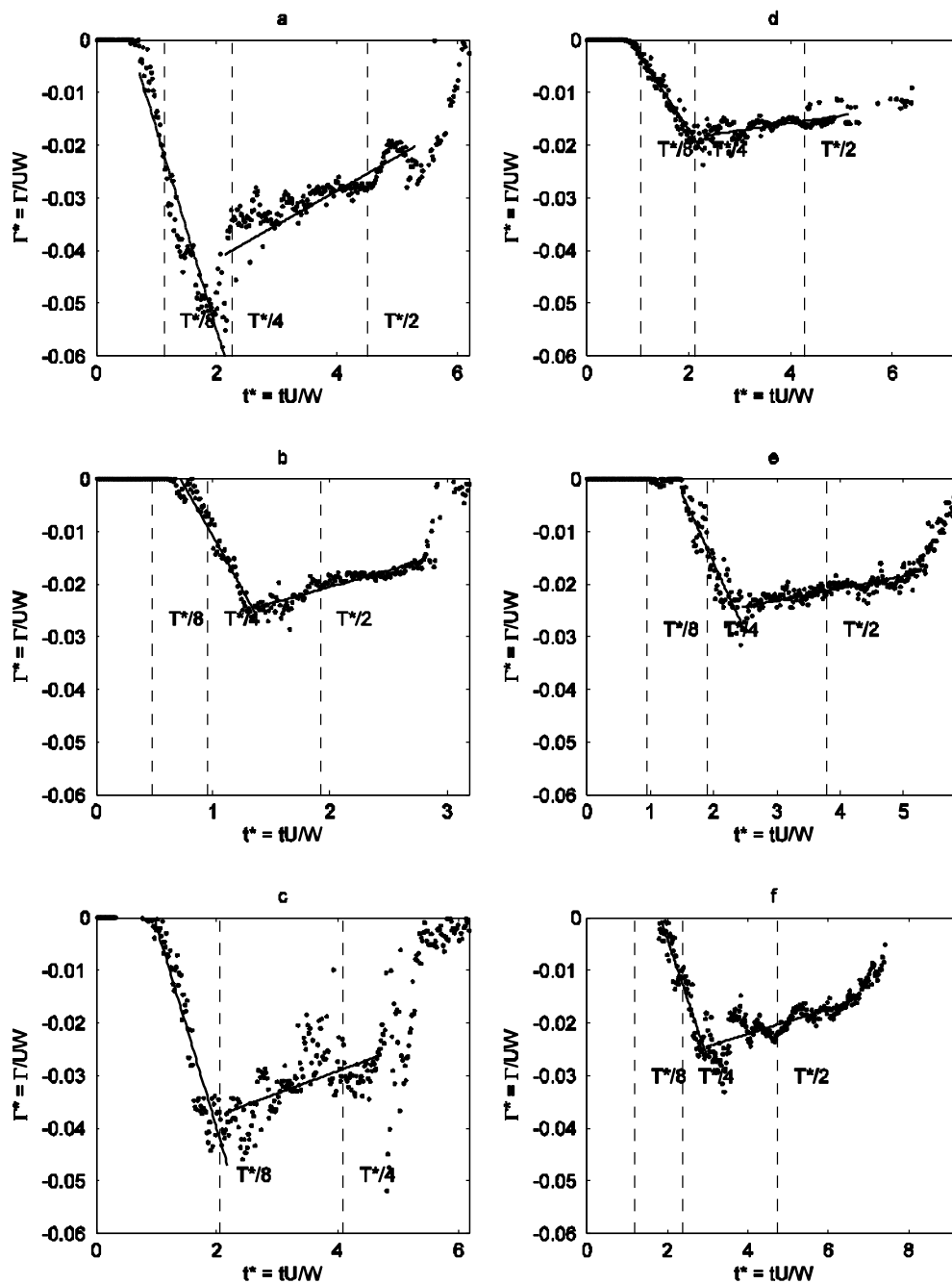


Figure 13 a) Circulation around the main vortex for life-history Type I, Layout A. b) Circulation around the main vortex for life-history Type II, Layout A. c) Circulation around the main vortex for life-history Type III, Layout A. d) Circulation around the main vortex for life-history Type I, Layout B. e) Circulation around the main vortex for life-history Type I, Layout C. a) Circulation around the main vortex for life-history Type I, Layout D.

Observing the lines fitted to the data, we can appreciate that the slopes of these are similar comparing the six experiments. The slopes were calculated with a linear regression between the data contemplated in the growing or decaying sections. The numerical values of these slopes are shown in the Table 7. A propagation of error analysis was done for this calculation of the slope, to take in account the errors of measurement that can be made. The time between to images has an associated error of  $\pm 0.001$  [s]; and the associated error for the root mean square error (rmse) the circulation is  $\pm 0.0001$ . Then, the estimated error for the slope calculation is  $\pm 0.02$ .

Table 7 Slopes of the fitted curves for the growth and decay of the circulation of the main vortex for the first cycle, with an associated error of  $\pm 0.020$ .

LAYOUT	LIFE-HISTORY TYPE	K <sub>w</sub> REAL VALUE	CIRCULATION SLOPE	
			Growth	Decay
		□	□	□
A	I	0.11	-0.038	0.007
	II	0.06	-0.039	0.005
	III	0.29	-0.040	0.007
B	I	0.12	-0.015	0.012
C	I	0.13	-0.026	0.003
D	I	0.11	-0.023	0.003

For the simulations done for Layout A the slopes have almost the same value. For the rest of the layouts the growth and decay rates are similar, but not equal. The values suggest that the circulation is slightly decreasing its intensity once the vortex reaches the maximum value, so the vortex will decay also in area and strength.

The secondary vortices formed in the stationary and escape case, are due to the separation of the flow at the edge of the inlet or barrier island. A secondary vortices analysis was done by observing the movies of the dye studies. The

Strouhal number associate the frequency that the vortices are forming at the peak of the tidal cycle, the radius of curvature of the edge of the barrier island, and the maximum cross sectional average velocity.

$$S_t = \frac{R_c f}{U_{MAX}} \quad (12)$$

Where  $R_c$  is the radius of curvature of the barrier island,  $f$  is the frequency of the formation of the vortices, and  $U_{MAX}$  is the maximum velocity.

A propagation of error analysis was done for this calculation, to take in account the errors of measurement that can be made. The frequency of the vortices has an associated error of  $\pm 0.1$  [Hz]; the radius of curvature of the barrier island has an associated error of  $\pm 0.05$  [cm]; and the associated error for the maximum velocity is  $\pm 0.01$  [m/s]. Then, the estimated error for the Strouhal Number is  $\pm 0.1$ .

Table 8 shows the frequency of the formation of the vortices for layouts A through D, and Table 9 shows the Strouhal Number for layouts A through D, only for Life-History types I and II. The type III was not calculated because it was difficult to observe the formation of the secondary vortices.

Table 8 Frequency of the formation of the secondary vortices in the peak of the first and second tidal cycles, with an associated error of  $\pm 0.1$  [Hz].

EXPERIMENT	$K_w = 0.11$		$K_w = 0.06$	
	Frequency		Frequency	
	1st Cycle	2nd Cycle	1st Cycle	2nd Cycle
	[1/s]	[1/s]	[1/s]	[1/s]
Layout A	0.9	0.7	0.6	0.5
Layout B	1.0	0.6	-	-
Layout C	0.7	0.7	-	-
Layout D	1.1	1.1	-	-

Table 9 Strouhal Number of the secondary vortices present in the first and second cycles of the tidal flow, with an associated error of  $\pm 0.1$ .

EXPERIMENT	RADIUS OF CURVATURE	$K_w = 0.11$		$K_w = 0.06$	
		Strouhal Number		Strouhal Number	
		1st Cycle	2nd Cycle	1st Cycle	2nd Cycle
	[cm]	[]	[]	[]	[]
Layout A	0.075	0.4	0.2	0.2	0.2
Layout B	0.075	0.4	0.2	-	-
Layout C	0.075	0.3	0.2	-	-
Layout D	0.15	0.8	0.6	-	-

A sinusoidal behavior can be identified once the circulation reaches the maximum value and during the slightly decay of this in the Figure 13. Also, it can be observed that the detached secondary structures from the edge of the barrier island, flows away from the inlet to finally join the main vortex. The frequency in which they join the main vortex is similar to the frequency of formation of the structures. In the circulation plots in Figure 13 shows that once the maximum value is reached, then the intensity of the circulation starts decaying with a sinusoidal behavior. This sinusoidal performance is due to the presence of these secondary vortices that are joining the main vortex, and inputting extra vorticity increasing the circulation once they amalgamate the main structure.

Table 9 shows that the Strouhal number for the Layout D is greater than the values for the others layouts. This is corroborated in the Figure 13 f) were the circulation of this layout is shown for the first cycle, and we can appreciate that the sinusoidal tendency with an evidently larger period.

Finally, we can say that the maximum vorticity behavior is similar to the circulation but with narrower limits. The maximum vorticity grow and then slightly decays. For the equivalent diameter we can observe that once the vortex reaches the maximum this remains with a constant width.

Regarding the upwelling flowing from the main vortex we can say that takes part on the process of dissipation of the vortex that is probably dominated by the bottom friction. The upwelling is derivated from the continuity equation (13).

$$\frac{\partial u}{\partial x} + \frac{\partial v}{\partial y} + \frac{\partial w}{\partial z} = 0 \quad (13)$$

Then assuming that  $(\partial u/\partial x + \partial v/\partial y)$  is constant over the vertical, the divergence is calculated as following:

$$Q_{up} = -\left(\frac{\partial u}{\partial x} + \frac{\partial v}{\partial y}\right)h\Delta x\Delta y \quad (14)$$

Where  $Q_{up}$  is the upwelling flow,  $h$  is the depth of the flow,  $\Delta x$  and  $\Delta y$  defines the area where the upwelling is calculated, and  $(x,y)$  and  $(u,v)$  the direction and velocities stream-wise and normal to the direction of the initial flow.

## 2.6 Summary and Conclusions

Experiments developed in the shallow water basin of the Institute of Hydromechanics of the University of Karlsruhe, Germany have been presented and analyzed. Typical flows through tidal inlets were modeled varying the tidal period  $T$ , and the average cross sectional maximum velocity  $U_{MAX}$ . The mixing and transport properties, and physical parameters were calculated using visualization and Particle Image Velocimetry (PIV) techniques.

For idealized inlets, the behavior of the three types of life-history of the vortex dipoles simulated (stationary, entrains and escape dipoles) were predicted accurately by the mixing number  $K_W$ , for the first tidal cycle. For the subsequent tidal cycles the structures behave differently than predicted by  $K_W$ . This different behavior may be caused because in the first tidal cycle the water is standing still, and for the following cycles the mass of water has a momentum in the moment of inputting the next cycle. The most critical case is when the mixing number is inputted as  $K_W = 0.26$ , because in the second and following cycles the vortex dipole does not get entrained.

Regarding the formation of the vortex dipole, for characteristics non-dimensional times  $t^* = tU/W$  less than 2.2 the structure is attached to the inlet and forms rapidly for all the cases simulated. For later times the dipole advects

downstream and start slowly decaying in intensity. If the tide reverses before this characteristic time is reached, then the eddy will get drawn back to the “estuary” side of the inlet.

The circulation plots shows that once the vortex reaches the maximum value, the magnitude of the circulation starts decaying (dissipating) with a sinusoidal behavior. This sinusoidal conduct is due to the presence of the secondary vortices that join the main vortex with a certain frequency that matches the sinusoidal peaks. The formation of the secondary vortices can be observed in the Figure 6 a) and c).

The decaying of the circulation after the vortex is detached from the inlet may be caused by the bottom friction and the upwelling of low-momentum bottom water. The decaying rate is similar for most the idealized inlet simulations and the life-history Type I for the complex inlets (jetties and barrier island).

Is interesting to observe that longitudinal position  $X^*$  the vortex in Layout A flows away and remain stationary at the end of the curve. In the other layouts, the vortex flows away and then goes back towards the inlet around half of the travel distance. This tells us that the vortex, eventhough remains stationary, it is influenced by the flood tide that is pulling it slightly towards the inlet.

## CHAPTER III

### NUMERICAL MODELING

A series of numerical simulations using the shallow water wave equation and depth average model ADCIRC, were developed to predict the formation of the vortex dipole.

#### 3.1 Model Description

The Advanced Circulation model (ADCIRC), is a two-dimensional, depth-integrated, barotropic time-dependent long wave, hydrodynamic circulation model (Luettich and Westerink 2000). ADCIRC can be run either as a two-dimensional depth integrated model or as a three-dimensional model.

In the present investigation, the two dimensional momentum equations are solved by the model. Then, ADCIRC solves the vertically-integrated momentum equations to determine the depth-averaged velocity (Luettich and Westerink 2000). Specifically ADCIRC uses the shallow water form of the momentum equations (applying the Boussinesq and hydrostatic pressure approximations).

#### 3.2 Methodology

The objective of the numerical modeling is to simulate the experiments of the idealized inlet conducted in the shallow water basin of the Institute of Hydromechanics of the University of Karlsruhe, in Karlsruhe, Germany. To take the formation of the vortex dipole to simulation domain, the same methodology used in Appendix A.1 was used. This means that the behavior of the flow regime



was matched using the Froude number, a geometrical parameter and the Mixing number. Table 10 presents the geometric parameters of the layout and the characteristics of the flow for different life-history types of vortex dipole formation.

Table 10 Geometric parameters and the characteristic of the flow for different life-history types of vortex dipole formation

LIFE-HISTORY TYPE	MIXING NUMBER	WIDTH	DEPTH	PERIOD	VELOCITY	FROUDE
	$K_w$	$W$	$h$	$T$	$U_{MAX}$	$F_r$
	[-]	[m]	[m]	[min]	[m/s]	[-]
Type I	0.11	1170	10	90	2.0	0.20
Type II	0.26	1170	10	63	1.2	0.12
Type III	0.06	1170	10	164	2.0	0.20

### 3.3 Results

In Figures 14 and 15 sample images are shown of the numerical simulations done with ADCIRC.

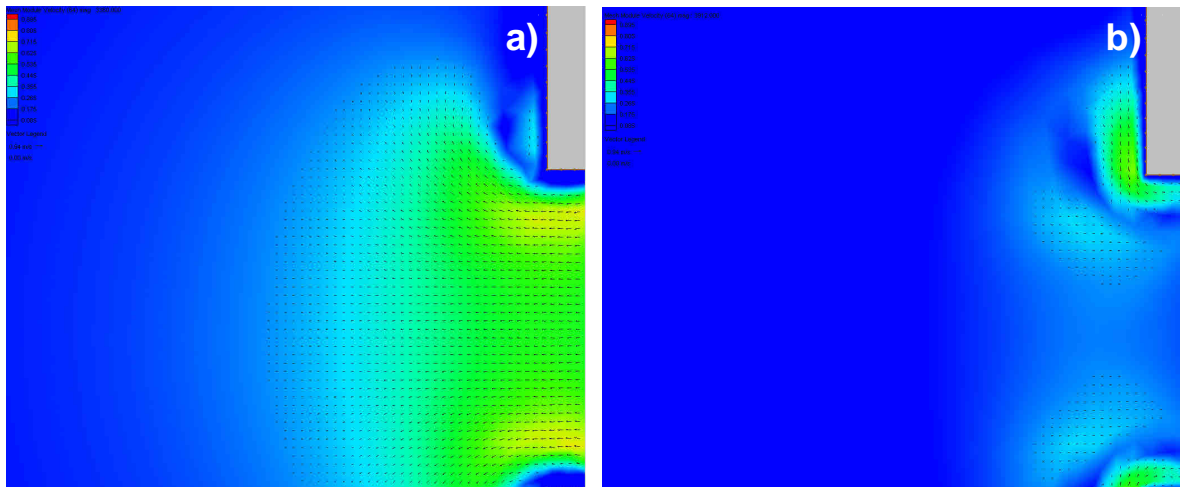


Figure 14 Numerical simulation of Layout A. Life-history Type II ( $K_W = 0.26$ )

Figure 14 provides sample images of the time evolution of the simulation with the idealized inlet and life-history Type II (entrained case): a) Formation of the vortex dipole at the ebb of the first tidal cycle. b) The structure get drawn back to the estuary as predicted by the Mixing number  $K_W = 0.26$ .

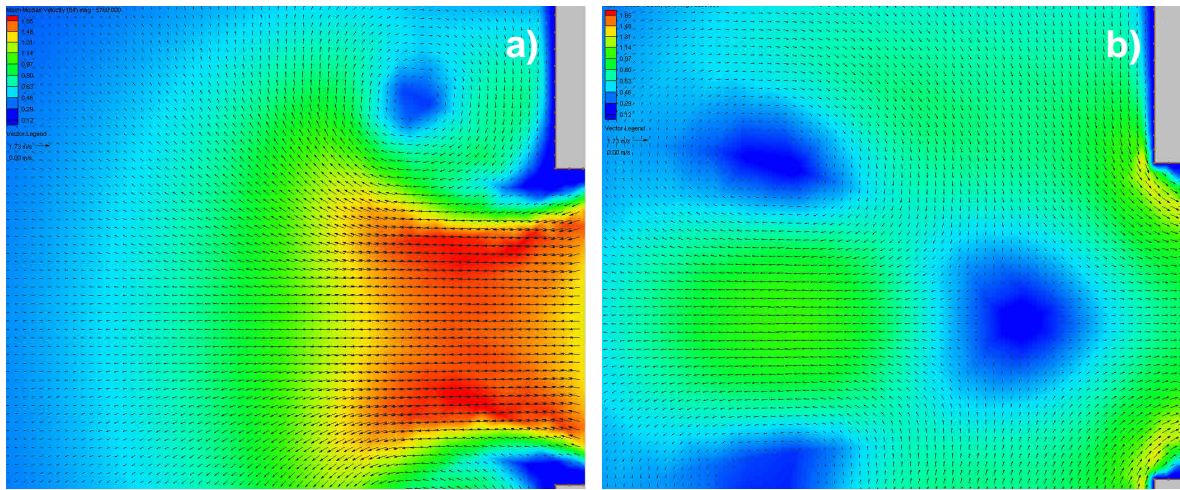


Figure 15 Numerical simulation of Layout A. Life-history Type III ( $K_W = 0.06$ )

Figure 15 has sample images of the time evolution of the simulation with the idealized inlet and life-history Type III (escape case): a) Formation of the vortex dipole at the ebb of the first tidal cycle. b) The structure escapes away from the inlet as predicted by the Mixing number  $K_W = 0.06$ .

### 3.4 Application Discussion

After analyzing the numerical modeling simulations, the following comments can be made:

- The results of the numerical simulations shows that the model can predict with precision the formation of the vortex dipole as expected by the calculation of the Mixing number  $K_W$ .
- To have accurate results, is better to run the ADCIRC model with shallow cells. This means that not only the entire domain has to have a shallow flow, but also each cell by itself has to accomplish this. This assumption is made because the model solves the shallow water wave equation, hence solving the equation that takes care of that condition, improves the results.
- The grid and parameters had to be up scaled in order to get better numerical stability and grid resolution. This also helps to accomplish the shallowness of each cell.
- If the secondary vortices wanted to be simulated, better resolution is needed, this is because the sizes of the vortices are small and fit in one cell. This may be incompatible if the shallowness of each cell wanted to be maintained.

## CHAPTER IV

### CONCLUSIONS

Experiments developed in the shallow water basin of the Institute of Hydromechanics of the University of Karlsruhe, Germany have been presented and analyzed. Typical flows through tidal inlets were modeled varying the tidal period  $T$ , and the average cross sectional maximum velocity  $U_{MAX}$ . The mixing and transport properties, and physical parameters were calculated using visualization and Particle Image Velocimetry (PIV) techniques.

For idealized inlets, the behavior of the three types of life-history of the vortex dipoles simulated (stationary, entrains and escape dipoles) were predicted accurately by the mixing number  $K_W$ , for the first tidal cycle. For the subsequent tidal cycles the structures behave differently than predicted by  $K_W$ . This different behavior may be caused because in the first tidal cycle the water is standing still, and for the following cycles the mass of water has a momentum in the moment of inputting the next cycle. The most critical case is when the mixing number is inputted as  $K_W = 0.26$ , since in the second and following cycles the vortex dipole does not get entrained.

The non-idealized geometries can behave differently as predicted by the mixing number. And the jetties and barrier islands give most complex flow structures with multiple eddies flowing from each side of the inlet, because the formation of vortex on the flood tide inside the channel flows out towards the "open coast" during the subsequent ebb tide.

Regarding the formation of the vortex dipole, for characteristics non-dimensional times  $t^* = tU / W$  less than about 2.2 the structure is attached to the inlet and

forms rapidly for all the cases simulated. For later times the dipole advects downstream and start slowly decaying in intensity. If the tide reverses before this characteristic time is reached, then the eddy will get drawn back to the “estuary” side of the inlet.

In the circulation plots can be observed that once the vortex reaches the maximum value, the magnitude of the circulation starts decaying (dissipating) with a sinusoidal behavior. This sinusoidal conduct is due to the presence of the secondary vortices that join the main vortex with a certain frequency that matches the sinusoidal peaks. The secondary vortices can be observed in the movies of dye studies simulations in Appendix C.

The decaying of the circulation after the vortex is detached from the inlet may be caused by the bottom friction and the upwelling of low-momentum bottom water. The decaying rate is similar for most of the idealized inlet simulations and the life-history Type I for the complex inlets (jetties and barrier island).

Is interesting to observe that longitudinal position  $X^*$  the vortex in Layout A flows away and remain stationary at the end of the curve. In the other layouts, the vortex flows away and then goes back towards the inlet around half of the travel distance. This tells us that the vortex, eventhough remains stationary, it is influenced by the flood tide that is pulling it slightly towards the inlet.

Building inlets with oblique angles simulates the behavior of an inlet with cross-shore current. This can be appreciated since the vortex dipole does not go in a straight line after leaving the inlet area.

The numerical modeling simulation results shows that the model predict accurately the formation and behavior of the tidal dipole vortex expected by the

mixing number  $K_w$ . However, to have correct physical results is better to run ADCIRC with shallow cells not only in the entire domain, but also each cell by itself.

## REFERENCES

- Adrian, R. J., Christensen, K. T., and Liu, Z. C. (2000). "Analysis and interpretation of instantaneous turbulent velocity fields." *Experiments in Fluids* 29(3): 275-290.
- Afanasyev, Y. D. (2006). "Formation of vortex dipoles." *Physics of Fluids* 18(3): 340-358.
- Brown, C. A., Jackson, G. A., and Brooks, D. (2000). "Particle transport through a narrow tidal inlet due to tidal forcing and implications for larval transport." *Journal of Geophysical Research-Oceans* 105(C10): 24141-24156.
- Carmer, C. V. (2005). "Shallow turbulent wake flows: momentum and mass transport due to large-scale coherent vortical structures." PhD Dissertation. Karlsruhe, Germany. Institute of Hydromechanics of Karlsruhe. PhD Period 1998-2005.
- Davies, P., Dakin, J., and Wolanski, E. (1995). "Eddy formation behind a coastal headland." *Journal of Coastal Research* 11: 154-167.
- Davies, P. A., Besley, P., and Boyer, D. L. (1990). "An experimental-study of flow past a triangular cape in a linearly stratified fluid." *Dynamics of Atmospheres and Oceans* 14(6): 497-528.
- Feng, H., Olsen, M. G., Liu, Y., Fox, R. O., and Hill, J. L. (2005). "Investigation of turbulent mixing in a confined planar-jet reactor." *AIChE Journal* 51(10): 2649-2664.
- Foucaut, J. M. and Stanislas, M. (2002). "Some considerations on the accuracy and frequency response of some derivative filters applied to particle image velocimetry vector fields." *Measurement Science & Technology* 13(7): 1058-1071.
- Ganapathisubramani, B., Longmire, E. K., and Marusic, I. (2006). "Experimental investigation of vortex properties in a turbulent boundary layer." *Physics of Fluids* 18(5): 1040-1056.
- Ganapathisubramani, B., Longmire, E. K., Marusic, I., and Pothos, S. (2005). "Dual-plane PIV technique to determine the complete velocity gradient tensor in a turbulent boundary layer." *Experiments in Fluids* 39(2): 222-231.



- Hench, J. L., Blanton, B., and Luettich, R. A. (2002). "Lateral dynamic analysis and classification of barotropic tidal inlets." *Continental Shelf Research* 22(18-19): 2615-2631.
- Hench, J. L. and Luettich, R. A. (2003). "Transient tidal circulation and momentum balances at a shallow inlet." *Journal of Physical Oceanography* 33(4): 913-932.
- Jirka, G. H. (2001). "Large scale flow structures and mixing processes in shallow flows." *Journal of Hydraulic Research* 39(6): 567-573.
- Kashiwai, M. (1984). "Tidal residual circulation produced by a tidal vortex. part I: life-history of a tidal vortex." *Journal of the Oceanographical Society of Japan* 40: 279-294.
- Kashiwai, M. (1985). "TIDICS - Control of tidal residual circulation and tidal exchange in a channel-basin system." *Journal of the Oceanographical Society of Japan* 41: 1-10.
- Kashiwai, M. (1985). "A hydraulic experiment on tidal exchange." *Journal of the Oceanographical Society of Japan* 41: 11-24.
- Lin, J. C., Ozgoren, M., and Rockwell, D. (2003). "Space-time development of the onset of a shallow-water vortex." *Journal of Fluid Mechanics* 485: 33-66.
- Lophaven, S., Nielsen, H., and Sondergrand, J. (2002). "DACE: A matlab kriging toolbox." <http://citeseer.ist.psu.edu/nielsen02dace.html>
- Luettich, R. A. and Westerink, J. J. (2000). "ADCIRC: advanced circulation model for oceanic, coastal and estuarine waters." [http://adcirc.org/document/ADCIRC\\_title\\_page.html](http://adcirc.org/document/ADCIRC_title_page.html)
- Mori, N. and Chang, K. A. (2003). "Introduction to MPiV." <http://sauron.urban.eng.osaka-cu.ac.jp/~mori/software/mpiv/index.php>
- NASA. (2004). "Chlorophyll concentration off the Queen Charlotte Islands, CANADA." Courtesy NASA SeaWiFS <http://visibleearth.nasa.gov/usetems.php>
- Negretti, M. E., Socolofsky, S. A., Rummel, A., and Jirka, G. H. (2005). "Stabilization of cylinder wakes in shallow water flows by means of roughness elements: an experimental study." *Experiments in Fluids* 38(4): 403-414.

- Raffel, M., Willert, C., and Kompenhams, J. (1998). *Particle Image Velocimetry*. Berlin, Germany, Springer.
- Rummel, A. C., Socolofsky, S. A., Carner, C., and Jirka, G. H. (2005). "Enhanced diffusion from a continuous point source in shallow free-surface flow with grid turbulence." *Physics of Fluids* 17(7): 567-584.
- Shinneeb, A. M., Bugg, J. D., and Balachandar, S. (2004). "Variable threshold outlier identification in PIV data." *Measurement Science & Technology* 15(9): 1722-1732.
- Socolofsky, S. (2006). "Progress report on a sea project: laboratory studies of mixing processes in estuaries and coastal flows on the Texas coast." <http://texas-sea-grant.tamu.edu>
- Socolofsky, S. and Carner, C. (2003). "Shallow turbulent wakes: Linear stability analysis compared to experimental data." *IAHR International Symposium on Shallow Flows*, Delft, The Netherlands.
- Socolofsky, S. A. and Adams, E. E. (2005). "Role of slip velocity in the behavior of stratified multiphase plumes." *Journal of Hydraulic Engineering-Asce* 131(4): 273-282.
- Socolofsky, S. A. and Jirka, G. H. (2004). "Large-scale flow structures and stability in shallow flows." *Journal of Environmental Engineering and Science* 3(5): 451-462.
- Weiss, J. (1991). "The Dynamics of Enstrophy Transfer in 2-Dimensional Hydrodynamics." *Physics of Fluids* 48(2-3): 273-294.
- Wells, M. G. and van Heijst J. F. (2003). "A model of tidal flushing of an estuary by dipole formation." *Dynamics of Atmospheres and Oceans* 37(3): 223-244.
- Zhou, J., Adrian, R. J., Bacachandar, S., and Kendall, T. (1999). "Mechanisms for generating coherent packets of hairpin vortices in channel flow." *Journal of Fluid Mechanics* 387: 353-396.

## APPENDIX A

### METHODOLOGY OF THE EXPERIMENTS

A series of experiments were conducted the summer of 2006 in the University of Karlsruhe, in Karlsruhe, Germany. The present Appendix explains the methodology of how these experiments were developed.

#### 1     **Scaling**

The objective of the experiments is to simulate a flow that occurs in nature on a laboratory facility where measures can be taken, and the parameters that control the flow are easily adjustable. To take the formation of 2DCS from the actual field scale to the laboratory scale, a methodology to match the behavior of both flows was developed. A set of 4 parameters that define the characteristics of the formation of the vortex was used. These 4 parameters are: tidal period  $T$ , width of the inlet  $W$ , depth of the channel  $h$ , and the maximum average velocity over one tidal cycle in the middle of the inlet  $U_{MAX}$ . Using the previously mentioned factors, 3 dimensionless parameters were constructed which are the Froude Number, geometric width / depth inlet ratio, and the mixing number.

#### Froude number

The Froude number is a dimensionless number that can be interpreted as the ratio of the inertial forces to the gravity forces in the flow.

$$Fr = \frac{U_{MAX}}{\sqrt{gh}} \quad (15)$$

Where  $U$  is the characteristic velocity of the flow,  $g$  is the acceleration of gravity, and  $L$  is the characteristic length of the flow. When the Froude number is equal to one, the speed of the surface wave and that of the flow is the same. The flow is in the critical state. When the Froude number is less than one, the flow velocity is smaller than the speed of a disturbance wave traveling on the surface. Flow is considered to be subcritical. Gravitational forces are dominant and the surface waves will propagate upstream. When the Froude number is greater than one, the flow is supercritical and inertial forces are dominant and the surface waves will not propagate upstream.

In the experiments that were carried out, the characteristic velocity used was set to be  $U_{MAX}$ , and the length scale was the water depth  $h$ . The value of the Froude number cannot be larger than 0.20, to match the behavior of the flow in the nature.

$$Fr = \frac{U_{MAX}}{\sqrt{gh}} \leq 0.20 \quad (16)$$

The value for the Froude number of 0.20 was calculated from inlets along the Texas coast. This was obtained with a characteristic maximum tidal velocity of 2 [m/s], and a depth of 10 [m].

Geometric ratio

One of the basic assumptions of these experiments is that the flow is shallow; therefore in order to maintain the shallowness of the flow in the simulations the

parameters has to match a geometric ratio. This parameter for this particular experiment was found to be:

$$\frac{W}{h} \geq 10 \quad (17)$$

### Mixing number

The Mixing number is similar to the Strouhal number, which is a dimensionless factor used in studying the vibrations of a body past which a fluid is flowing; it is equal to a characteristic dimension of the body times the frequency of vibrations divided by the fluid velocity relative to the body.

$$S_t = \frac{Wf}{U_{MAX}} \quad (18)$$

Where  $St$  is the dimensionless Strouhal number,  $f$  is the frequency of vortex shedding,  $L$  is the characteristic length (for example hydraulic diameter) and  $V$  is the velocity of the fluid.

The Mixing number that is used in this research takes the tidal period, instead of the frequency to compute this dimensionless factor:

$$K_w = \frac{W}{U_{MAX} T} \quad (19)$$

Where  $K_w$  is the dimensionless Mixing number,  $W$  is the width of the inlet,  $T$  is the tidal period in the zone which is located the inlet, and  $U_{MAX}$  is the maximum mean velocity in the middle of the inlet over a tidal cycle.

In the Table 11 is shown the interpretation of the Mixing number. The information provided by the Table 11 is a summary of the researches done by Kashiwai (1984) and Wells and van Heijst (2003).

Table 11 Summary of the researches done by Kashiwai (1984) and Van Heijst (2003) of the interpretation of the mixing number

$K_w$	LIFE-HISTORY TYPE	CASE	MIXING
$\approx 0.13$	Type I	Stationary	Intermediate
$\gg 0.13$	Type II	Entrain	Poor
$\ll 0.13$	Type III	Escape	Efficient

This means that if the Mixing number is less than 0.13 the vortex dipole will escape from the inlet, and if  $K_w$  is larger 0.13 the structure will get drawn back into the estuary. Also, there is a critical case were the structure is supposed to remain stationary near the mouth of the inlet.

The dimensionless number is named as mixing number in this research, to adopt an environmental meaning for the parameter. The factor measure how efficient is the mixing done by the characteristics of the flow.

## 2 Experimental Set Up

A set of experiments were developed in the shallow water basin of the University of Karlsruhe, Germany. There were used 8 different geometries for the simulations:

- Layout A: Idealized inlet (Figure 16).
- Layout B: Inlet with jetties with equal length than the inlet (Figure 17).
- Layout C: Inlet with jetties length longer than the inlet (Figure 18).
- Layout D: Inlet with a wider width, simulating a barrier island (Figure 19).
- Layout E: Inlet with one big obstacle at the mouth of the inlet (Figure 20).
- Layout F: Inlet with small obstacles at the mouth of the inlet (Figure 21).
- Layout G: Inlet with small obstacles at the mouth of the inlet (Figure 22).
- Layout H: Inlet in an oblique angle (Figure 23).

For layouts A to D there were developed 3 types of flows, reproducing the Stationary case ( $K_W \approx 0.13$ ), Entrain case ( $K_W \gg 0.13$ ), and the case that the structure is suppose to Escape ( $K_W \ll 0.13$ ).

For layouts E to H, only the Stationary Case was analyzed, because only the effect of the structures and the angle wanted to be investigated.

### A.1.1 Layouts

In the Figures A.1 to A.8 the layouts of the experiments are shown.

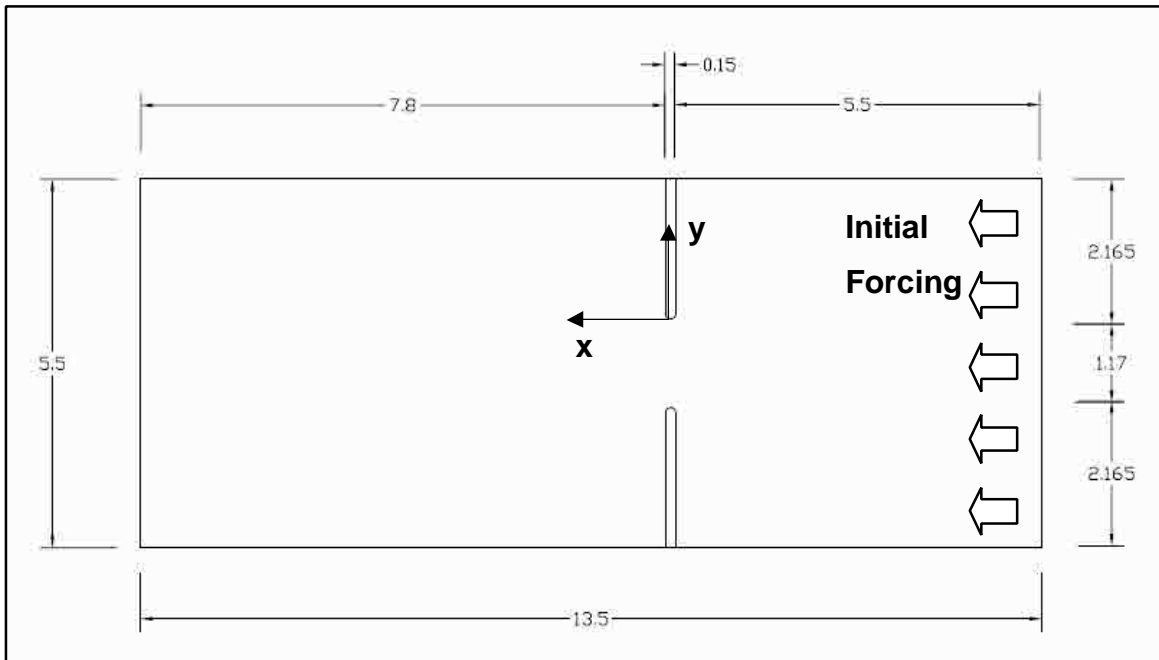


Figure 16 Layout A: Idealized inlet

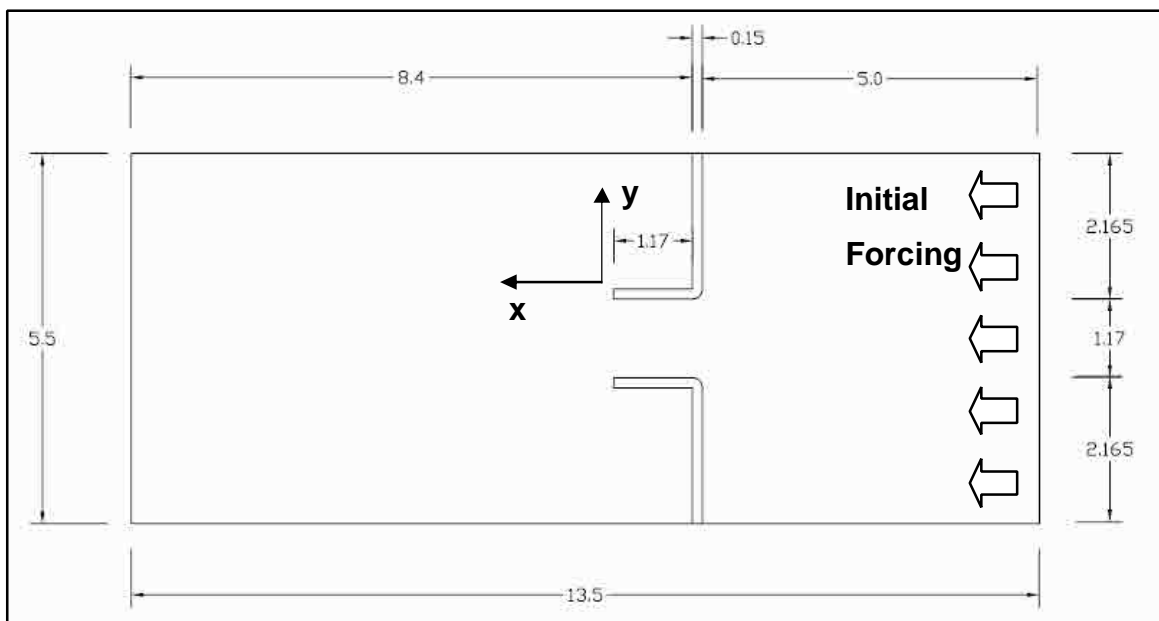


Figure 17 Layout B: Inlet with jetties with equal length than the inlet



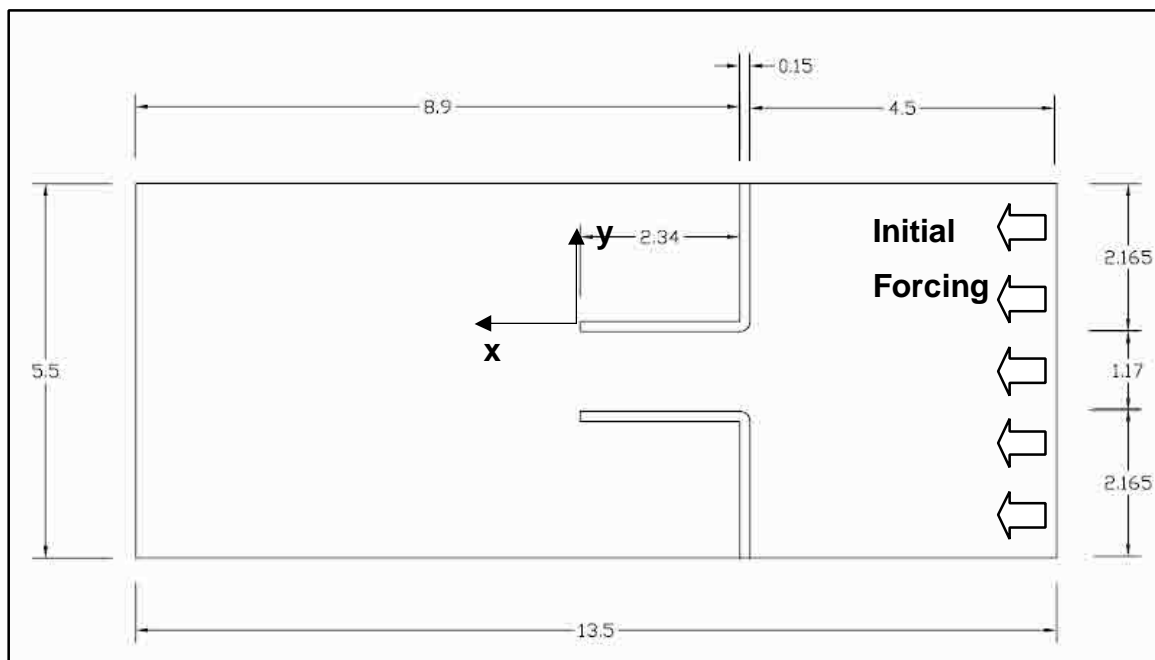


Figure 18 Layout C: Inlet with jetties length longer than the inlet

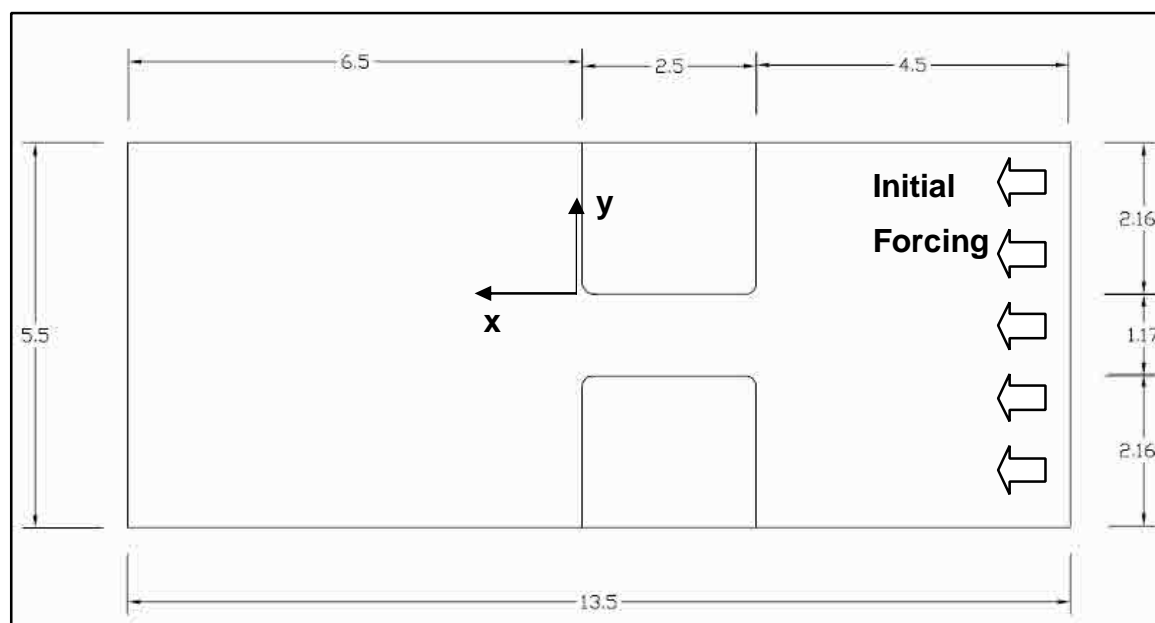


Figure 19 Layout D: Inlet with a wider width, simulating a barrier island

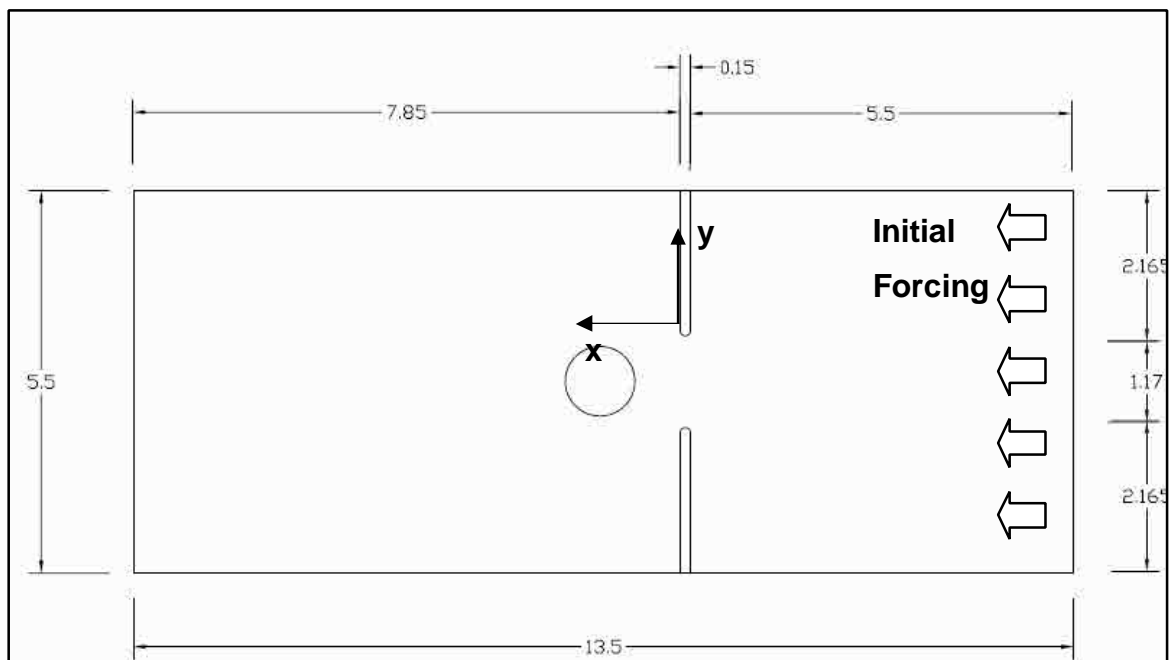


Figure 20 Layout E: Inlet with obstacles in the mouth of the inlet. Case A

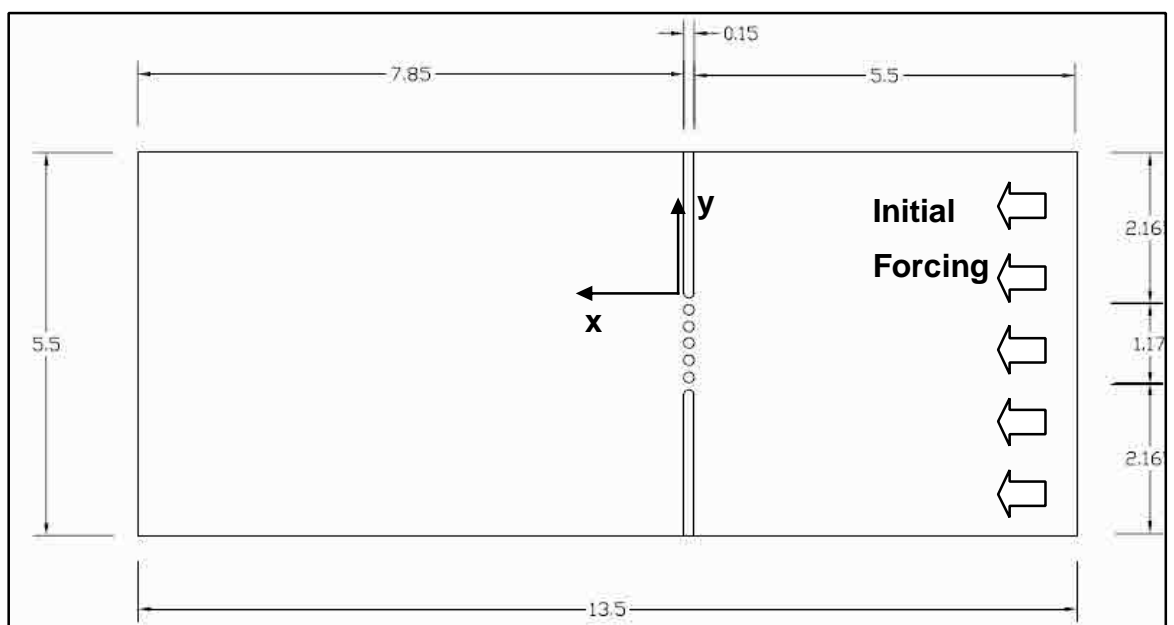


Figure 21 Layout F: Inlet with obstacles in the mouth of the inlet. Case B

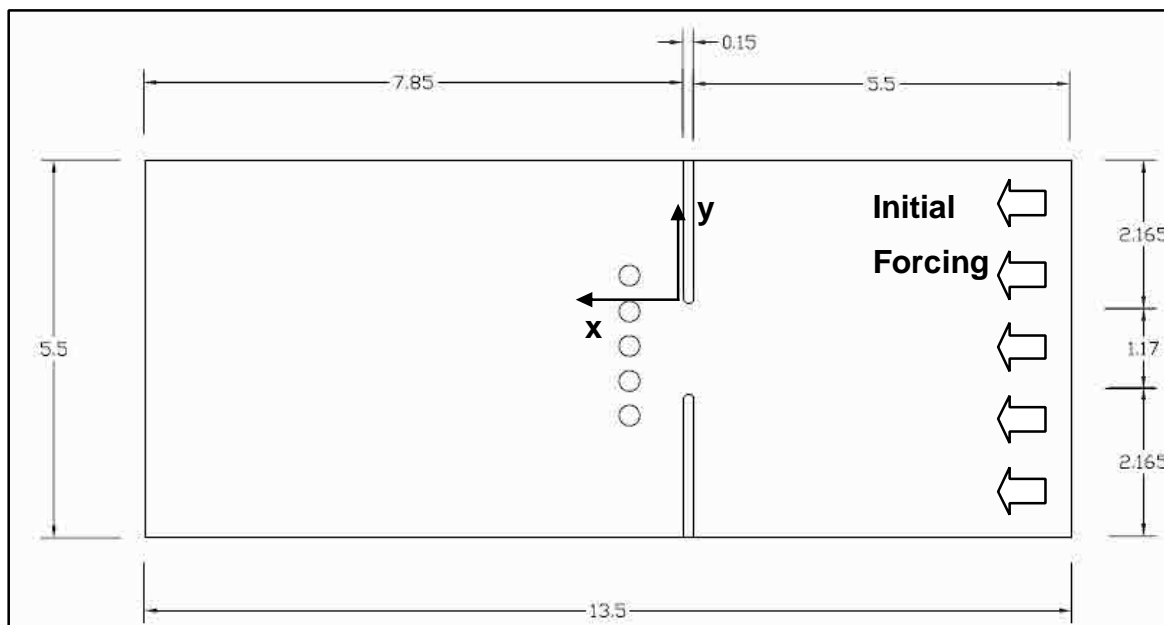


Figure 22 Layout G: Inlet with obstacles in the mouth of the inlet. Case C

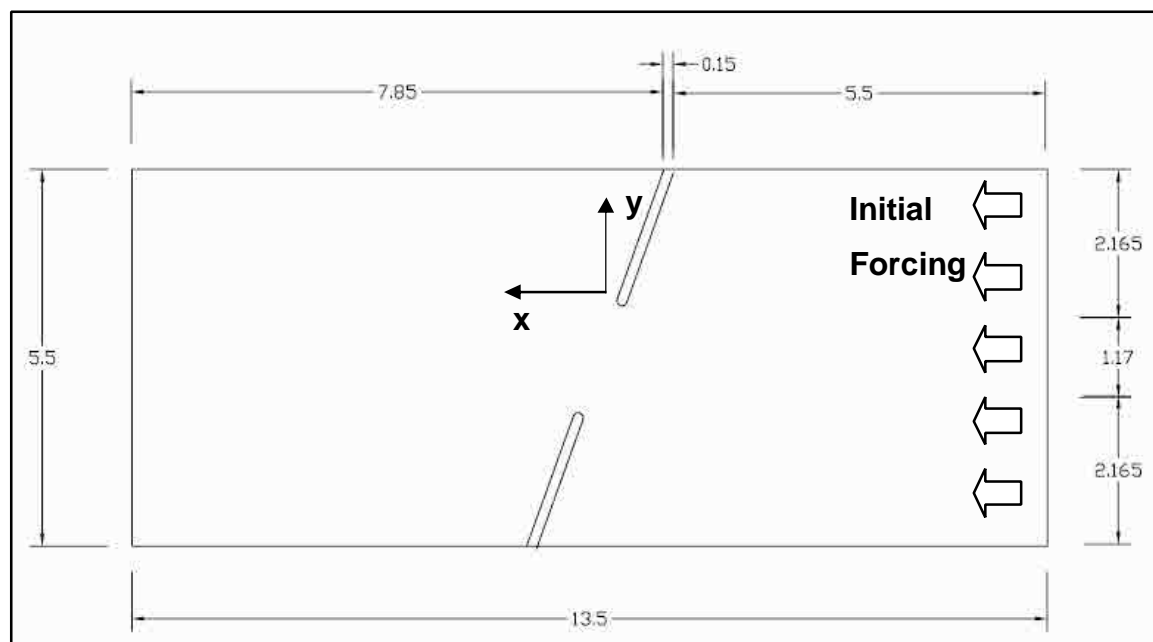


Figure 23 Layout H: Inlet in an oblique angle

### Characteristics of the flows

As was mentioned before, for experiments A through D there were developed 3 kinds of flows, reproducing the Stationary Case ( $K_W \approx 0.13$ ), Entrain Case ( $K_W \gg 0.13$ ), and the Case that the structure is suppose to Escape ( $K_W \ll 0.13$ ). For experiments E through H, only the Stationary Case was analyzed, because only the effect of the structures and the angle wanted to be investigated.

The flows simulated a sinusoidal tide, with 5 cycles for experiment A and 3 cycles for the rest of the experiments. This sinusoidal tide was forced with a current, not with a head. This is possible because the shallow water basin has the capability to reverse the flow, by operating 4 valves in order to overturn the direction of the flow.

The pump that generates the currents had to be operated at least in a 10% of its maximum capacity, in order to have accuracy of the flow that was inputting. The maximum flow that the pump can force is 120 [l/s]. Consequently, the minimum value that the pump could be operated was 12 [l/s].

The characteristics of the flows were selected and calculated carefully to achieve the restrictions that the physical parameters needed to meet, and also taking into account the limitations of the facilities of the University of Karlsruhe.

A hydrodynamic stability analysis of the flow was developed as well (Socolofsky and Jirka 2004), to study the stability of the tailing jet. The calculations show that for the given size of the shallow water basin only the unstable case was able to be simulated. To be unstable in this case means that the centerline of the jet will meander and multiple secondary vortices will develop at the sides of the jet

Table 12 presents the geometric parameters of the layouts, and the Table 13 presents the characteristics of the different flow inputted to the layouts.

Table 12 Geometric parameters used in the different layouts

EXPERIMENT	JETTIES	BARRIER ISLAND	ANGLE	WIDTH
	L	D	$\alpha$	W
	[m]	[m]	[degrees]	[m]
Layout A	-	0.15	0	1.17
Layout B	1.17	0.15	0	1.17
Layout C	2.3	0.15	0	1.17
Layout D	-	1.17	0	1.17
Layout E	-	1.17	0	1.17
Layout F	-	1.17	0	1.17
Layout G	-	0.15	0	1.17
Layout H	-	0.15	10 and 20	1.17

Table 13 Flow parameters used in the different types of life-history

LIFE-HISTORY TYPE	DEPTH	PERIOD	FLOW	VELOCITY	STABILITY	FROUDE
	H	T	$Q_{MAX}$	$U_{MAX}$	$S_f$	$F_r$
	[m]	[s]	[l/s]	[m/s]	[]	[]
Type I	0.1	55	23	0.20	0.08	0.20
Type II	0.1	37	14	0.12	0.09	0.12
Type III	0.1	100	23	0.20	0.08	0.20

### 3 Dye Visualizations Studies

Dye studies were conducted in the shallow water basin to help in the visualization of the formation of the vortex. This technique was applied for layouts A through D, and layout H.

#### Measurement equipment

The equipment used for the simulation of the experiments for the visualization with dye is the following:

- Flow meter
- Red dye
- Dye injector with different frequency of injection
- Cannon A 75 Photo Camera used as a video camera

#### Dye visualization studies measuring methodology

The procedure for filming the movies of the visualization studies was the following:

- 1) Turn on the camera.
- 2) Activate the dye disposal jets.
- 3) Set in motion the pump to start the flow.
- 4) Every time that the pump reaches half a cycle of the sinusoidal flow, operate the valves to change the direction of the flow (2 people needed for this).

## 4 PIV Studies

The PIV method (Particle Image Velocimetry) was developed to obtain qualitative and quantitative data. This means that movies of the velocity and vorticity fields are obtained, but also each frame is analyzed to acquire information about the vortex evolution, and the secondary eddies as well. This technique was applied for all the layouts.

### Measurement equipment

The equipment used for the simulation of the experiments for the PIV studies are the following:

- Flow meter.
- Depth sensors (2).
- Cameras Photonfocus MV-D1024, 10 frames per second, 1024x768 pixels.
- 300 GB of storage capacity.
- Polyurethane seeding particles, 2 [mm].
- Seeding dispensator.

### PIV studies measuring methodology

After reviewing the movies of the dye visualizations the two cameras were set in a position to maximize the vortex time in focus. The cameras were mounted in a crane 3 meters above the basin.

It was assumed that the surface of the water was representative of the depth average flow velocity since the flow was shallow. This is important because the seeding particles were floating in the surface of the water.

The seeding dispensator was located at the entrance of the inlet where the flow is forced initially.

The stopwatch was used to measure the time between the moment the cameras start capturing images and when the flow starts.

The procedure for acquiring the images for the PIV analysis was the following:

- 1) Seed the particles in the whole domain of the basin.
- 2) Turn on the seeding dispensator.
- 3) Trigger the cameras. Activate the stopwatch.
- 4) Set in motion the pump to start the flow. Stop the stopwatch.
- 5) Activate the depth measuring device.
- 6) Every time that the pump reaches half a cycle of the sinusoidal flow, operate the valves to change the direction of the flow (2 people needed for this).

The camera took 10 images per second, for a total of 5 tidal cycles for the idealized inlet and 3 cycles for the rest of the experiments.



## **APPENDIX B**

### **DATA ANALYSIS**

The present Appendix shows the results and analysis of the experiments and the methodology that was used to study them.

#### **1 Visualization**

The visualization of the characteristics of the flow was made with colored dye (red) injected on the sides of the inlet. Below are exposed some sample shots of specific cases that were filmed, with their correspondent explanation of the phenomenon observed.

All the complete movies filmed are provided in the Appendix C.

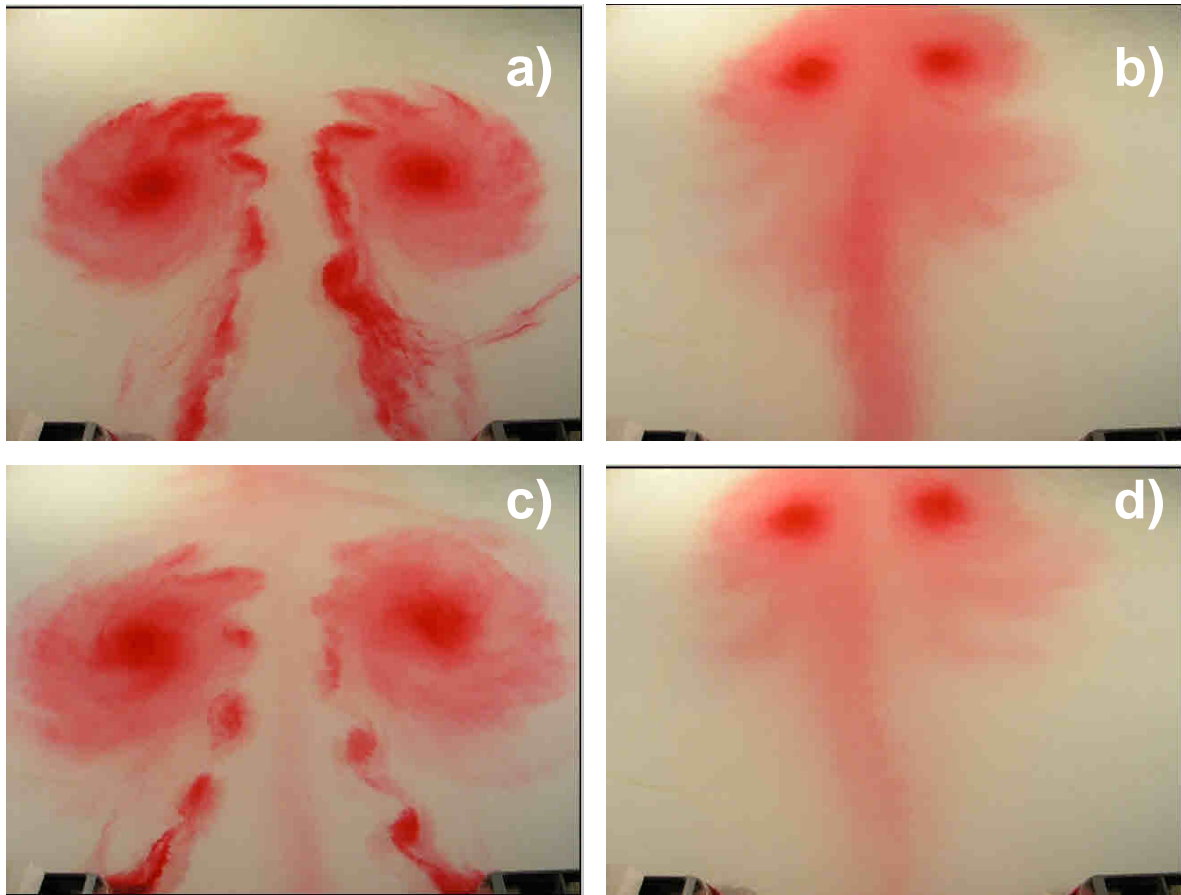


Figure 24 Layout A: Idealized inlet ( $K_W = 0.11$ )

Figure 24 has sample images of the time evolution of the experiment with the idealized inlet and life-history Type I (stationary case): a) Formation of the 2DCS at the end of the ebb of the first cycle. b) The structure remains stationary as predicted in the first cycle at the end of the flood tide. c) Formation of the vortex on the second cycle; it can be observed that are several secondary structures forming and getting together with the main structure. d) Ending of the flood of the second cycle, and the structure remains stationary but slightly further away than the first cycle.

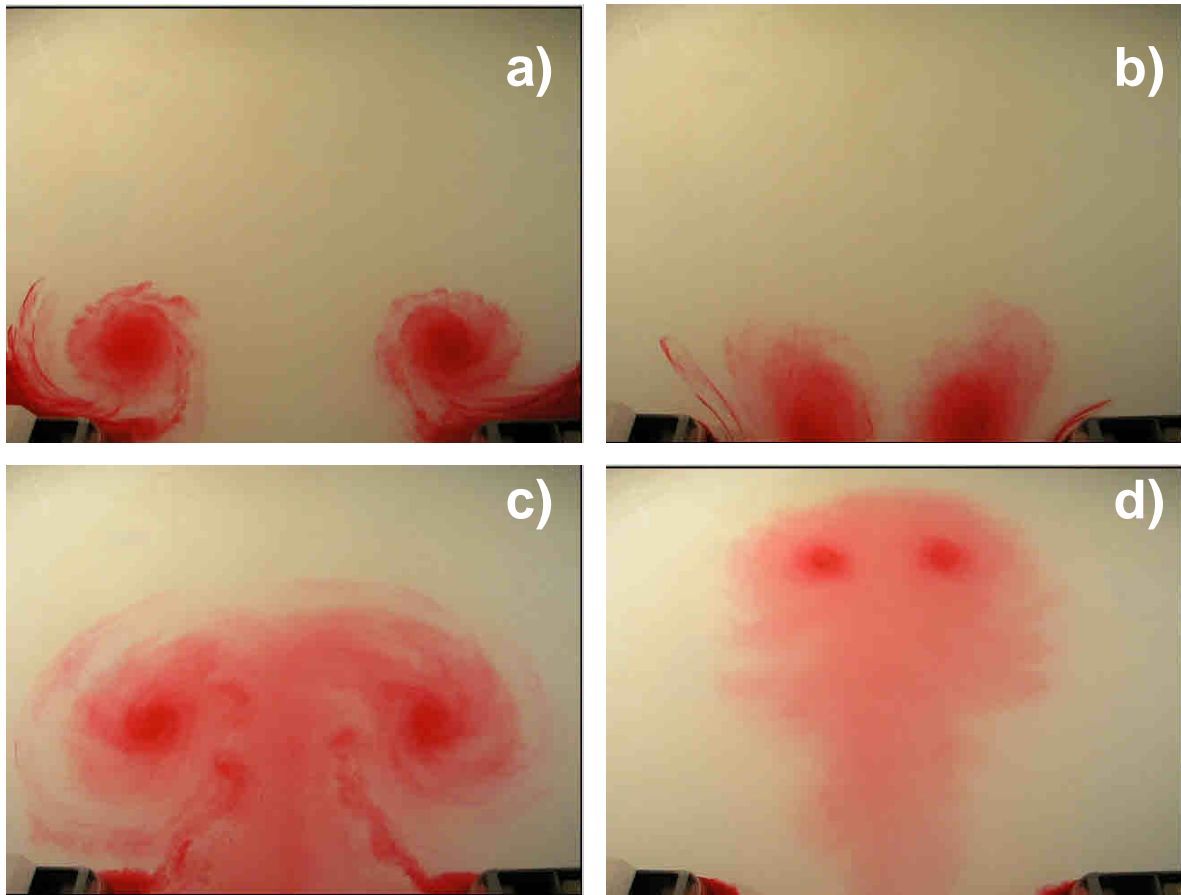


Figure 25 Layout A: Idealized inlet ( $K_W = 0.26$ )

Figure 25 has sample images of the time evolution of the experiment with the idealized inlet and life-history Type II (entrained case): a) Formation of the 2DCS at the end of the ebb of the first cycle. b) The structure gets drawn back to the inlet as predicted in the flood tide of the first cycle. c) Formation of the vortex on the second cycle; it can be observed (not as clear as the previous figure) that are several secondary structures forming and getting together with the main structure. d) At the end of the flood of the second cycle the structure remains stationary, in a different way as predicted.

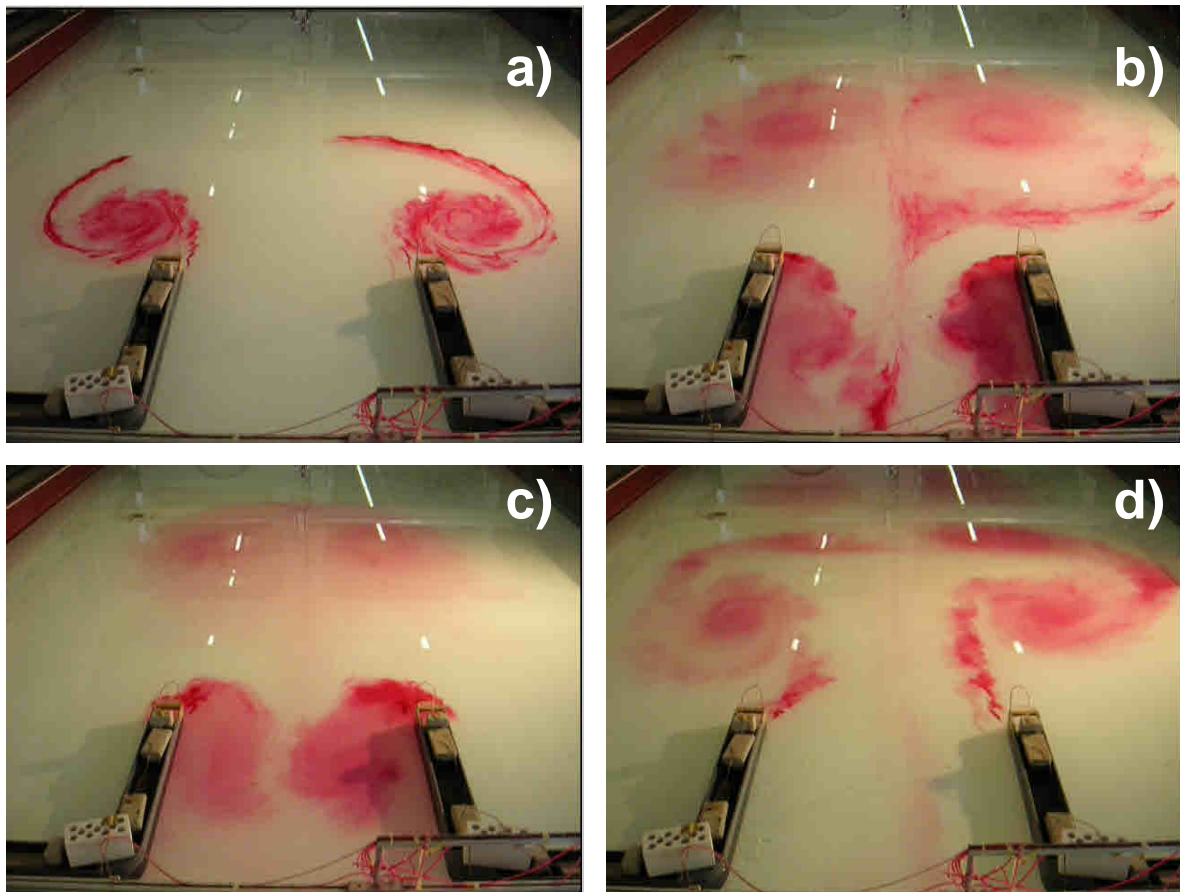


Figure 26 Layout B: Inlet with jetties with equal length than the inlet ( $K_W = 0.06$ )

Figure 26 has sample images of the time evolution of the experiment with the jetties equal to the length of the inlet and life-history Type III (escape case): a) Formation of the 2DCS at the middle of the ebb of the first cycle; the structures are closer to sides of the basin than the idealize inlet. b) The structure is in the limit of being escaping, and inside the jetties vortex are forming driven by the flood tide passing through the inlet. c) The second cycle is starting, and the structures formed during the flood are now flowing out with the ebb tide. d) Two vortex can be identified in each side, the ones formed by the ebb tide flowing to open coast (round shape), and the structures formed during the flood tide (further away from the inlet); the structures are spinning in opposite directions. Also secondary vortexes are forming.

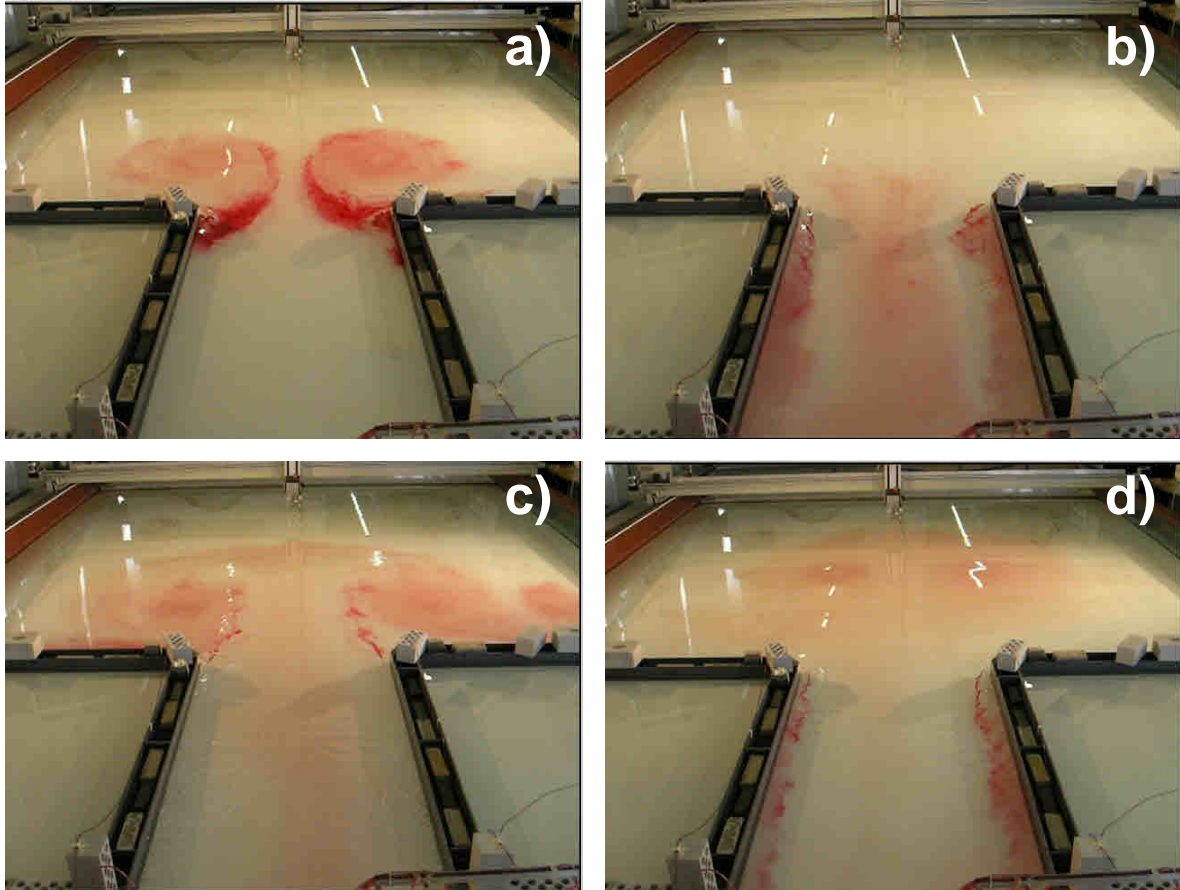


Figure 27 Layout D: Inlet with a wider width, simulating a barrier island ( $K_W = 0.13$ )

Figure 27 has sample images of the time evolution of the experiment simulating a barrier island and life-history Type I (stationary case): a) Formation of the 2DCS at the end of the ebb of the first cycle. b) The structures get drawn back to the inlet instead of remain stationary; eddy formation at the sides of the channel generated by the flood tide. c) Second cycle: Two vortex can be identified in each side, the ones formed by the ebb tide flowing to open coast (round shape), and the structures formed during the flood tide (to the sides of the basin); the structures are spinning in opposite directions. Also secondary vortexes are forming. d) The vortex remains stationary in the second cycle at the flood tide; the vortex formed in the flood tide of the first cycle got drawn into the inlet.

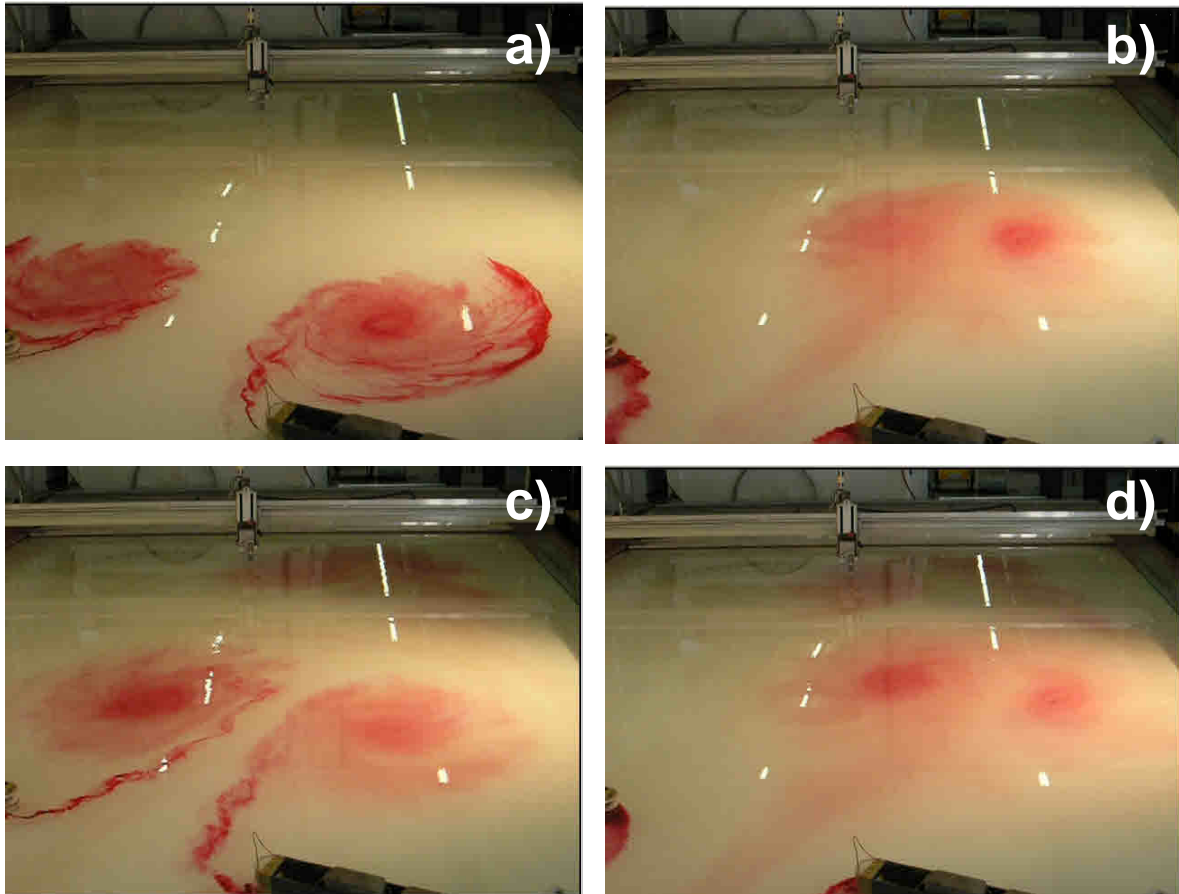


Figure 28 Layout H: Inlet in an oblique angle:  $20^\circ$  ( $K_W = 0.13$ )

Figure 28 has sample images of the time evolution of the experiment with the inlet in an oblique angle of  $20^\circ$  and life-history Type I (stationary case): a) Formation of the 2DCS; the right side vortex is slightly more detached from the inlet than the other. b) The vortex remains stationary as predicted, but taking a straight line perpendicular to the inlet the right-hand vortex is further away from it. c) The 2DCS formed in the second tidal cycle; the secondary vortex can be observed. d) Again the right-hand vortex is slightly further away from the inlet in the second cycle.

From the figures commented above, and the movies that are in electronic format in the Appendix C, the following can be identified:

- The mixing number predicts well the behavior of the vortices for the first cycle on idealized inlets.
- For subsequent tidal cycles, the structures behave differently than predicted by  $K_W$  on idealized inlets. The most critical case is when  $K_W = 0.26$ , since it is clear that in the following cycles the 2DCS remains stationary.
- Inlets with different geometries than the idealized inlet can behave differently than predicted by  $K_W$ .
- Jetties and thick barrier islands give most complex flow structure with multiple eddies off each side, because of the formation of eddies on the flood tide inside the channel flows out towards the “open coast” on the subsequent ebb tide.
- The 2DCS formed in the first cycle on the jetties and barrier island set up in the beginning goes near the sides of the basin, and the end of the ebb tide and the beginning of the flood tide they move towards the middle of the basin.
- Secondary vortices appear in all the simulated cases with different intensities.
- For visualization purposes the structures were not set up on the middle of the basin, thus this may be a factor explaining why the following cycles of the life-history Type II did not behave as predicted.
- Building inlets with oblique angles simulates the behavior of an inlet interacting with a cross-shore current.

## 2 Particle Image Velocimetry (PIV) Analysis

The PIV method is a technique to measure fluid velocity. A PIV system does this by taking two digital images of a fluid (gas or liquid), seeded with particles in quick succession. Hence, the position of the particles in two successive images and the time-step used by the camera are known, the velocity can be computed with simple physics. The velocity is calculated in several windows within the image, and then each window analyzed will have a specific velocity for that exact region (Raffel, Willert et al. 1998).

The MPIV toolbox written in MATLAB and developed by Nobuhito Mori and Kuang-An Chang (2003), was used to analyze the images taken in the shallow water basin. Specifically, the Minimum Quadratic Difference (MQD) method was used since the data studied gave the most accurate results.

Since the computer time estimated for calculating the velocity field using this toolbox would have taken too long, the MQD method of the MPIV toolbox was reprogrammed in FORTRAN in order to gain time and compute the images faster. Only the MQD method was ran in FORTRAN, obtaining the data set of the raw velocity fields without interpolation for each camera separately.

A complete code in MATLAB was developed for calculating the velocity field for the two cameras joined together, the vorticity field, and for identify the region where the vortex were forming. This code is shown in the Appendix C.

Then using the interpolated data, physical parameters of the vortexes were analyzed along the time series of each experiment. The parameters studied were the circulation, vertical and horizontal position, width, maximum vorticity, and upwelling of the vortex at each frame took in the experiment. For the first cycle, the slope of the growth and decay of the vortex were calculated.



## Velocity Field

The first thing done was removing the data that was in the region where the structure (Jetties, Barrier Island or Obstacles) was standing. The PIV method analyzes the images and does not recognize if the data is water or structure, so the values structures (Inlets, jetties, barrier island) were set up to be zero before any calculation was developed.

The calculation of the velocity field was done by applying the MPIV toolbox to all the images taken for each experiment. After the data was obtain from the reprogrammed FORTRAN code, it was necessary to filter the data to remove the vectors that didn't represent accurately the velocity field in the region that they were standing (Foucaut and Stanislas 2002). The removing of the noise was done using the median filter in several sub-regions of the image.

The velocity field obtained after removing the bad vectors had missing data in some regions. For a good visualization and calculation limitations the data was interpolated using the Kriging Method by applying a modified version of the DACE Kriging toolbox (Lophaven, Nielsen et al. 2002). This means that the Kriging interpolation was not applied to the whole domain of the velocity field all at once, it was divided into sub-windows. Each image was initially divided into 20 windows in the current direction, and 10 windows in the wall normal direction, if the method did not found more than 3 vectors to interpolate any sub-window the program automatically drop the resolution until it was able to perform the interpolation. There was a 50% of overlap between sub-windows. Using this methodology the data turn out to be smoother than the whole region interpolated straight away.

### Vorticity Field

The vorticity field was obtained by calculating the circulation (20) at each data point of the velocity field, using for this the 8 surrounding vectors of a specific location. It was necessary to calculate the velocity gradients using the least squared method (21) for every data point of the velocity field. The vorticity of a specific data point is given by Equation (22).

$$\Gamma = \int_{dl} u dl = \int_A \omega dA \quad (20)$$

$$\left( \frac{df}{dx} \right)_i \approx \frac{2f_{i+2} + f_{i+1} - f_{i-1} - 2f_{i-2}}{10\Delta x} \quad (21)$$

$$\omega = \frac{\Gamma}{A} \quad (22)$$

Where  $f$  is the velocity component in the  $i$  location, and  $\Delta x$  is the distance between two nearby locations. Where  $\omega$  is the vorticity of a specific data point;  $\Gamma$  is the circulation; and  $A$  is the area in which the circulation is calculated.

The least squared approach was used because have a tendency to smooth the circulation because the outer values are more weighted than the inner data.

### Vortex identification

A universal definition of vortex has not been accepted yet, but it can be describe as a tube shaped structure with persistent and coherent rotation along its center of mass (Zhou, Adrian et al. 1999). Using this definition two methodologies where studied to identify the vortex formation in the present research.

The first method, proposed by Adrian and Christiansen (2000), uses an equivalent 2-dimensional velocity gradient tensor computed in the plane where the PIV data was acquired.

$$D^{2-D} = \begin{pmatrix} \frac{du}{dx} & \frac{du}{dy} \\ \frac{dv}{dx} & \frac{dv}{dy} \end{pmatrix} \quad (23)$$

Where  $(x,y)$  and  $(u,v)$  the direction and velocities stream-wise and normal to the direction of the initial flow. In this case, the matrix  $D^{2-D}$  will have two real eigenvalues  $\lambda_r$ , or a pair of complex conjugate eigenvalues  $\lambda_{ci}$ . Taking the positive value of the complex values,  $\lambda_{ci} > 0$ , and plotting the iso-regions of these values, the location where the vortices are forming can be identified.

$$\lambda_{ci} = \sqrt{\frac{1}{4} \left( \frac{du}{dx} - \frac{dv}{dy} \right)^2 + \left( \frac{dv}{dx} + \frac{du}{dy} \right)^2 - \left( \frac{dv}{dx} - \frac{du}{dy} \right)^2 + \frac{du}{dy} \frac{dv}{dx}} \quad (24)$$

The second method proposed by Carmer (2005), uses the Weiss Function (Weiss 1991) that compares the magnitudes of the rates of strain and vorticity.

$$Q = \left( \frac{du}{dx} - \frac{dv}{dy} \right)^2 + \left( \frac{dv}{dx} + \frac{du}{dy} \right)^2 - \left( \frac{dv}{dx} - \frac{du}{dy} \right)^2 \quad (25)$$

Where  $(x,y)$  and  $(u,v)$  the direction and velocities stream-wise and normal to the direction of the initial flow. The named Q Values are calculated in the planar field where the PIV data was taken. The regions where these values are negative  $Q < 0$ , are dominated by vorticity. The regions where these values are positive  $Q > 0$ , are dominated by strain.

The results obtained using the two methods were similar. Both predicted the formation of eddies in the same locations, but the values of  $\lambda_{ci} > 0$  were found to be more consistent for the type of data that this research was analyzing, after squared these values before plotting the iso-regions. The values were squared to make easier the observation of the forming vortex.

## Results

The Figures 29 through 31 show examples of results of the velocity field, vorticity field and vortex identification, for the three types of life-history cases for Layout A.

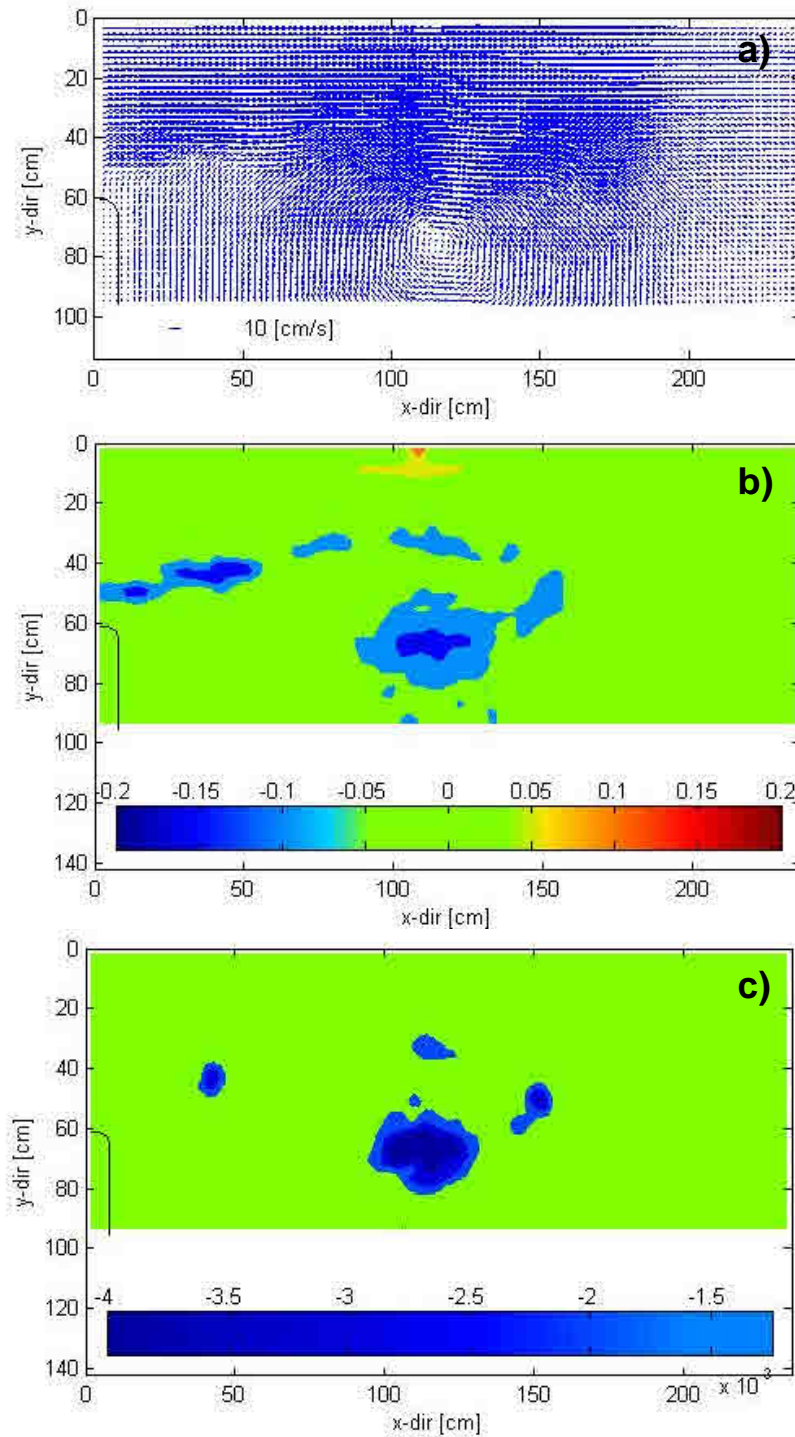


Figure 29 Example of a result for the data analysis of and image for the Life-history Type I of the idealized case: a) Velocity field; b) Vorticity field; c) Vortex formation identification.

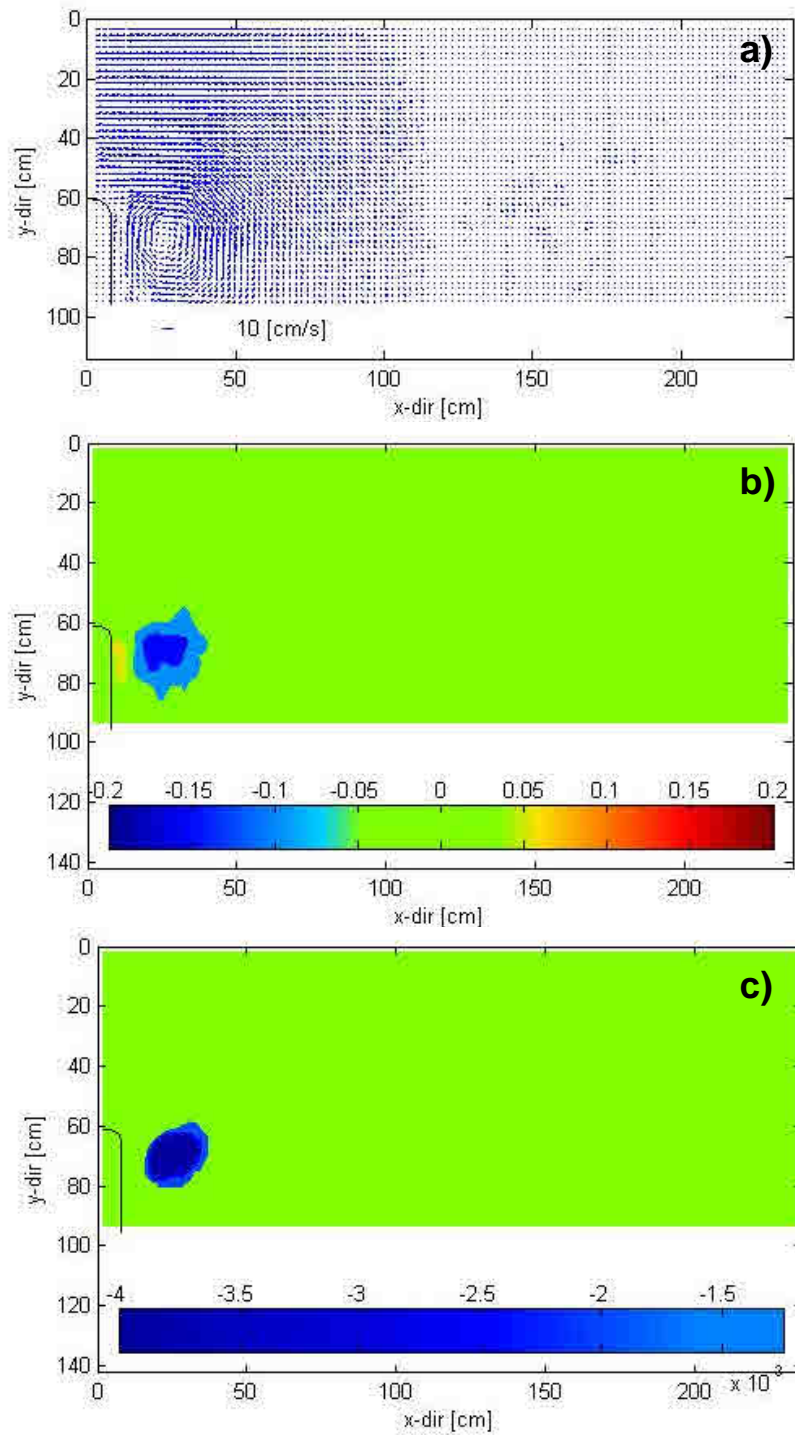


Figure 30 Example of a result for the data analysis of and image for the Life-history Type II of the idealized case: a) Velocity field; b) Vorticity field; c) Vortex formation identification.

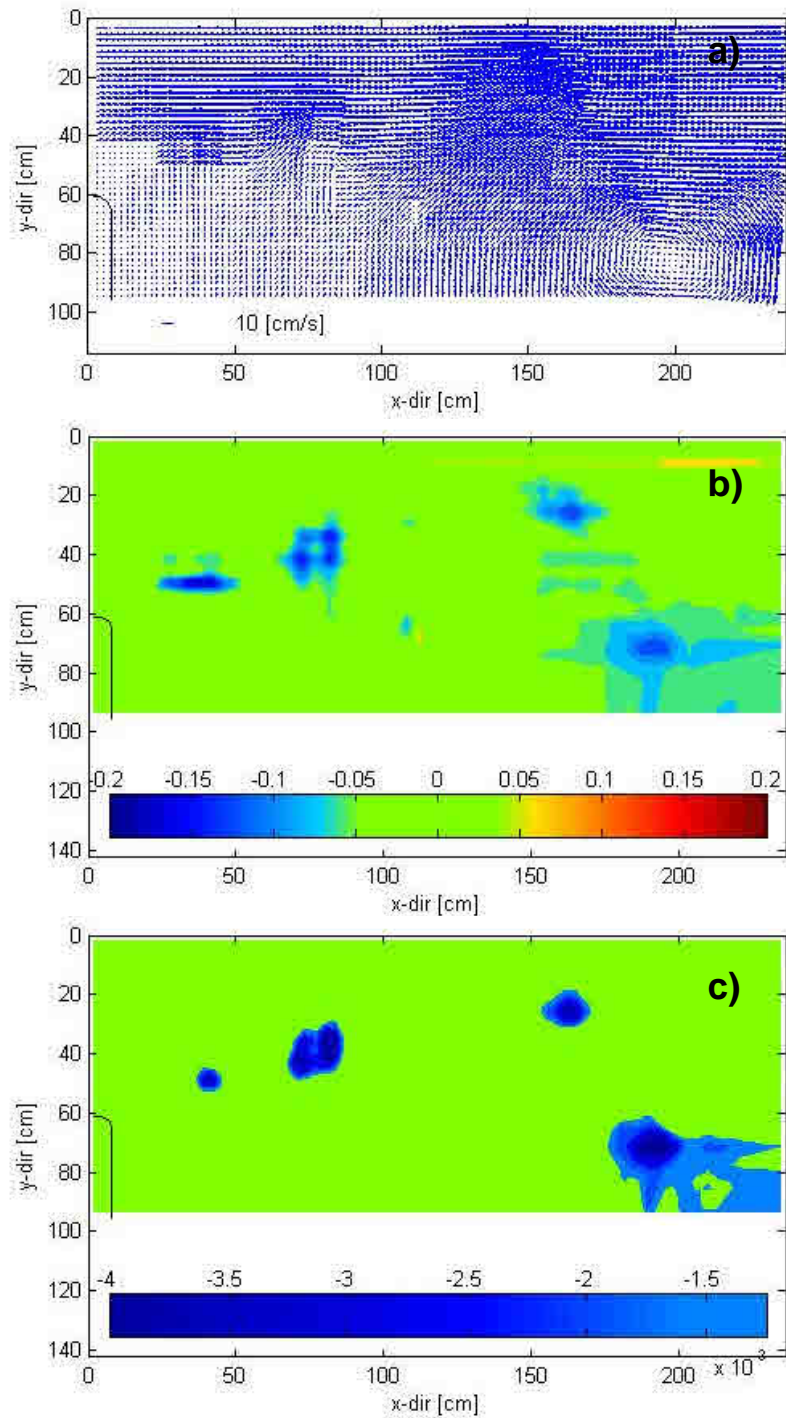


Figure 31 Example of a result for the data analysis of and image for the Life-history Type III of the idealized case: a) Velocity field; b) Vorticity field; c) Vortex formation identification.

### 3 Vortex Evolution

A series of physical parameters of the 2DCS were calculated to understand the behavior of the vortices depending of the different cases studied. The physical parameters of the vortex evolution are the following:

- Average cross sectional velocity,  $u$ .
- Longitudinal position of the center of the main vortex,  $X$ .
- Lateral position of the center of the main vortex,  $Y$ .
- Circulation around the main vortex,  $\Gamma$ .
- Maximum vorticity inside the main vortex,  $\omega_{MAX}$ .
- Equivalent diameter of the main vortex,  $D$ .
- Total upwelling generated by the main vortex,  $Q_{up}$ .
- Slopes of the growth and decay of the circulation for the first cycle, and the time that these curves start.

The Longitudinal position of the center of the vortex  $X$ , the maximum vorticity inside the main vortex  $\omega_{MAX}$ , and the equivalent diameter of the main vortex  $D$ , were previously used by Davies et al (1995).

Before computing all the physical parameters it was necessary to evaluate the real value of the mixing number  $K_W$  of each experiment, by calculating the maximum average velocity from the analyzed PIV data. The results are shown below in the Table 14.

The Experiments are defined taking in account three classifications:

- Layout
- Life-History type
- Repetition of the experiment (or angle of the inlet for Layout H)



Table 14 Nominal and real values of the mixing number  $K_w$ , and maximum cross sectional average velocity over a tidal cycle for the first and the following cycles of each experiment.

LAYOUT	LIFE-HISTORY TYPE		$K_w$ NOMINAL VALUE	MAXIMUM VELOCITY		$K_w$ REAL VALUE	
				1 <sup>st</sup> Cycle	Following Cycles	1 <sup>st</sup> Cycle	Following Cycles
			□	[m/s]	[m/s]	□	□
A	I	1	0.11	0.19	0.23	0.11	0.09
	I	2	0.11	0.19	0.22	0.11	0.10
	II	1	0.06	0.22	0.19	0.05	0.06
	II	2	0.06	0.19	0.18	0.06	0.06
	III	1	0.26	0.12	0.16	0.27	0.19
	III	2	0.26	0.11	0.16	0.29	0.19
B	I	1	0.11	0.20	0.24	0.11	0.09
	I	2	0.11	0.18	0.24	0.12	0.09
	II	1	0.06	0.18	0.20	0.06	0.06
	II	2	0.06	0.17	0.18	0.07	0.06
	III	1	0.26	0.07	0.15	0.44	0.22
	III	2	0.26	0.09	0.16	0.35	0.19
C	I	1	0.11	0.16	0.22	0.13	0.10
	I	2	0.11	0.16	0.22	0.13	0.10
	II	1	0.06	0.20	0.18	0.06	0.06
	II	2	0.06	0.18	0.19	0.06	0.06
	III	1	0.26	0.07	0.15	0.44	0.21
D	I	1	0.11	0.20	0.27	0.11	0.08
	I	2	0.11	0.20	0.25	0.11	0.08
	II	1	0.06	0.20	0.21	0.06	0.06
	II	2	0.06	0.20	0.20	0.06	0.06
	III	1	0.26	0.06	0.15	0.50	0.22
	III	2	0.26	0.07	0.14	0.44	0.23
E	I	1	0.11	0.19	0.22	0.11	0.10
	I	2	0.11	0.19	0.22	0.11	0.10
F	I	1	0.11	0.19	0.22	0.11	0.10
	I	2	0.11	0.19	0.22	0.11	0.10
G	I	1	0.11	0.19	0.22	0.11	0.10
	I	2	0.11	0.19	0.22	0.11	0.10
H	I	10	0.11	0.20	0.23	0.11	0.10
	I	20	0.11	0.21	0.23	0.10	0.09

Using the real values of the mixing number and the maximum average velocity, the physical parameters were non-dimensionalized. The characteristic length scales used were, the tidal period  $T$ , the width of the inlet  $W$ , the average cross sectional maximum velocity over a tidal cycle  $U$ , and the depth of the basin  $h$ . The parameters are shown in the Table 15.

Table 15 Non-dimensional factors used for the calculation of the physical parameters of the vortex evolution

PHYSICAL PARAMETER	NON-DIMENSIONAL PARAMETER
$u$	$u^* = u / U$
$X$	$X^* = X / UT$
$Y$	$Y^* = Y / UT$
$\Gamma$	$\Gamma^* = \Gamma / UW$
$\omega_{MAX}$	$\omega_{MAX}^* = \omega_{MAX} W / U$
$D$	$D^* = D / UT$
$Q_{up}$	$Q_{up}^* = Q_{up} / (UWh / \pi)$

The value of  $U$  varies depending on which cycle the calculation is made.

As the physical parameters were calculated in time series evolution, it was necessary to non-dimensionalize the time scale too.

$$t^* = tU / W \quad (26)$$

In this case the value of  $U$  was taken as the average of the maximum average velocities of the tidal cycles in each experiment.

The first cycle was analyzed in more detail because the data obtained from the PIV analysis had a better quality and less noise than the rest of the cycles. This is because the seeding for the first cycle had a better quality than the rest of the experiments. But not for all experiments this is true, that is why the first cycle is not investigated for all experiments.

## Results

The following Figures show the results of the calculation of the physical parameters of the vortex evolution.

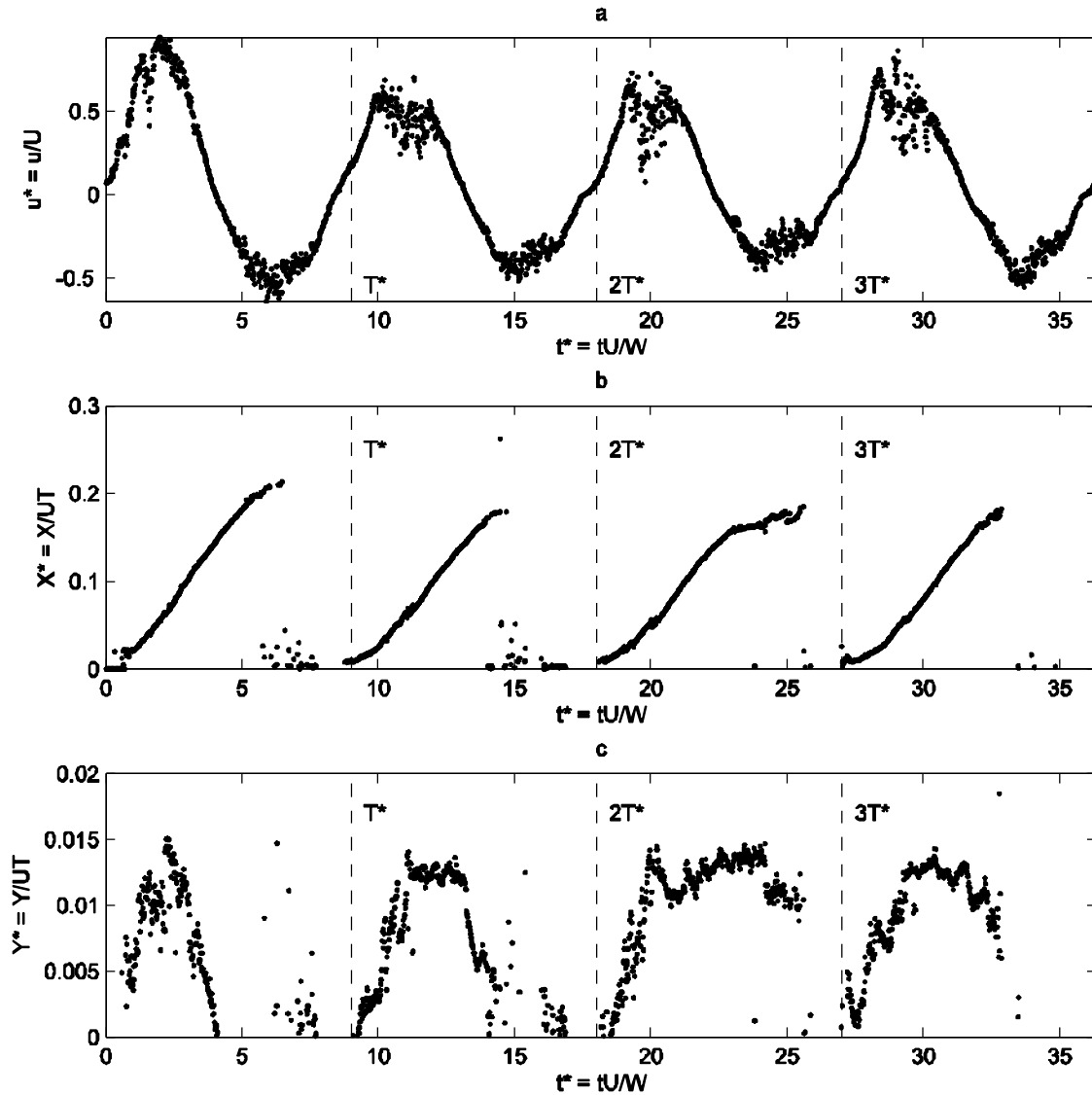


Figure 32 Life-history Type I for Layout A, repetition 1: a) Average cross sectional velocity at the mouth of the inlet. b) Longitudinal position of the center of the main vortex starting from the edge of the barrier island. c) Lateral position of the center of the main vortex starting from the edge of the barrier island.

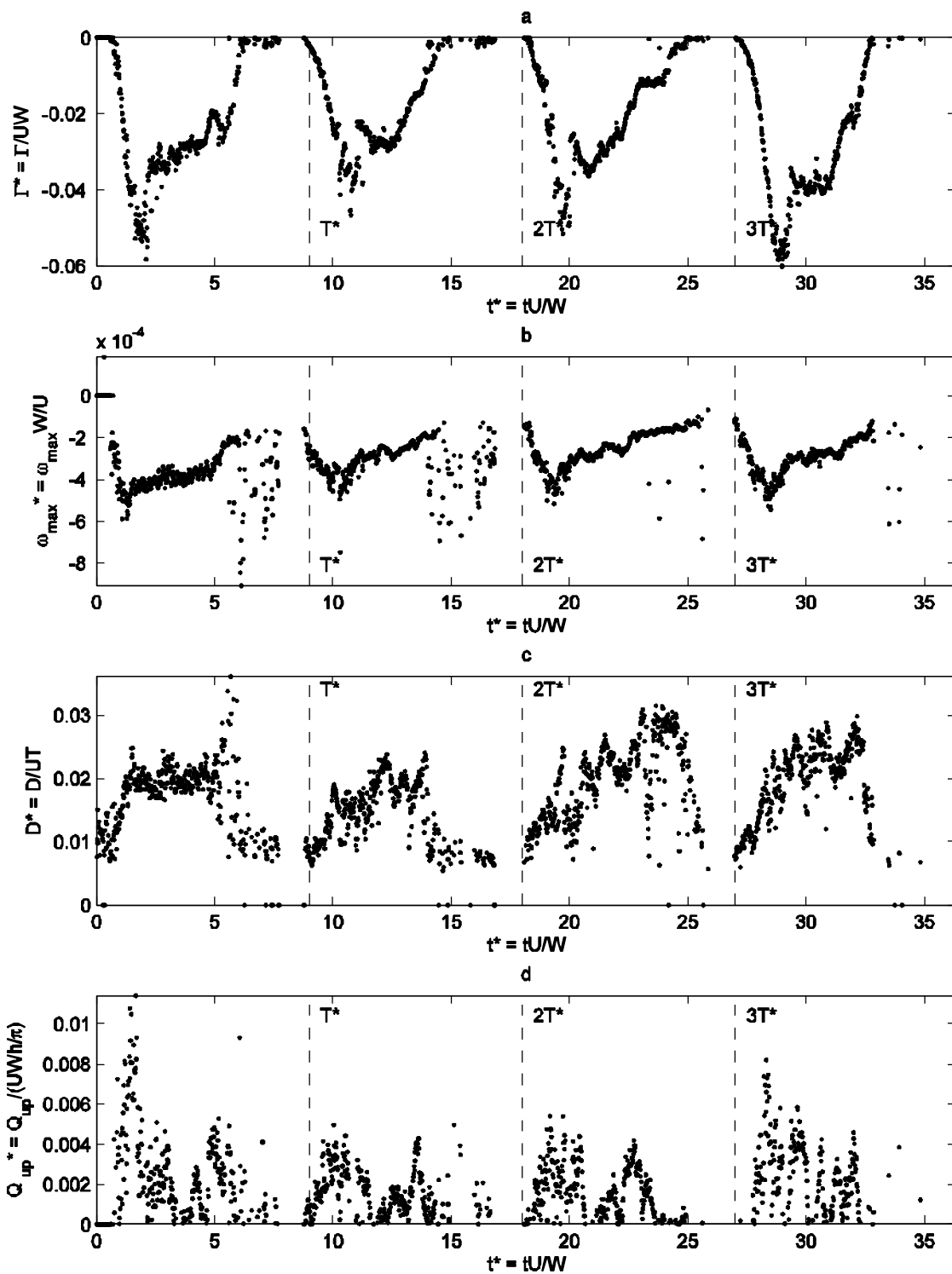


Figure 33 Life-history Type I for Layout A, repetition 1: a) Circulation around the main vortex b) Maximum vorticity in the main vortex c) Equivalent diameter of the main vortex. d) Upwelling flowing from the main vortex.

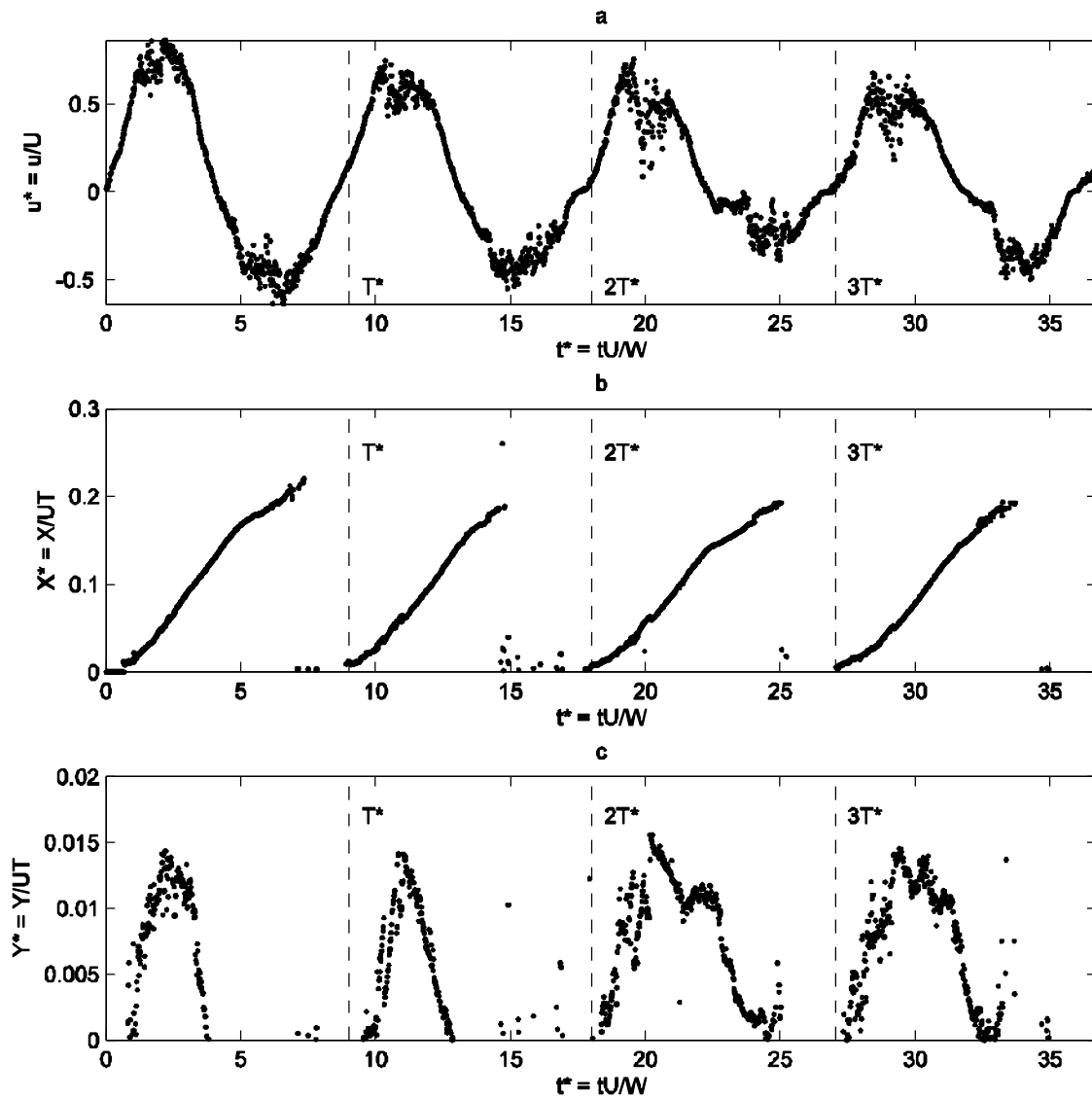


Figure 34 Life-history Type I for Layout A, repetition 2: a) Average cross sectional velocity at the mouth of the inlet. b) Longitudinal position of the center of the main vortex starting from the edge of the barrier island. c) Lateral position of the center of the main vortex starting from the edge of the barrier island.

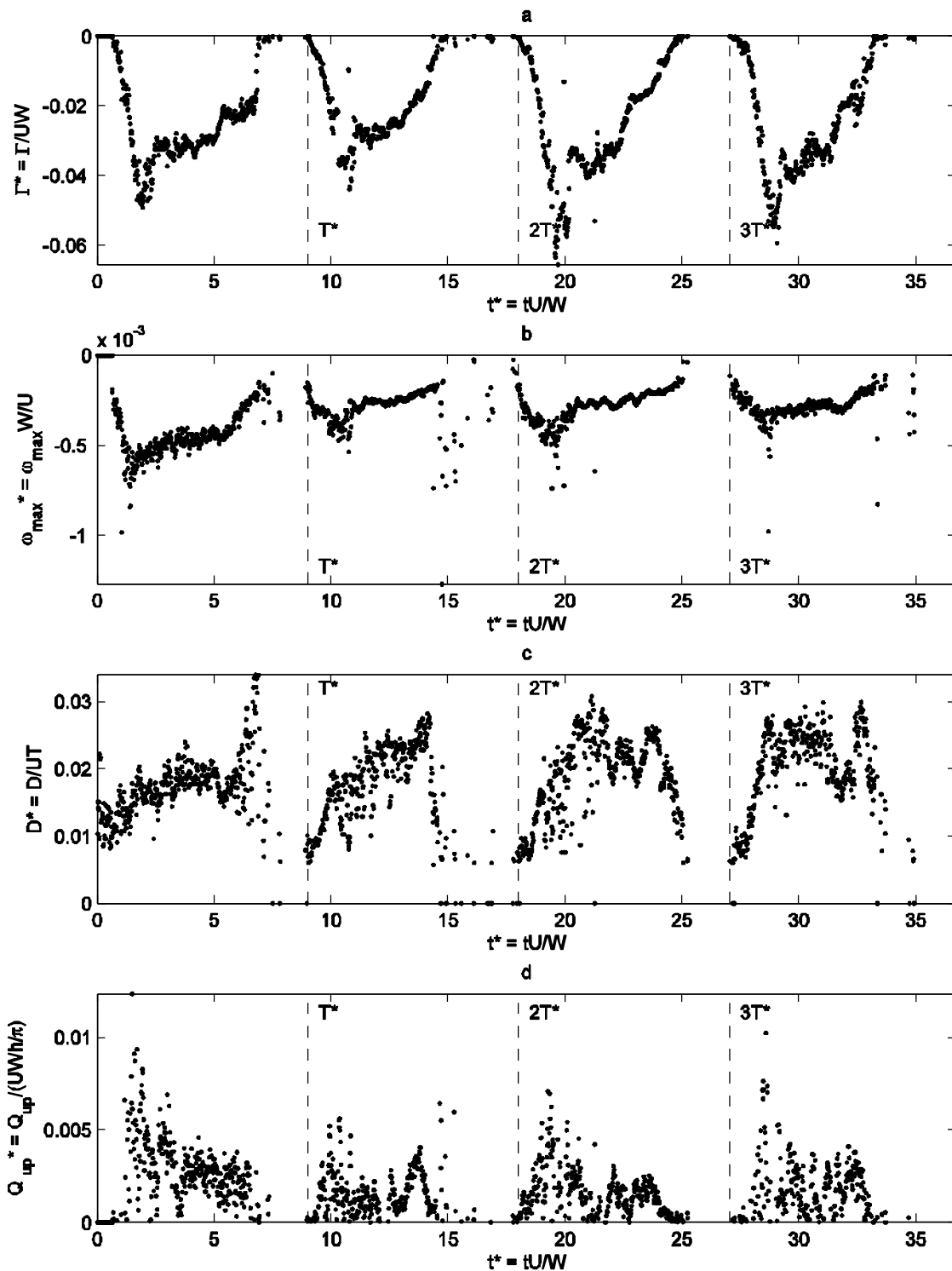


Figure 35 Life-history Type I for Layout A, repetition 2: a) Circulation around the main vortex b) Maximum vorticity in the main vortex c) Equivalent diameter of the main vortex. d) Upwelling flowing from the main vortex.

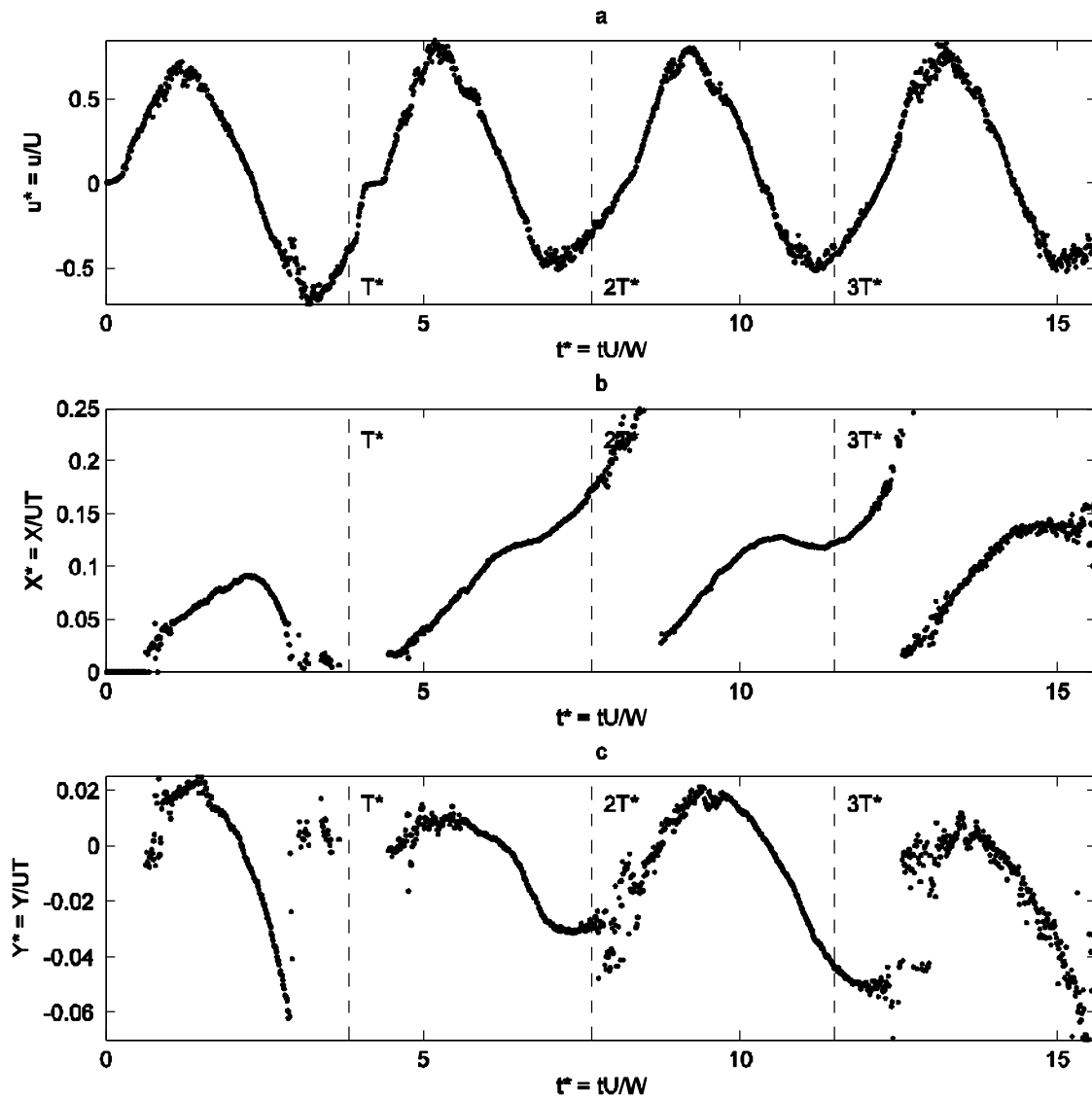


Figure 36 Life-history Type II for Layout A, repetition 1: a) Average cross sectional velocity at the mouth of the inlet. b) Longitudinal position of the center of the main vortex starting from the edge of the barrier island. c) Lateral position of the center of the main vortex starting from the edge of the barrier island.



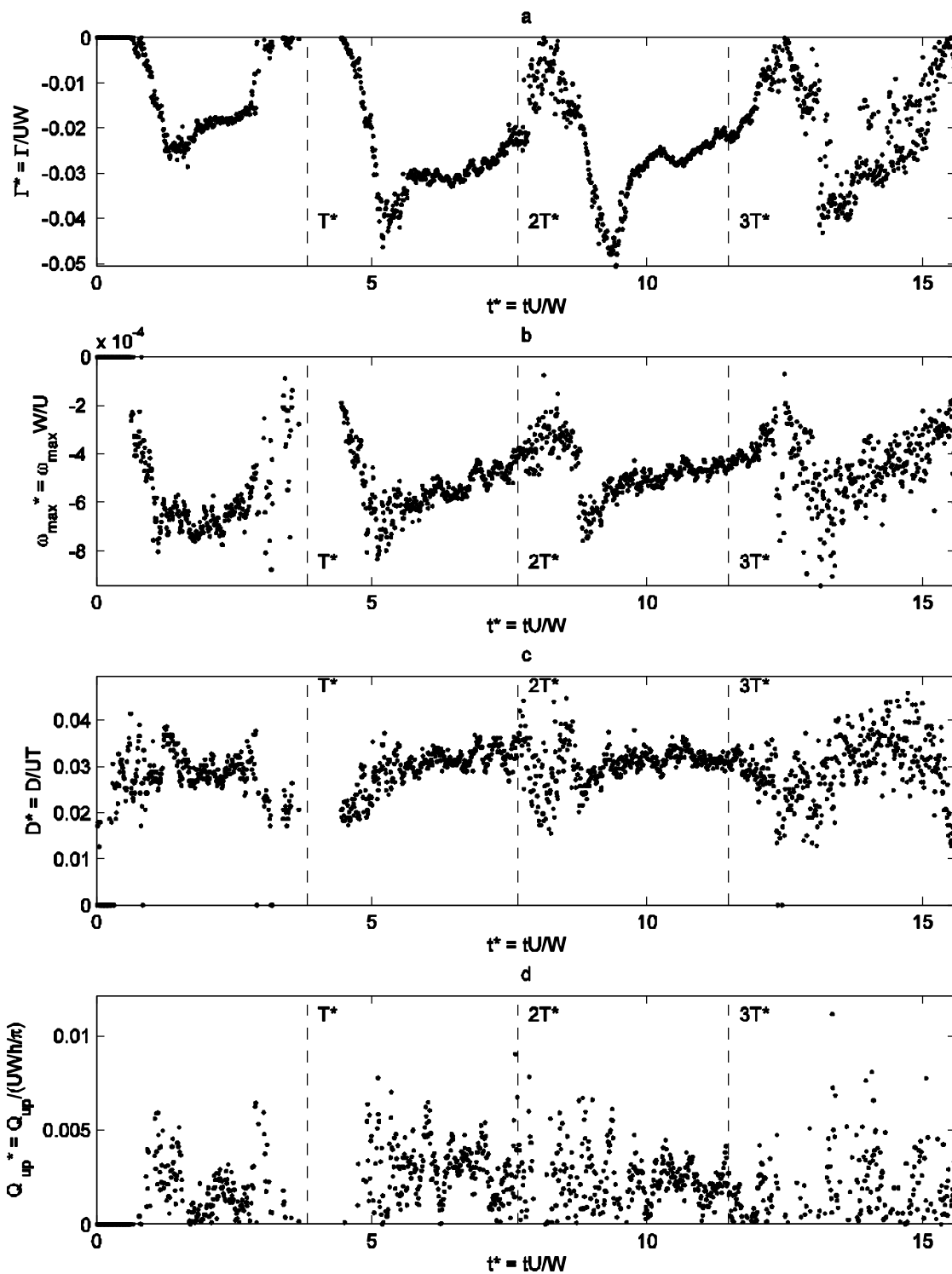


Figure 37 Life-history Type II for Layout A, repetition 1: a) Circulation around the main vortex b) Maximum vorticity in the main vortex c) Equivalent diameter of the main vortex. d) Upwelling flowing from the main vortex.

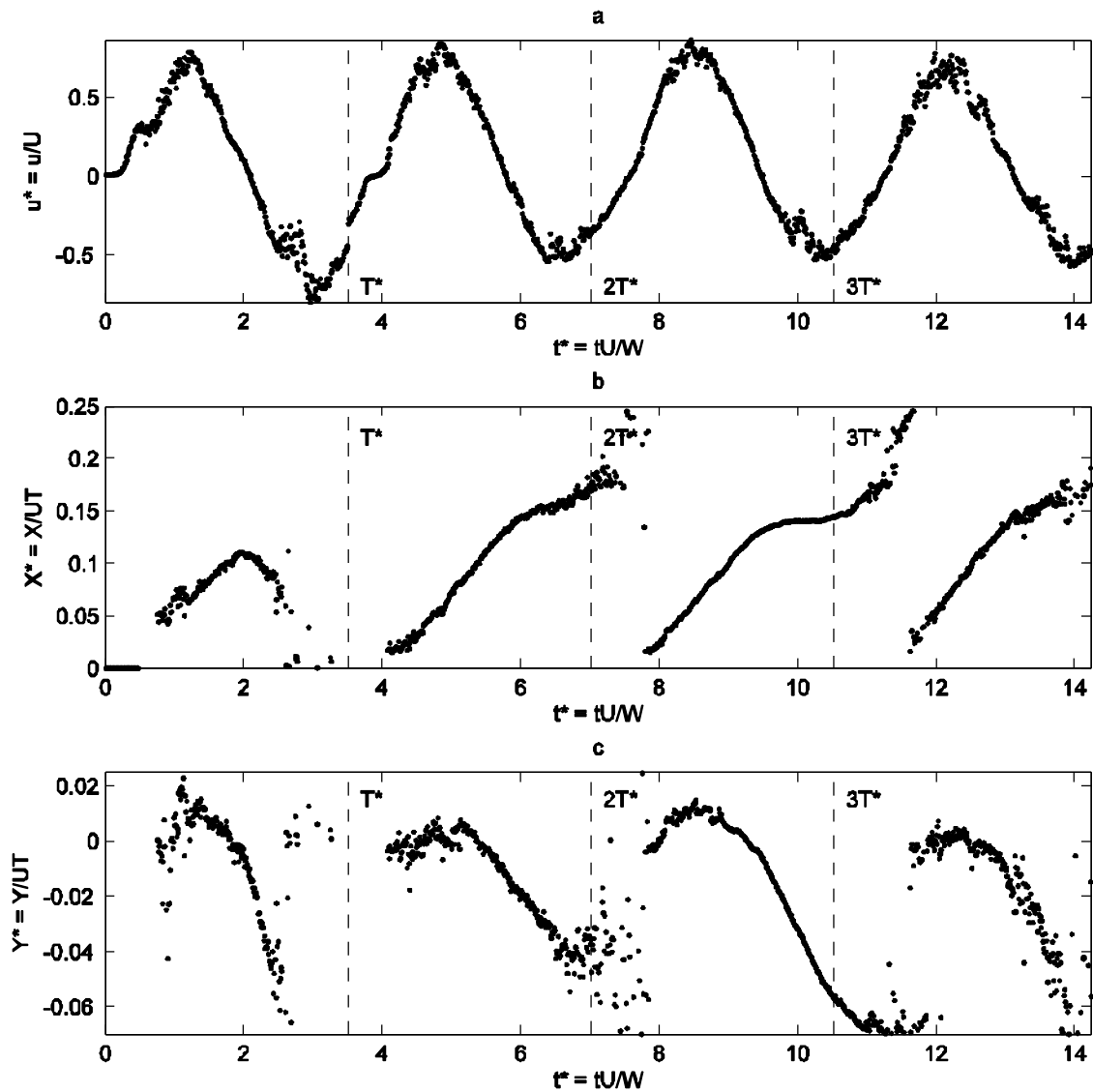


Figure 38 Life-history Type II for Layout A, repetition 2: a) Average cross sectional velocity at the mouth of the inlet. b) Longitudinal position of the center of the main vortex starting from the edge of the barrier island. c) Lateral position of the center of the main vortex starting from the edge of the barrier island.

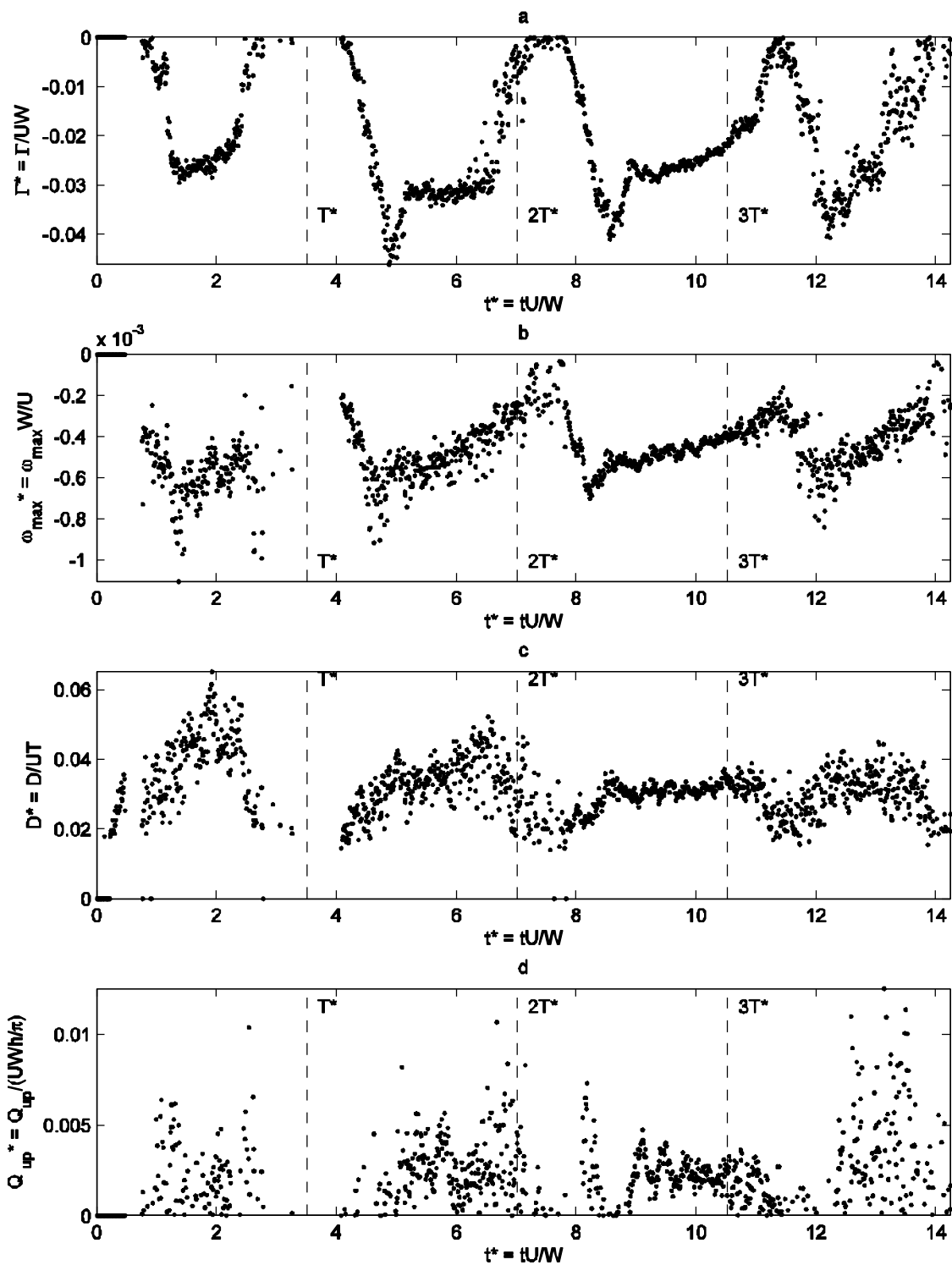


Figure 39 Life-history Type II for Layout A, repetition 2: a) Circulation around the main vortex b) Maximum vorticity in the main vortex c) Equivalent diameter of the main vortex. d) Upwelling flowing from the main vortex.

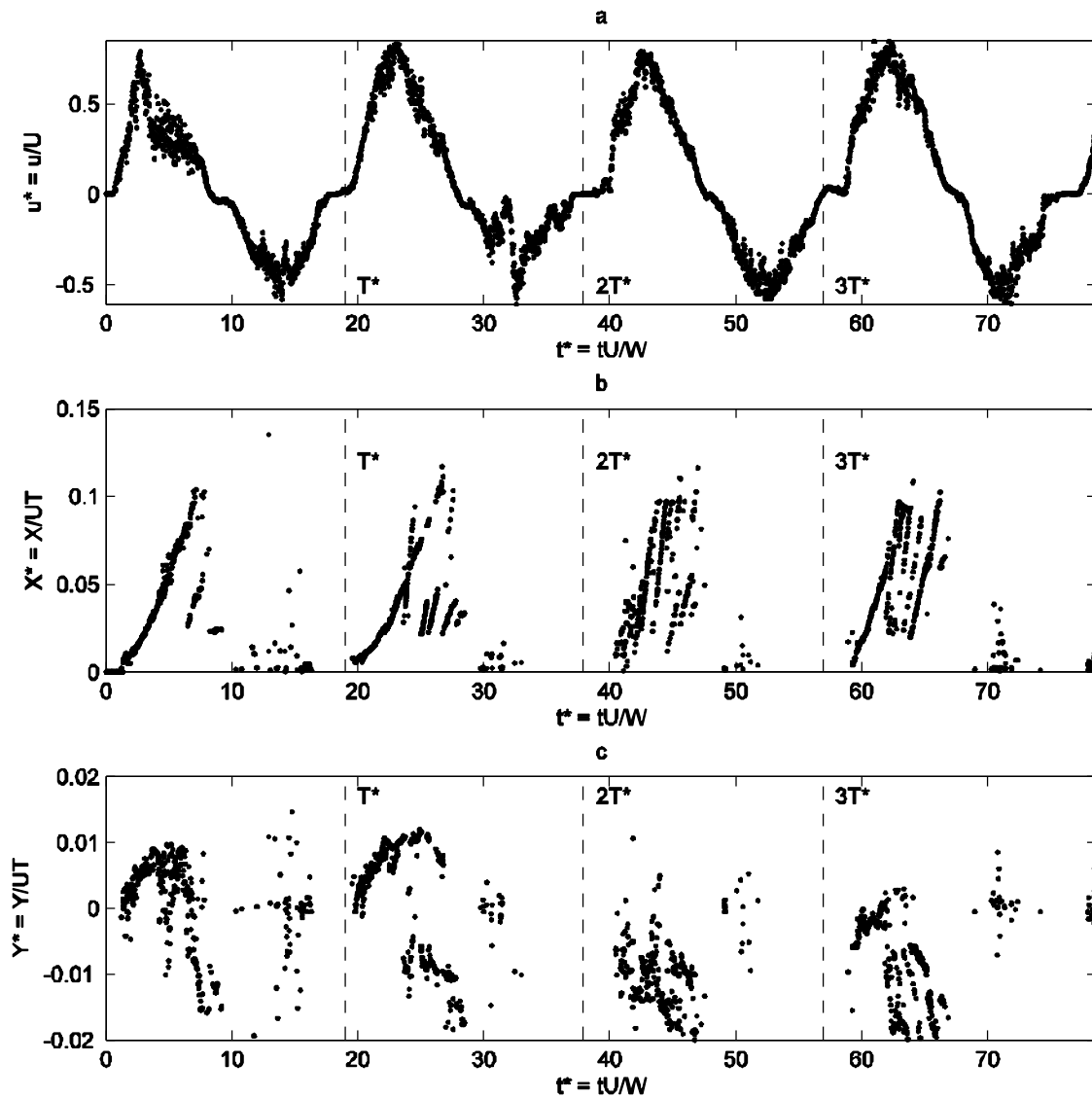


Figure 40 Life-history Type III for Layout A, repetition 1: a) Average cross sectional velocity at the mouth of the inlet. b) Longitudinal position of the center of the main vortex starting from the edge of the barrier island. c) Lateral position of the center of the main vortex starting from the edge of the barrier island.

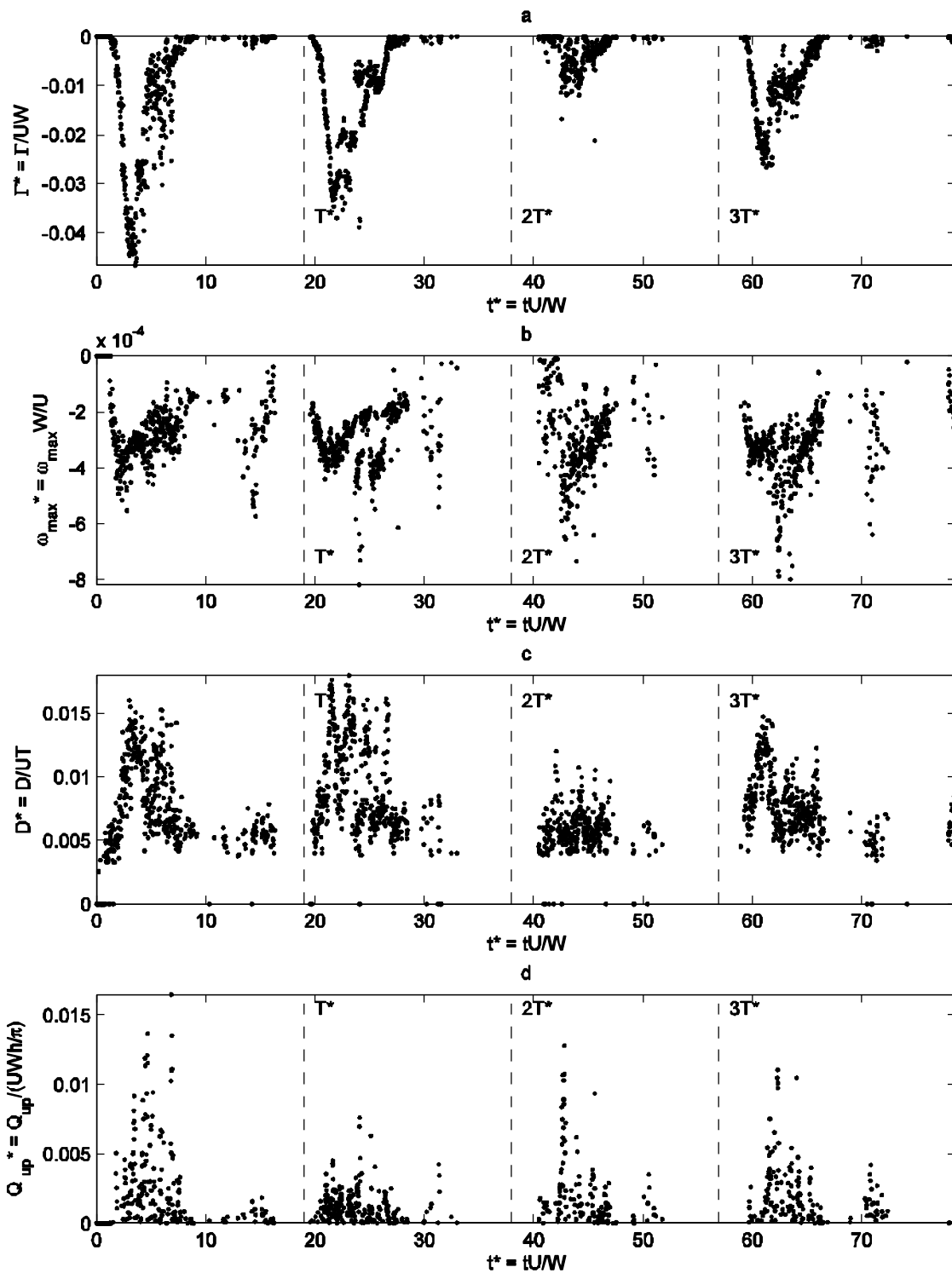


Figure 41 Life-history Type III for Layout A, repetition 1: a) Circulation around the main vortex b) Maximum vorticity in the main vortex c) Equivalent diameter of the main vortex. d) Upwelling flowing from the main vortex.

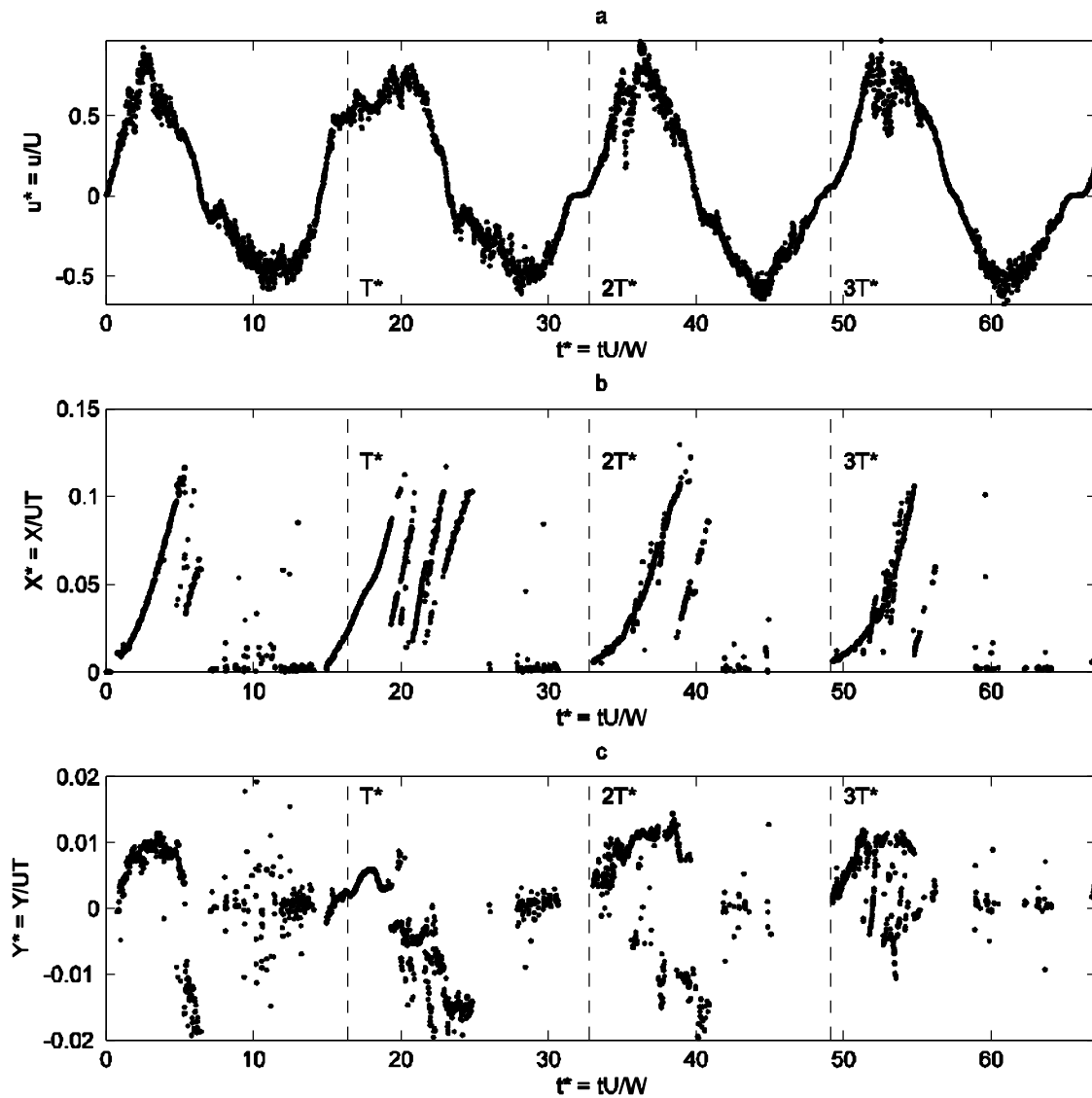


Figure 42 Life-history Type III for Layout A, repetition 2: a) Average cross sectional velocity at the mouth of the inlet. b) Longitudinal position of the center of the main vortex starting from the edge of the barrier island. c) Lateral position of the center of the main vortex starting from the edge of the barrier island.

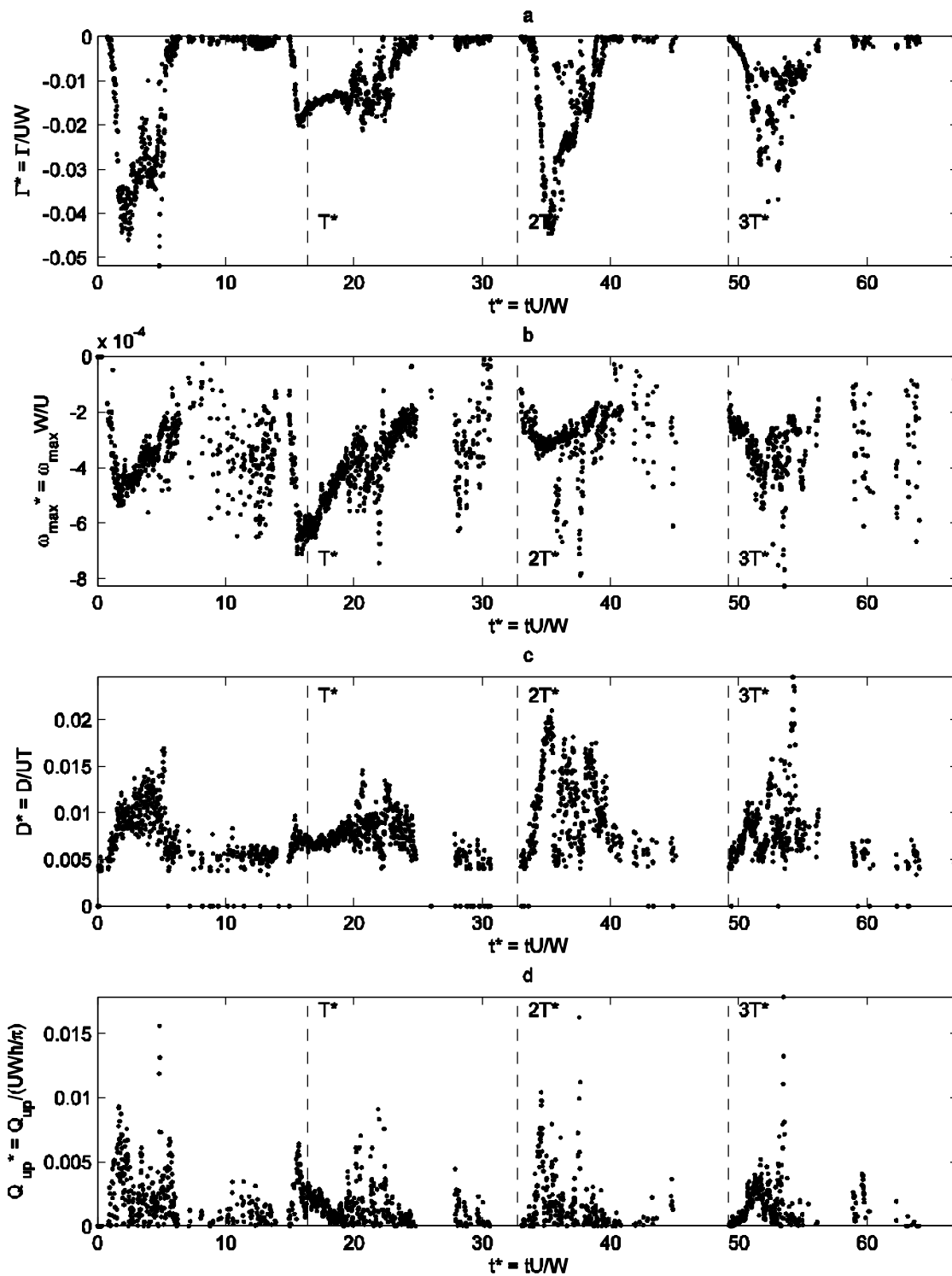


Figure 43 Life-history Type III for Layout A, repetition 2: a) Circulation around the main vortex b) Maximum vorticity in the main vortex c) Equivalent diameter of the main vortex. d) Upwelling flowing from the main vortex.

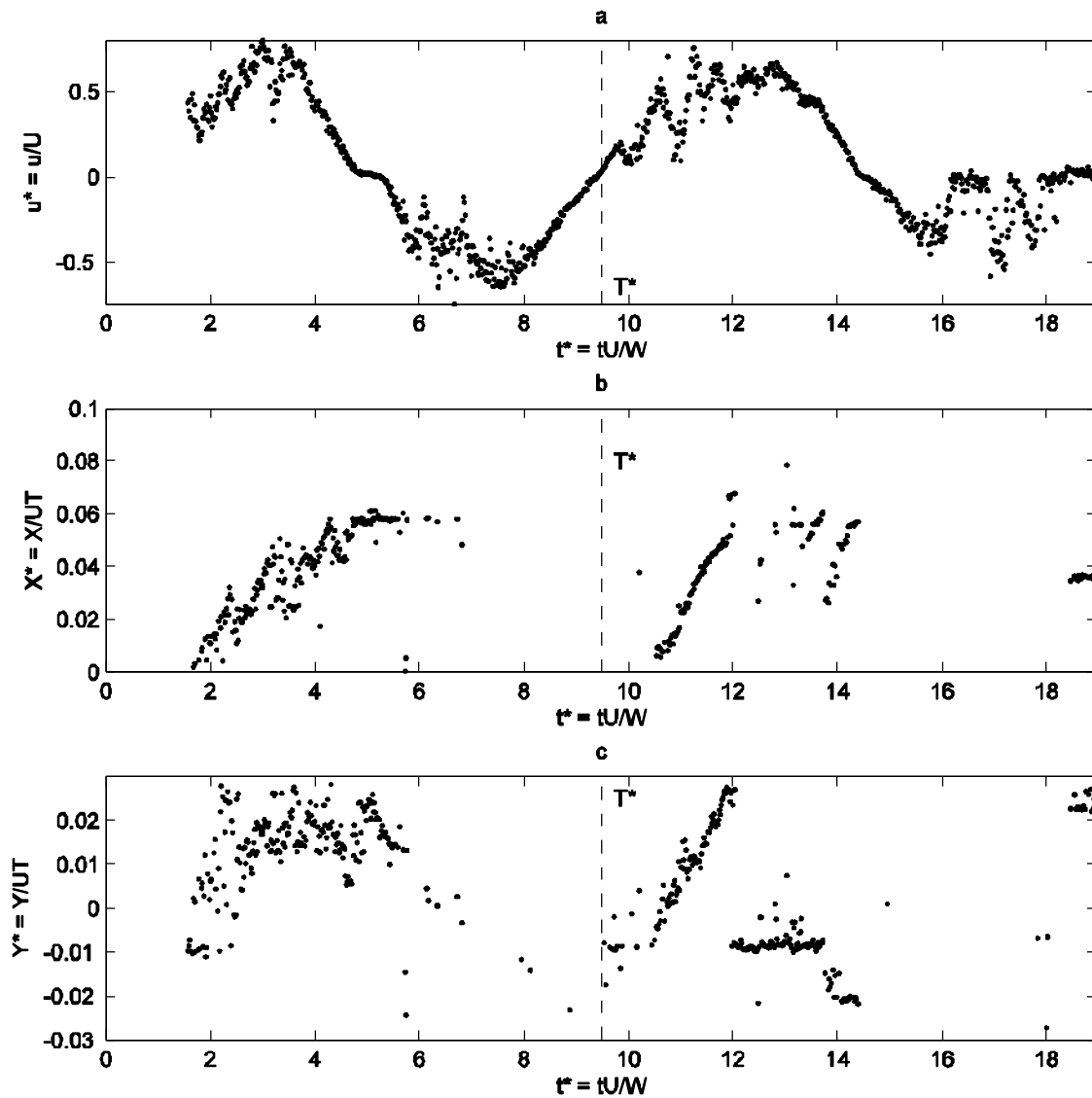


Figure 44 Life-history Type I for Layout B, repetition 1: a) Average cross sectional velocity at the mouth of the inlet. b) Longitudinal position of the center of the main vortex starting from the edge of the barrier island. c) Lateral position of the center of the main vortex starting from the edge of the barrier island.



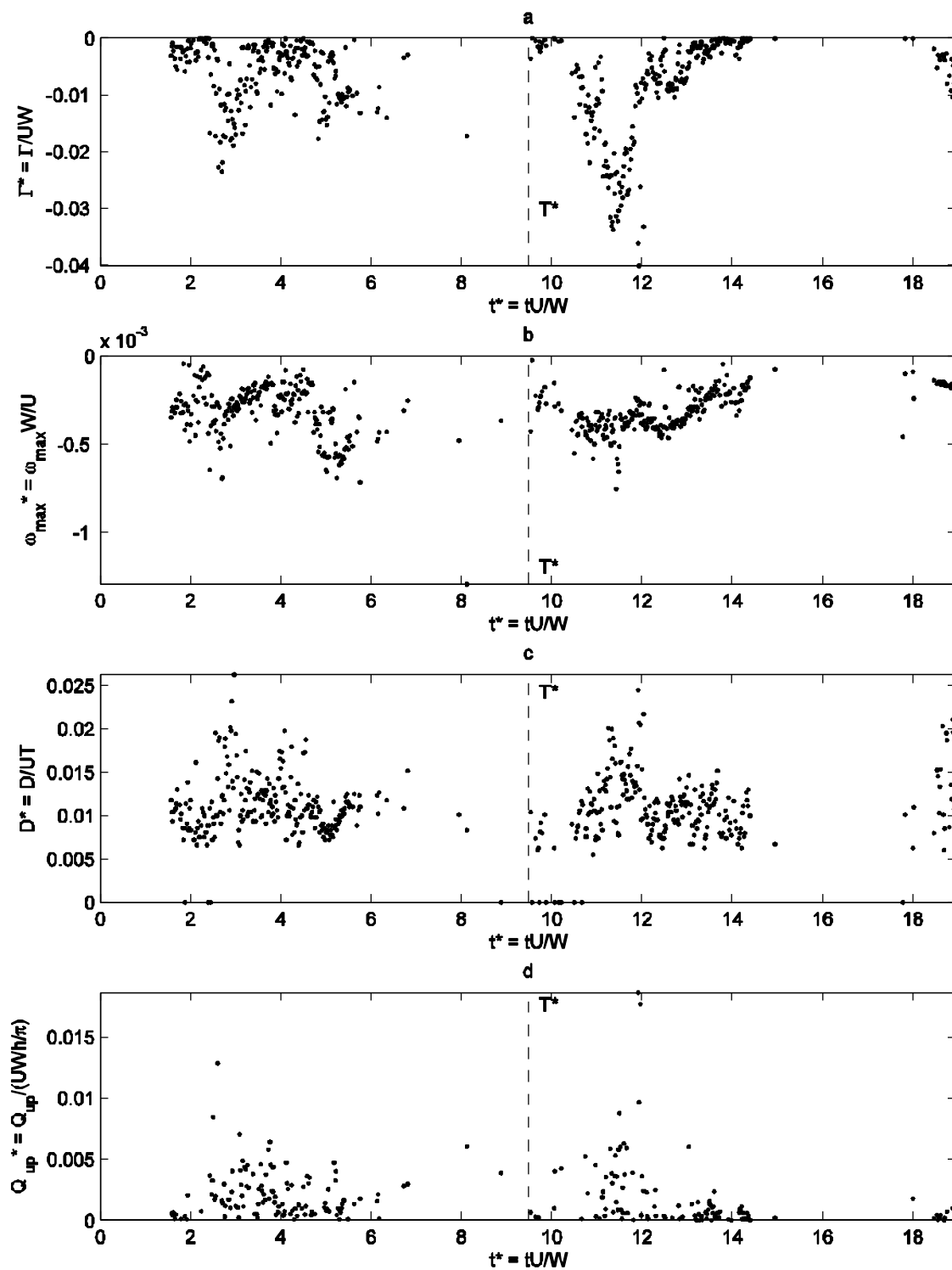


Figure 45 Life-history Type I for Layout B, repetition 1: a) Circulation around the main vortex b) Maximum vorticity in the main vortex c) Equivalent diameter of the main vortex. d) Upwelling flowing from the main vortex.

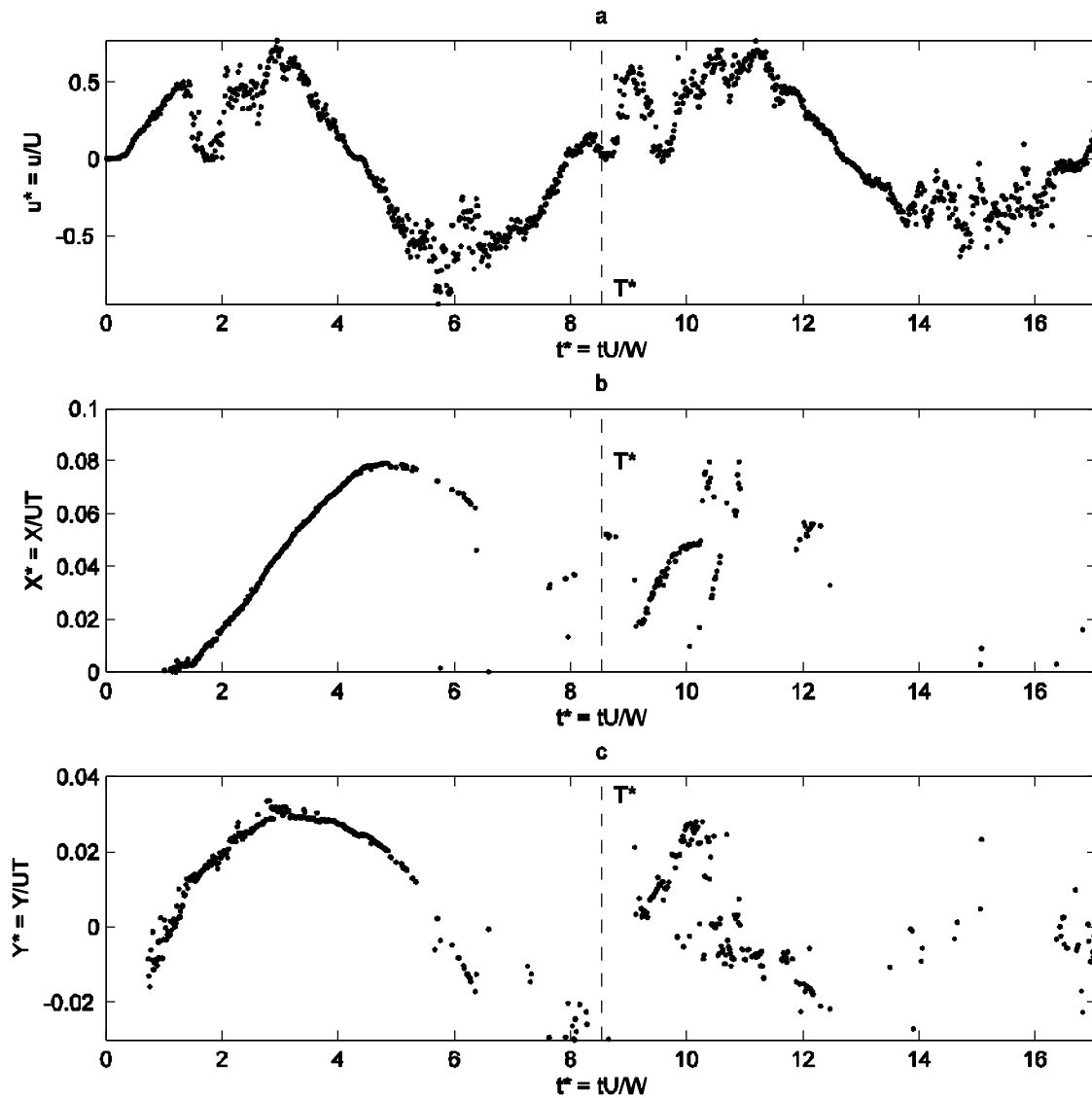


Figure 46 Life-history Type I for Layout B, repetition 2: a) Average cross sectional velocity at the mouth of the inlet. b) Longitudinal position of the center of the main vortex starting from the edge of the barrier island. c) Lateral position of the center of the main vortex starting from the edge of the barrier island.

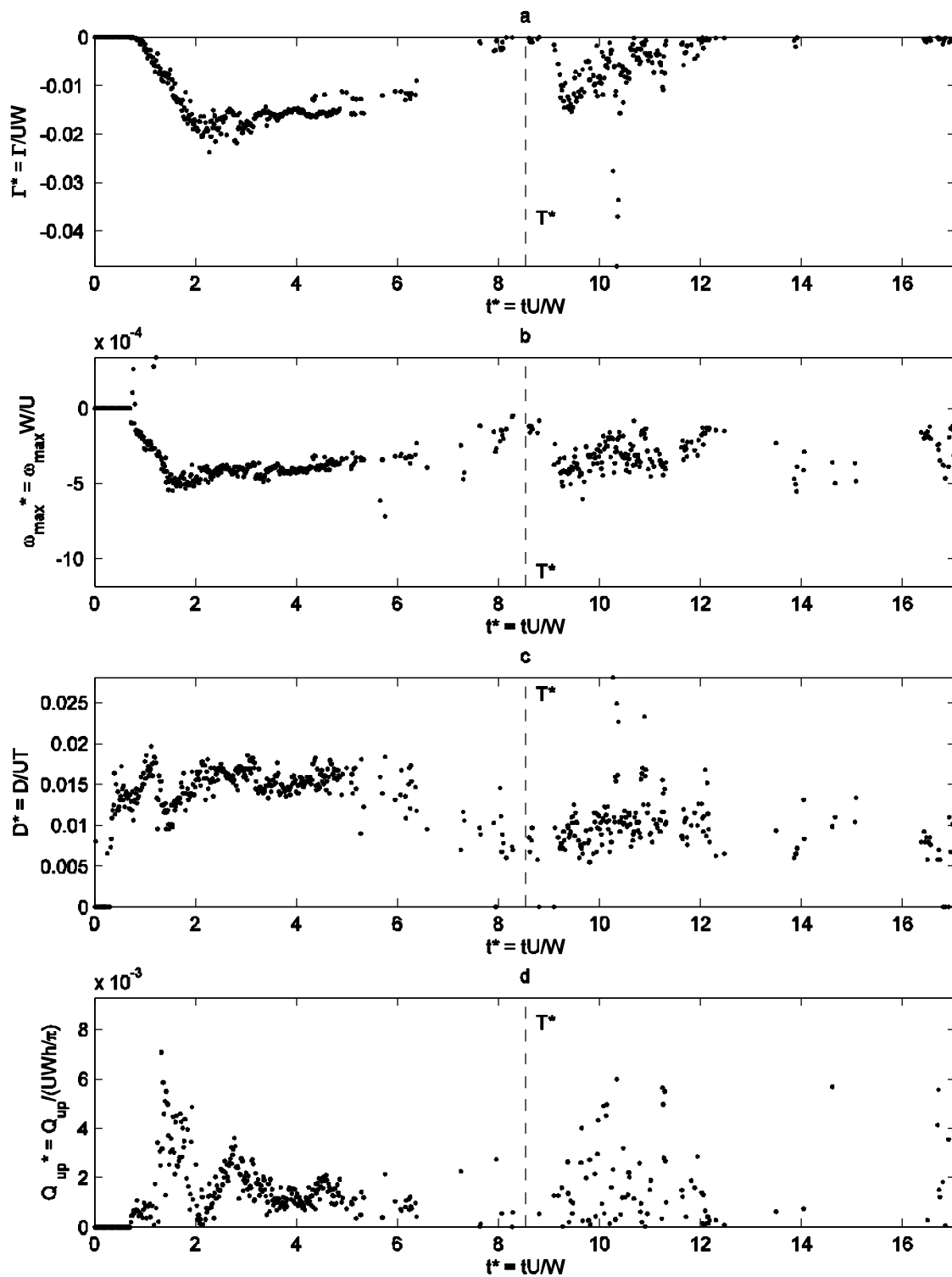


Figure 47 Life-history Type I for Layout B, repetition 2: a) Circulation around the main vortex b) Maximum vorticity in the main vortex c) Equivalent diameter of the main vortex. d) Upwelling flowing from the main vortex.

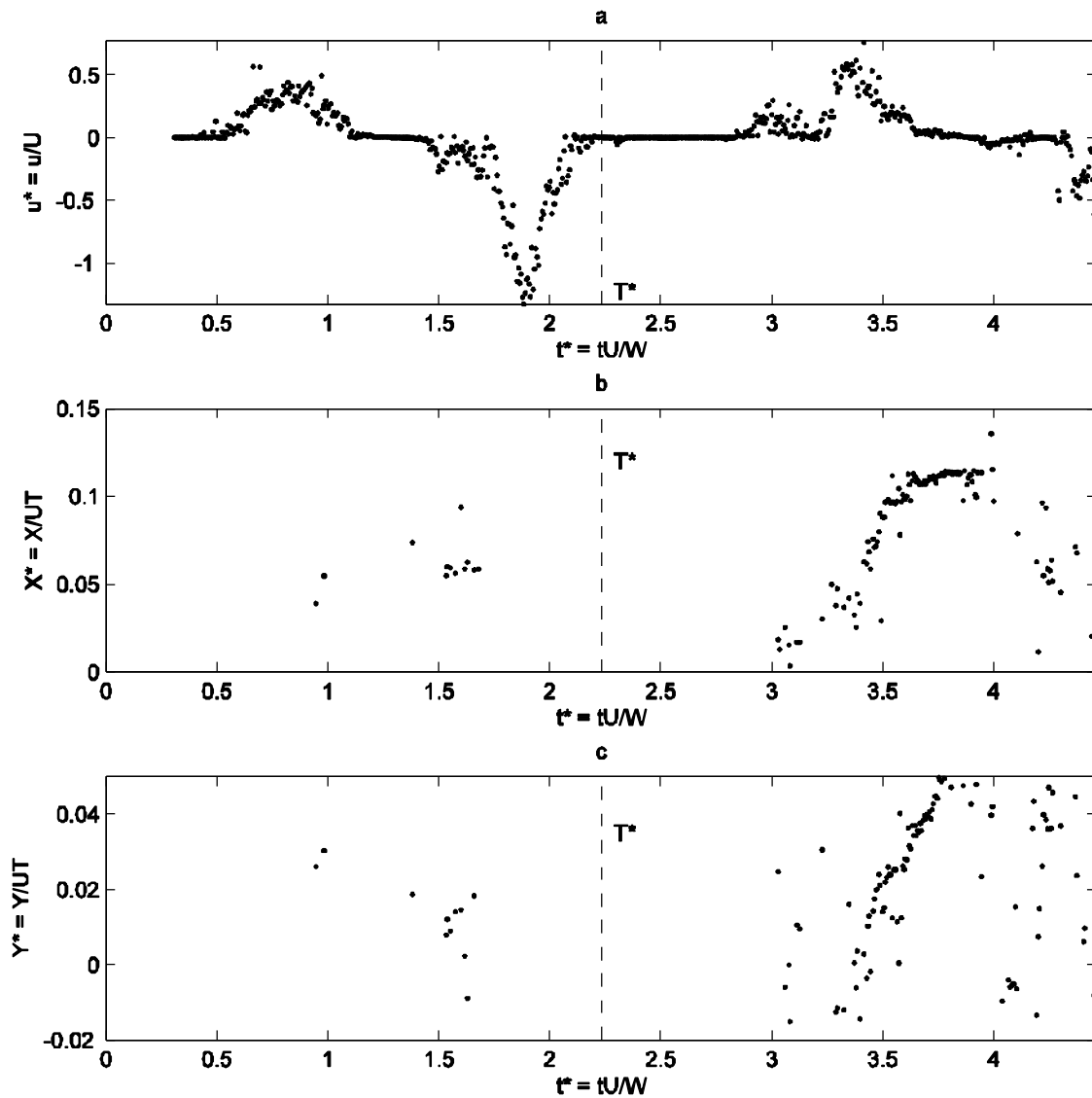


Figure 48 Life-history Type II for Layout B, repetition 1: a) Average cross sectional velocity at the mouth of the inlet. b) Longitudinal position of the center of the main vortex starting from the edge of the barrier island. c) Lateral position of the center of the main vortex starting from the edge of the barrier island.

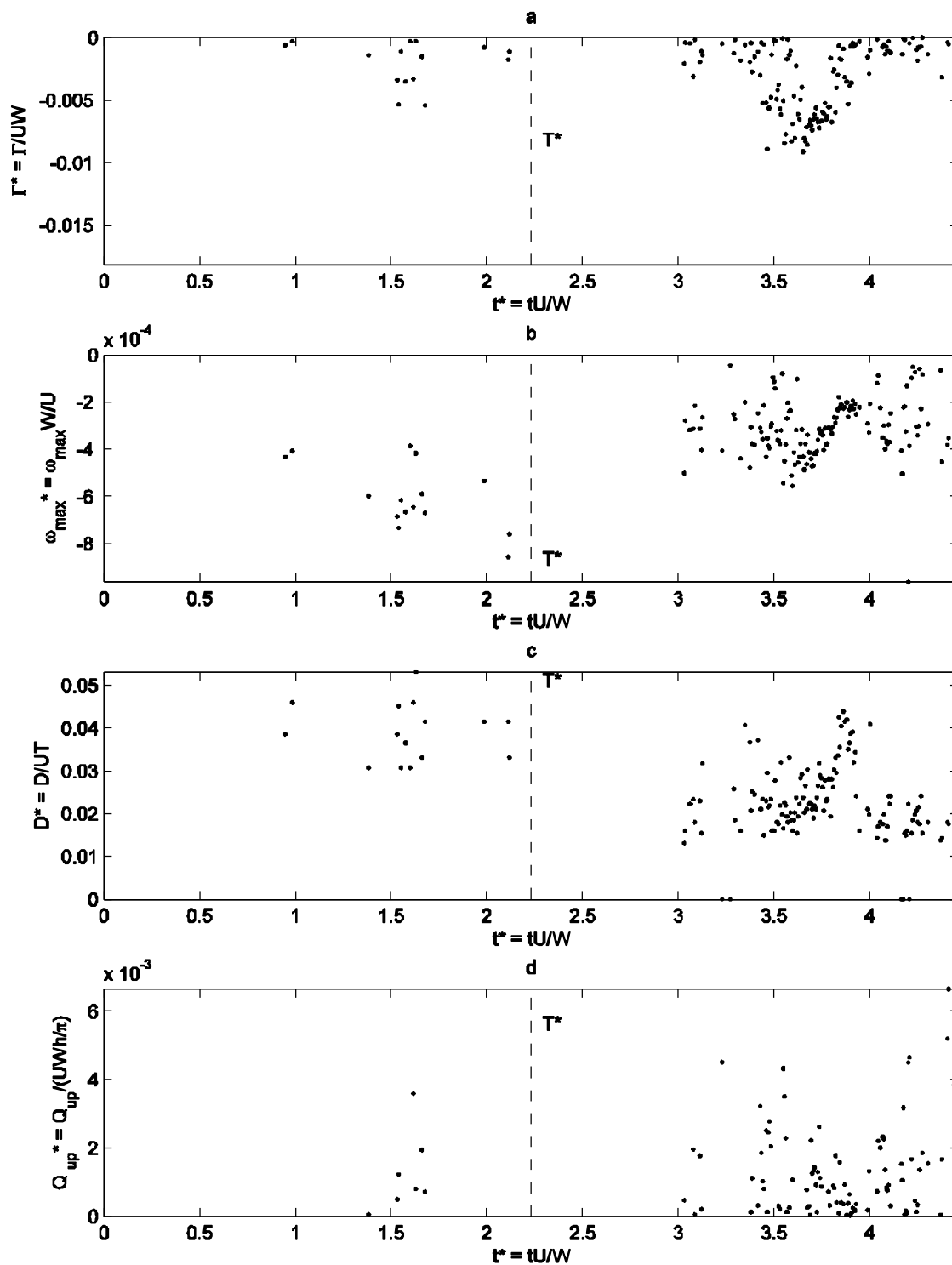


Figure 49 Life-history Type II for Layout B, repetition 1: a) Circulation around the main vortex b) Maximum vorticity in the main vortex c) Equivalent diameter of the main vortex. d) Upwelling flowing from the main vortex.

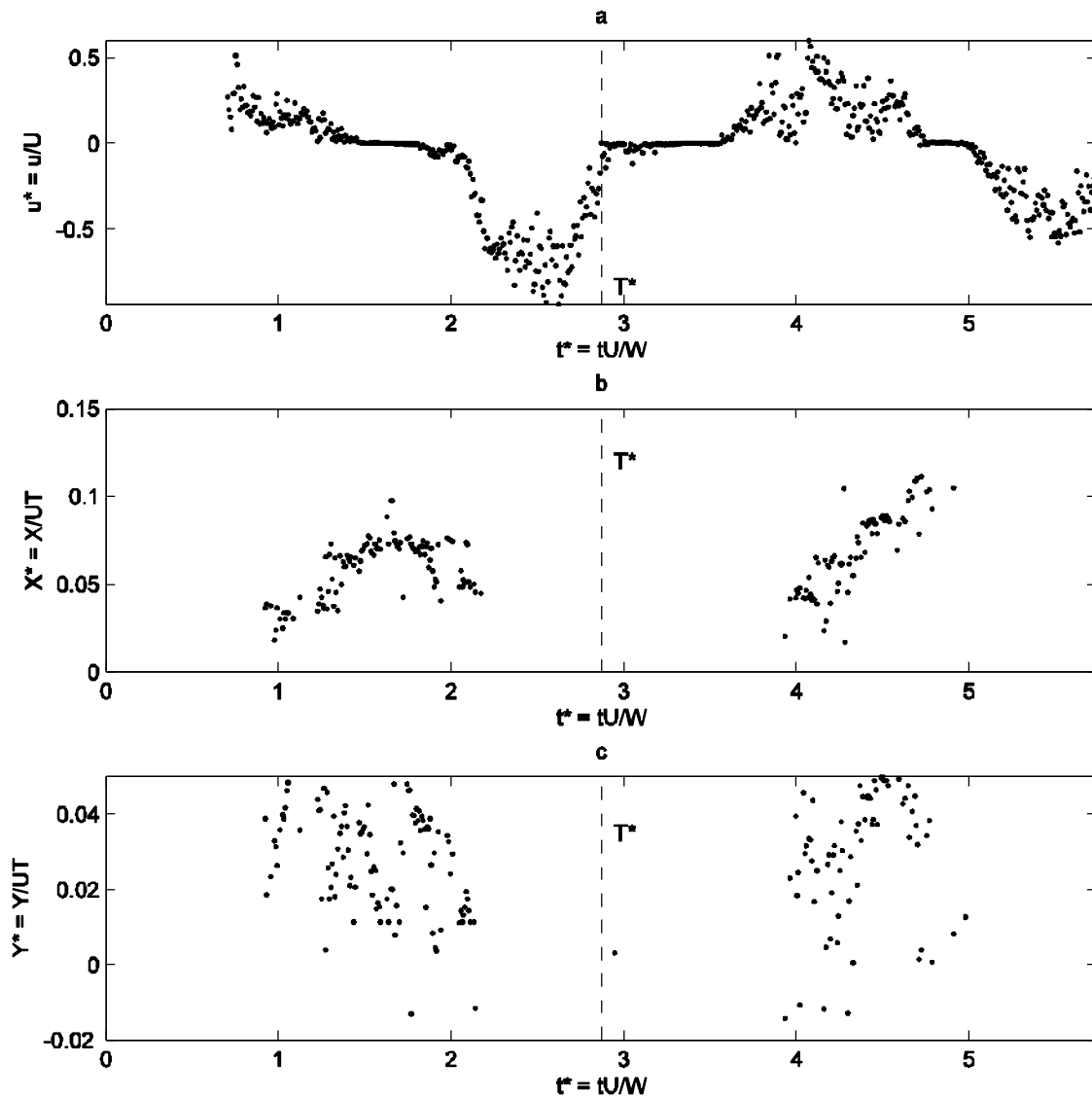


Figure 50 Life-history Type II for Layout B, repetition 2: a) Average cross sectional velocity at the mouth of the inlet. b) Longitudinal position of the center of the main vortex starting from the edge of the barrier island. c) Lateral position of the center of the main vortex starting from the edge of the barrier island.

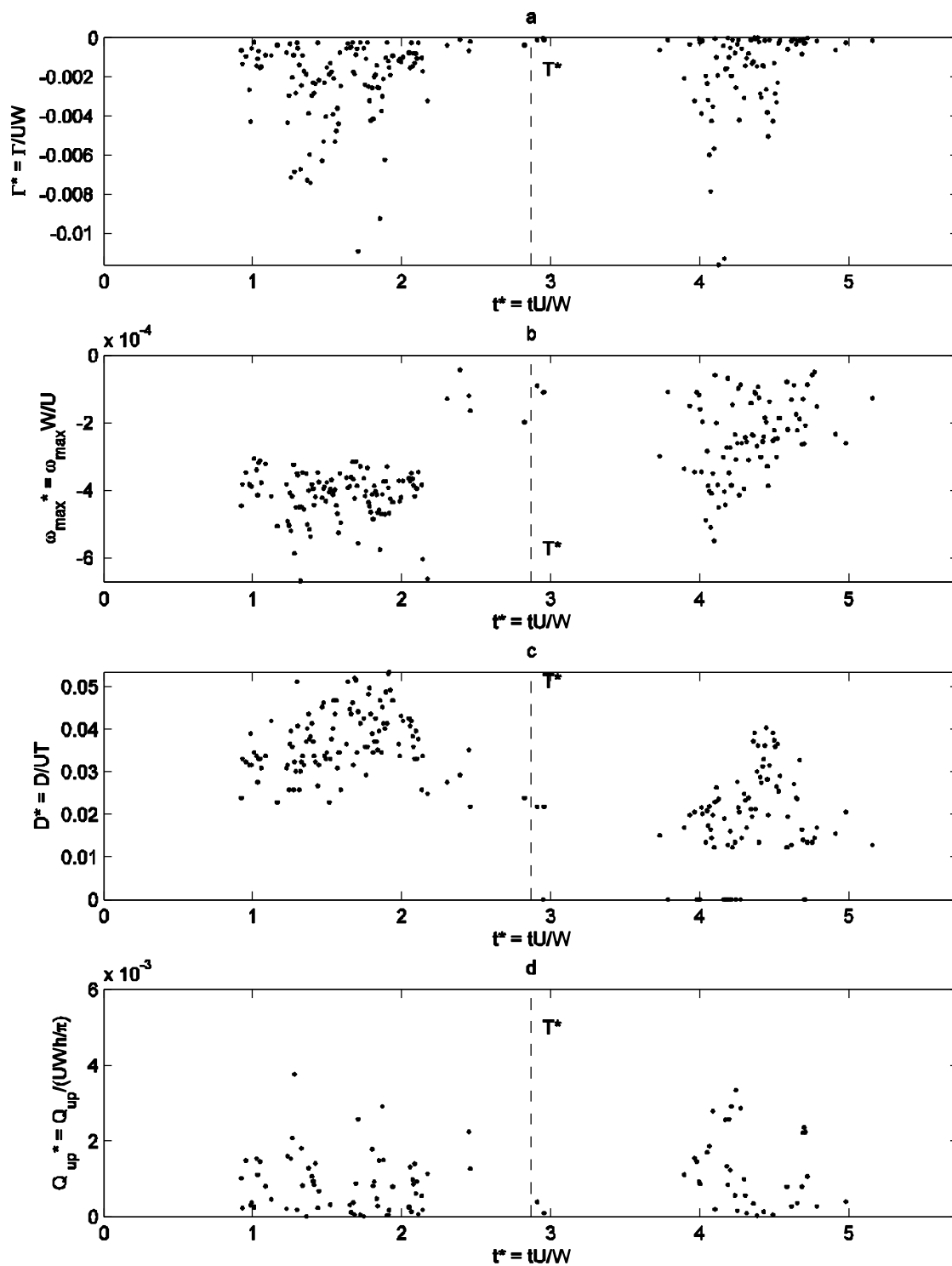


Figure 51 Life-history Type II for Layout B, repetition 2: a) Circulation around the main vortex b) Maximum vorticity in the main vortex c) Equivalent diameter of the main vortex. d) Upwelling flowing from the main vortex.

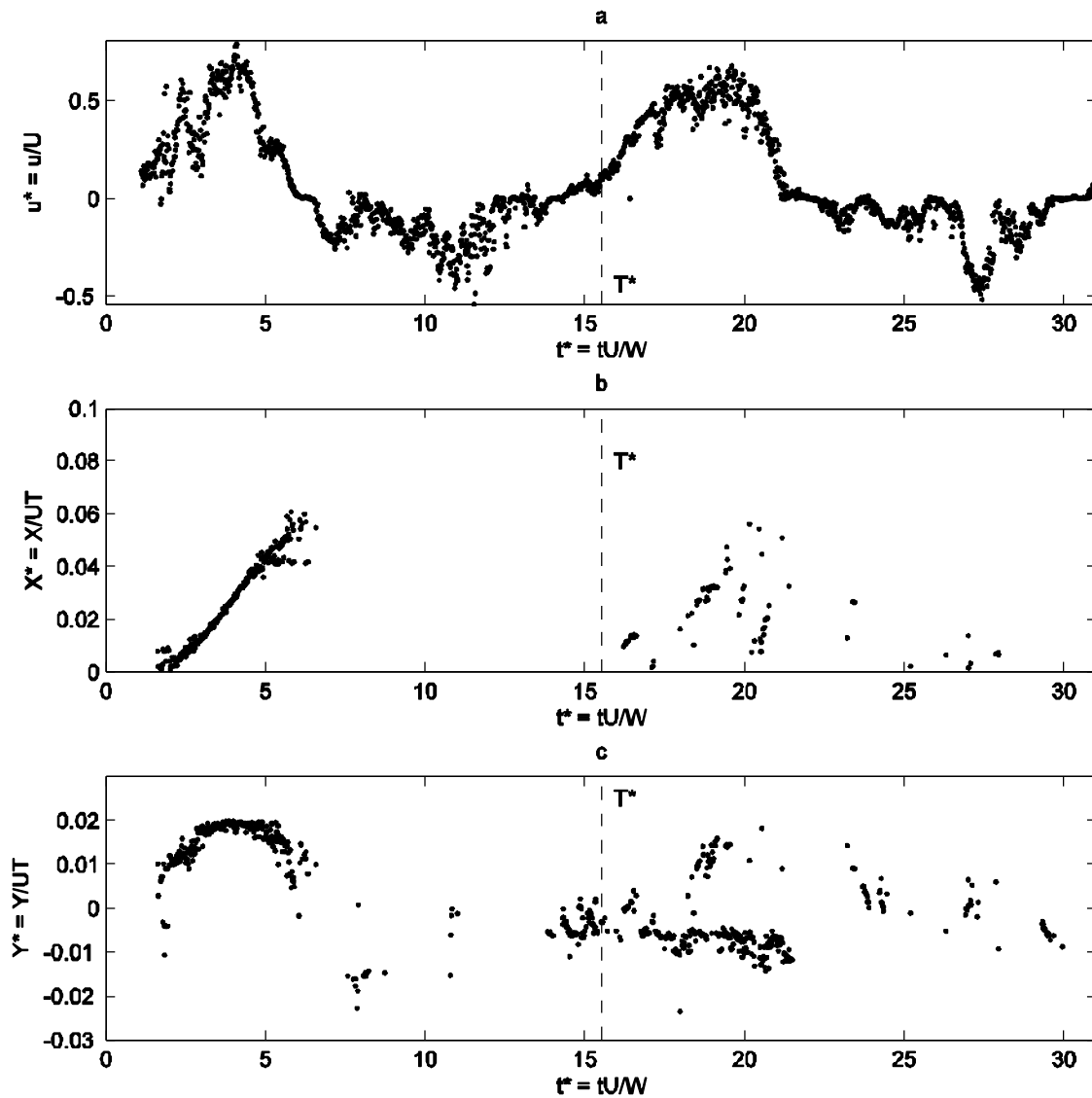


Figure 52 Life-history Type III for Layout B, repetition 1: a) Average cross sectional velocity at the mouth of the inlet. b) Longitudinal position of the center of the main vortex starting from the edge of the barrier island. c) Lateral position of the center of the main vortex starting from the edge of the barrier island.



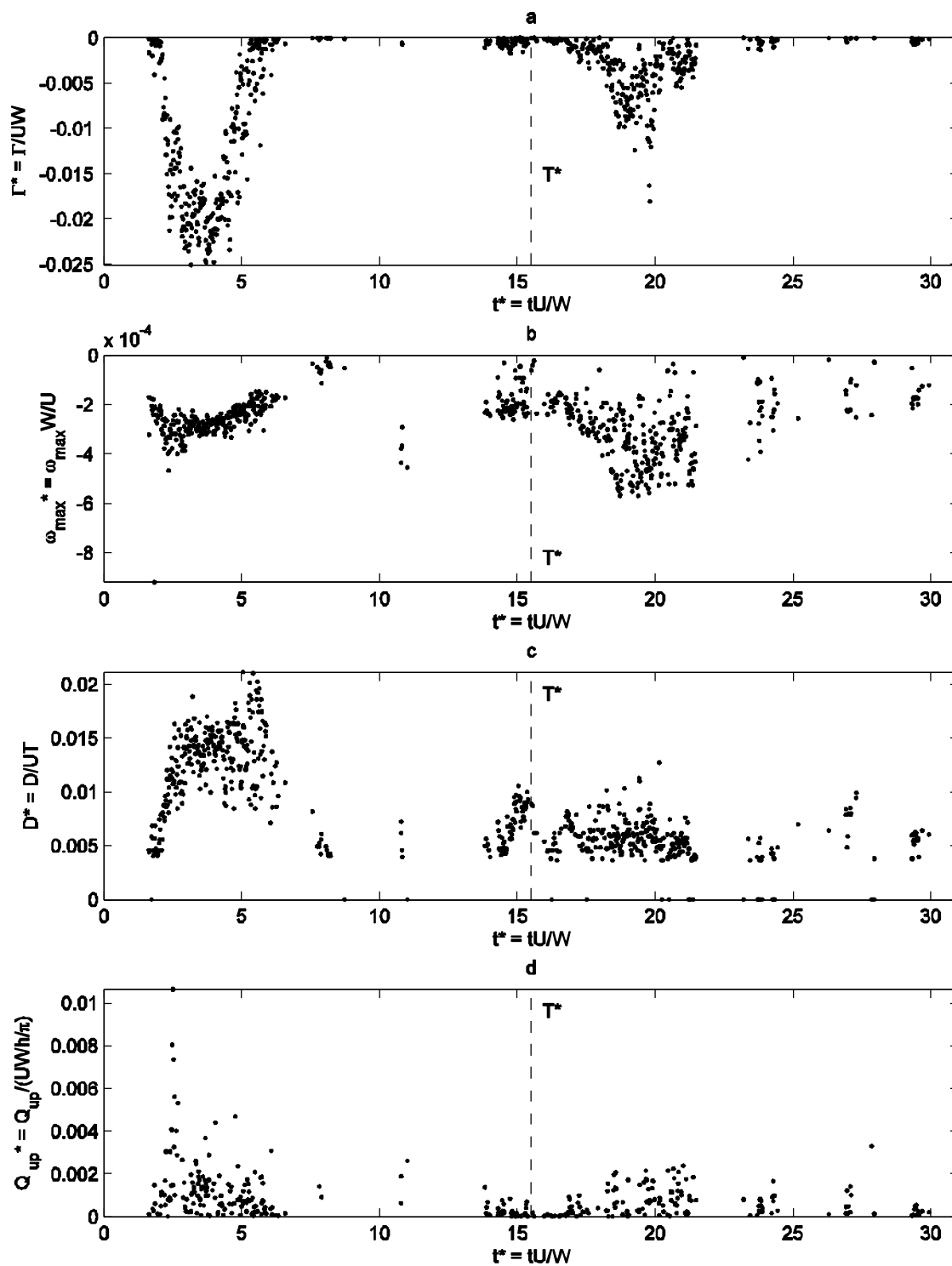


Figure 53 Life-history Type III for Layout B, repetition 1: a) Circulation around the main vortex b) Maximum vorticity in the main vortex c) Equivalent diameter of the main vortex. d) Upwelling flowing from the main vortex.

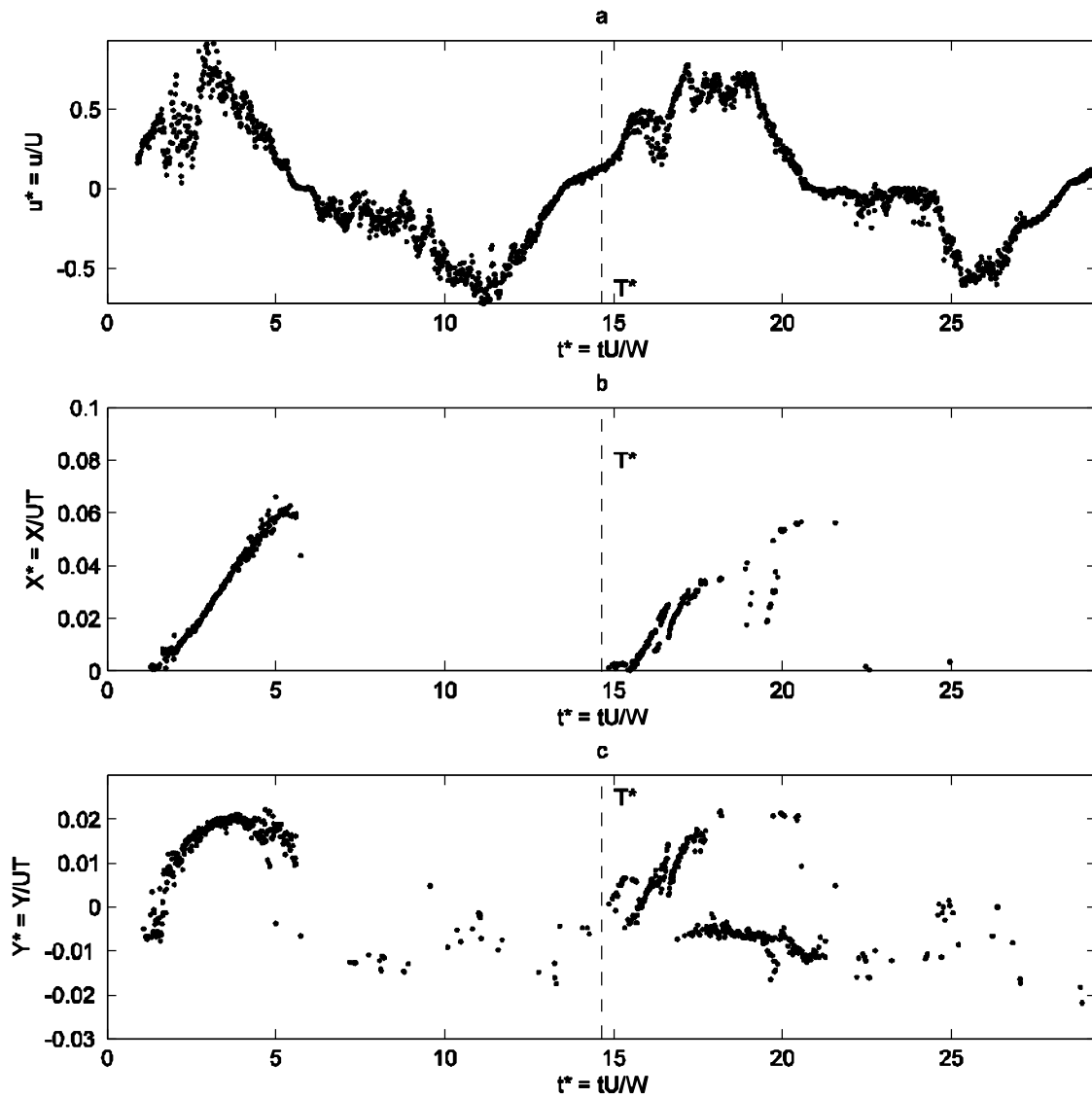


Figure 54 Life-history Type III for Layout B, repetition 2: a) Average cross sectional velocity at the mouth of the inlet. b) Longitudinal position of the center of the main vortex starting from the edge of the barrier island. c) Lateral position of the center of the main vortex starting from the edge of the barrier island.

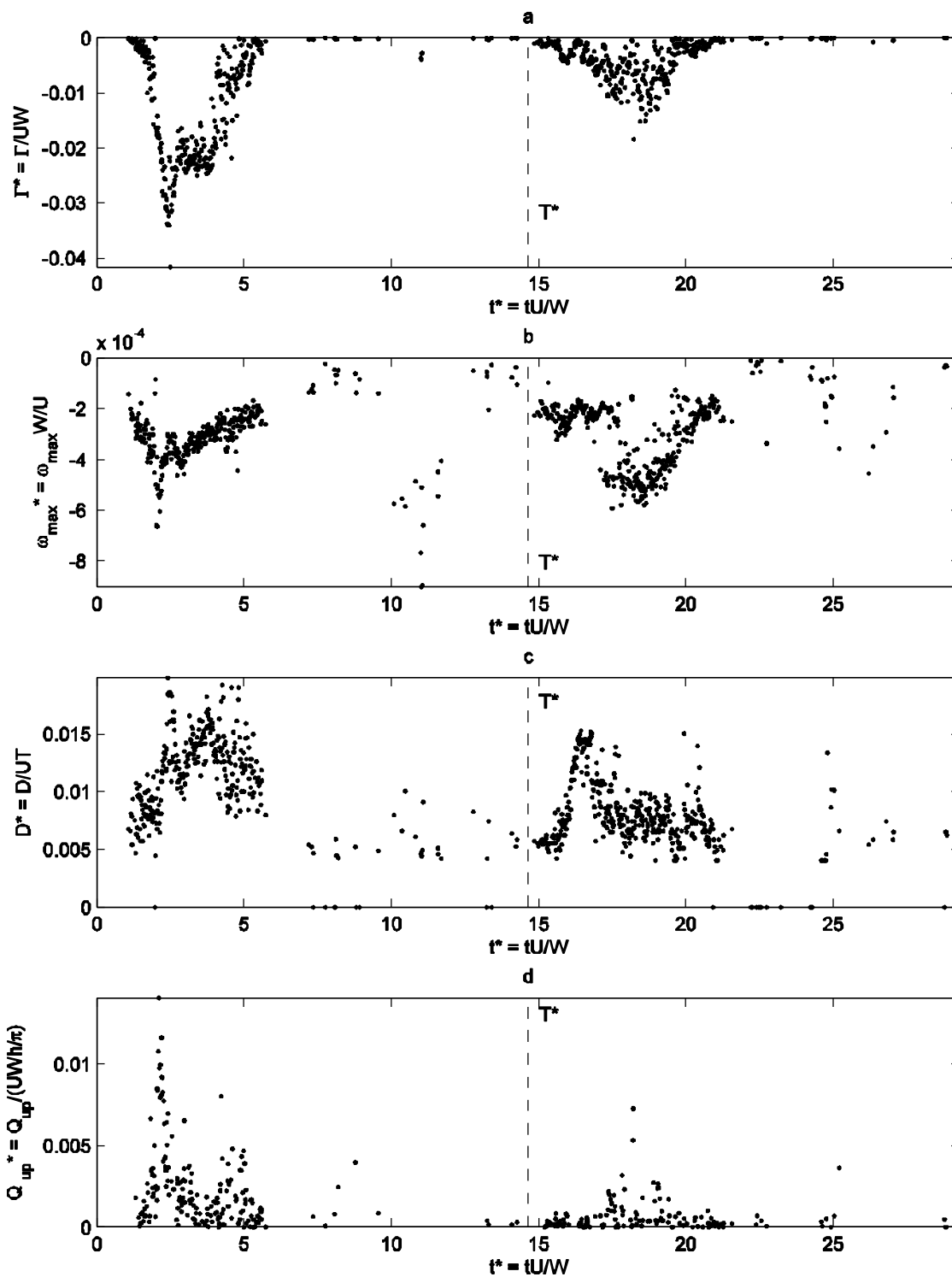


Figure 55 Life-history Type III for Layout B, repetition 2: a) Circulation around the main vortex b) Maximum vorticity in the main vortex c) Equivalent diameter of the main vortex. d) Upwelling flowing from the main vortex.

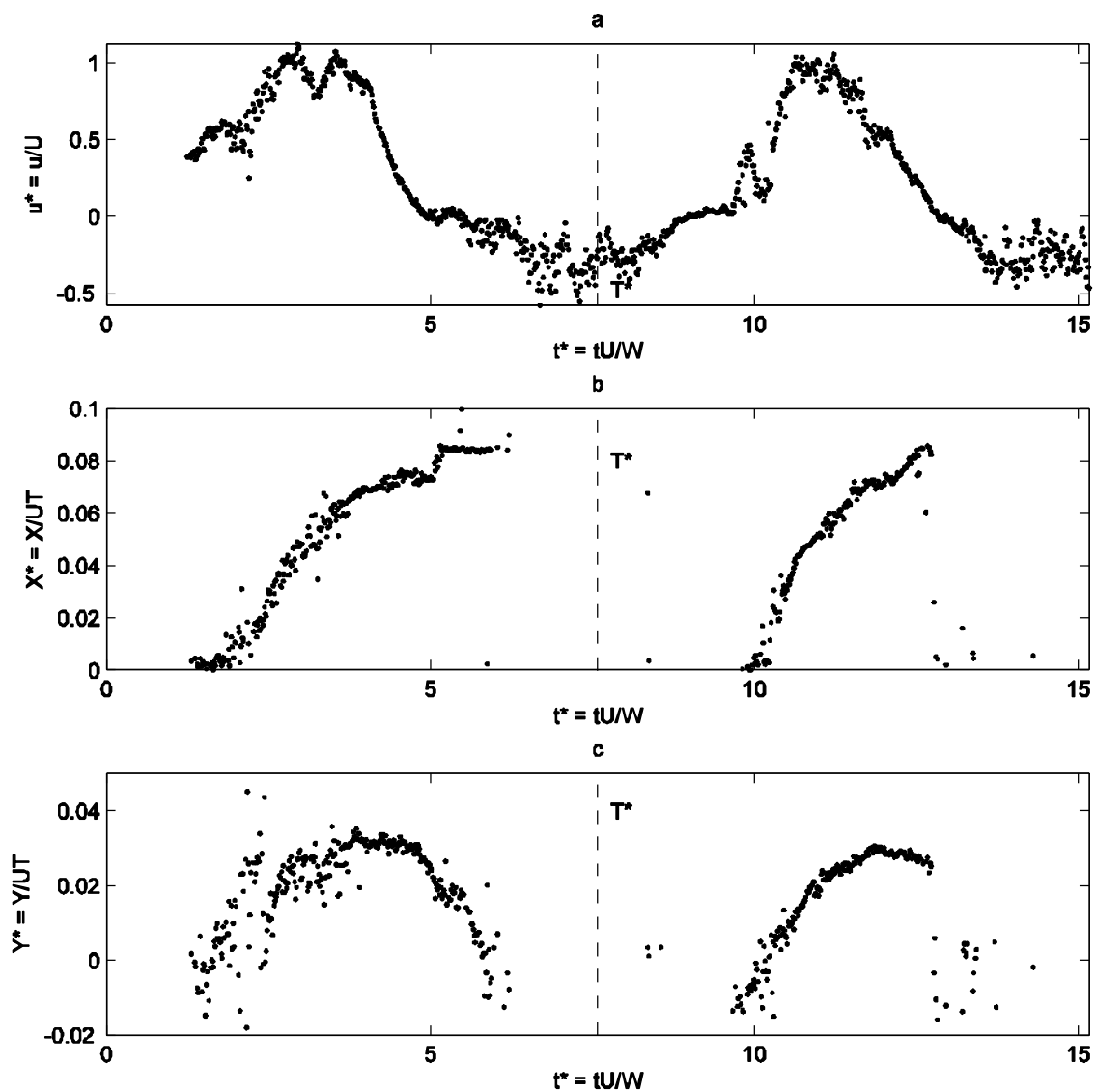


Figure 56 Life-history Type I for Layout C, repetition 1: a) Average cross sectional velocity at the mouth of the inlet. b) Longitudinal position of the center of the main vortex starting from the edge of the barrier island. c) Lateral position of the center of the main vortex starting from the edge of the barrier island.

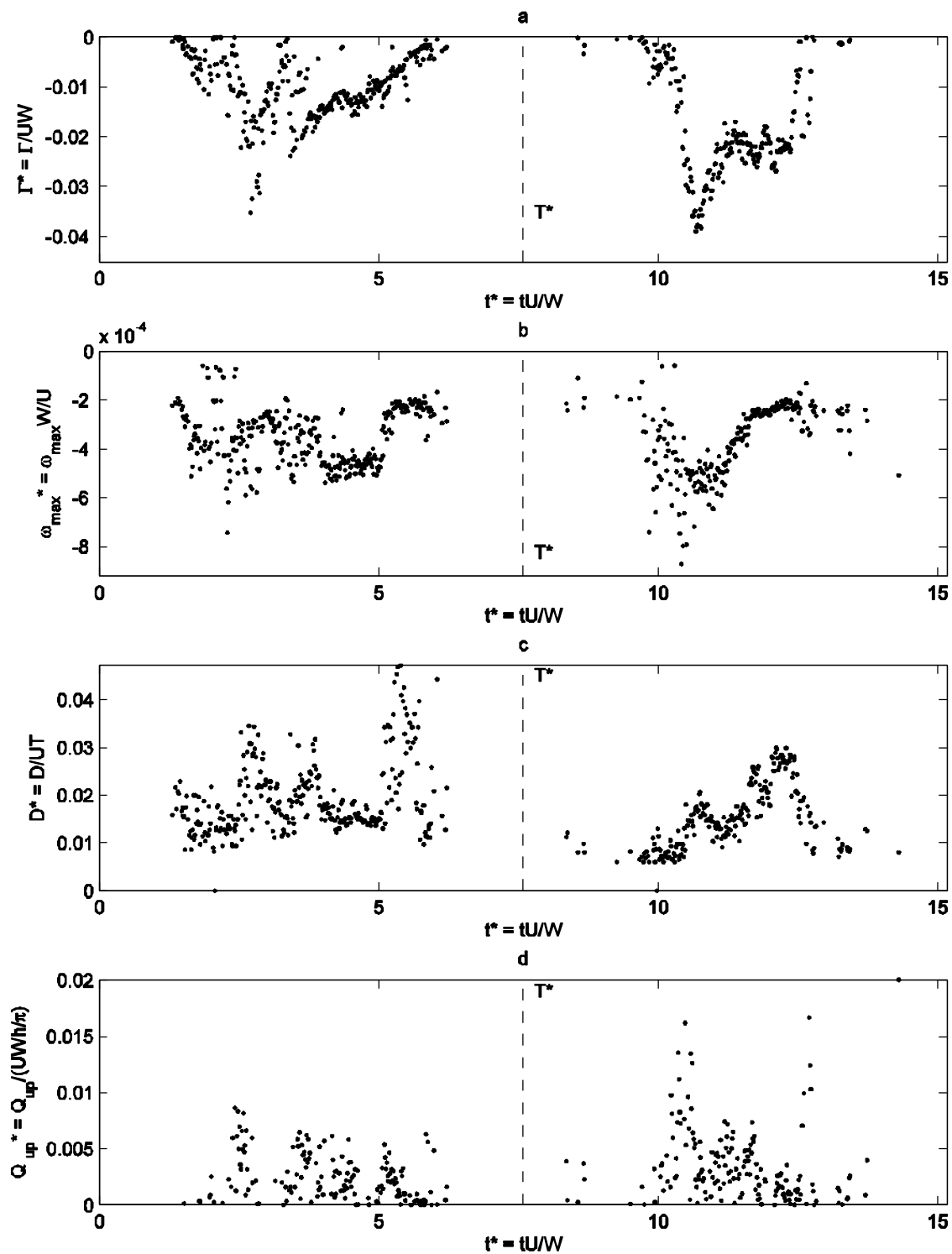


Figure 57 Life-history Type I for Layout C, repetition 1: a) Circulation around the main vortex b) Maximum vorticity in the main vortex c) Equivalent diameter of the main vortex. d) Upwelling flowing from the main vortex.

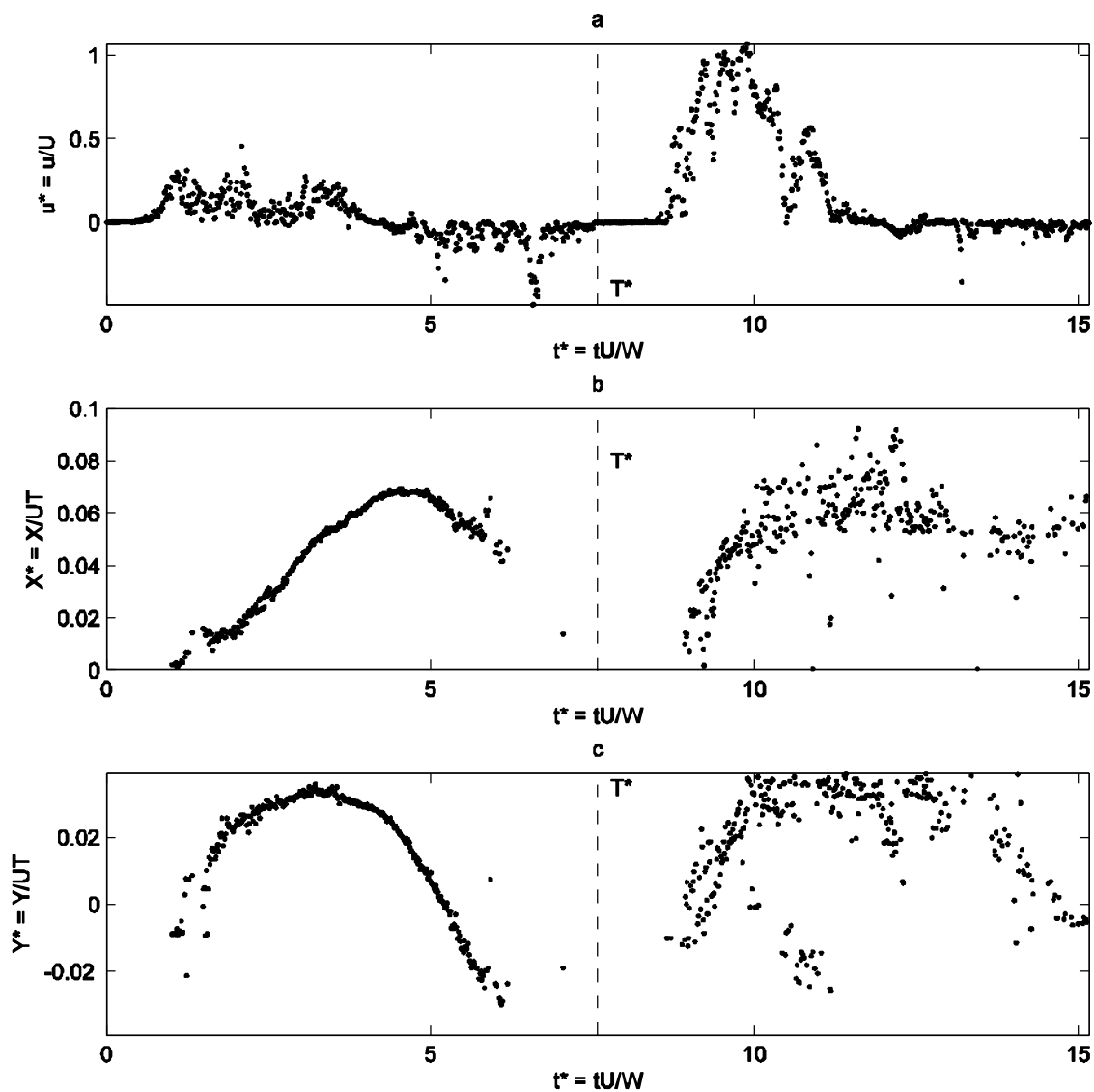


Figure 58 Life-history Type I for Layout C, repetition 2: a) Average cross sectional velocity at the mouth of the inlet. b) Longitudinal position of the center of the main vortex starting from the edge of the barrier island. c) Lateral position of the center of the main vortex starting from the edge of the barrier island.

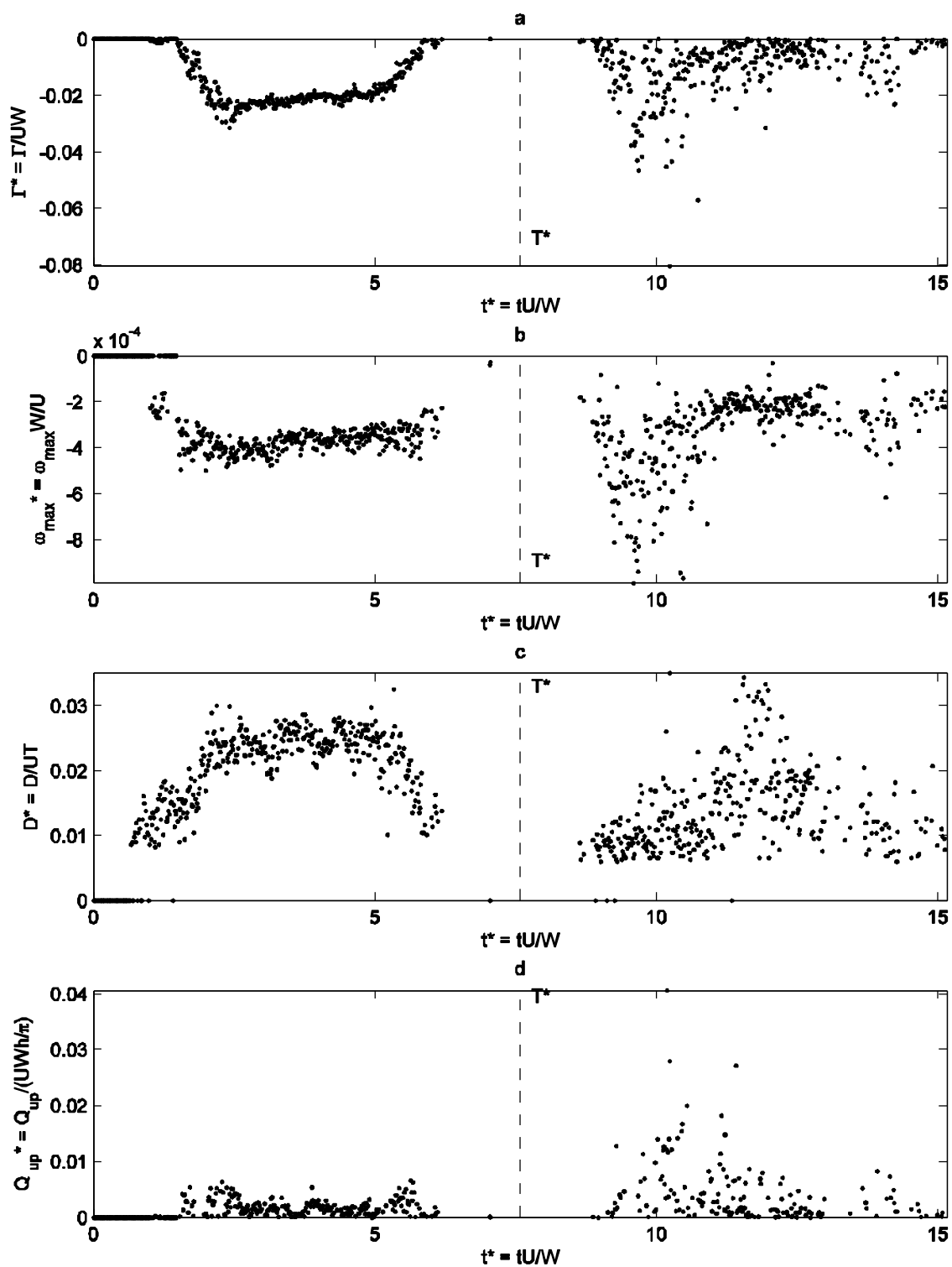


Figure 59 Life-history Type I for Layout C, repetition 2: a) Circulation around the main vortex b) Maximum vorticity in the main vortex c) Equivalent diameter of the main vortex. d) Upwelling flowing from the main vortex.

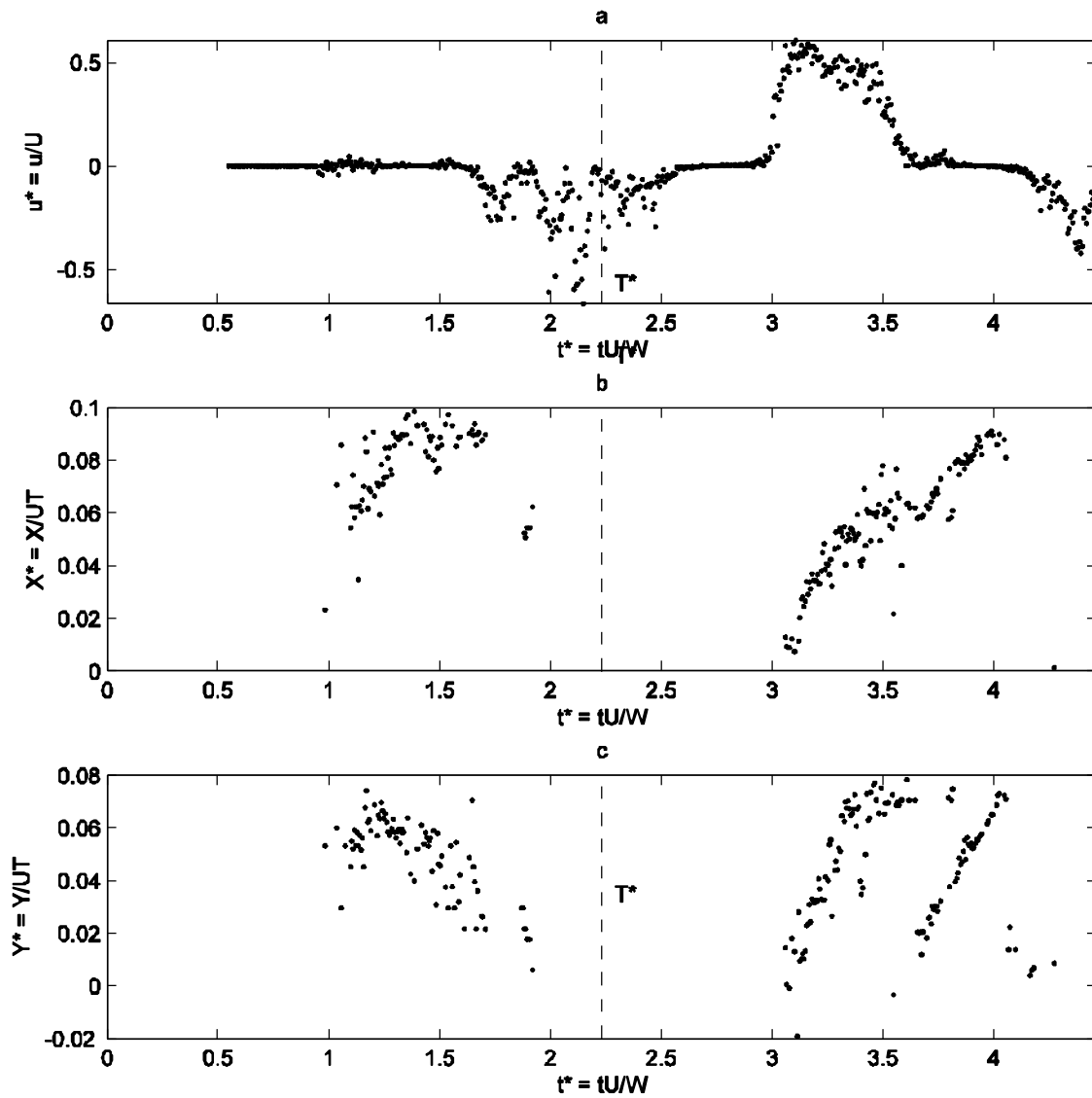


Figure 60 Life-history Type II for Layout C, repetition 1: a) Average cross sectional velocity at the mouth of the inlet. b) Longitudinal position of the center of the main vortex starting from the edge of the barrier island. c) Lateral position of the center of the main vortex starting from the edge of the barrier island.



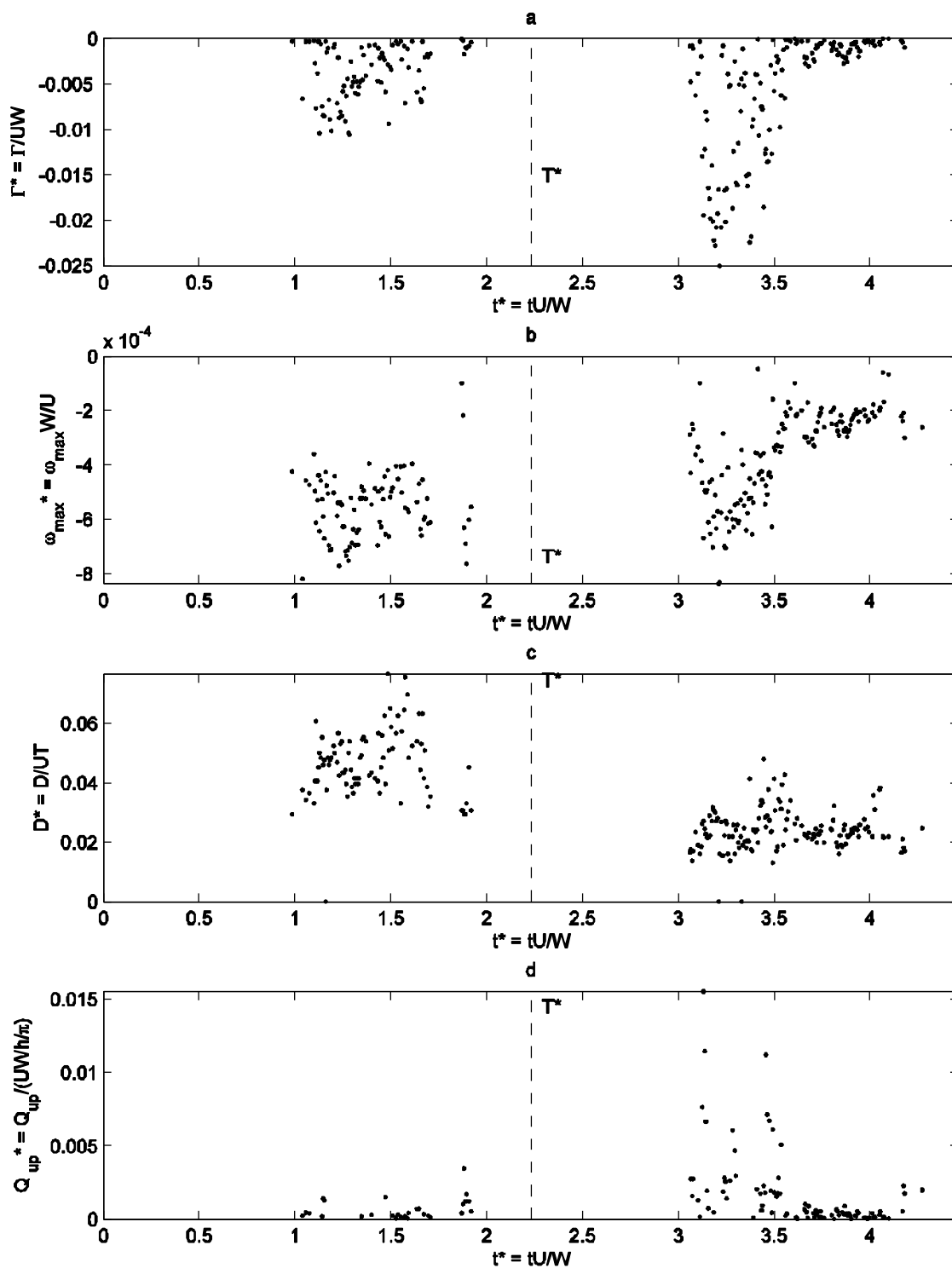


Figure 61 Life-history Type II for Layout C, repetition 1: a) Circulation around the main vortex b) Maximum vorticity in the main vortex c) Equivalent diameter of the main vortex. d) Upwelling flowing from the main vortex.

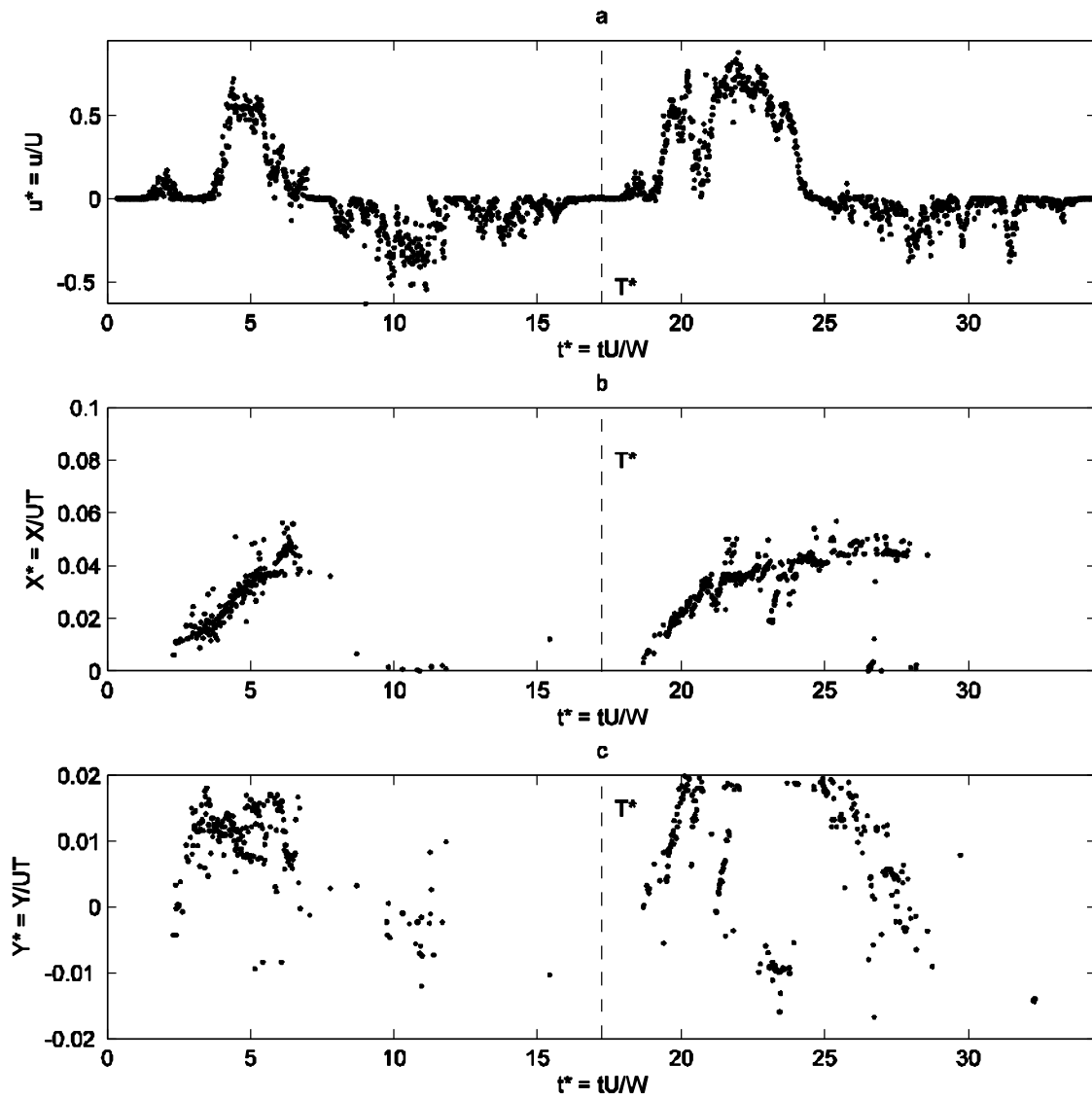


Figure 62 Life-history Type III for Layout C, repetition 1: a) Average cross sectional velocity at the mouth of the inlet. b) Longitudinal position of the center of the main vortex starting from the edge of the barrier island. c) Lateral position of the center of the main vortex starting from the edge of the barrier island.

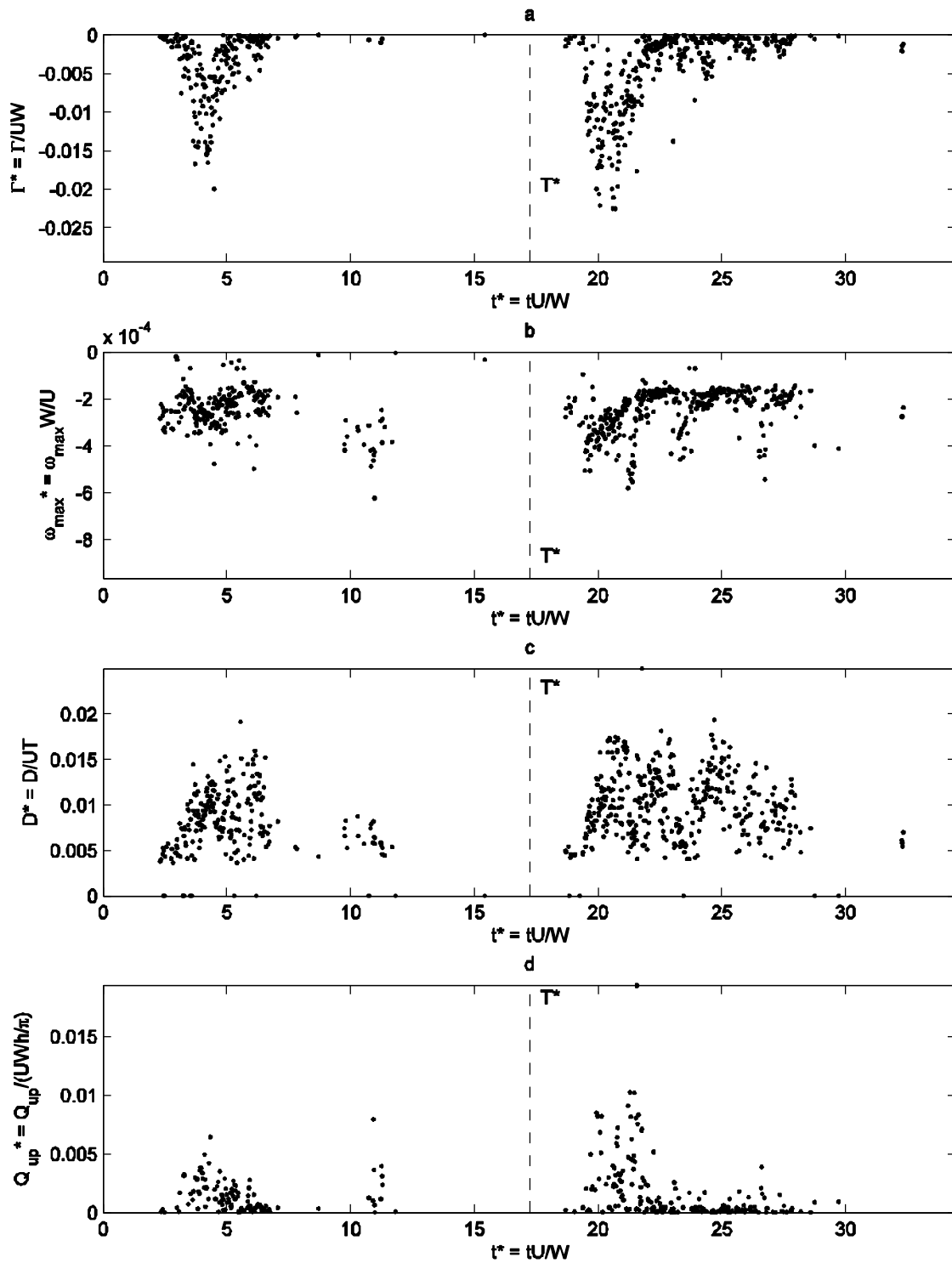


Figure 63 Life-history Type III for Layout C, repetition 1: a) Circulation around the main vortex b) Maximum vorticity in the main vortex c) Equivalent diameter of the main vortex. d) Upwelling flowing from the main vortex.

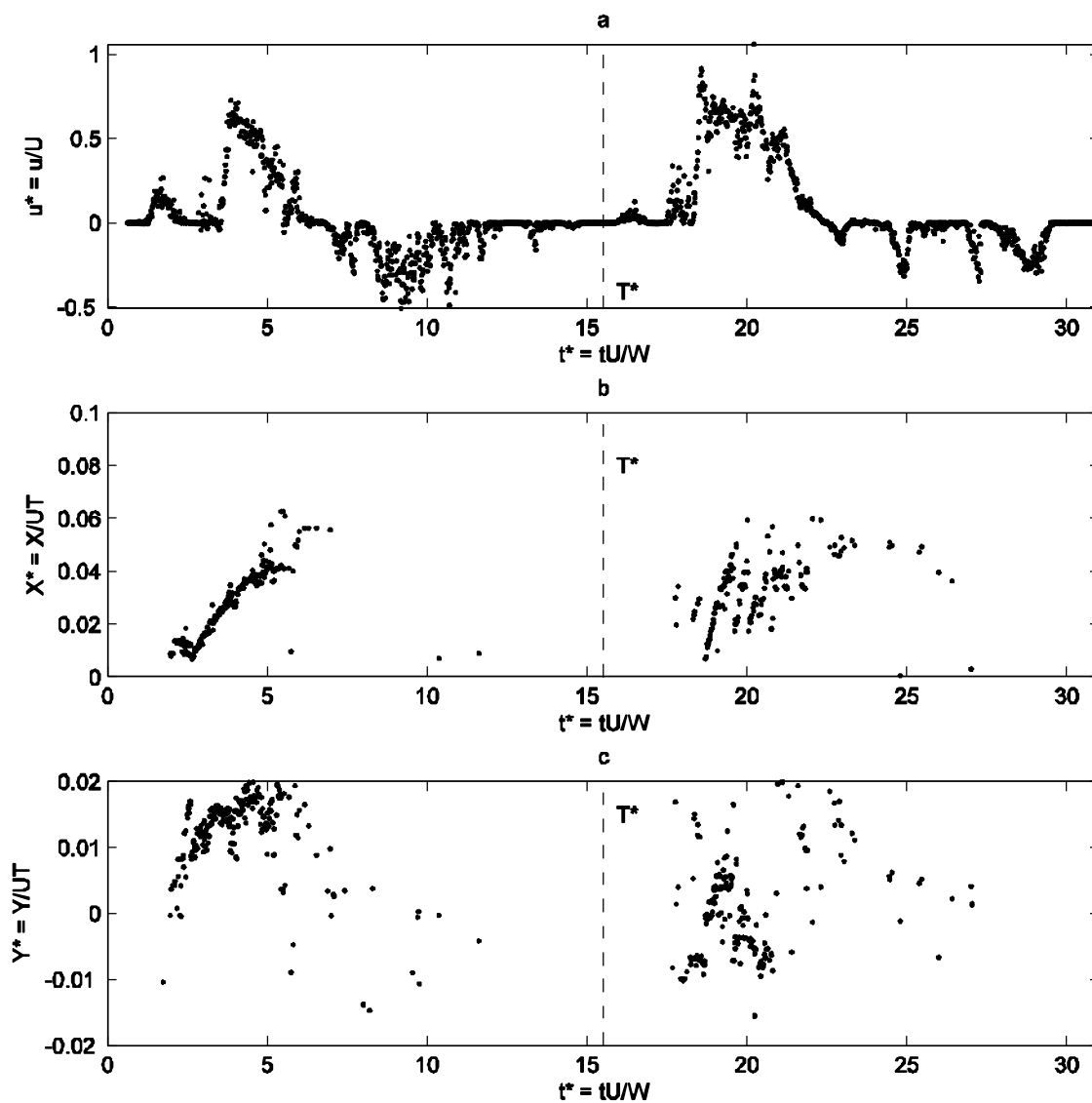


Figure 64 Life-history Type III for Layout C, repetition 2: a) Average cross sectional velocity at the mouth of the inlet. b) Longitudinal position of the center of the main vortex starting from the edge of the barrier island. c) Lateral position of the center of the main vortex starting from the edge of the barrier island.

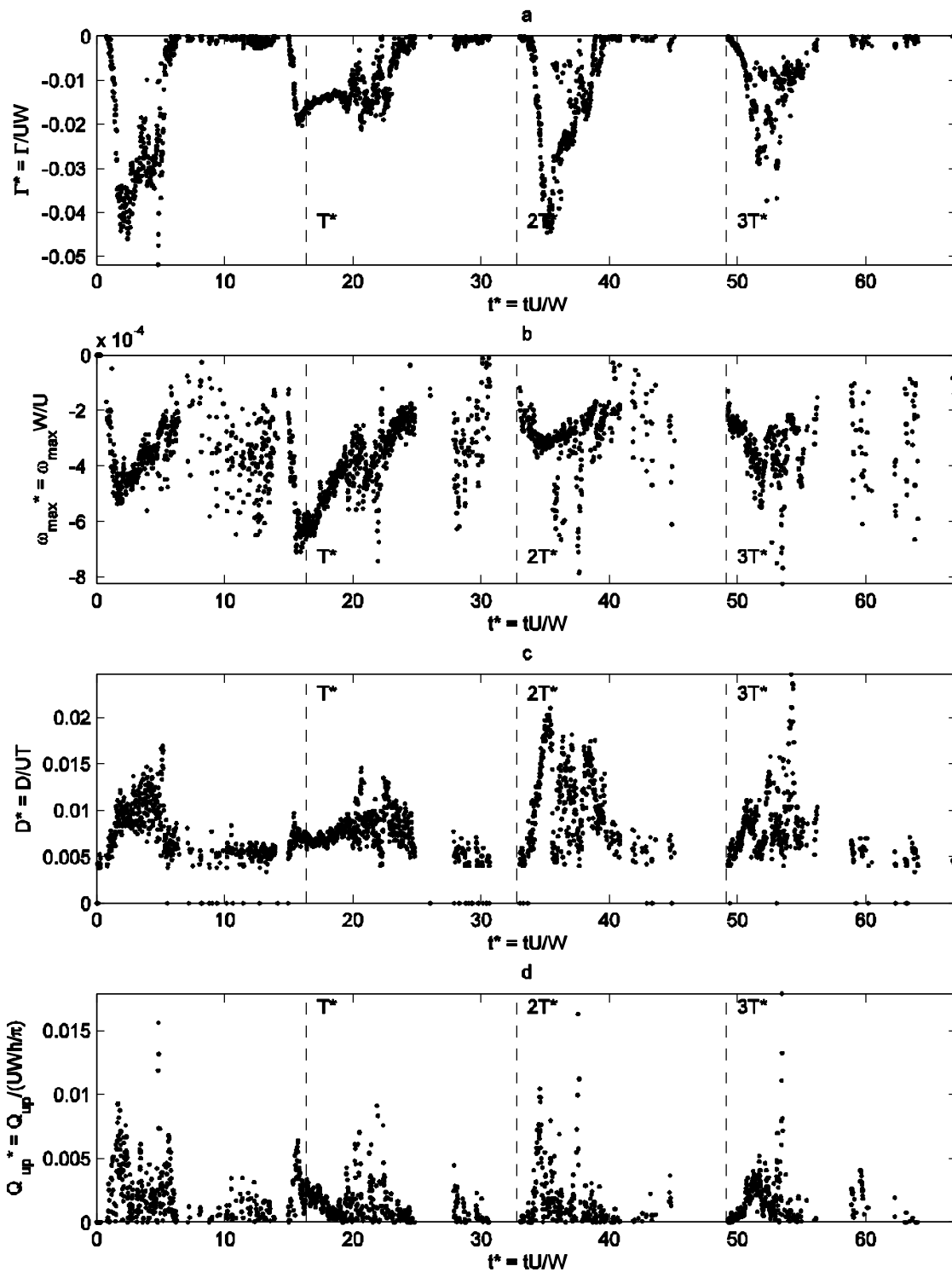


Figure 65 Life-history Type III for Layout C, repetition 2: a) Circulation around the main vortex b) Maximum vorticity in the main vortex c) Equivalent diameter of the main vortex. d) Upwelling flowing from the main vortex.

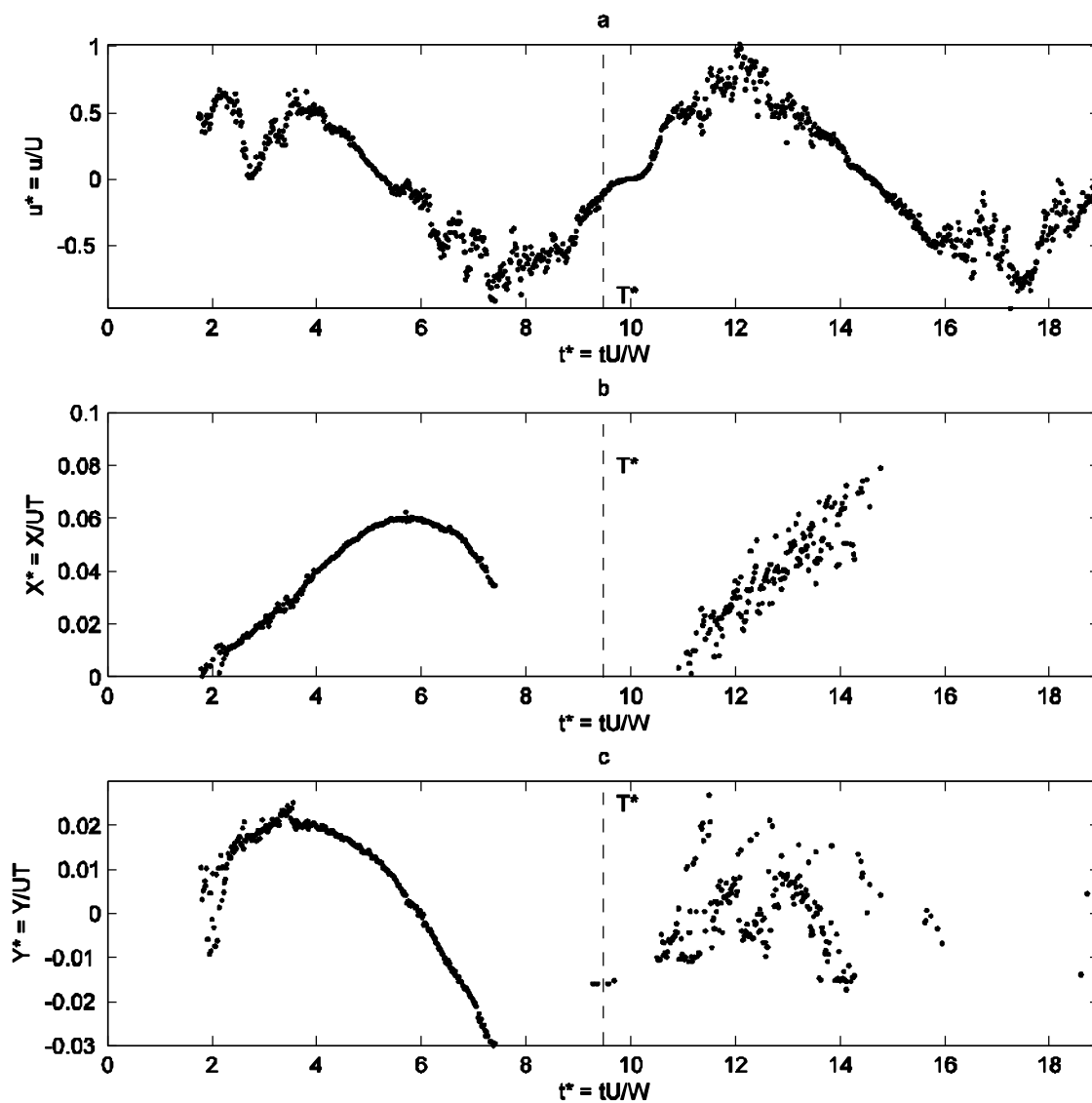


Figure 66 Life-history Type I for Layout D, repetition 1: a) Average cross sectional velocity at the mouth of the inlet. b) Longitudinal position of the center of the main vortex starting from the edge of the barrier island. c) Lateral position of the center of the main vortex starting from the edge of the barrier island.

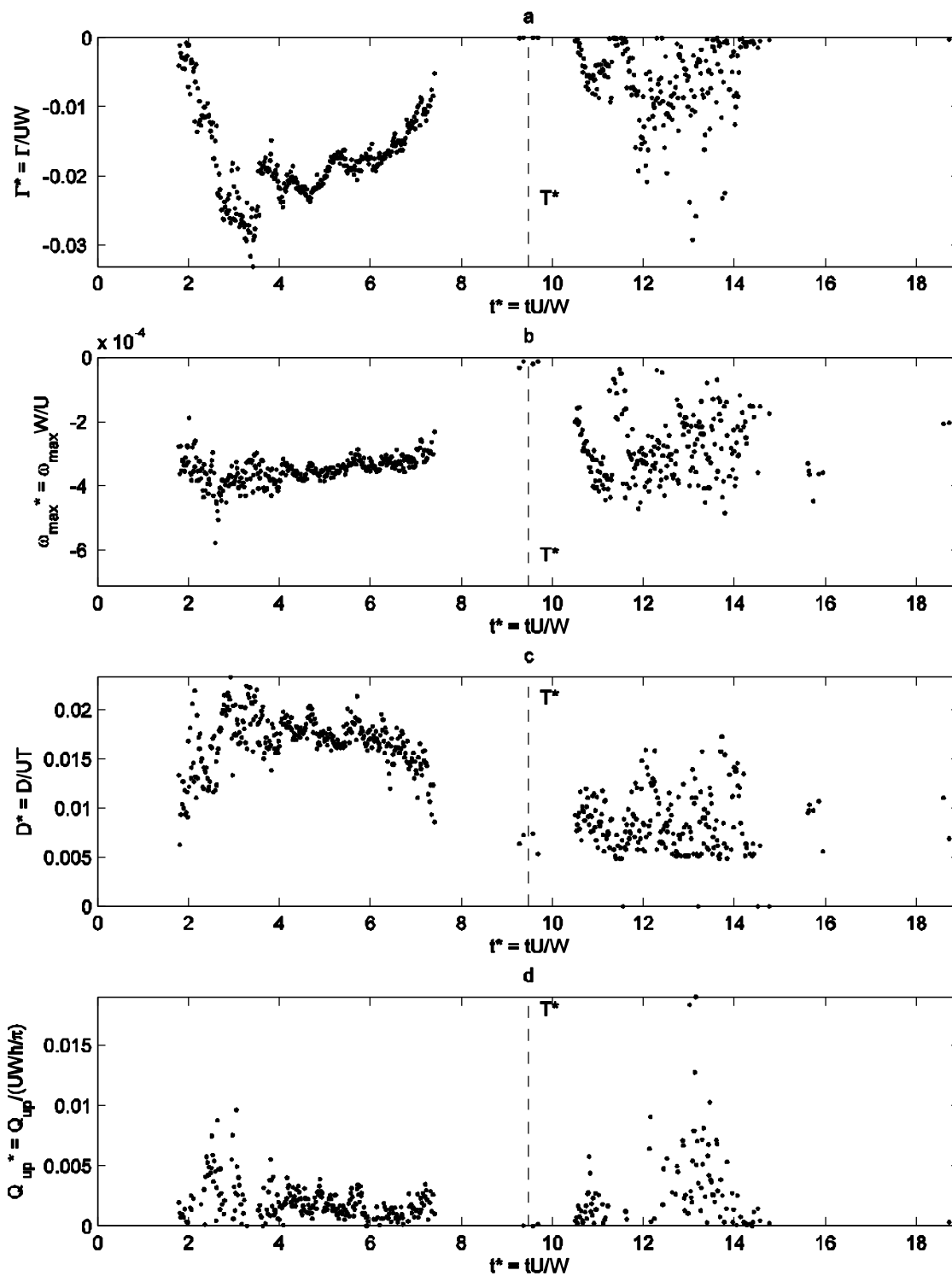


Figure 67 Life-history Type I for Layout D, repetition 1: a) Circulation around the main vortex b) Maximum vorticity in the main vortex c) Equivalent diameter of the main vortex. d) Upwelling flowing from the main vortex.

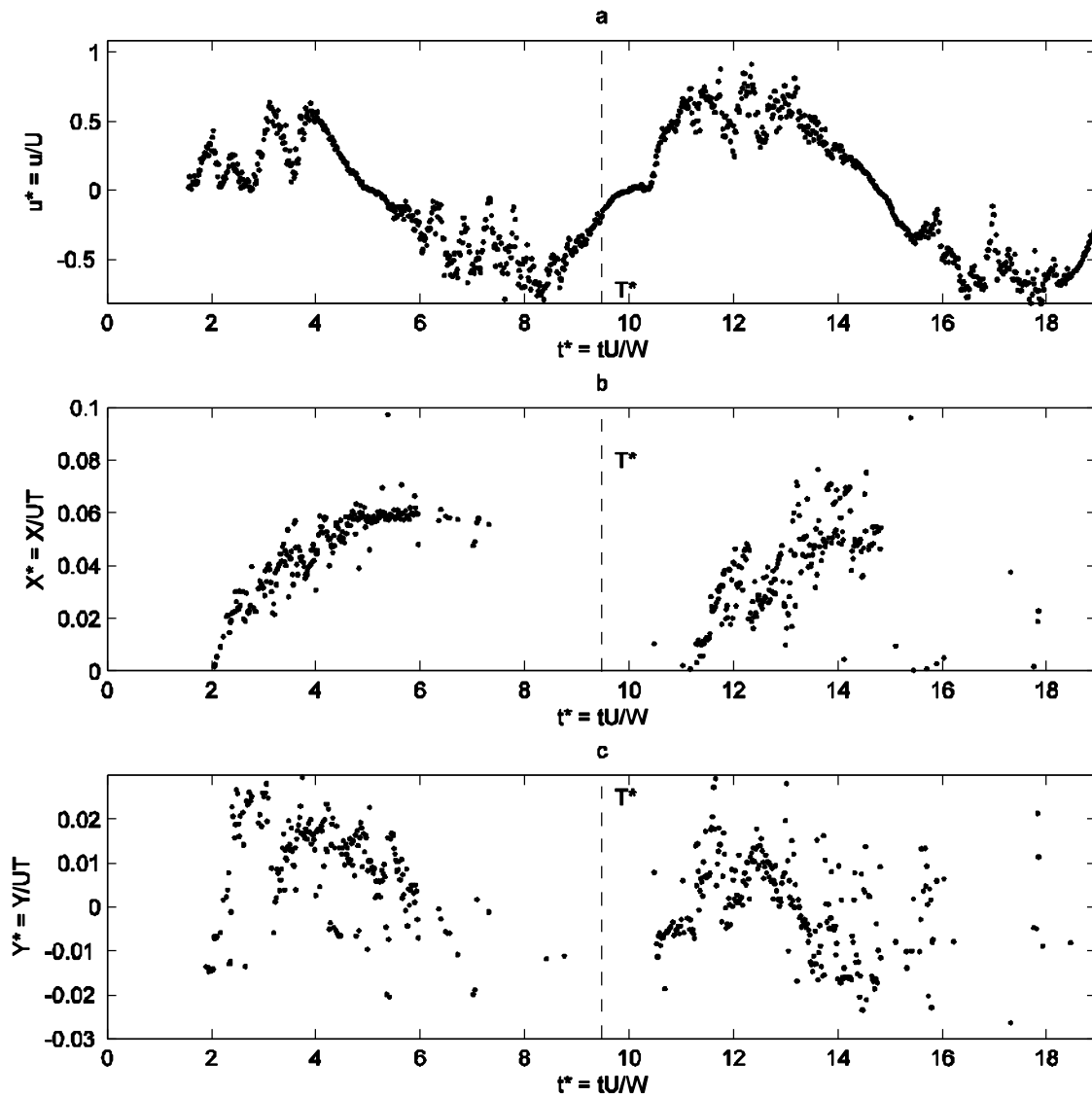


Figure 68 Life-history Type I for Layout D, repetition 2: a) Average cross sectional velocity at the mouth of the inlet. b) Longitudinal position of the center of the main vortex starting from the edge of the barrier island. c) Lateral position of the center of the main vortex starting from the edge of the barrier island.



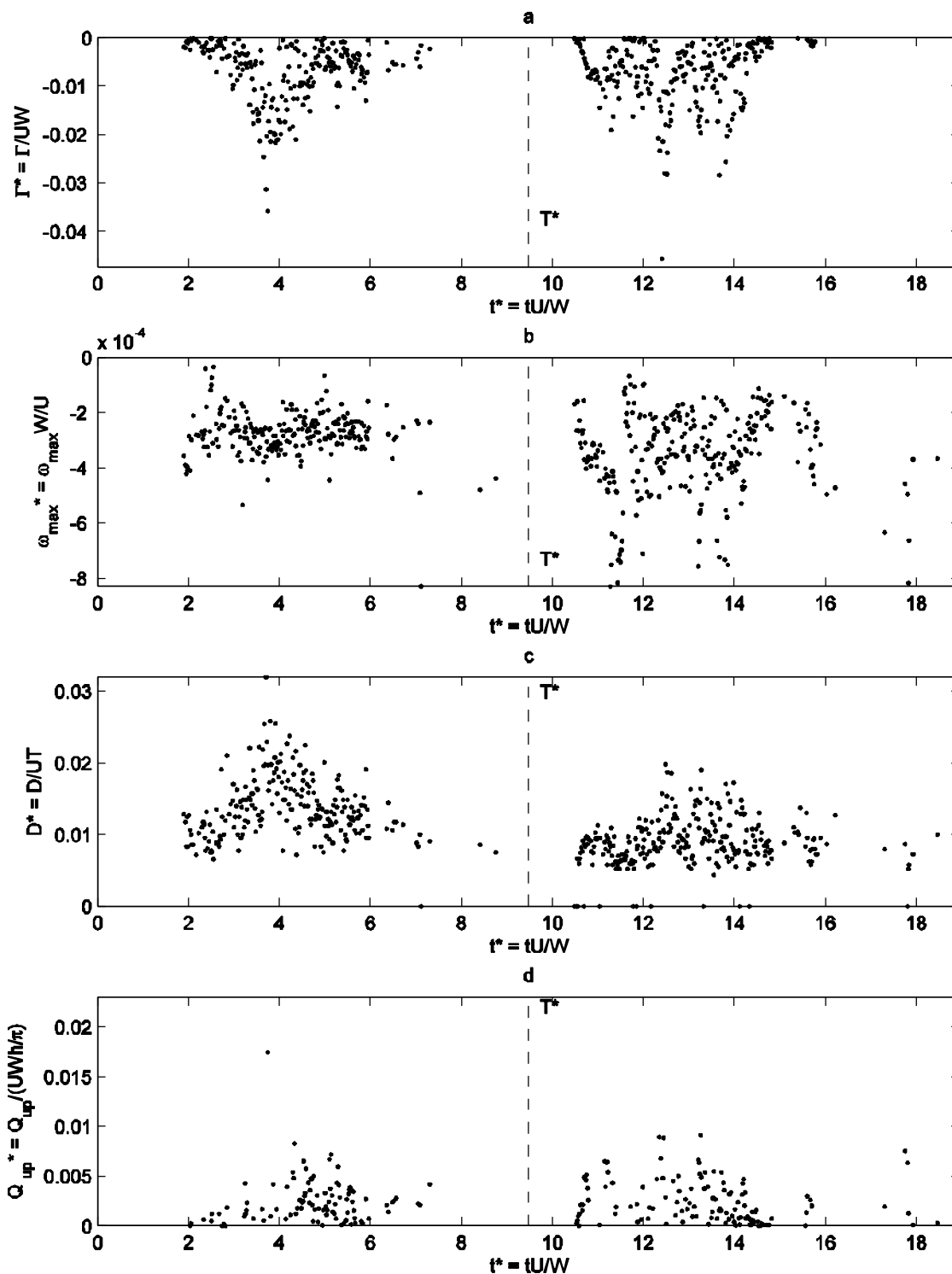


Figure 69 Life-history Type I for Layout D, repetition 2: a) Circulation around the main vortex b) Maximum vorticity in the main vortex c) Equivalent diameter of the main vortex. d) Upwelling flowing from the main vortex.

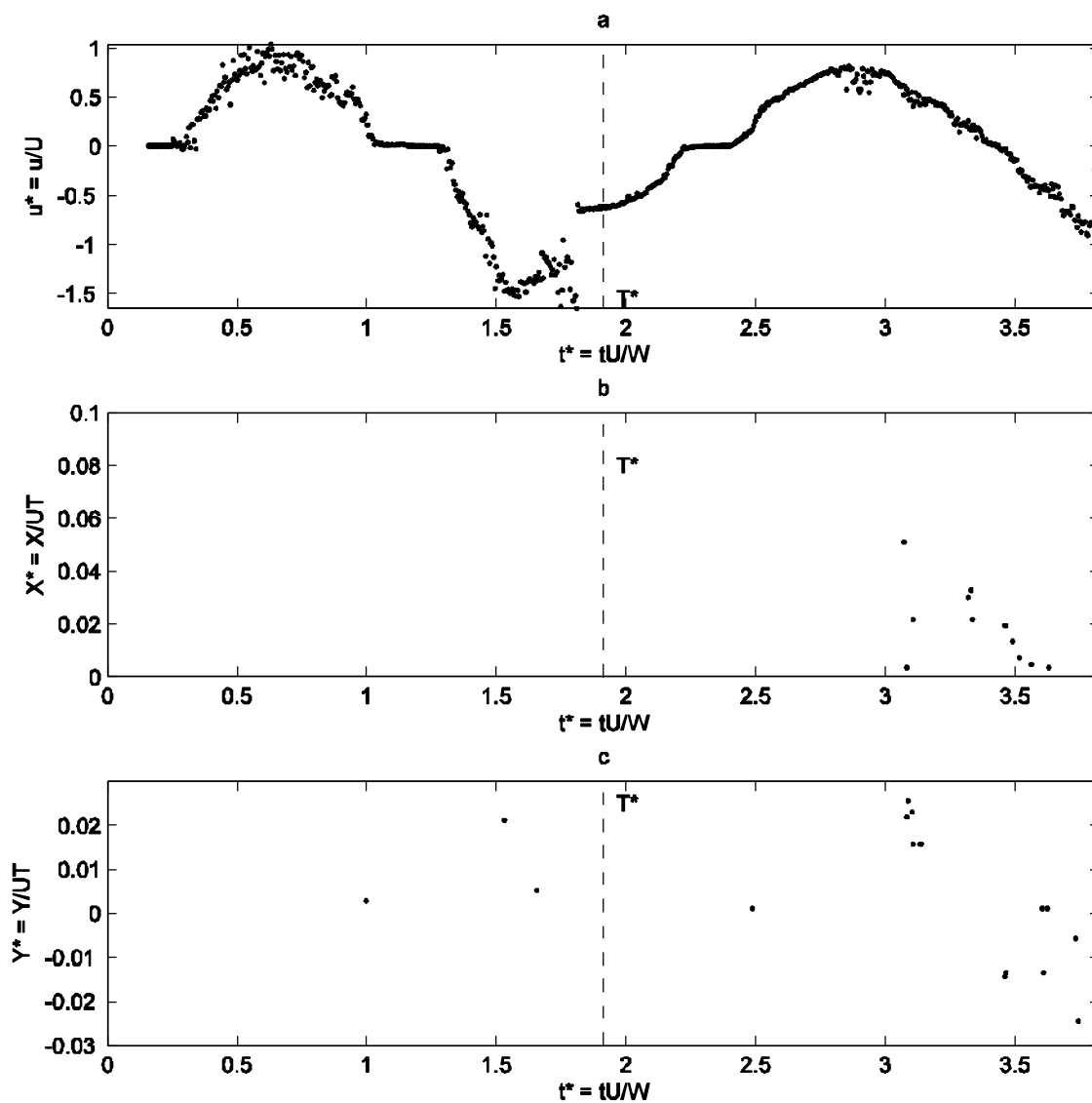


Figure 70 Life-history Type II for Layout D, repetition 1: a) Average cross sectional velocity at the mouth of the inlet. b) Longitudinal position of the center of the main vortex starting from the edge of the barrier island. c) Lateral position of the center of the main vortex starting from the edge of the barrier island.

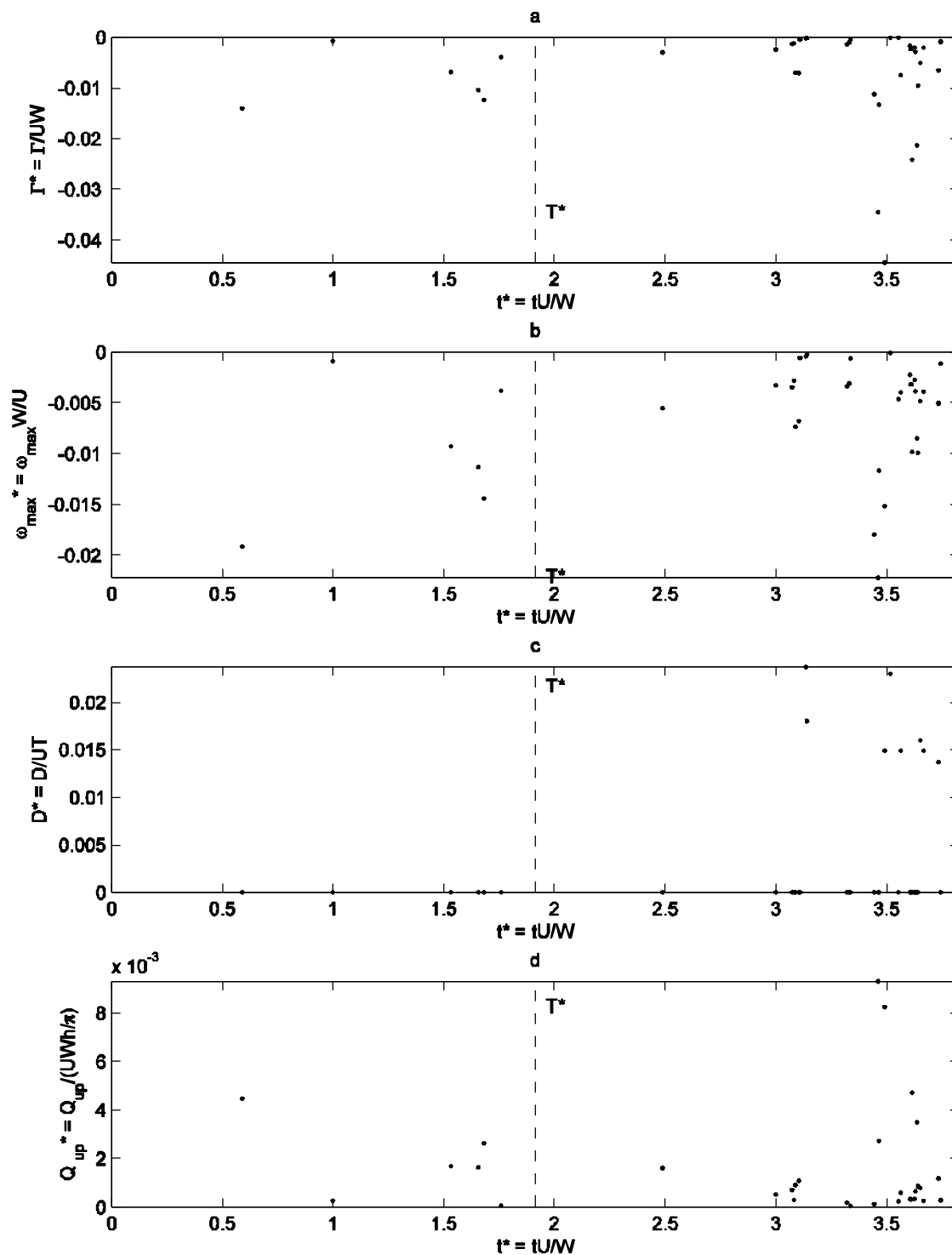


Figure 71 Life-history Type II for Layout D, repetition 1: a) Circulation around the main vortex b) Maximum vorticity in the main vortex c) Equivalent diameter of the main vortex. d) Upwelling flowing from the main vortex.

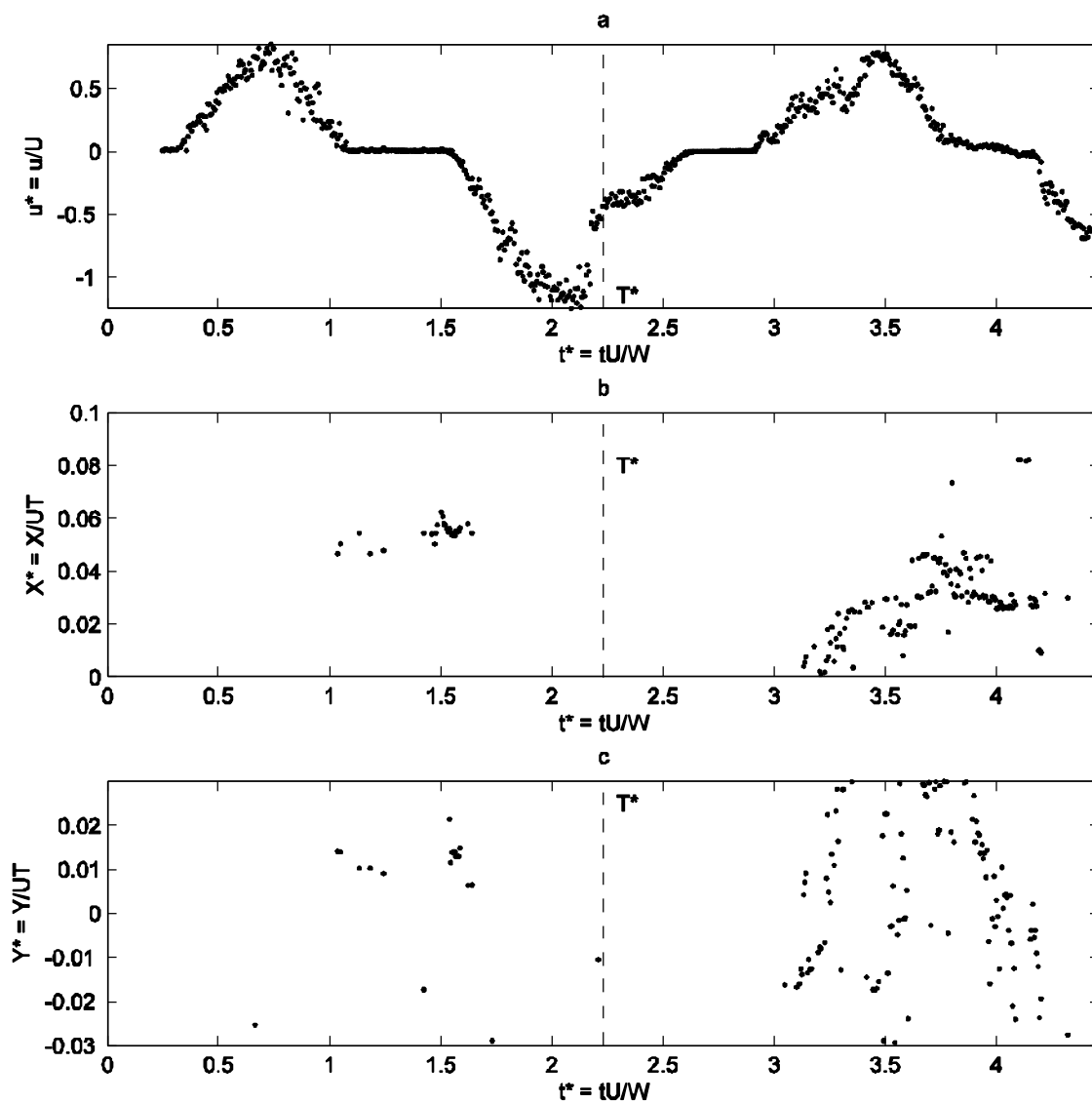


Figure 72 Life-history Type II for Layout D, repetition 2: a) Average cross sectional velocity at the mouth of the inlet. b) Longitudinal position of the center of the main vortex starting from the edge of the barrier island. c) Lateral position of the center of the main vortex starting from the edge of the barrier island.

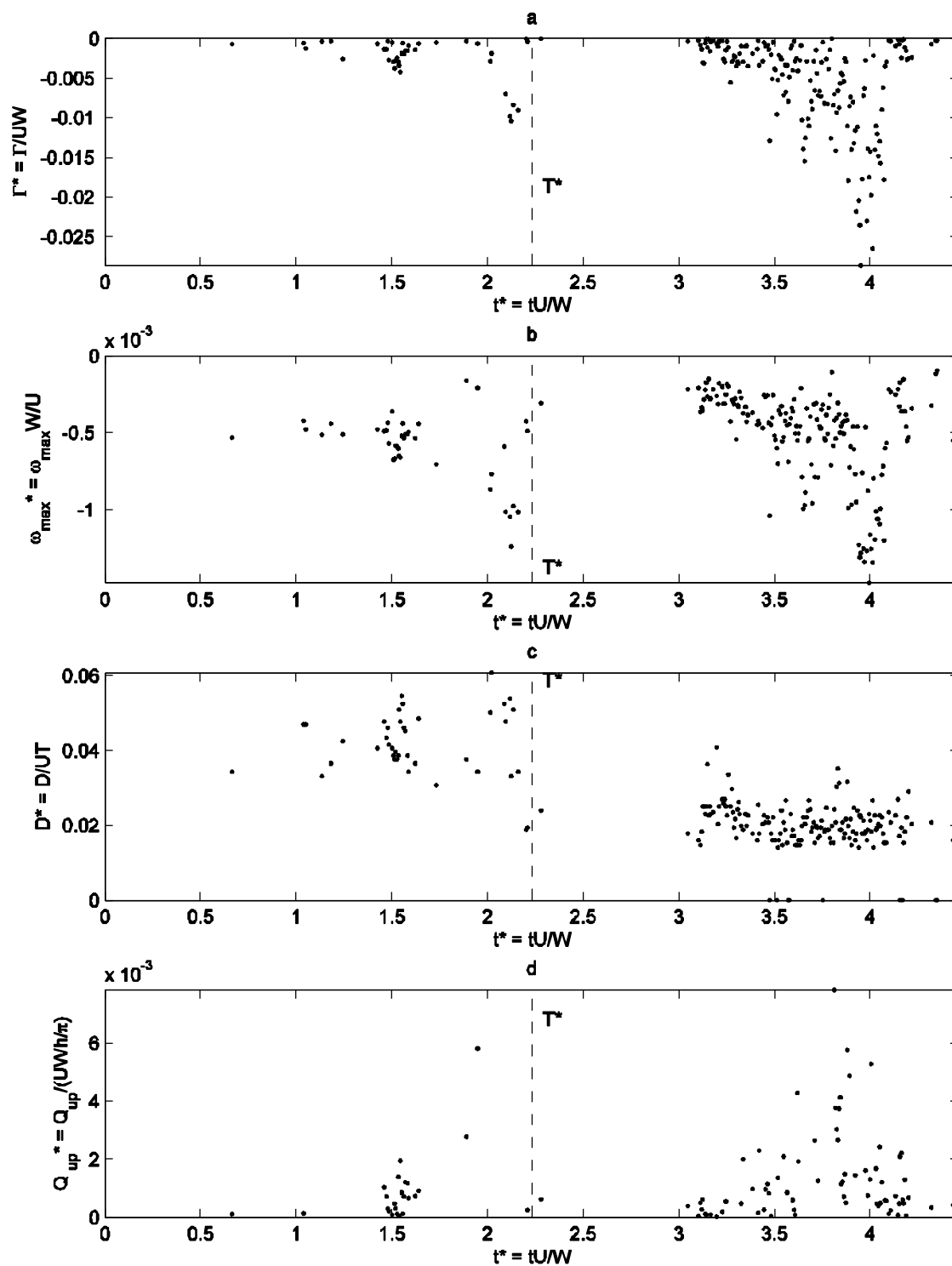


Figure 73 Life-history Type II for Layout D, repetition 2: a) Circulation around the main vortex b) Maximum vorticity in the main vortex c) Equivalent diameter of the main vortex. d) Upwelling flowing from the main vortex.

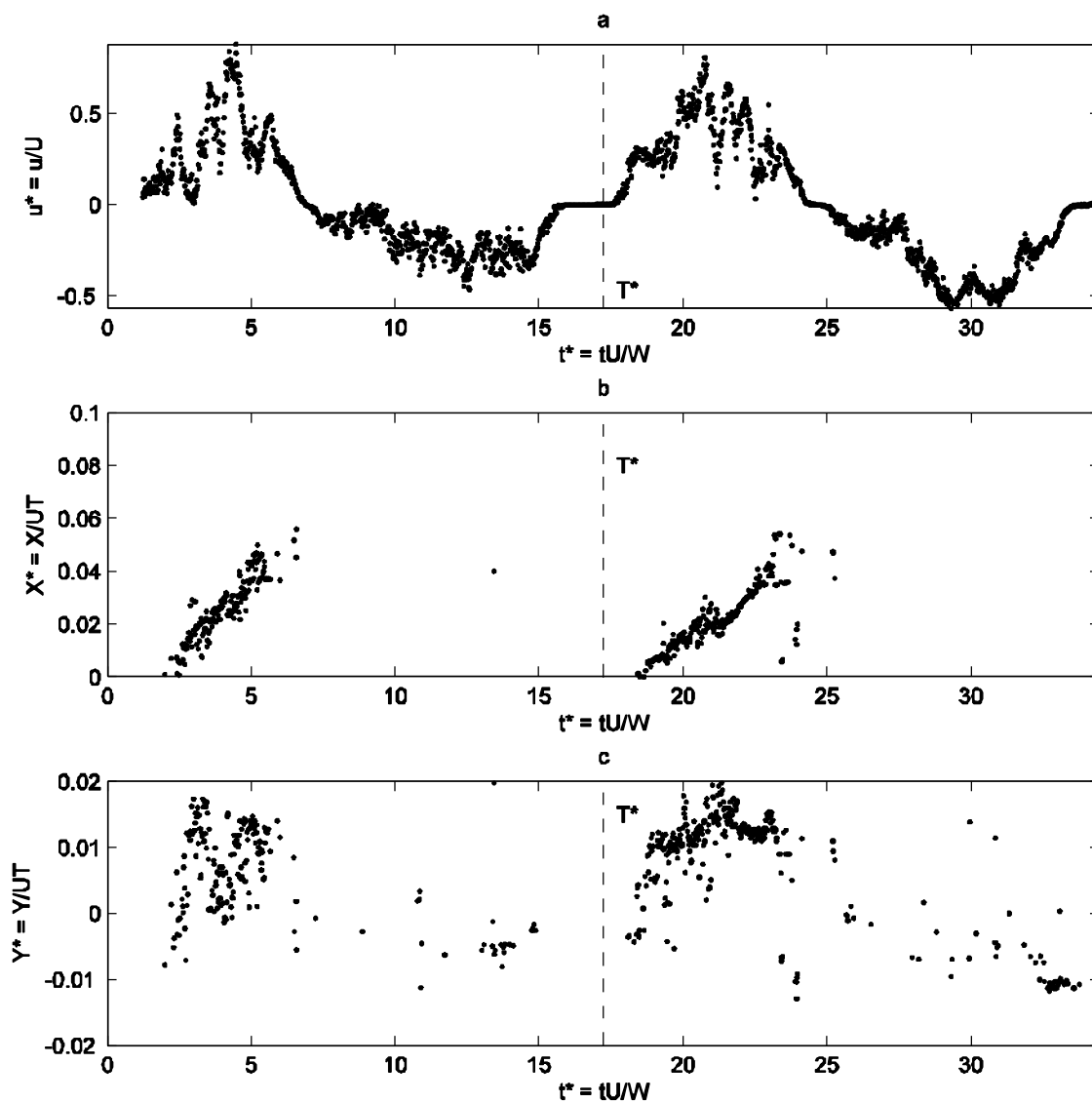


Figure 74 Life-history Type III for Layout D, repetition 1: a) Average cross sectional velocity at the mouth of the inlet. b) Longitudinal position of the center of the main vortex starting from the edge of the barrier island. c) Lateral position of the center of the main vortex starting from the edge of the barrier island.

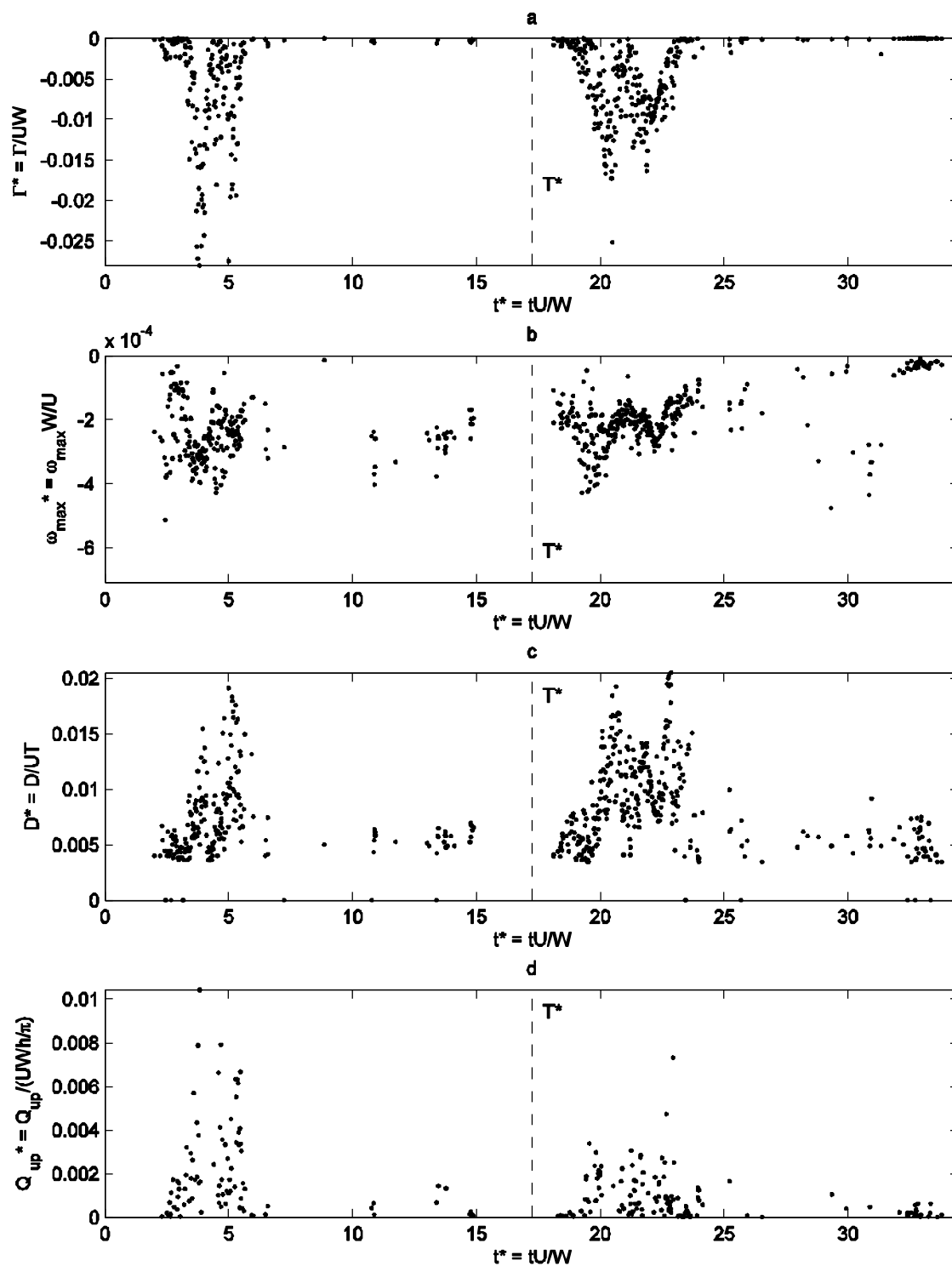


Figure 75 Life-history Type III for Layout D, repetition 1: a) Circulation around the main vortex b) Maximum vorticity in the main vortex c) Equivalent diameter of the main vortex. d) Upwelling flowing from the main vortex.

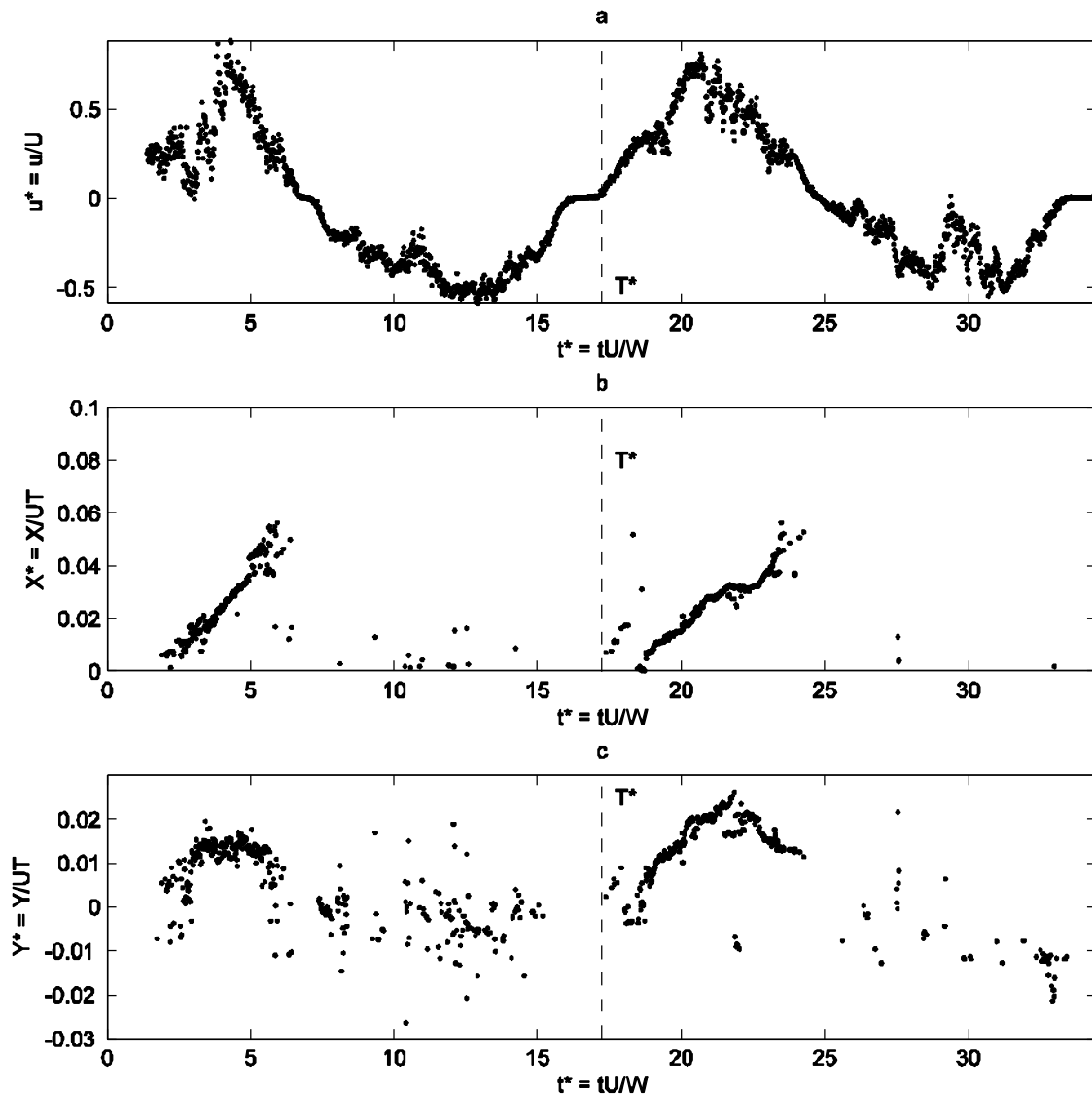


Figure 76 Life-history Type III for Layout D, repetition 2: a) Average cross sectional velocity at the mouth of the inlet. b) Longitudinal position of the center of the main vortex starting from the edge of the barrier island. c) Lateral position of the center of the main vortex starting from the edge of the barrier island.



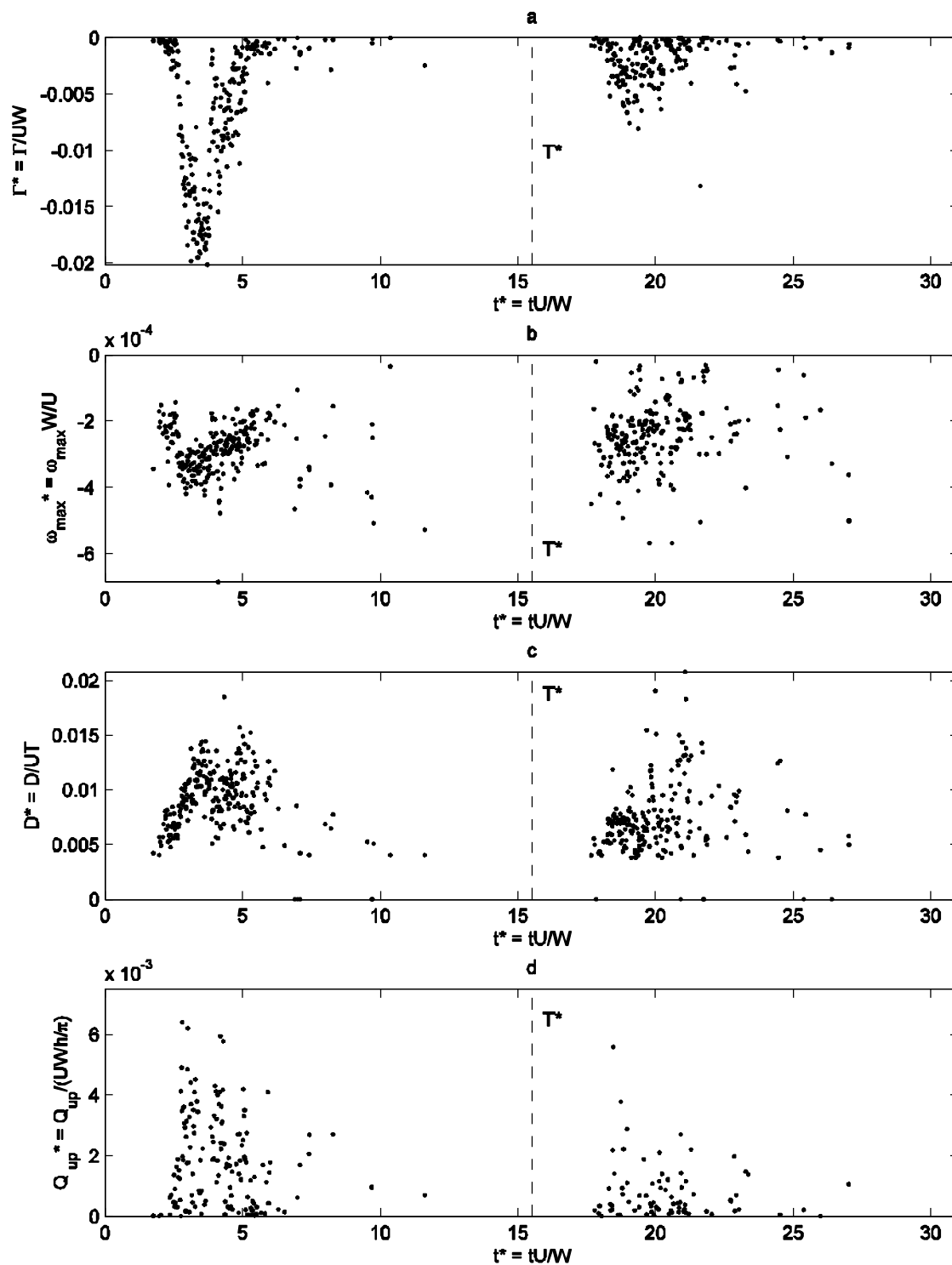


Figure 77 Life-history Type III for Layout D, repetition 2: a) Circulation around the main vortex b) Maximum vorticity in the main vortex c) Equivalent diameter of the main vortex. d) Upwelling flowing from the main vortex.

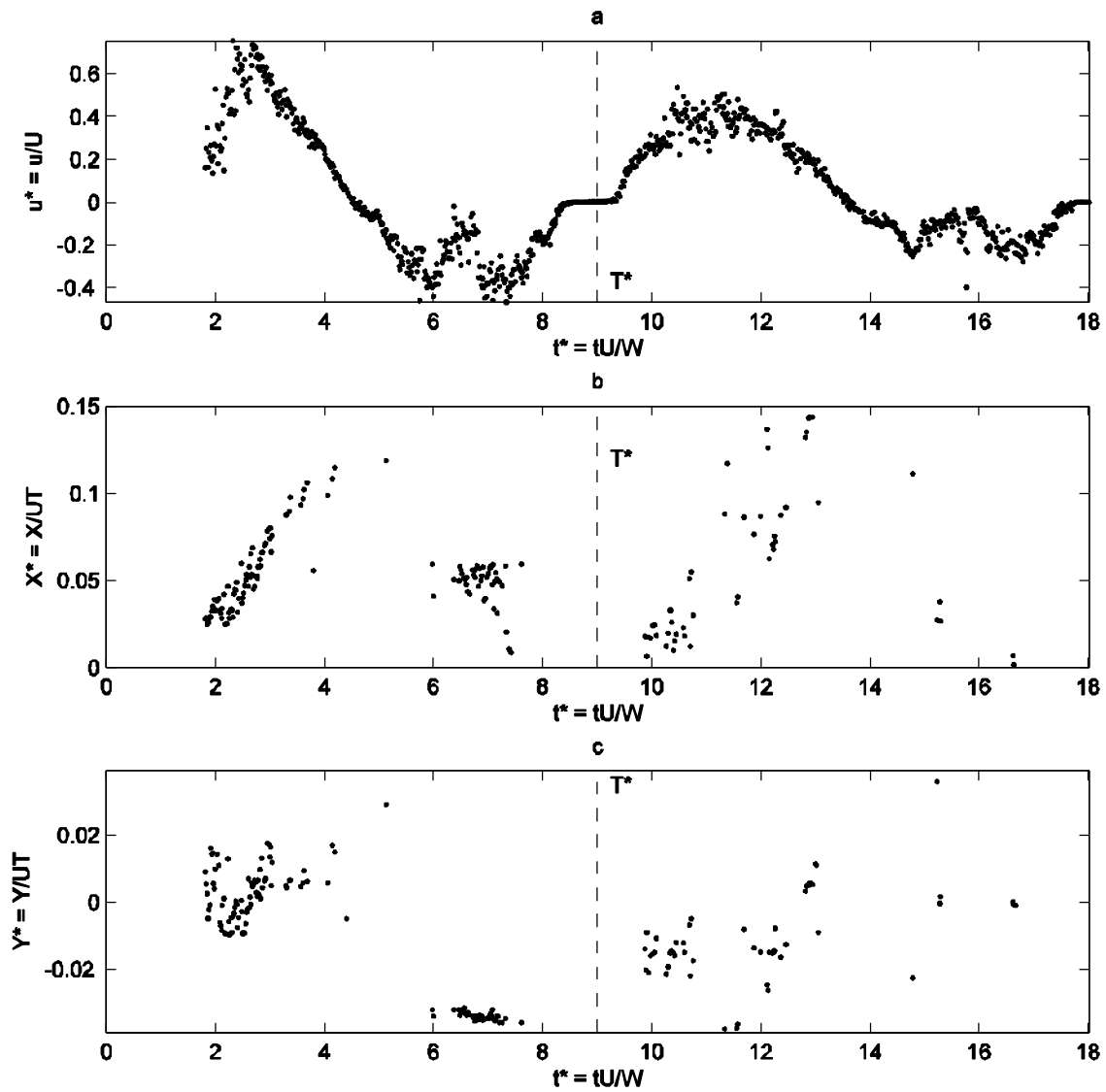


Figure 78 Life-history Type I for Layout E, repetition 1: a) Average cross sectional velocity at the mouth of the inlet. b) Longitudinal position of the center of the main vortex starting from the edge of the barrier island. c) Lateral position of the center of the main vortex starting from the edge of the barrier island.

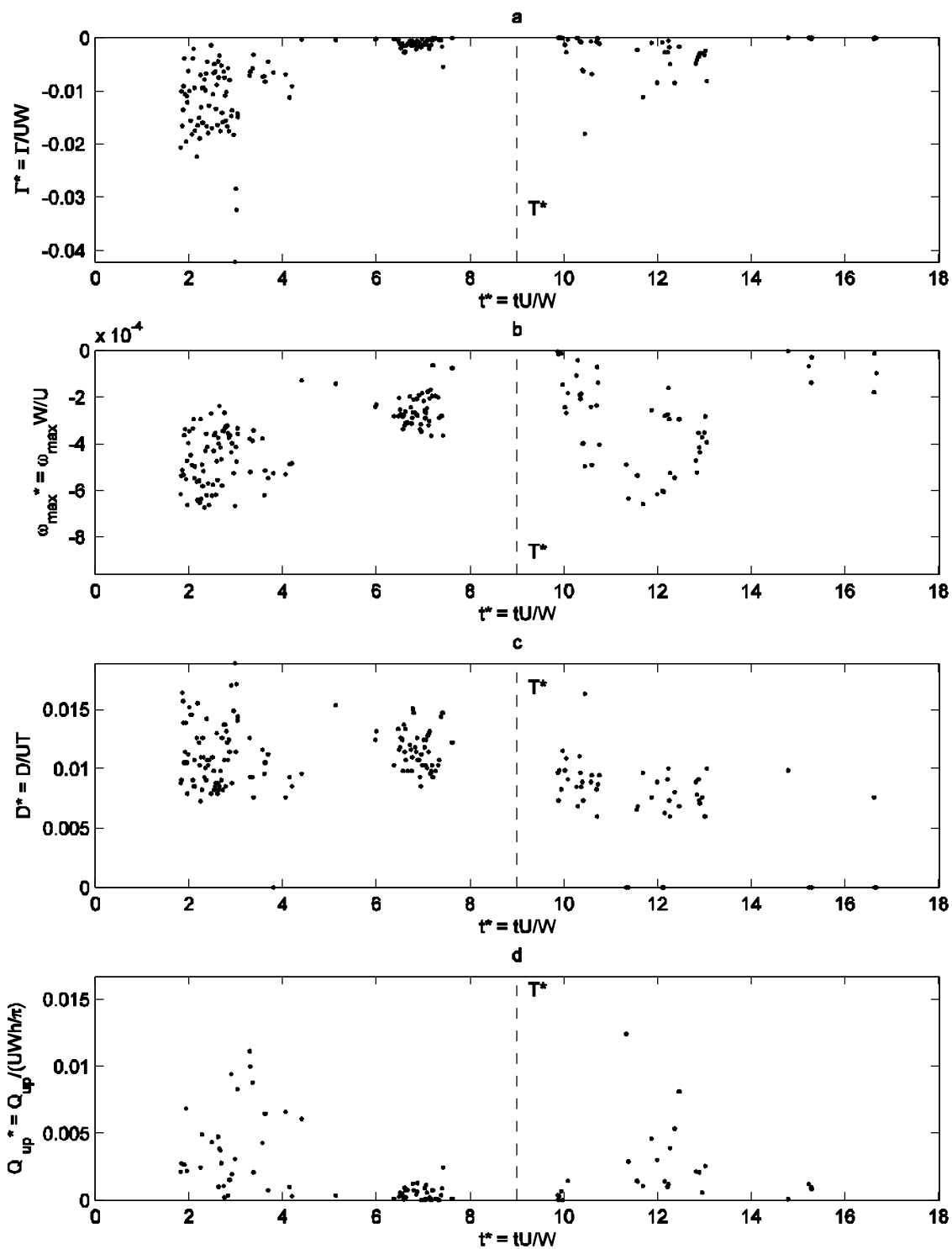


Figure 79 Life-history Type I for Layout E, repetition 1: a) Circulation around the main vortex b) Maximum vorticity in the main vortex c) Equivalent diameter of the main vortex. d) Upwelling flowing from the main vortex.

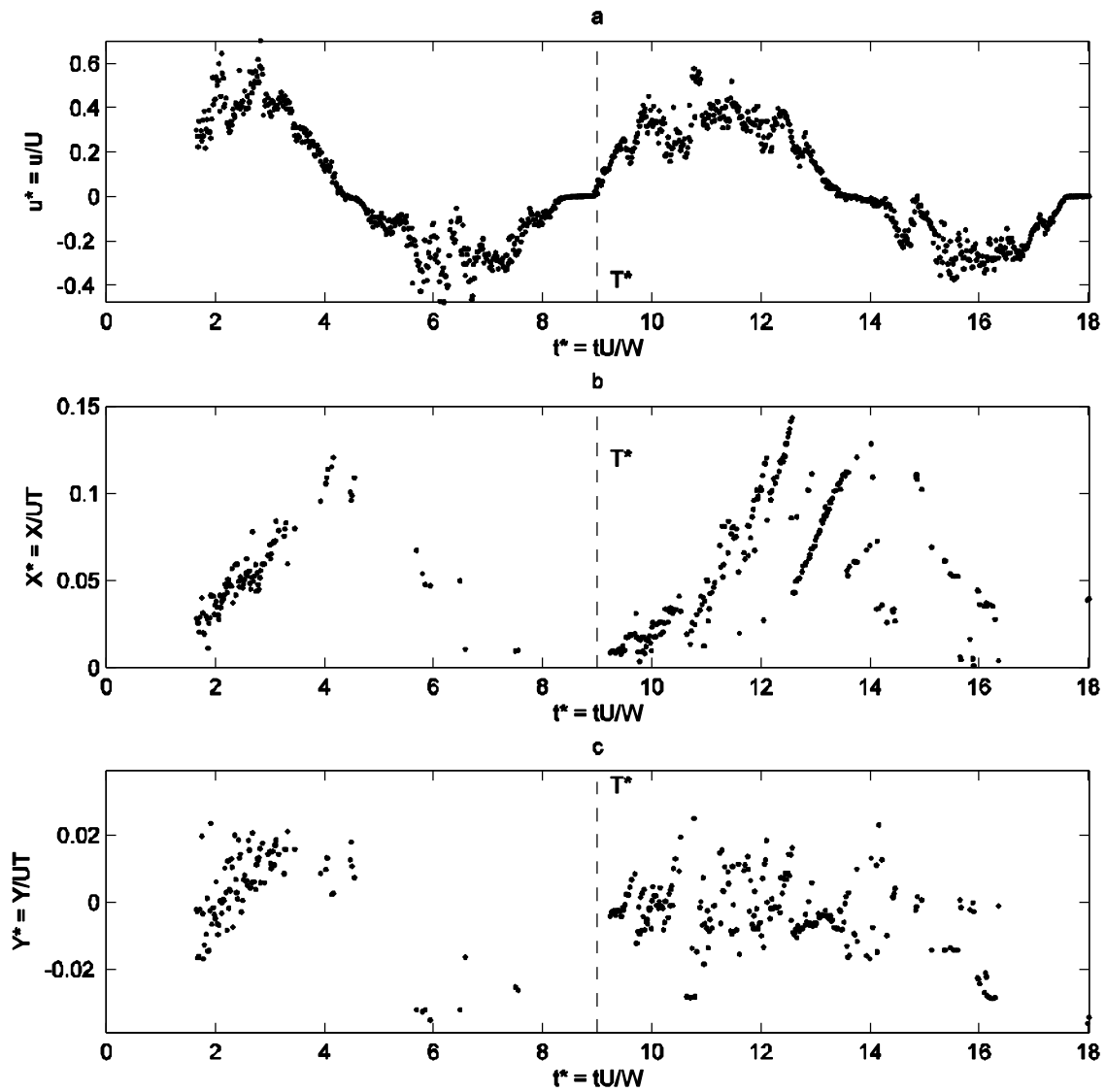


Figure 80 Life-history Type I for Layout E, repetition 2: a) Average cross sectional velocity at the mouth of the inlet. b) Longitudinal position of the center of the main vortex starting from the edge of the barrier island. c) Lateral position of the center of the main vortex starting from the edge of the barrier island.

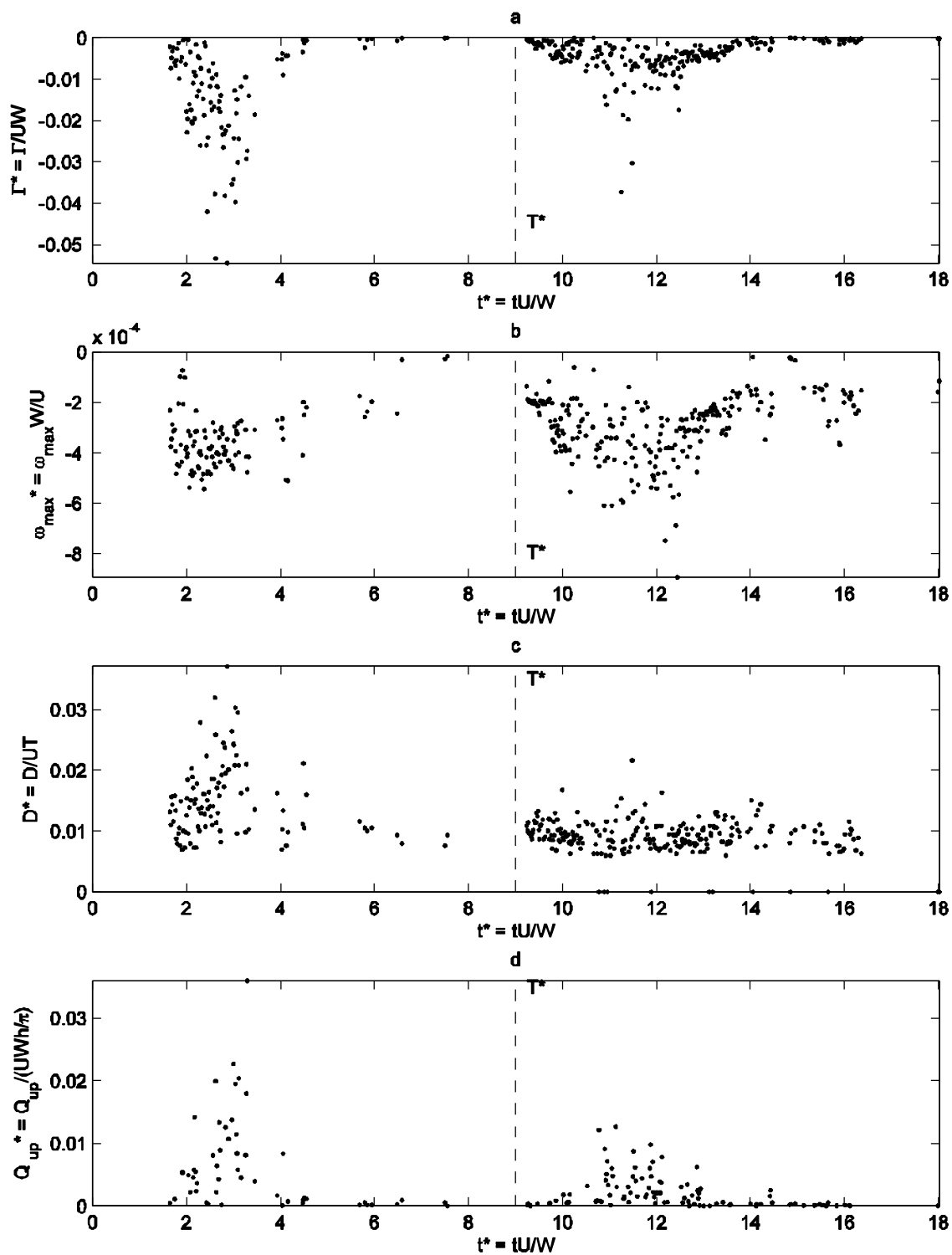


Figure 81 Life-history Type I for Layout E, repetition 2: a) Circulation around the main vortex b) Maximum vorticity in the main vortex c) Equivalent diameter of the main vortex. d) Upwelling flowing from the main vortex.

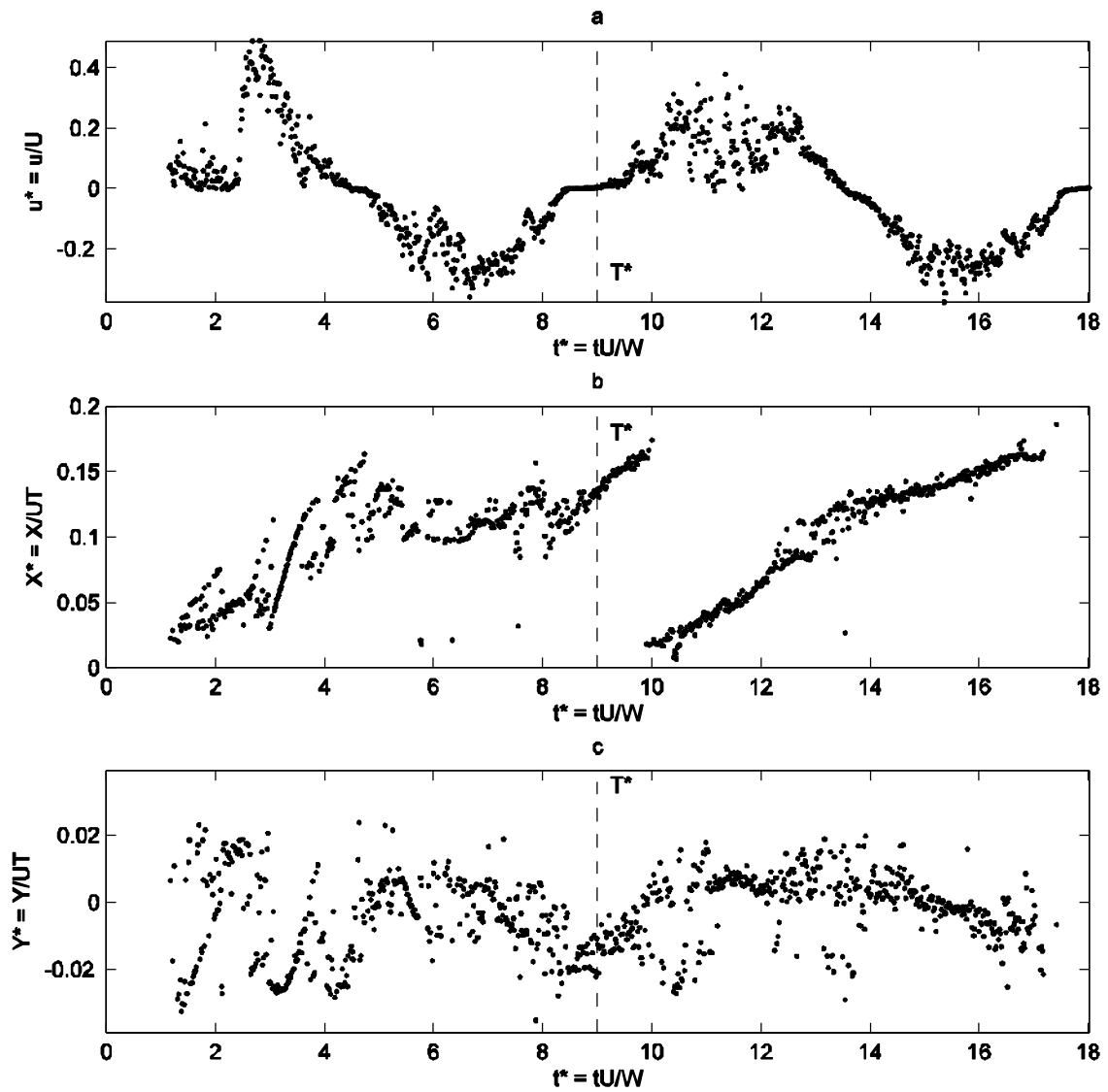


Figure 82 Life-history Type I for Layout F, repetition 1: a) Average cross sectional velocity at the mouth of the inlet. b) Longitudinal position of the center of the main vortex starting from the edge of the barrier island. c) Lateral position of the center of the main vortex starting from the edge of the barrier island.

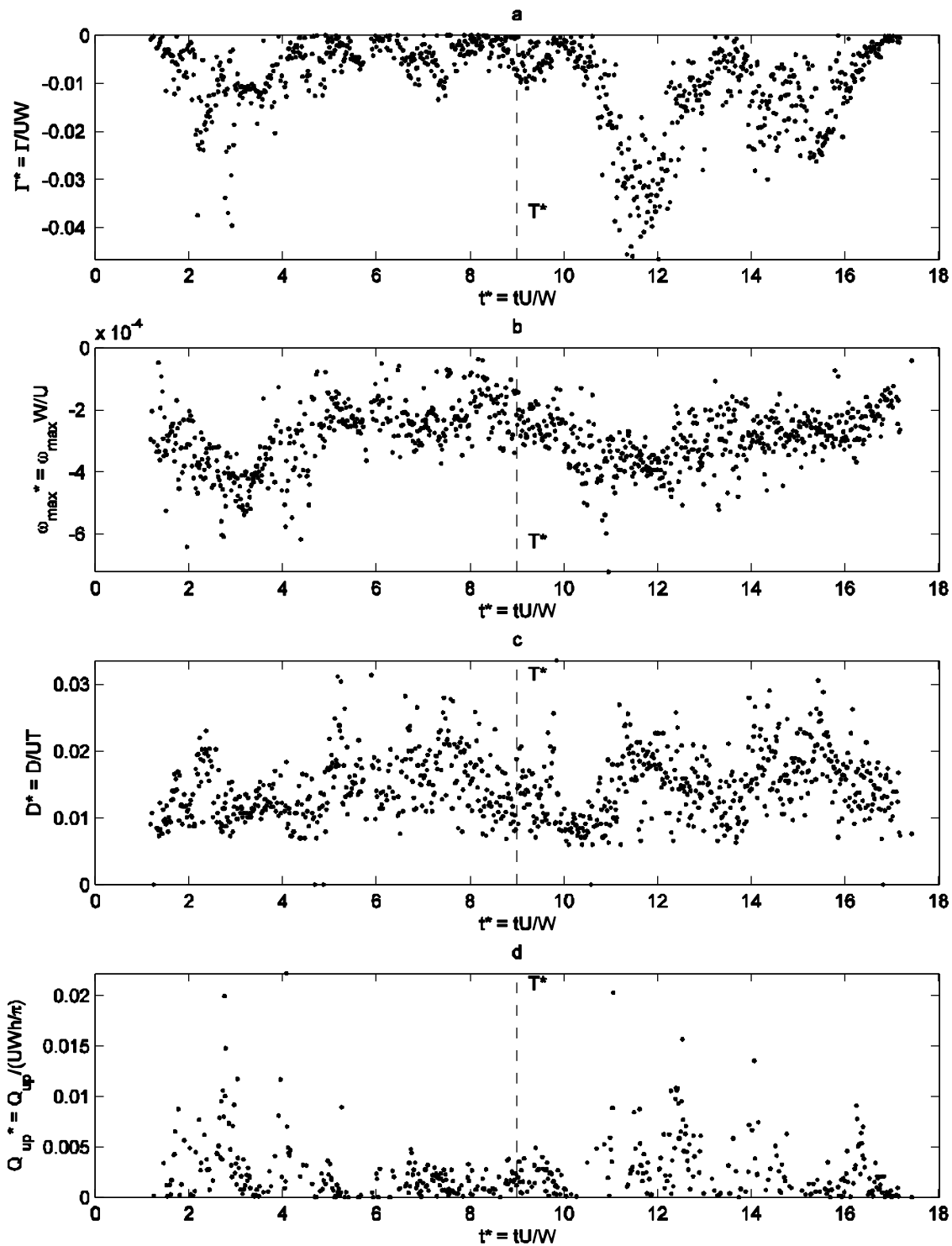


Figure 83 Life-history Type I for Layout F, repetition 1: a) Circulation around the main vortex b) Maximum vorticity in the main vortex c) Equivalent diameter of the main vortex. d) Upwelling flowing from the main vortex.

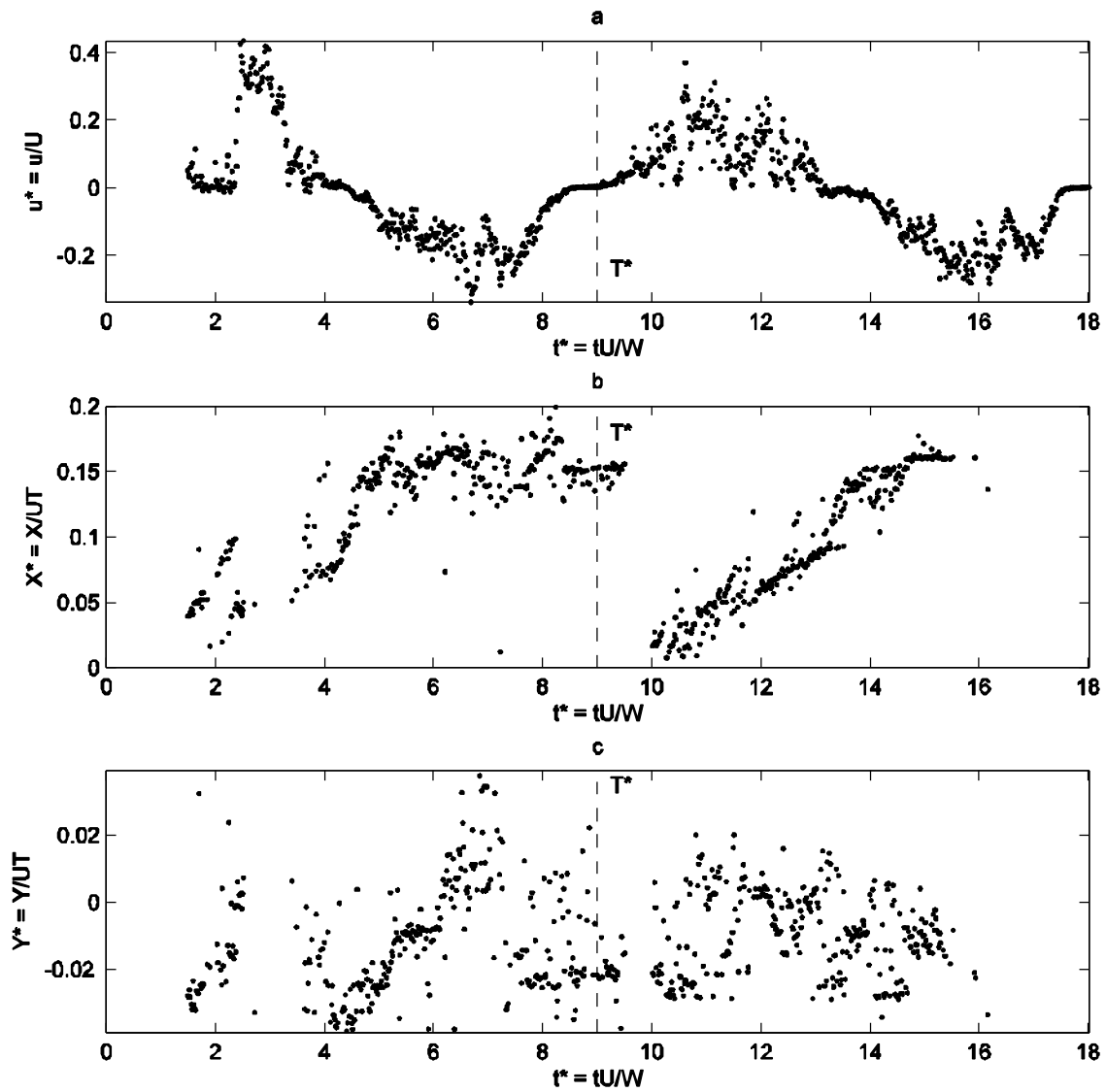


Figure 84 Life-history Type I for Layout F, repetition 2: a) Average cross sectional velocity at the mouth of the inlet. b) Longitudinal position of the center of the main vortex starting from the edge of the barrier island. c) Lateral position of the center of the main vortex starting from the edge of the barrier island.



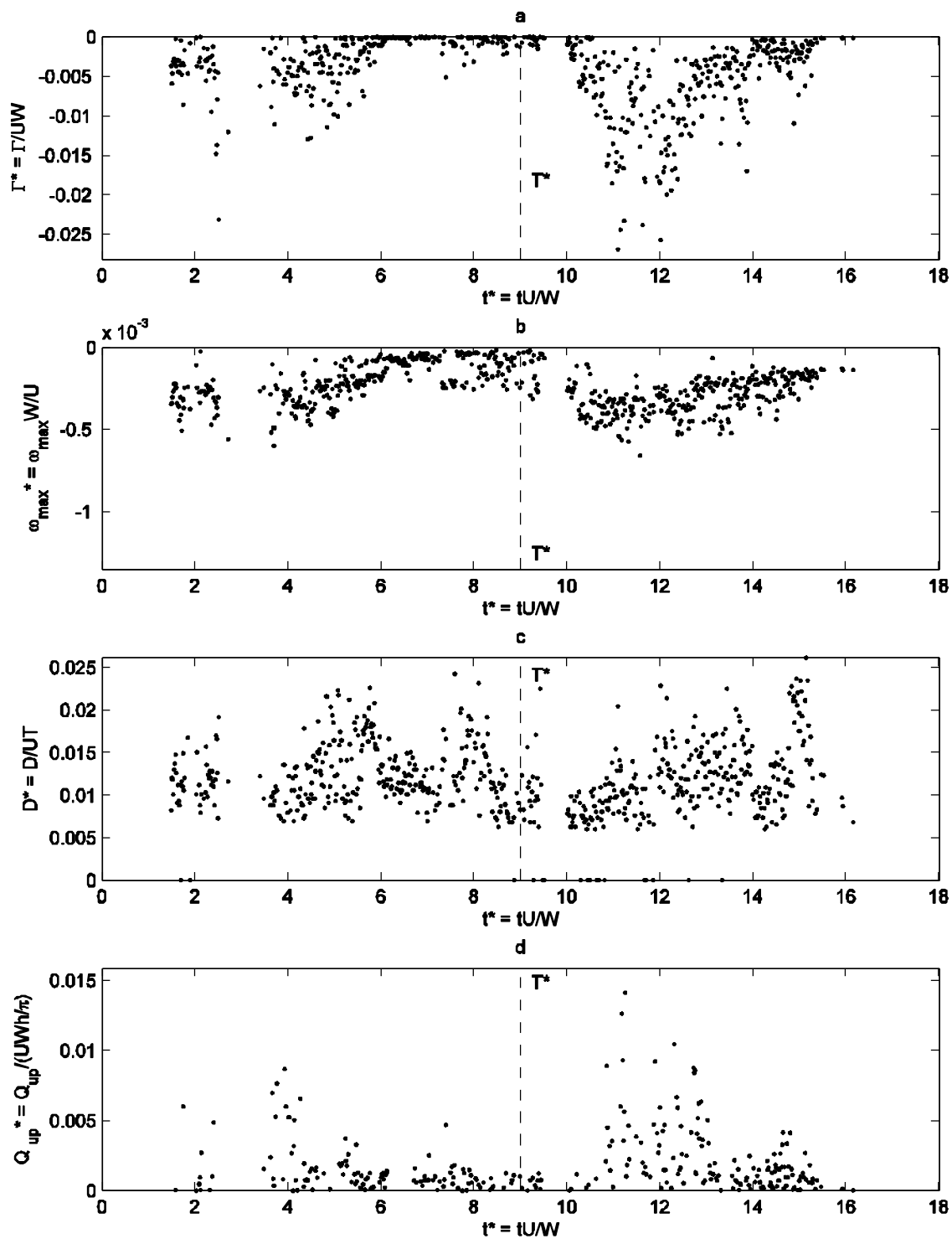


Figure 85 Life-history Type I for Layout F, repetition 2: a) Circulation around the main vortex b) Maximum vorticity in the main vortex c) Equivalent diameter of the main vortex. d) Upwelling flowing from the main vortex.

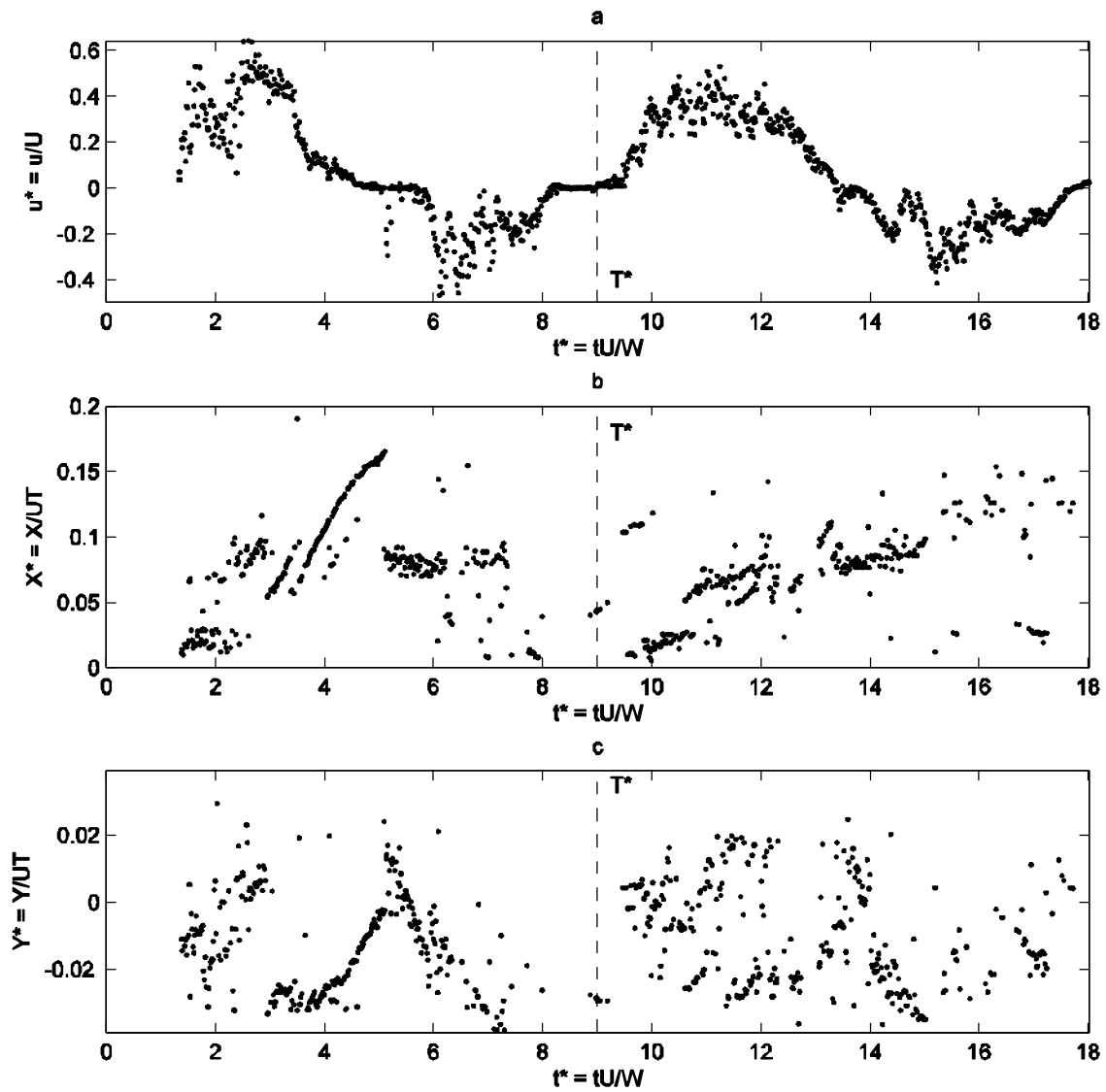


Figure 86 Life-history Type I for Layout G, repetition 1: a) Average cross sectional velocity at the mouth of the inlet. b) Longitudinal position of the center of the main vortex starting from the edge of the barrier island. c) Lateral position of the center of the main vortex starting from the edge of the barrier island.

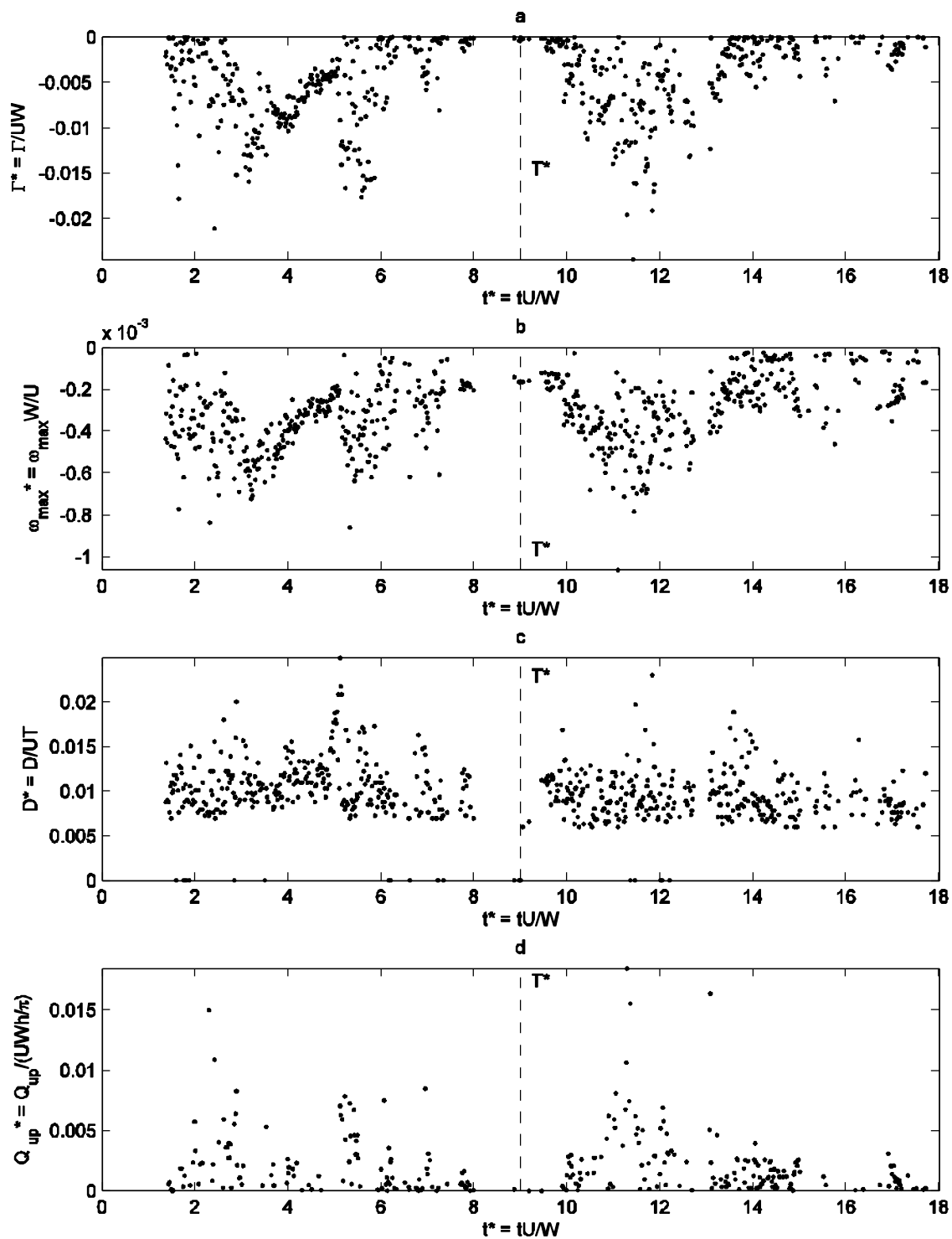


Figure 87 Life-history Type I for Layout G, repetition 1: a) Circulation around the main vortex b) Maximum vorticity in the main vortex c) Equivalent diameter of the main vortex. d) Upwelling flowing from the main vortex.

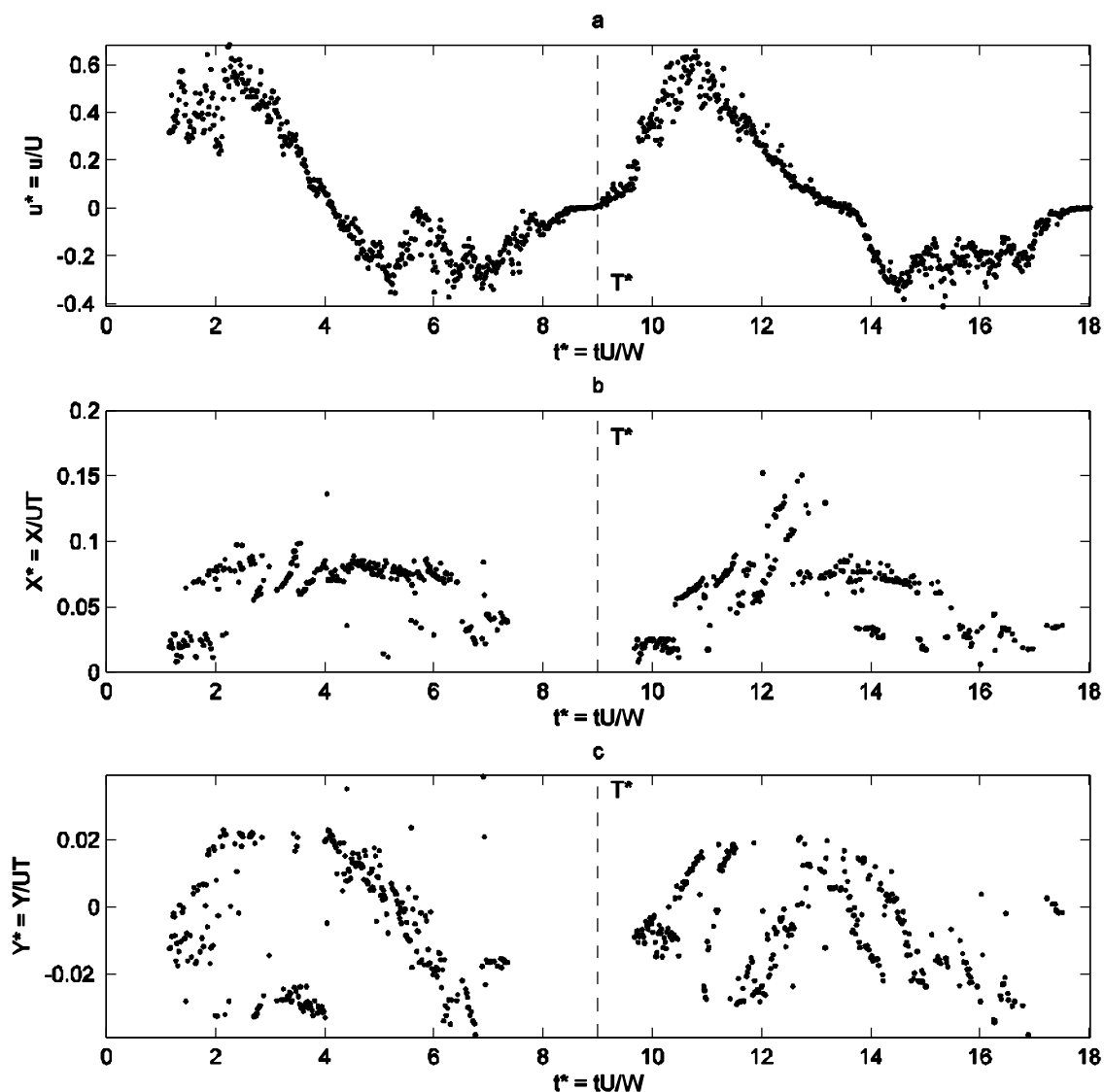


Figure 88 Life-history Type I for Layout G, repetition 2: a) Average cross sectional velocity at the mouth of the inlet. b) Longitudinal position of the center of the main vortex starting from the edge of the barrier island. c) Lateral position of the center of the main vortex starting from the edge of the barrier island.

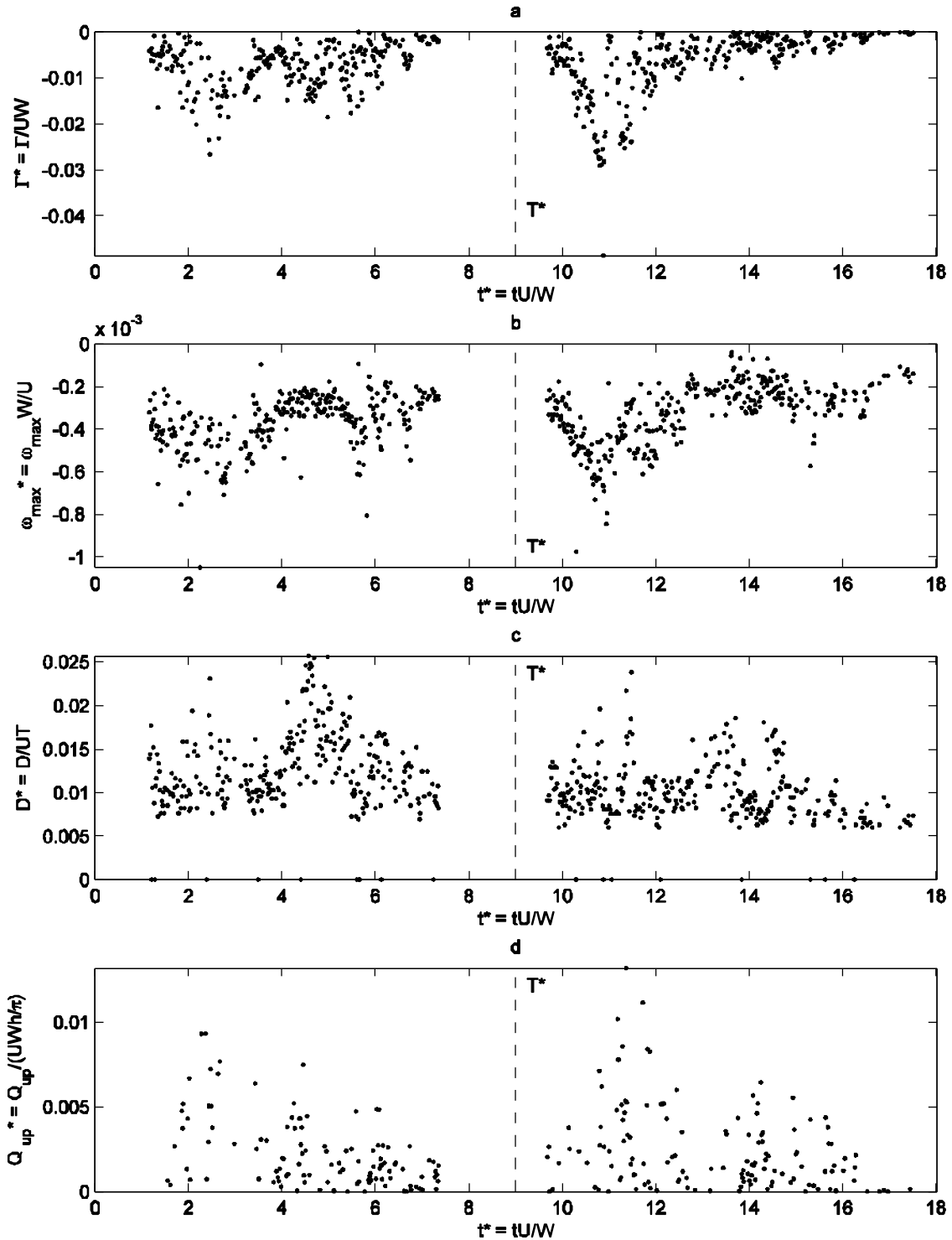


Figure 89 Life-history Type I for Layout G, repetition 2: a) Circulation around the main vortex b) Maximum vorticity in the main vortex c) Equivalent diameter of the main vortex. d) Upwelling flowing from the main vortex.

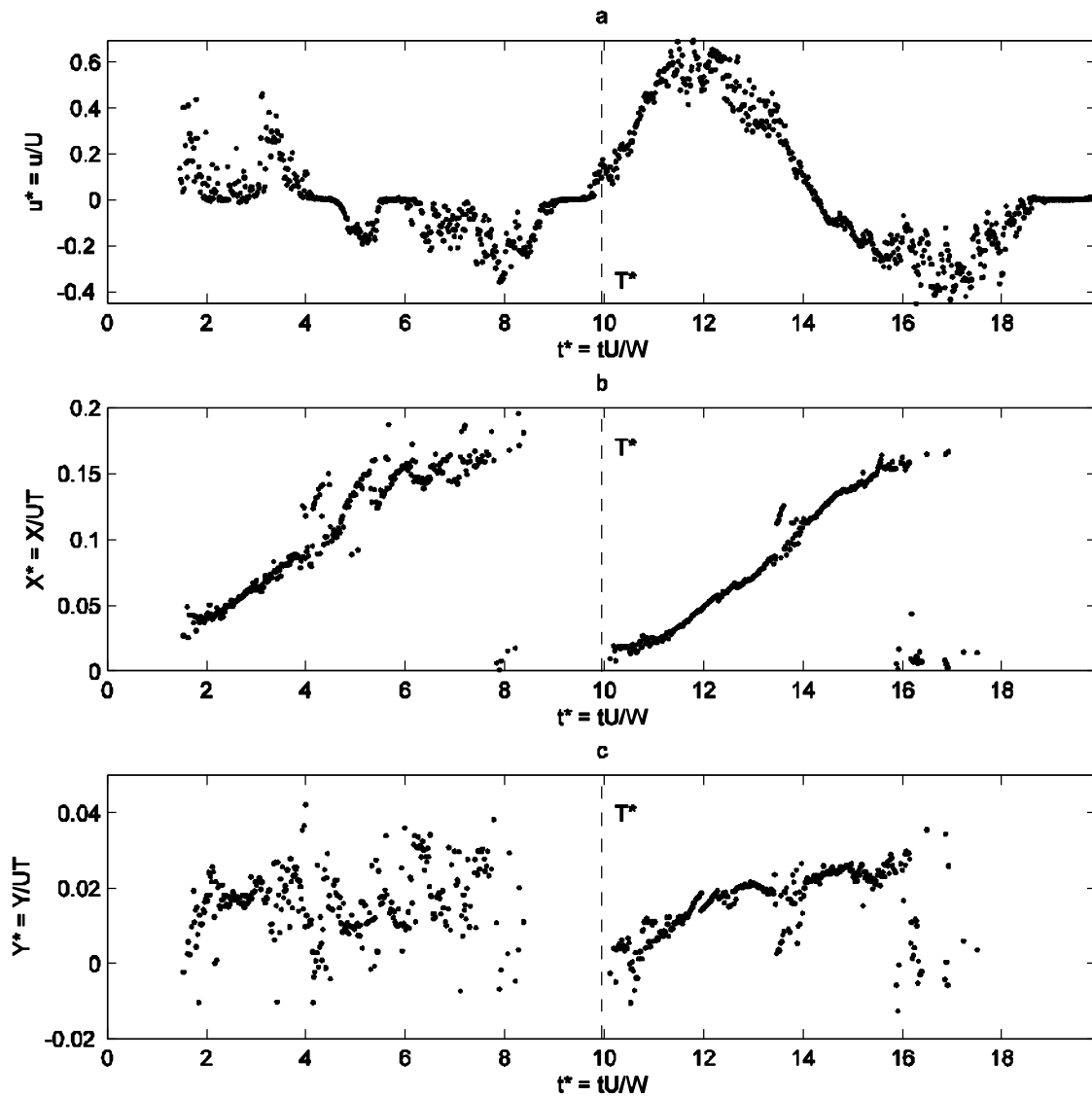


Figure 90 Life-history Type I for Layout H, 10 Degrees: a) Average cross sectional velocity at the mouth of the inlet. b) Longitudinal position of the center of the main vortex starting from the edge of the barrier island. c) Lateral position of the center of the main vortex starting from the edge of the barrier island.

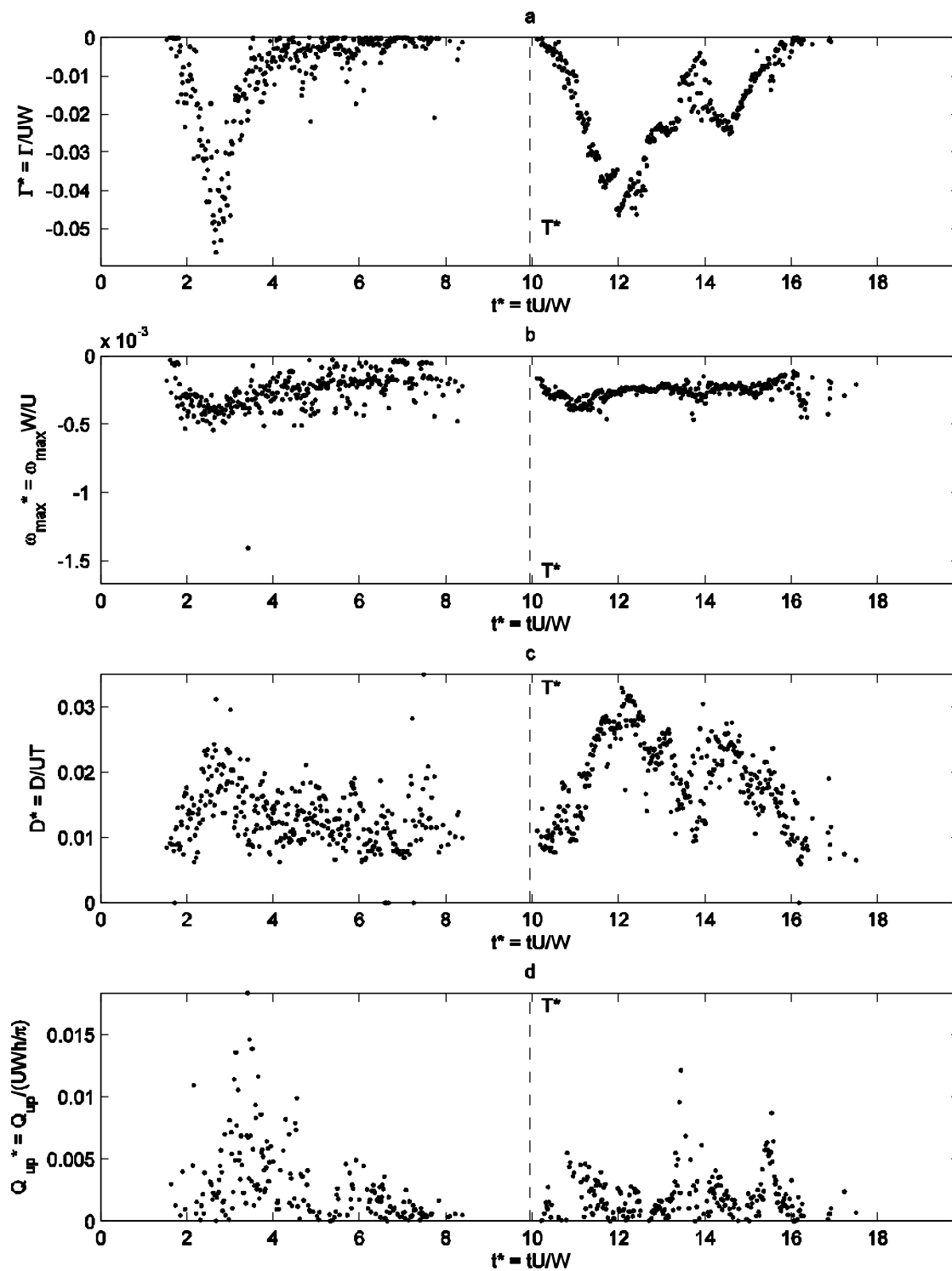


Figure 91 Life-history Type I for Layout H, 10 Degrees: a) Circulation around the main vortex b) Maximum vorticity in the main vortex c) Equivalent diameter of the main vortex. d) Upwelling flowing from the main vortex.

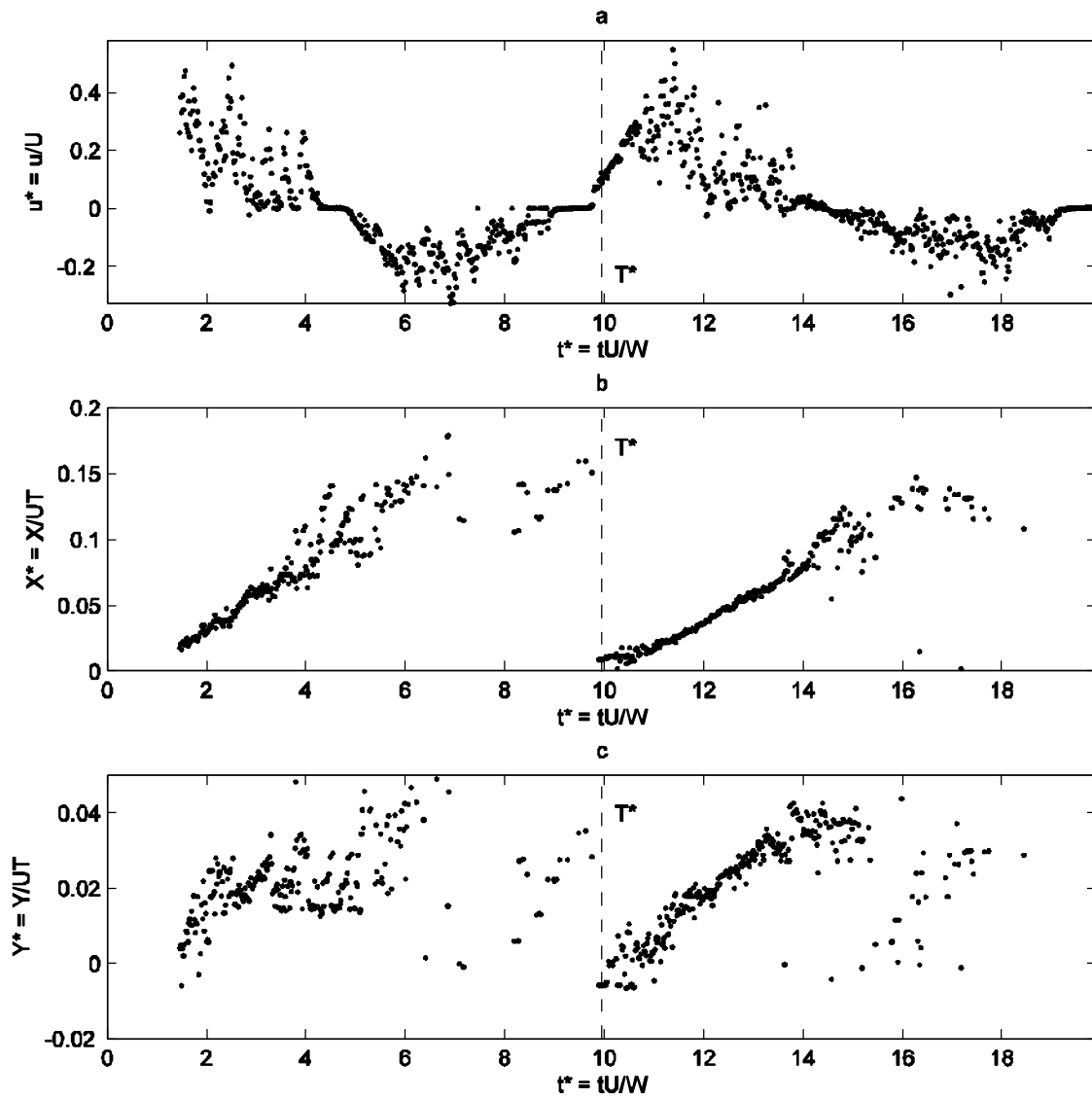


Figure 92 Life-history Type I for Layout H, 20 Degrees: a) Average cross sectional velocity at the mouth of the inlet. b) Longitudinal position of the center of the main vortex starting from the edge of the barrier island. c) Lateral position of the center of the main vortex starting from the edge of the barrier island.



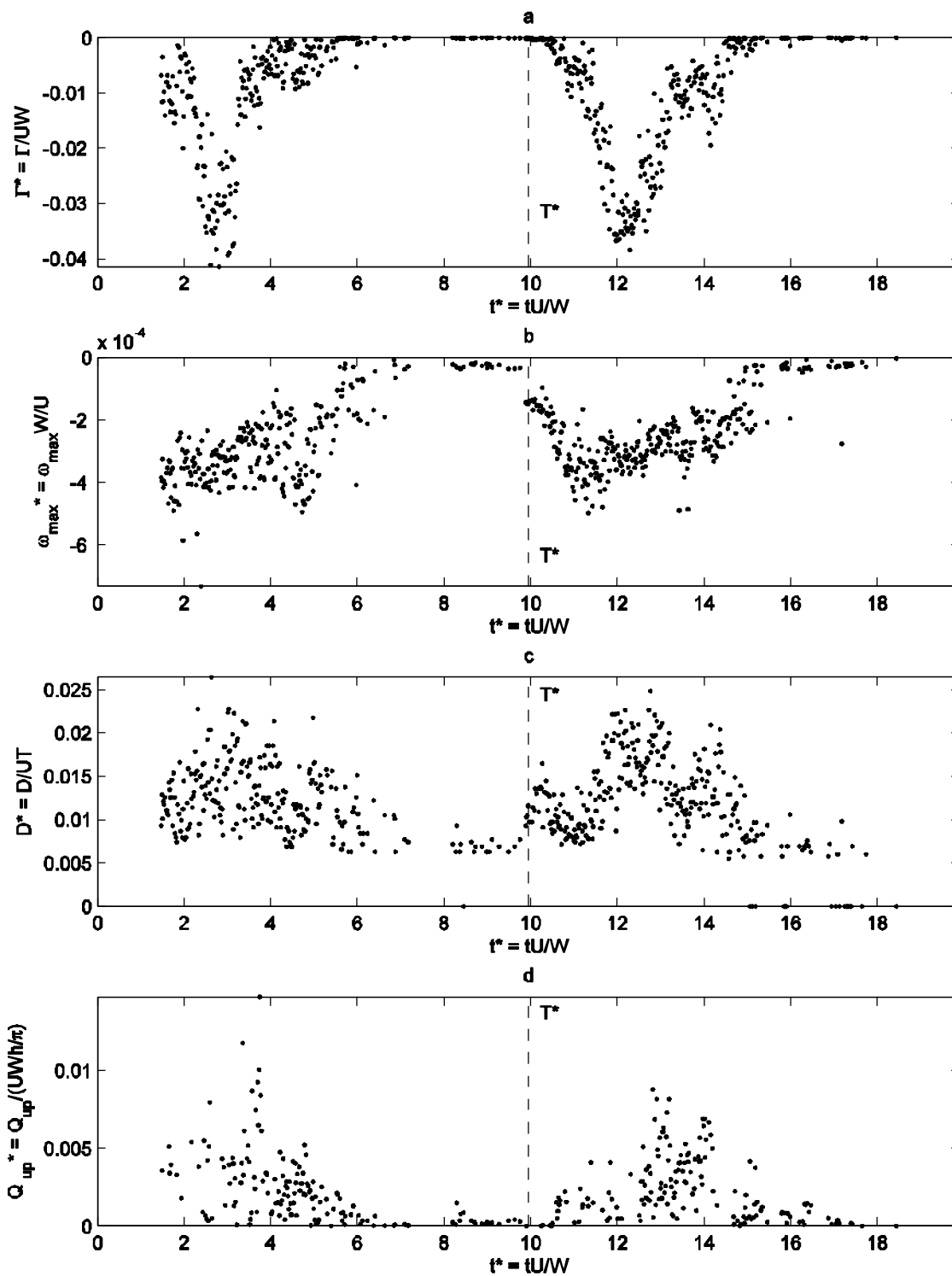


Figure 93 Life-history Type I for Layout H, 20 Degrees: a) Circulation around the main vortex b) Maximum vorticity in the main vortex c) Equivalent diameter of the main vortex. d) Upwelling flowing from the main vortex.

Table 16 shows the slopes of the fitted curves for the growth and decay of the circulation of the main vortex for the first cycle. The slopes were calculated until the vortex starts leaving the field of view.

A propagation of error analysis was done for this calculation of the slope, to take in account the errors of measurement that can be made. The time between to images has an associated error of  $\pm 0.001$  [s]; and the associated error for the root mean square error (rmse) the circulation is  $\pm 0.0001$ . Then, the estimated error for the slope calculation is  $\pm 0.02$ .

Table 16 Slopes of the fitted curves for the growth and decay of the circulation of the main vortex for the first cycle, with an associated error of  $\pm 0.020$ .

LAYOUT	LIFE-HISTORY TYPE		K <sub>w</sub> REAL VALUE	CIRCULATION SLOPE	
				Growth	Decay
				□	□
A	I	1	0.11	-0.038	0.007
	I	2	0.11	-0.040	0.005
	II	1	0.05	-0.024	0.012
	II	2	0.06	-0.039	0.004
	III	1	0.27	-0.040	0.006
	III	2	0.29	-0.044	0.007
B	I	1	0.11	-0.006	0.012
	I	2	0.12	-0.015	0.056
	II	1	0.06	-0.016	0.001
	II	2	0.07	-0.027	0.006
	III	1	0.44	-	-
	III	2	0.35	-	-
C	I	1	0.13	-0.012	0.003
	I	2	0.13	-0.027	0.003
	II	1	0.06	-0.006	0.006
	II	2	0.06	-0.014	0.007
	III	1	0.44	-	-
D	I	1	0.11	-0.023	0.003
	I	2	0.11	-0.010	0.013
	II	1	0.06	-0.011	0.007
	II	2	0.06	-0.016	0.011
	III	1	0.50	-	-
	III	2	0.44	-	-
E	I	1	0.11	-	-
	I	2	0.11	-	-
F	I	1	0.11	-	-
	I	2	0.11	-	-
G	I	1	0.11	-	-
	I	2	0.11	-	-
H	I	10	0.11	-0.045	0.020
	I	20	0.10	-0.021	0.015

#### 4 Secondary vortices analysis

Secondary vortices are formed because of the unstable characteristics of the tidal jets that are simulated in this research. For an unstable jet, the centerline has a meandering behavior and multiple secondary vortices form at each side of the inlet.

The secondary vortices analysis was done by observing the movies of the dye studies (Appendix C). The Strouhal number associate with the frequency that the vortices were forming at the peak of the tidal cycles, the radius of curvature of the edge of the barrier island, and the maximum average cross sectional velocity was calculated.

$$S_t = \frac{R_c f}{U_{MAX}} \quad (27)$$

Where  $R_c$  is the radius of curvature of the barrier island,  $f$  is the frequency of the formation of the vortices, and  $U_{MAX}$  is the maximum velocity.

A propagation of error analysis was done for this calculation, to take in account the errors of measurement that can be made. The frequency of the vortices has an associated error of  $\pm 0.1$  [Hz]; the radius of curvature of the barrier island has an associated error of  $\pm 0.05$  [cm]; and the associated error for the maximum velocity is  $\pm 0.01$  [m/s]. Then, the estimated error for the Strouhal Number is  $\pm 0.1$ .

Table 17 shows the frequency of the formation of the vortices for layouts A through D, and Table 18 shows the Strouhal Number for layouts A through D, only for Life-History types I and II. The type III was not calculated because it was difficult to observe the formation of the secondary vortices.

Table 17 Frequency of the formation of the secondary vortices in the peak of the first and second tidal cycle, with an associated error of  $\pm 0.1$  [Hz].

EXPERIMENT	$K_w = 0.11$		$K_w = 0.06$	
	Frequency		Frequency	
	1st Cycle	2nd Cycle	1st Cycle	2nd Cycle
	[1/s]	[1/s]	[1/s]	[1/s]
Layout A	0.9	0.7	0.6	0.5
Layout B	1.0	0.6	0.6	0.5
Layout C	0.7	0.7	0.5	0.4
Layout D	1.1	1.1	1.1	0.8

Table 18 Strouhal Number of the secondary vortices present in the first and second cycles of the tidal flow, with an associated error of  $\pm 0.1$ .

EXPERIMENT	RADIUS OF CURVATURE	$K_w = 0.11$		$K_w = 0.06$	
		Strouhal Number		Strouhal Number	
		1st Cycle	2nd Cycle	1st Cycle	2nd Cycle
	[cm]	[]	[]	[]	[]
Layout A	0.075	0.4	0.2	0.2	0.2
Layout B	0.075	0.4	0.2	0.2	0.2
Layout C	0.075	0.3	0.2	0.2	0.2
Layout D	0.15	0.8	0.6	0.8	0.6

## APPENDIX C

### ELECTRONIC SUPPLEMENT

The present appendix explains what does the electronic supplement has in it, and how is it organized. This supplement can be found in the Texas A&M Library.

The supplement is divided into 3 Folders (compresed into zip files) that provide the following:

- Matlab Programs: This folder has all the necessary programs to reproduce the analysis that was done for the thesis. The MPIV Code and the DACE program can be downloaded from the web page stated. Also the codes developed for the analysis of the PIV data and the vortex evolutions are included.
- Dye Studies: This folder has the videos for the visualization studies.
- PIV: This folder has the movies for the simulation of the velocity and vorticity field, and the vortex identification movies as well.

**VITA**

Francisco Nicolau del Roure was born in Concepcion, Chile. He received his Bachelor of Science degree in civil engineering in 2004 from Universidad de Chile in Santiago, Chile. He came to Texas A&M University, College Station in the fall of 2005 to pursue his Master of Science in ocean engineering. His research interests include numerical and laboratory simulations of exchange processes on tidal inlets. His permanent address is

Francisco Nicolau del Roure  
Av. Las Perdices #847-B  
La Reina, Santiago  
CHILE